Regulation of actomyosin contractility by p110α P13-kinase in sprouting angiogenesis

Ana Angulo Urarte

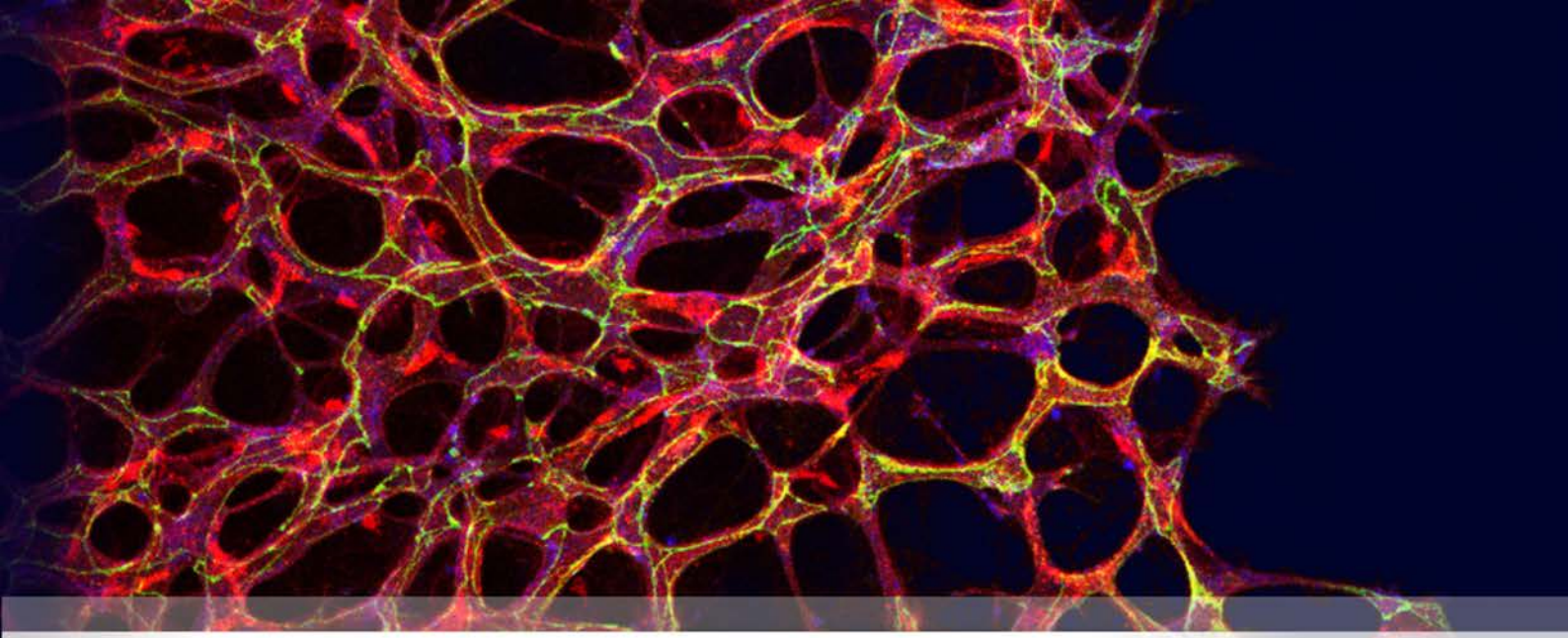

Regulation of actomyosin contractility by p110α PI3-Kinase in sprouting angiogenesis

ANA ANGULO URARTE

PhD Thesis. Barcelona, February 2017

Facultat de Farmàcia , UB

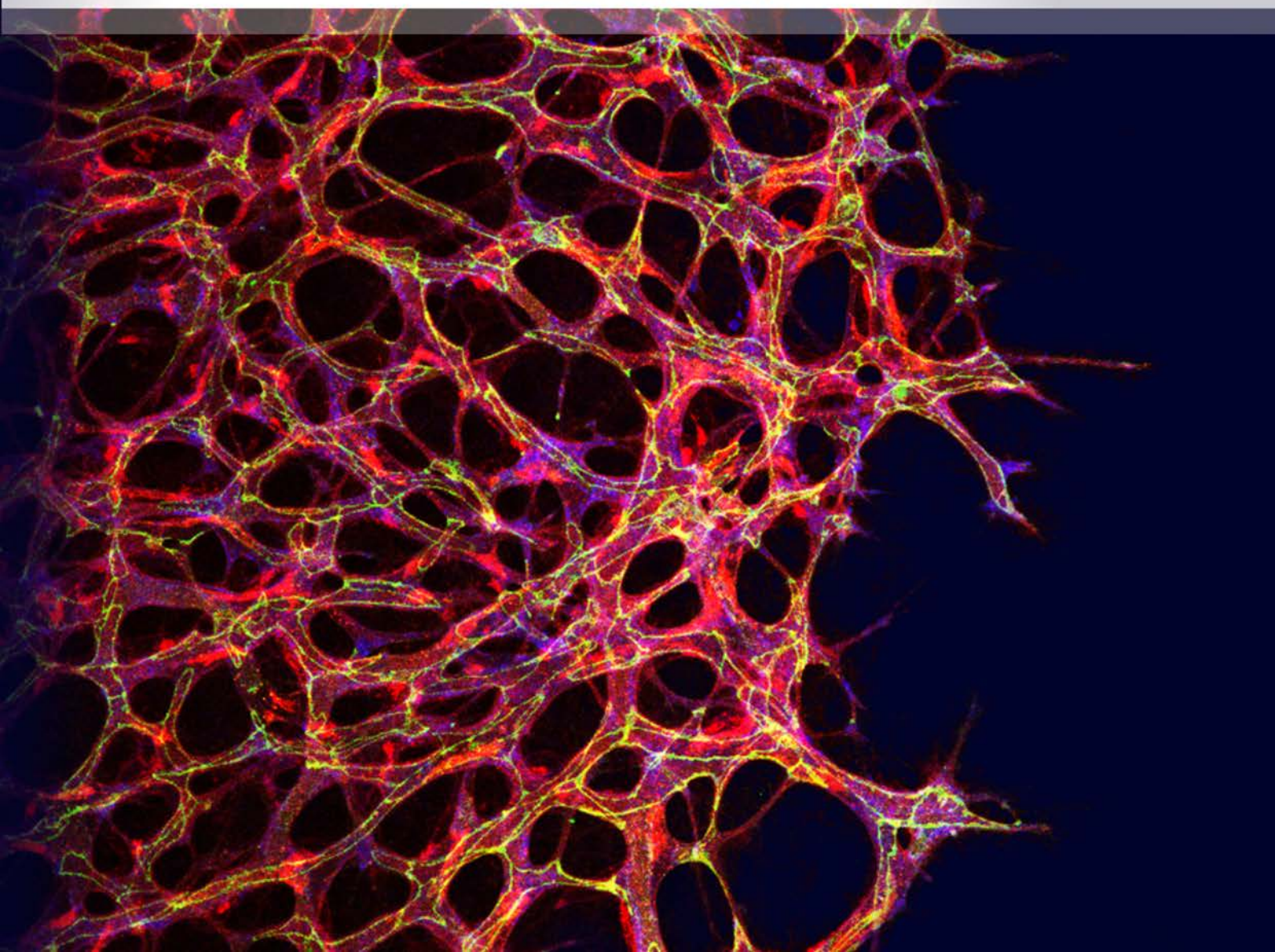

UNIVERSITAT DE BARCELONA

IDIBELL
Institut d'Investigació Biomèdica de Bellvitge

FACULTAT DE FARMÀCIA I CIÈNCIES DE L'ALIMENTACIÓ
UNIVERSITAT DE BARCELONA

Programa de Doctorado en Biomedicina

Regulation of actomyosin contractility by p110α PI3-kinase in sprouting angiogenesis

Memòria presentada per
Ana Angulo Urarte
per optar al títol de doctora per la Universitat de Barcelona.

Aquesta tesi ha estat realitzada sota la direcció de
Mariona Graupera i Garcia-Milà
en el Laboratori de Senyalització Vascular ubicat en l'Institut d'Investigació Biomedica de Bellvitge (IDIBELL).

Directora de tesi	Tutor	Doctoranda
Dra. Mariona Graupera i Garcia-Milà	**Dr. Fransesc Viñals Canals**	**Ana Angulo Urarte**

Ana Angulo Urarte, Febrer 2017

This thesis work titled *" Regulation of actomyosin contractility by p110α-PI3K during sprouting angiogenesis*" has been developed in the Vascular Signalling Laboratory at IDIBELL (L'Hospitalelt de Llobregat, Barcelona).

Financial Support:

- Gobierno de España - Ministerio de Ciencia e Inovación (MICINN). SAF2010-15661 and SAF2013-46542-P
- People Programme (Marie Curie Actions) of the European Union's Seventh Framework Programme FP7/2013-2016/ under REA grant agreement 317250. VESSEL-317250. Title of the project: "Vascular Endothelial Interactions and Specialization"
- Instituto de Salud Carlos III (ISCIII). PIE13/00022 (ONCOPROFILE, 2014-2016)
- Generalitat de Catalunya - Agència de Gestió d'Ajust Universitaris i de Recerca (AGAUR) - 2014-SGR-725

During the present work Ana Angulo Urarte performed a secondment (8th February 2016 to 12th May 2016) in Dr. Markus Affolter's laboratory and under the supervision of Dr.Heinz-George Belting at the Biozentrum, Basel (Switzerland) thanks to the financial support from EMBO (EMBO short-term fellowship).

EMBO excellence in life sciences

IDIBELL Institut d'Investigació Biomèdica de Bellvitge

A mi padre Licerio,

Por compartir conmigo el entusiasmo por la ciencia.

Por enseñarme a no rendirme.

Por enseñarme a soñar.

Acknowledgement

En mi primer lugar quería agradeceros a todas las personas que durante esta etapa de mi vida habéis estado *al meu costat* y habéis hecho que este largo proyecto haya sido una experiencia inolvidable y suuuper enriquecedora. Gracias a vosotros siento que he crecido a nivel personal y profesional.

A **Mariona Graupera**; no tengo palabras para agradecerte la oportunidad que me diste al confiar en mí para desarrollar este proyecto. Para mí ha sido apasionante aprender tanto sobre una proteína tan genial como la PI3K como introducirme en el campo del desarrollo vascular, el cual ha terminado fascinándome. Gracias por haber sido una jefa tan positiva y alentadora siempre, pero aun más en los momentos en los que las cosas no salían y yo me estresaba. Gracias por haber confiado en mí durante estos años y haberme enseñado que se puede hacer buena ciencia de una forma humilde y generosa. También gracias por ser un ejemplo de que se puede ser mujer, excelente científica y madre. Sé que tú me quedas tanto a nivel profesional como personal, y no puedo pedir más. Gràcies.

I am extremely grateful to **Susana de la Luna**, **Stephan Huveneers** and **Rui Benedito** for being willing to read my work and be part of my thesis committee. **Sandra**, **Pilar** y **Jordi**, muchísimas gracias por haber aceptado con tanto entusiasmo ser suplente de mi tribunal, os lo agradezco muchísimo!

I would like to thank to **Markus Affolter** to give me the opportunity to be in his Lab for three months and allows me to enjoy that fascinating and inspiring scientific environment. I would like to give special thanks to **Heinz-Georg Belting**. Henry, I really appreciate your help and supervision during my stay. Thank to you I learnt a lot about vascular development in zebrafish embryos. You were always available for good scientific discussion and advice. I would also like to thank to all the members of the Affolter's Lab, specially to **Minkyoung, Etienne, Niels, Charles Bentz, Vahap, Ilkka, Mario, Ilaria, Shinya, Cora, Gustavo, Helen**… for making incredibly pleasant my stay.

Gracias **Francesc y Oriol** porque habéis sido una pieza indispensable en el crecimiento de este trabajo. Gracias por vuestros consejos y por las inspiradoras discusiones científicas.

Mil gracias a todos los ONAs que han estado y están en Lab porque han hecho que los momentos buenos del doctorado fueran geniales y los malos y duros no lo fueran tanto. Este grupo siempre ha sido una piña, y se ha ayudado entre sí cuando alguien lo ha necesitado. Gracias chic@s, sois todos especiales

para mí. Gracias **Helena y Adriana. Gracias Ana, Erika, Iñi, Jordi, Gabi, María, Eric, Laia, Piotr, Jasmine...**

Y llegó la fusión y la llegada de los CMPs al Lab y con ello la etapa más divertida del doctorado. Llegasteis como un huracán de buen rollo y pudimos compartir muchas risas y confidencias. Gracias **Clara, Raffa, Javi, Estefanía, Didac y Fransin** habéis sido unos compañeros geniales.

También a todas las personas que han pasado por Angio durante este periodo y por los consejos en los meetings y los ánimos por los pasillos. Gracias **Gabi, Lara, Agnès, Mar, Lydia, Roser, Susana, Nick, Iratxe, Patricia, Mariona, Álvaro,** y los muchos que ahora no me vienen☺. Mil gracias a todos!! En especial gracias **Laura, Elisenda y Alba.**

Gracias a toda la gente del COM, porque da gusto ir a trabajar. Gracias por tratarme con tanto cariño. Gracias **Cristina, Isabel, Àngels, Antonia, Edu, Maribel, Dani, Joan, Edgar, Eva, Esther, Joaquim, Dani, Andrea, Judit, Miguel, Laura, Olga, Roser, Juan, David, Santi, Silvia**. Gracias a otros compañeros de pasillos como **Marta, Giulio, Antonio, Pepelu, Pablo y Javi.** Gracias **Carmen** por ayudarme con el Confocal. Gracias a las chicas de lavado y a la gente del Estabulario. También quería dar las gracias a mis compis del CE, porque sois un ejemplo de trabajo y lucha y sobre todo unas personas formidables. Gracias a muchísima más gente que me dejo que han sido vitales durante estos años!!

Y por supuesto gracias a mi familia, por estar ahí siempre.

También a todos mis amigos en Madrid, en Barcelona y por el mundo que me han ayudado a airear la mente y por supuesto hacer la vida más bonita!! Gracias **Sara, Paloma, Itziar, Berta, Raquel, Irene, Laura, Atenea, Inma, Edi, Ana, Lau, Raquel, Joaquim, Manon, Carla, Miquel, Laia, Aura, Miriam, Blanca, Pau, Edurne**….

Per últim, vull donar les GRÀCIES a la persona que ha estat al meu costat en tot aquest viatge, al Edu.

Abstract

Class I PI3K signalling is required in a cell-autonomous manner in endothelial cells (ECs) for proper blood vessel growth. Although ECs express all class I PI3K isoforms, only the catalytic subunit p110α is required for vascular development. However, little is known about the role of p110α/PI3K signalling in the different steps of vascular morphogenesis. By using a tamoxifen-inducible endothelial Cre line in mouse and genetic and pharmacological approaches in zebrafish embryos, we have found that p110α signalling is required to maintain vessel stability. The lack of p110α activity leads to endothelial tubular structures composed of single cells that show an elongated shape with multiple protrusions and no lumen. These aberrant structures fail to stabilize upon anastomosis and are associated with an increase in the formation of cortical actin cables and hyper-phosphorylation of myosin light chain. We identify that p110α negativity controls actomyosin contractility independently of Rho/ROCK signalling pathway and that this control could be exert through the regulation of MLC phosphatase activity by the impact on mRIP and/or MYPT proteins.

Contents

List of Tables

List of Figures

List of abbreviations

α-SMA Alpha-smooth muscle actin

AA Aaortic arches

AJ Adheren junction

Akt Protein kinase B

Alk-5 TGFβ type I receptor kinase

AMIS Apical membrane initiation site

Ang Angiopogetin

aPKC Atypical protein kinase C

Arap3 ArfGAP With RhoGAP Domain, Ankyrin Repeat And PH Domain 3

Arf6 ADP Ribosylation Factor 6

Axl Axl receptor tyrosine kinase

BAD Bcl-2 associated death promoter

BM Basement membrane

CCV Common cardinal vein

CLOVES Congenital lipomatous overgrowth, vascular malformations & epidermal nevi

CMV Communicating vessels

ColIV Collagen IV

CV Caudal vein

DA Dorsal aorta

DAPI 4',6-diamidino-2-phenylindole

DAPT N-[N-(3,5-Difluorophenacetyl)-L-alanyl]-S-phenylglycine t-butyl ester

DAPP Dual-adapter for phosphotyrosine and 3-phosphoinositides

Dll4 Delta-like 4

DLAV Dorsolateral anastomotic vessels

DMSO Dimethyl sulfoxide

DNA Deoxyribonucleic acid

dpf Days post fertilization

DTT Dithiothreitol

Cdc42 cell division control protein 42 homologue

EC Endothelial cell

ECM Extracellular matrix

EdU 5-ethynyl-2-deoxyuridine

EGFP Enhanced GFP

ELC Myosin essential light chain

eNOS Endothelial nitric oxide synthase

ERG ETS-related gene

ESAM Endothelial Cell-Selective Adhesion Molecule

FAJ Focal adherens junction

Fli-1a Friend leukemia integration 1 a

Flk-1 Fetal liver kinase 1 (In mouse also Kdr or VEGFR-2, In zebrafish Kdrl or VEGFR4)

Flt-1 Fms-like tyrosine kinase 1 (VEGFR-1)

Flt-4 Fms related tyrosin kinase 4 (VEGFR-3)

FBS fetal bovine serum

FGFs Fibroblast growth factors

FoxO Forkhead box O transcription factors

FoxC1 Forkhead box protein C1

FoxC2 Forkhead box protein C2

GAB GRB2-associated-binding protein

GAPs GTPases-activating proteins

GEFs Guanine nucleotide exchange factors

GFP Green fluorescent protein

GPCR G protein-coupled receptor

GSK3 Glycogen synthase kinase 3

HEKs Human embryonic kidney cells 293, HEK-293 cells

Hes Hairy enhancer of split

Hey Hairy and enhancer-of-split related with YRPW motif protein

HIF Hypoxia inducible factor

hpf Hours post fertilization

ICAM-2 Intercellular adhesion molecule 2

IF Immunofluorescence

INL Inner nuclear layer

IP Immunoprecipitation

ISV Intersegmental vessel

iSH2 Inter-SH2 domain

JAM Junctional adhesion molecule

Kdr Kinase insert domain receptor. In zebrafish also Flk-1b or VEGFR-2.

Kdrl Kinase insert domain receptor like. In zebrafish also Flk-1 or VEGFR-4.

KTS Klippel–Trénaunay syndrome

LC-MS/MS Liquid chromatography tandem mass spectrometry

LM Lymphatic malformation

miRs microRNAs

mTORC1 Mammalian target of rapamycin complex 1

mTORC2 Mammalian target of rapamycin complex 2

MVD Microvascular density

MLC-(RLC) Myosin light chain

MLCP Myosin light chain phosphatase

MLCK Myosin light chain kinase

mLECs Mouse lung endothelial cells

MO morpholino

MPRIP Myosin Phosphatase Rho Interacting Protein, also called mRIP

MRCK Myotonic dystrophy kinase-related CDC42-binding kinase

mRIP Myosin Phosphatase Rho Interacting Protein, also called MPRIP

MT1-MMP Membrane type 1-matrix metalloproteinase 1

N-cadherin Neural cadherin

NGCs Neuronal guidance cues

NHE1 Sodium-hydrogen antiporter 1

NICD NOTCH intracellular domain

NLS Nuclear localization signal or sequence

NMII Non-muscle myosin II

Nrarp NOTCH-Regulated Ankyrin Repeat Protein

NRP Neuropilin, also NP

NUAK1 NUAK family SNF1-like kinase 1, also called ARK5

ON Overnight

p110α Protein encoded by the PIK3CA gene

p16INK4A Cyclin-dependent kinase 4 inhibitor A

$p21^{Cip1/Waf1}$ Cyclin-dependent kinase inhibitor

PAGE Polyacrylamide gel electrophoresis

PAK Serine/threonine-protein kinase

PAR3 Partitioning defective 3 homolog

PAR6 Partitioning defective 6 homolog

PBS Phosphate-buffered saline

PBST Phosphate-buffered saline-Tween 20

PBSTX Phosphate-buffered saline-Tween 20- Triton-X 100

PCeC Posterior cerebral vein

PCR Polymerase chain reaction

PCV Posterior cardinal vein

PDGF-B Platelet-derived growth factor-B

PDGFR-B Platelet-derived growth factor receptor-B

PDK-1 Phosphoinositide-dependent kinase 1

Pdxl2 Podocalyxin 2

PFA Paraformaldehyde

PHS Primary head sinus

PI Phosphatidylinositide; see also PtdIns

PlGF Placenta growth factor

PIK3CA Phosphatidylinositol-4,5-Bisphosphate 3-Kinase Catalytic Subunit Alpha; p110α

PI3Ks Phosphoinositide 3-kinases

PIKfyve Phosphatidylinositol-3-Phosphate/Phosphatidylinositol 5-Kinase, Type III

PIP Phosphatidylinositol 3-phosphate; see also PtdIns(3)P

PIP_2 PtdIns 4,5-bisphosphate; see also PtdIns(4,5)P_2

PIP_3 PtdIns 3,4,5-trisphosphate; see also PtdIns(3,4,5)P_3

PLA Palatocerebral artery

PPP1R12A Protein Phosphatase 1 Regulatory Subunit 12A, also known as MYPT1

PRAS40 Proline-rich Akt substrate of 40 kDa

PTEN Phosphatase and tensin homolog

PTU Phenylthiourea

PtdIns Phosphatidylinositide; see also PI

PtdIns(3)P Phosphatidylinositol 3-phosphate; see also PIP

PtdIns(3,4)P_2 PtdIns 3,4-bisphosphate

PtdIns(3,4,5)P_3 PtdIns 3,4,5-trisphosphate; see also PIP_3

PtdIns(4,5)P_2 phosphatidylinositol 4,5-bisphosphate; see also PIP_2

Pyk2 Proline-rich tyrosine kinase 2

qPCR Quantitative polymerase chain reaction

pS6 Phospho-s6 ribosomal protein

RAC1 GTPase: Ras-related C3 botulinum substrate 1

RBD Ras-binding domain

RLC-(MLC) Myosin regulatory light chain

ROBO4 Roundabout Guidance Receptor 4

ROCK Rho-associated protein kinase

RT Room temperature

RTKs Tyrosine kinase receptors

S6K p70 ribosomal protein S6 kinase

SA-βgal Senescence-associated beta-galactosidase

SeA Segmental artery

SEM Standard error of the mean

Sema3 Semaphorin3

SeV Segmental vein

SH2 Src-homology 2

siRNA Small interference RNA

SIV Zebrafish subintestinal vein

Src Proto-oncogene tyrosine-protein kinase

SREBP Sterol regulatory element-binding protein

TAPP Tandem PH-Domain-Containing Protein

TBS Tris-buffered saline

TBST Tris-buffered saline with tween

TEM Transendothelial migration

TiO_2 Titanium dioxide

TJs Tight junctions

TCL Total cell lysate

TNFα Tumor necrosis factor alfa

TSC-2 Tuberous sclerosis protein 2

UNC5B Netrin receptor UNC5B

UCHD Utrophin calponin homology domain

VCAM-1 Vascular cell adhesion molecule 1

VE-cadherin Vascular endothelial cadherin

vSMC Vascular smooth muscle actin

VEGF Vascular endothelial growth factor

VEGFR Vascular endothelial growth factor receptor

VM Venous malformations

ZIPK Zipper interacting protein kinase, also called DAPK3

ZO1 Zonula occuldens-1 protein

1 Introduction

1.1 The circulatory system

The circulatory system is made up of two primary components: the cardiovascular system and the lymphatic system. The cardiovascular system is the first functional organ to develop during vertebrate embryogenesis. It includes the heart, blood vessels and blood and is not only important to supply body tissues with oxygen and nutrients, distribute water, electrolytes and hormones all over the body and allow the clearance of CO2 and metabolic waste products but also contributes to the infrastructure of the immune system and to the thermoregulation. Vertebrates have a closed cardiovascular system in which highly oxygenated blood is driven from the heart through arteries into smaller arterioles and, finally into capillary beds. Here, oxygen and nutrients move out into the cells of the body's tissues and wastes move into the capillaries to flow throughout the venules and then moves to the veins carrying the deoxygenated blood back to the heart to enter into the pulmonary circulatory system to be replenished with oxygen. Exceptionally, the pulmonary circulation transports oxygen-depleted blood away from the heart through the pulmonary arteries to the lungs, and returns oxygenated blood back to the heart through pulmonary veins to be incorporated into the systemic circulation. In parallel, the lymphatic system is composed by the lymph, lymphatic vessels and organs that contain lymphoid tissue (lymph nodes, tonsils, spleen and thymus) and in contrast to the cardiovascular system, lymphatic fluid is not pumped but passively flow from the tissue to the lymphatic tissues. About 90% of interstitial fluid is absorbed by the venous capillaries but the rest (10%) is collected into the lymph fluid, filtrated and brought back into the blood. The main function of the lymphatic system is to restore the excess of interstitial fluid and proteins to the blood and absorb fats and fat-soluble vitamins from the digestive system and transport these elements to the venous circulation. Lymphatic vessels also serve as conducts to transport immune cells and facilitates the immune response against invading organism (reviewed in Swartz, 2001; Margaris and Black, 2012).

The complex networks of blood and lymphatic vessels are not only important to supply nutrients and control the fluid homoeostasis during physiology but are also required for organ growth during development and repair of wounded tissues.

1.1.1 Blood vessel structure and physiology

In vertebrates there are three major types of blood vessels: arteries and veins (large vessels) and the capillaries (small vessels). Blood vessel are composed by several layers that differ between vessels of different size and function. In general, large vessels have three layers: 1) the tunica intima, composed by ECs lining the lumenal surface, the basement membrane (BM) and an internal elastic layer, 2) the tunica media, comprises multiple sheets of smooth muscle cells (vSMCs) and elastin and 3) the tunica adventitia, consists of loose connective tissue. Arteries present thicker the tunica media layer to support high blood pressure while the veins have valves to ensure the unidirectional blood flow. Besides, capillaries are formed by ECs, perycites and the basement membrane (BM).

1.1.2 Blood vessel development and growth

The mechanisms and the genetic control of vascular development are highly conserved among a number of species that serve as model systems to study this process, including the mouse, chicken, frog and zebrafish. Blood vessels are formed in the embryo by two different mechanisms, vasculogenesis and angiogenesis. During the embryogenesis, the first step of blood vessel formation is the differentiation of endothelial cells. The formation of blood vessels from *de novo* is called vasculogenesis and begins very early after the initiation of gastrulation in the mammalian embryo. A subset of primitive mesodermal cells (angioblasts) is committed to differentiate into endothelial cells and organized in a lumenazed primitive vascular plexus (Risau and Flamme, 1995). In mouse, angioblasts are found in the yolk sac clustered with haematopoietic cells in blood island, whereas in zebrafish, blood islands are found intraembryoncally in the lateral mesoderm. At this very early stage, capillaries already acquire arterial and venous fate. Around E9.5, new blood vessels are formed from pre-existing ones in a process that is called angiogenesis. Vascularization of developing organs rely

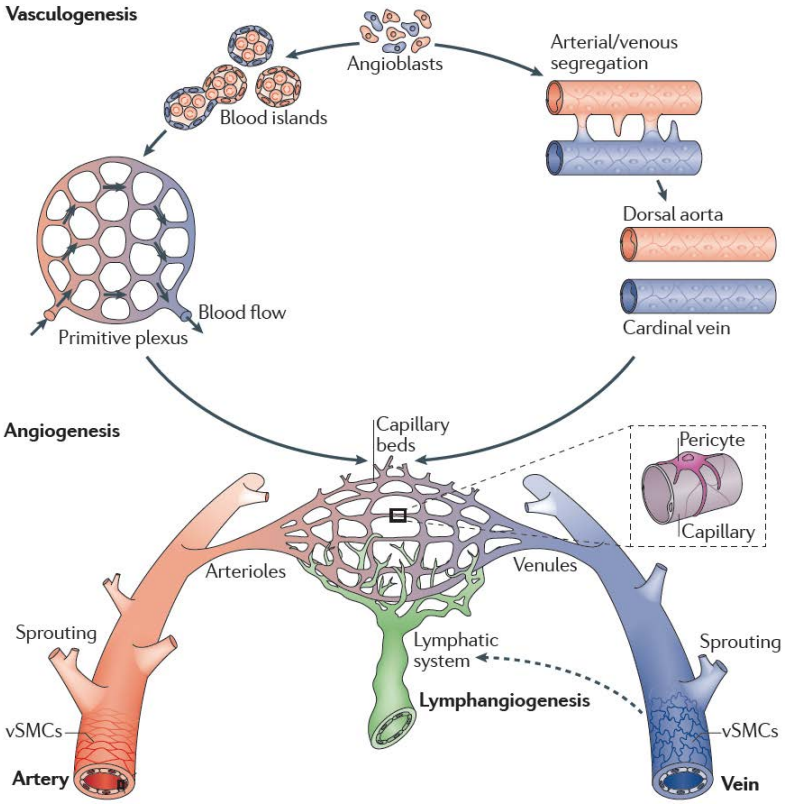

Figure 1.1: **Blood vessel development.** Mesodermal cells in the early embryo differentiate into endothelial precursor cells (angioblasts) that agregates forming blood islands. Fusion of blood islands leads to the vasculogenic formation of a primary capillary plexus. Angioblasts also may acquire arterial (red) or venous (blue) fates and coalesce to generate the first embryonic blood vessels, the dorsal aorta and cardinal vein. Blood circulation is established and primary plexus are remodelled into a hierarchical network of arteries, arterioles, capillary beds, venules and veins. Subsequent recruitment of mural cells (pericytes and vascular smooth-muscle cells (vSMCs)) stabilizes nascent vessels and promotes vessel maturation. In addition, the sprouting of lymphatic endothelial cells from venous vessels (lymphangiogenesis) seeds the lymphatic system. (modified and adapted from Herbert and Stainier, 2011)

to different extent to vasculogenesis and angiogenesis. **Figure 1.1**

1.2 Angiogenesis

Angiogenesis occurs during the embryogenesis but also in adults and is a highly regulated process that takes place through two non-exclusive events, the so-called endothelial sprouting (SA) (Risau, 1997) or non-sprouting (intussusceptive) microvascular growth (Burri et al., 2004; Djonov et al., 2000). Postnatal angiogenesis, unlike embryonic angiogenesis, participates in physiological processes as in female reproductive cycle and also in numerous pathophysiologic processes, such as ischemic, cardiovascular disease, cancer and wound repair.

1.2.1 Intussusceptive angiogenesis

Intussusceptive angiogenesis, is also called splitting angiogenesis or non-sprouting angiogenesis. The intussusceptive angiogenesis is based in the splitting of pre-exiting vessels. This process starts with protrusions from the walls from opposite sides into the vessel lumen. After a contact is established, the endothelial bi-layers are perforated and a transluminal pillar is formed. This pillar is cover of mural cells, fibroblast and ECM giving rise to two parallel vessels (reviewed in Djonov et al., 2000; Burri et al., 2004). This mechanism of intussusceptive pillar formation was shown to contribute also to the formation of vascular trees and to be involved in vascular remodelling. However, this process is often overlooked in angiogenesis research because it was discovered in the late eighties of the 20th century and has remained poorly investigated compared to sprouting angiogenesis. Nevertheless, intussusceptive angiogenesis seems to play a major role in the growth and remodelling of most vascular beds, including the vascular beds of tumours (Hlushchuk et al., 2008; Makanya et al., 2009; Hlushchuk et al., 2011).

1.2.2 Sprouting angiogenesis

Sprouting angiogenesis has been extensively studied during the last decades. This mechanism is principally regulated in a paracrine way by angiogenic

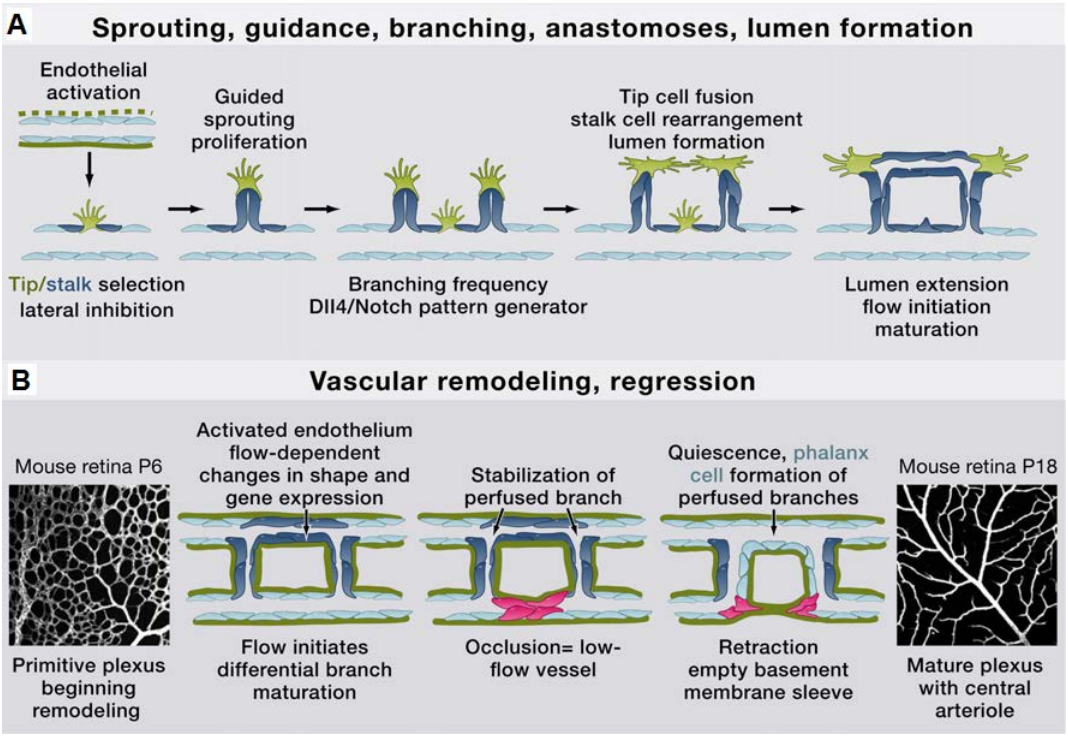

Figure 1.2: **Sprouting angiogenesis: a multi-step process.** Schematic representation of the principal steps of sprouting angiogenesis. (Adapted Potente et al., 2011).

growth factors expressed by poorly perfused tissues. Developmental sprouting angiogenesis is considered as a multi-step event that can be divided into several steps: activation of quiescence vessel, degradation of the capillary basement membrane, tip-cell selection, sprout outgrowth, connection between two neighbouring sprouts (anastomosis), lumen formation and extension. Then, the vasculature is remodelled via pruning. **Figure 1.2**

1.2.2.1 Extracellular cues - initiation and guidance of new vessels

The induction of a new sprout in a quiescence vessel is initiated by several pro-angiogenic factors, as the vascular endothelial growth factor (VEGF-A), expressed by surrounding hypoxic tissues, and is followed by changes in the endothelial polarity and endothelial junctions together with the degradation of the surrounding ECM (Glaser et al., 2008)(**Figure 1.3**). VEGF-A activates VEGFR-2 and promote Dll4 expression in exposed cells. Lateral inhibition between activated cells mediated by Dll4/Notch signalling enhances relative differences of Dll4, Notch and VEGFRs levels between neighbouring cells, which triggers the

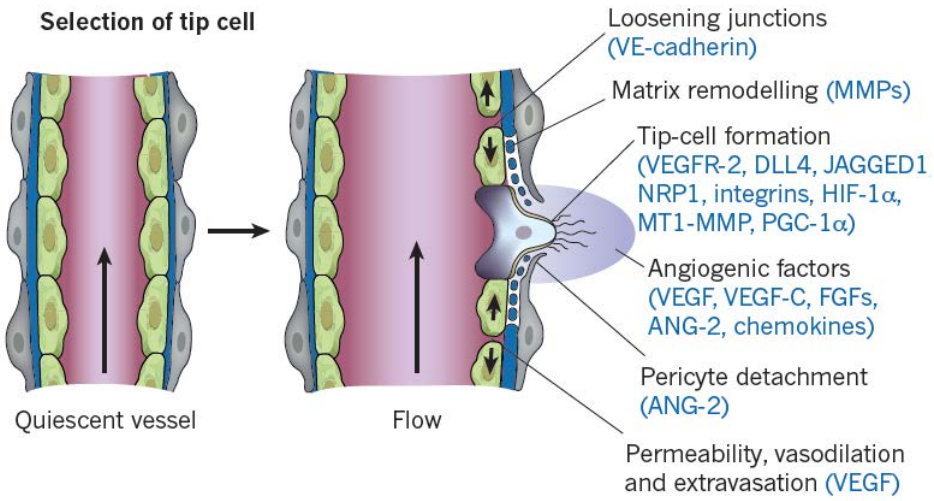

Figure 1.3: **Initiation of a new vessel sprout.** After stimulation with pro-angiogenic cues, basement membrane (BM) is degraded, pericytes detach and EC junctions are loosened. Only the BM of endothelial cells is represented but perycites also are embedded in this BM. (Modified and adapted from Carmeliet and Jain, 2011)

formation of a single tip cell from a group of cells (Gerhardt et al., 2003; Leslie et al., 2007; Suchting et al., 2007). Expression of VEGFR-1 in cells flanking the sprout reduced VEGF signalling in these cells. At the same time released soluble VEGFR-1 (sFlt1) binds extracellular VEGF-A reducing its availability at the base of the sprout (Jakobsson et al., 2010; Krueger et al., 2011) (reviewed in Siekmann et al., 2013). This process is strictly controlled to prevent vascular breakage and haemorrhage in the pre-existing vessel.

Within a new vessel sprout, two different EC populations can be distinguished, so-called tip cell and stalk cell. Tip and stalk cell specification is coordinated by the interplay between VEGF and Notch signalling (link to the explanation). These endothelial cells present different morphology and functional properties. Tip cells are the ones that upon VEGF stimulation leading the formation of the new sprout. The leading tip cells extend filopodia and actively migrate toward the increased gradient of pro-angiogenic cues and present a specific gene expression pattern, with high expression of Dll4, PDGFb, UNC5B, neuropilin-1 (NP1), MT1-MMP, VEGFR-2 and VEGFR-3 and low levels of Notch dependent genes (del Toro et al., 2010; Strasser et al., 2010). They rarely proliferate and secrete proteases to break down the ECM (Glaser et al., 2008). However, it has been observed that tip cells

can proliferate in the ISV sprouts in zebrafish. In contrast, stalk cells present fewer filopodia and enable the growth of the sprout, form the vascular lumen and establish interendothelial junctions to maintain the integrity of the new sprout. Stalk cells proliferate in response to pro-angiogenic cues (Gerhardt et al., 2003; Kearney, 2004), but recently Serra et al. demonstrate that stalk cells present two biological states. A first state, in which stalk cells are arrested to allow the proper patterning of the sprout and a second state, in which they proliferate to expand the plexus. These two states are regulated by PTEN-Notch signalling (Serra et al., 2015). Gene expression profile in stalk cell is characterized by VEGFR1 (Krueger et al., 2011), Notch-regulated ankyrin repeat protein (Nrarp) (Phng et al., 2009), Notch ligands Jagged1 and DLL1 (Roca and Adams, 2007), Robo4 (Jones et al., 2008), and VCAM1 (Harrington et al., 2008) enriched expression.

1.2.2.1.1 Tip and stalk cell selection and specification - Crosstalk between Notch and VEGFR signalling pathways

Notch signalling and VEGFR signalling have a key role in the process of tip cell selection in zebrafish and mouse. VEGF-A binds to VEGFR-2 inducing the expression of the Notch ligand Dll4 in ECs. Endothelial cells expressing highest Dll4 levels induce Notch activation in the neighbouring ECs, promoting the down-regulation of Dll4 expression and the up-regulation of the canonical Notch target genes, Hes, Hey and Nrarp. In this way, the differences in Dll4 expression between adjacent cells increased and leading to what is known as lateral inhibition (**Figure 1.4**). The endothelial cells that receive Dll4 stimulation inhibit their tip cell behaviour and differentiate in stalk cell. Furthermore, activation of Notch signalling in stalk cells inhibits VEGFR-2 expression, making them less sensitive to further VEGF stimulation. It also induces VEGFR-1 expression that inhibits tip cell differentiation even more, due to its high affinity to VEGF but low kinase activity. Depletion of Dll4 or Notch signalling in mouse and zebrafish results in increased tip cell numbers and causes an hyper-sprouting phenotype (Hellström et al., 2007; Suchting et al., 2007; Lobov et al., 2007; Siekmann and Lawson, 2007). The VEGFR/Dll4/Notch dependent tip cell selection is a very dynamic process. Accordingly, in the absence of Notch signalling-mediated lateral

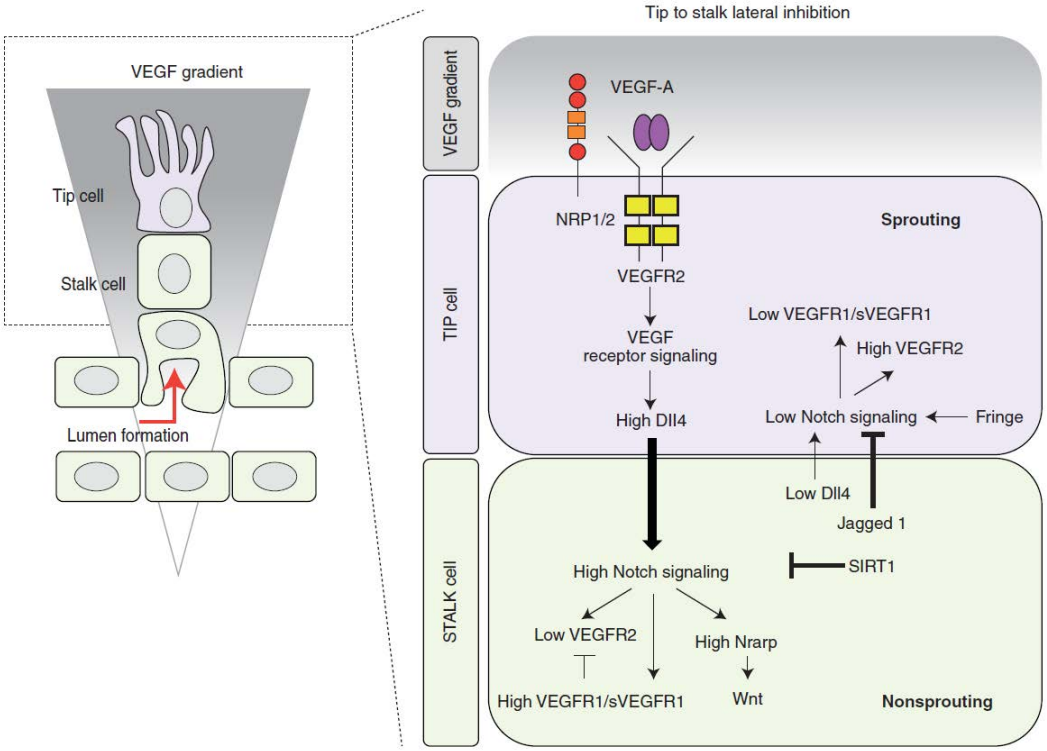

Figure 1.4: **Tip/stalk cell specification during sprouting angiogenesis.** Schematic representation of the crosstalk between Notch and VEGFR signalling pathways to control tip/stalk specification. (Adapted from Blanco and Gerhardt, 2012)

inhibition, all the endothelial cells stimulated by VEGF would become tip cells, however the differential expression of Dll4 and the consequent differential Notch activation and VEGF signalling trigger the formation of one single tip cell from a group of cells (Siekmann et al., 2013). However, this is not a static process, and the tip cell is in continuous exchange during vascular sprouting due to the mechanism of competition that ensure the optimal migration towards the VEGF-A gradient (Jakobsson et al., 2010).

1.2.2.1.2 Vessel patterning is regulated by repulsive cues

Molecular cues from neighbouring tissues shape developing blood vessels. In mouse and zebrafish, Sema3E/Plexin1 signalling has a major role regulating vessel patterning. Sema3E (Sema3a in the fish) is expressed in the caudal region of each developing somite, whereas Plexin-D1 is expressed in the intersomitic blood vessels adjacent to the somite boundary on the rostral region of each somite. Repulsive interaction of Semaphorin-Plexin1 signalling guides the sprout

outgrowing in the right direction. Both Sema3E and Plexin-D1 knockout mice showed disorganized intersomic vessel pattern (Gu et al., 2005). In zebrafish, PlexinD1 mutant-out of bounds (obd) (Childs et al., 2002) and morpholino knock-down experiments (Torres-Vazquez et al., 2004) show unorganized sprouting patterns with ISVs randomly distributed over the tail, often crossing the somite borders and connecting to neighbouring sprouts in their middle parts. This mechanism resembles the control of axonal outgrowth by Semaphorin signalling (reviewed in Tamagnone and Comoglio, 2000).

There are others “Neuronal guidance cues” (NGCs) secreted or membrane bound ligands that act as attractive or repulsive cues, depending on cognate EC receptors. They also regulate guidance events during vascular morphogenesis: the Eph receptor tyrosine kinases, which bind Ephrins; Robo receptors, which bind Slits and Unc5 receptors which bind to Netrins. For example, Lu et al. demonstrated that UNC5B is selectively expressed in the vascular system by arteries, a subset of capillaries and endothelial tip cells and its inactivation results in enhanced sprouting and uncontrolled filopodial extension in tip cells (Lu et al., 2004). Morphants lacking both UNC5B and Netrin1a also show an excessive branched vasculature. Supporting evidence comes from the chick model where Netrin-1 acts as a extracellular cue in the ECM that repels UNC5B expressing blood vessels (Bouvrée et al., 2008). This suggests that UNC5B is an evolutionary conserved repulsive receptor that is also used during blood vessel morphogenesis.

1.2.2.2 Sprout elongation and cell rearrangements

During the sprout outgrowth, there is a dynamic phenotypical specification shuffling between tip and stalk. This constant competition to leading the sprout is a team play that ensure the proper guidance and elongation of the sprout (Jakobsson et al., 2010). Guided sprout outgrowth is followed by its elongation. EC migration and proliferation sustain the growth of a new sprout (**Figure 1.2**). Only the tip cell is enough to exert a pulling force and allows the progression of the sprout but, at the end, the proliferation of stalk cells is needed to progress in the outgrowth of the vessel branch (Ausprunk and Folkman, 1977). Cell

rearrangements are based on a combination of dynamic cell adhesion and the modulation of the cytoskeleton at cell contacts. This attribute is essential for many morphogenetic processes. Recently, Sauter at al. have showed that EC elongation and cell rearrangements are also regulating the outgrowth of the sprouts. Endothelial cell-cell-adhesion-based motility is required for the advancement of vascular sprouts (Perryn et al., 2008; Sauteur et al., 2014). Cell rearrangements and cell shuffling during the sprout outgrowth depends on differential adhesion between endothelial cells, which is mediated by VE-cadherin at cell junctions (Bentley et al., 2014). There is also a tight interaction between actin cytoskeleton and EC junctions in the regulation of the EC elongation and cell rearrangements. F-actin fibres are important to exert deforming forces, which would elongate the junctional ring and allow EC elongation (Sauteur et al., 2014).

1.2.2.3 EC polarity and lumen formation

Lumen formation occurs during invasion and growth of the new vascular sprout. ECs are interconnected by interendothelial junctions but have not established yet the apicobasal polarity. First, Par3 is involved in the acquisition of EC apicobasal polarity and junctional proteins are redistributed in the lateral from the apical EC surface to the vascular cord periphery. The acquisition of apicobasal polarity seems to function partially by the accumulation of different proteins at the sites of lumen formation. More information about the molecular signalling implicated in the establishment of the apicobasal polarity and lumen morphogenesis is reviewed in Herbert and Stainier, 2011.

Lubarsky and Krasnow described five potential mechanisms by which epithelial cells could form lumens and tubular structures during morphogenetic processes: wrapping, budding, cavitation, cord hollowing and cell hollowing (Lubarsky and Krasnow, 2003). Lumen formation in angiogenic sprouts is thought to occur mainly by cell hollowing (formation of intracellular lumenal spaces initiated by vesicle formation and assembly in large vacuoles that later fuse together), and cord hollowing (a set of compact cells undergoes shape changes to create a central lumen) (Xu and Cleaver, 2011). Recently, Yu et al. detected the coexistence of seamless transcellular lumens and single or multicellular enclosed

lumens with autocellular or intercellular junctions, suggesting that heterogeneous mechanisms contribute to vascular lumen formation *in vivo*. In contrast, Gebala et al. have observed that blood pressure drives unicellular and multicellular lumen expansion in angiogenic sprouts through the induction of spherical deformations of the apical membrane of endothelial cells (inverse blebbings) by local and transient recruitment and contraction of actomyosin (Gebala et al., 2016). Analysing lumen formation in the developing ISVs, it is clear that different and heterogeneous mechanisms are responsible of lumen formation in angiogenic sprouts. The lumen formation in early sprouts is accomplished when blood flow is unstable or low whereas in sprouts developing at later times lumen formation is achieved in the presence of blood pressure (Lenard et al., 2013). In angiogenic sprouts from retinal vasculature also the lumen is formed concomitantly with the outgrowth sprout under blood pressure (Gerhardt et al., 2003; Gebala et al., 2016). Furthermore, during vasculogenesis or during the formation of other vessels as the cardinal vein other mechanisms lead to the formation of the tube (Strilic et al., 2009; Jin, 2005; Helker et al., 2013). Hence, lumen formation can occur via different mechanisms, depending on the vascular plexus that is being formed and/or the type of vessel that is being lumenized.

1.2.2.4 Cell-cell adhesion during sprouting angiogenesis

In the vascular system junctional proteins connect cells to each other allowing formation of well-sealed tubes. Not only EC junctions are essential to ensure vessel integrity, preventing areas of vascular damage and extravasation, and certain grade of permeability, to ensure oxygen and nutrients transport, but also, they have a key role during the sprout outgrowth. In the endothelium, junctional complexes mainly comprise adherent junctions and tight junctions (Bazzoni, 2004) (**Figure 1.5**). Endothelial cells are very thin and present the junctional complexes occupying most of the lateral cell membrane and defining the borders and shapes of the ECs. Junctional proteins contain transmembrane and intracellular proteins that connect endothelial cells to each-other, to other surrounding cells and to the ECM. They also interact with intracellular components, such as the cytoskeleton, to induce changes in cell shape and behaviour and take part in regulating gene

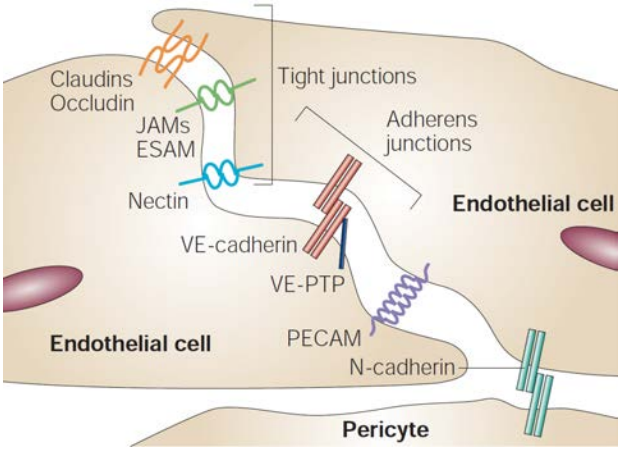

Figure 1.5: **The organization of endothelial cell-cell junctions.** Tight junction are located apically whereas adherens junctions are located more basolaterally. Outside these junctional structures, platelet endothelial cell adhesion molecule (PECAM) contributes to endothelial cell-cell adhesion. In EC, neuronal cadherin (N-cadherin) induces the adhesion of endothelial cells to pericytes and smooth muscle cells. (Modified and adapted from Dejana, 2004)

expression in response to extracellular signals provided by cell-cell contacts.

1.2.2.4.1 Adherens junctions

Adherens junctions (AJs) are multiprotein complexes of cadherins and catenins. Cadherins mediate homophilic transmembrane adhesion via multimeric complexes at cell borders, while catenins link cadherins to the actin cytoskeleton (**Figure 1.5**). Vascular endothelial cadherin (VE-Cadherin) is the principal endothelial-specific AJ molecule present across vessels in all vascular beds. VE–cadherin-deficient mice embryos die at mid-gestation resulting from severe vascular defects (Gory-Faure et al., 1999). Truncation of the domain that is responsible for binding to β-catenin and plakoglobin resemble the phenotype caused by complete absence of VE-cadherin, highlighting the implication of VE-cadherin in intracellular signalling (Carmeliet et al., 1999). In zebrafish, it has been reported that VE-cadherin plays a role in stabilizing new vascular vessels. Knocking-down VE-cadherin in zebrafish embryos results in a failure in the formation of new connections between ECs (Montero-Balaguer et al., 2009; Wang et al., 2010). Furthermore, in zebrafish embryos expressing a truncated form of VE-cadherin, ECs fail to anastomose and stabilize new contacts. Angiogenic sprouts in the absence of VE-cadherin establish a first contact but do not stabilize

it and ECs retract keeping searching for other connections (Lenard et al., 2013). Interestingly, Abraham et al. showed that VE-cadherin knock-down in zebrafish stimulates sprouting in ISVs due to a failure in blocking VEGF activity. VE-cadherin signalling to induce actomyosin contractility is necessary for the uniform distribution of VE-cadherin at cell junctions in the established quiescent state (Abraham et al., 2009). However, Lenard et al. study's suggests that the primary defect in VE-cadherin mutant is the failure in cell-cell recognition and not a VEGFR-2-dependet phenotype because inhibition of VEGFR-2 in VE-cadherin mutant does not result in normalization of the tip cell phenotype (Lenard et al., 2013).

Others *in vivo* and *in vitro* studies have shown that VE-cadherin is required for vascular integrity in quiescent vessels and to establish endothelial polarity and vascular lumen formation (reviewed in Dorland and Huveneers, 2016). VE-cadherin regulates several functions in ECs through different mechanism: transfers many different intracellular signalling communicating ECs in contact, inhibits cell growth by contact inhibition, signals indirectly through its binding partners that translocate to the nucleus to regulate transcription, by its anchorage to the cytoskeleton establish a tight regulation of EC shape, movement and permeability, and regulates endothelial barrier function (also reviewed in Giannotta et al., 2013).

VE-cadherin-based cell–cell junctions exist in different conformations depend on the coupling of the VE-cadherin intracellular domain via a cytoplasmic protein complex to the actin cytoskeleton both *in vitro* (Huveneers and de Rooij, 2013) and *in vivo* (van Geemen et al., 2014). Mature stabilized junctions present VE-cadherin localized linearly between endothelial cells and bound to parallel cortical actin bundles, whereas in response to permeability-inducing factors (thrombin, TNFa, VEGF among others), VE-cadherin-based junctions suffer conformational and morphological modifications that rely on changes in actomyosin contractility that impact in the pulling tension generating on the junctions. These remodelling junctions, also called focal adherens junctions (FAJs), present discontinuous morphology and VE-cadherin is connected to radial actin bundles (Huveneers et al., 2012; Millan et al., 2010). Although, Bentley et

al. showed a differential junctional organization along the vasculature essential to ensure proper endothelial cell rearrangements during sprouting angiogenesis, the impact that force-dependent changes on the junctions have *in vivo* is not well known yet (Bentley et al., 2014).

1.2.2.4.2 Tight junctions

Tight junctions (TJs) also mediate adhesion and communication between adjacent cells, but specifically they are responsible for regulating paracellular permeability and cell polarity. TJs form a continuous, impermeable seal between the adjacent cells (**Figure 1.5**). TJs control paracellular permeability displaying a barrier function that restricts the diffusion of solutes across intercellular spaces. Besides, they control cell polarity by restricting the movement of membrane molecules between the apical and basolateral domains of the plasma membrane (Bazzoni, 2004). TJs are protein complexes containing claudins, occludins, junctional adhesion molecules (JAMs) and endothelial cell-selective adhesion molecule (ESAM) (Bazzoni, 2004; Wallez and Huber, 2008). Zona occludens 1 and 2 (ZO-1 and 2) are intracellular components associated with TJs, also localizing to the cell-cell contacts. TJs participate in the formation of blood brain barrier, but their role in early vascular development is not known (Wallez and Huber, 2008).

1.2.2.5 Anastomosis

Vascular anastomosis is the process that generates connections between angiogenic sprouts and blood vessels. This process consist in the establishment of a new stable contact between two ECs. The new contact can be established between two angiogenic sprouts (“head-to-head” anastomosis) or between an angiogenic sprout with a functional blood vessel (“head-to-side” anastomosis). Two different cellular mechanisms have been described taking in account whether the sprouts that undergo anastomosis are lumenized and in presence of blood pressure (type I) or are non-lumenized (type II) (Lenard et al., 2013). In both cases, two tip cells set and break contacts through their filopodia until one single connection is stabilized and cells deposit de *novo* apical membrane (apical

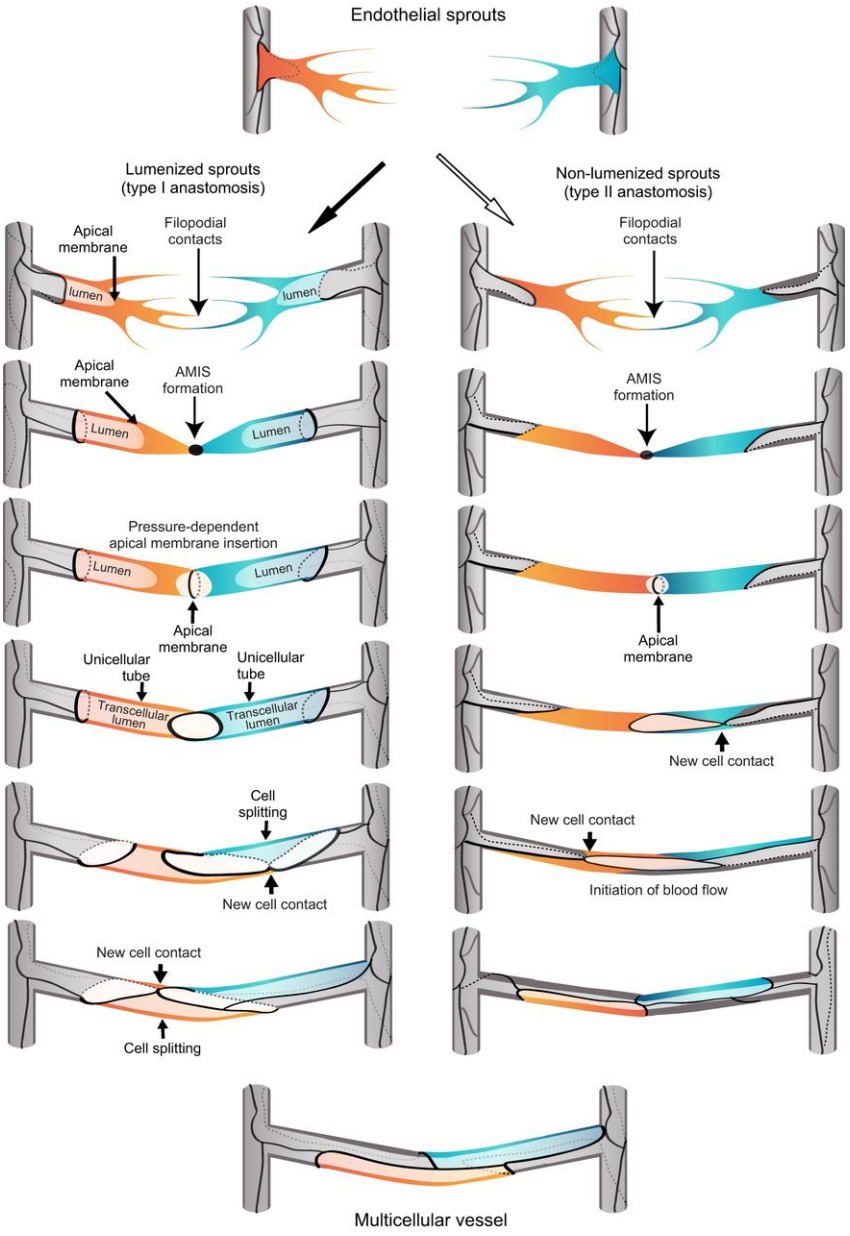

Figure 1.6: **Cell behaviours during anastomosis.** Scheme of the different stages of blood vessel fusion in the case of lumenized sprouts (type I anastomosis; left) and non-lumenized sprouts (type II anastomosis; right). Both processes are initiated by the contacts of two tip cells via filopodial extensions, until they form one stable connection. An apical membrane initiation site (AMIS) is formed at this novel contact site and apical membrane is inserted. In type I anastomosis, apical membrane invagination through blood pressure and subsequent apical membrane fusion generates a unicellular tube containing cells with a transcellular lumen. The subsequent transition from a unicellular to a multicellular tube in type I anastomosis involves cell rearrangements and cell splitting. In type II anastomosis, the apical membranes do not invaginate and only expand slowly due to the absence of pressure. Following, ECs suffer rearrangements and lead to lumen coalescence and the formation of a multicellular tube. Adapted from (Betz et al., 2016).

membrane initiation sites, AMISs). From this point the following steps for each type are summarized in **Figure 1.6**. In the case that an angiogenic sprout anastomoses with a perfused vessel the mechanism is very similar to anastomosis type I (Lenard et al., 2013).

1.2.2.6 Vascular maturation and stabilization

The stabilization of a newly formed vessel and maintenance of the vasculature are late events in the angiogenic process. The process of vascular stabilization includes three major steps: the formation of tight junctions between ECs constituting the vessels, the recruitment of mural cells that act as supporting cells for blood vessels and the formation of an extracellular matrix (ECM) that provides contacts between surrounding tissues and prevents vessels from collapsing. Pericytes and vSMCs stabilize the vessel wall, controlling endothelial cell proliferation and migration and stimulating the production of ECM and thereby the growth of new capillaries. Perycites are vascular mural cells found around blood capillaries, pre-capillary arterioles, pre-capillary venules and collecting venules that are embedded within the vascular basement. Perycites not only serve as supporting scaffold for vessels but also synthesize and promote assembly of basement membrane components (Davis and Senger, 2005; Bergers and Song, 2005; Stratman et al., 2009). Perycites and ECs interact and communicate directly by physical contact and indirectly by paracrine signalling pathways. On the other hand, vSMCs differ from perycites by their localization, their morphology and also their pattern of expression (Rensen et al., 2007). vSMVs cover bigger vessels forming an independent layer over the endothelium called the media that is separated from the vascular BM by a layer of mesenchymal cells and the intima.

During angiogenic remodelling ECs release platelet-derived growth factor B (PDGFB) that its bound to the extracellular matrix where acts as a chemoattractant for pericytes that express the PDGF receptor-β (PDGFR-β). Thereby, perycites are recruited into the wall of immature vessels and establish a direct contact with the ECs. Also, mural cells express Ang-1, that binds to and activates the Tie2 receptor, and therefore promotes EC survival, maintaining EC quiescence and mediating mural cell attachment. Secretion of S1P by platelets, haematopoietic

cells and ECs may promote S1PR1-mediated trafficking of neural cadherin (N-cadherin) to areas of EC-pericyte contact and the assembly of adherens junctions promoting vascular stability. Besides, TGF-β produced in endothelial cells induces vSMC differentiation in adjacent perivascular cells via Alk5-Smad2/3 to generate vSMC-ensheathed quiescent mature vessels (Gaengel et al., 2009; Herbert and Stainier, 2011).

The regulation of extracellular matrix (ECM) degradation and remodelling plays an essential role not only during the formation and expansion of nascent angiogenic sprouts but also for the stabilization and maturation of new vessels. The vascular ECM is composed of laminins, type IV collagen, perlecan, nidogen/entactin, fibulins, type XVIII collagean and fibronectins among others (Senger and Davis, 2011). The vascular ECM serve as an extension of the plasma membrane, protecting vessels from disruptive physical stresses, and provide an interactive interface between ECs and surrounding environment that can mediate local and distant signals within and between these compartments. Vascular and mural cells are connected to major structural ECM components by cell surface receptors including integrin and non-integrin molecules (Kalluri, 2003; Davis and Senger, 2005). By diverse mechanisms as diverse as cell anchorage, integrin-mediated activation and signalling to binding, release and activation of soluble growth factors and alteration in the supramolecular matrix architecture, vascular ECM controls vascular cell shape, behaviour, and the response to cytokines and growth factors (Boudreau and Jones, 1999). Although under lacking of collagen IV, perlecan or laminin α4, the vascular ECM can be formed, it becomes unstable and breaks-down over time leading to more dilated vessels highlighting the importance of the ECM also during mechanical stress (Costell et al., 1999; Poschl et al., 2004; Thyboll et al., 2002). Matrix metalloproteinases (MMPs) and vascular integrins have emerged as key mediators of angiogenic and anti-angiogenic action mediated by the vascular ECM.

1.2.2.7 Remodelling and pruning

After the establishment of primary vascular networks, they often suffer remodelling in order to optimize flow or adapt to changing demands in flow (**Figure 1.2**). Vessel

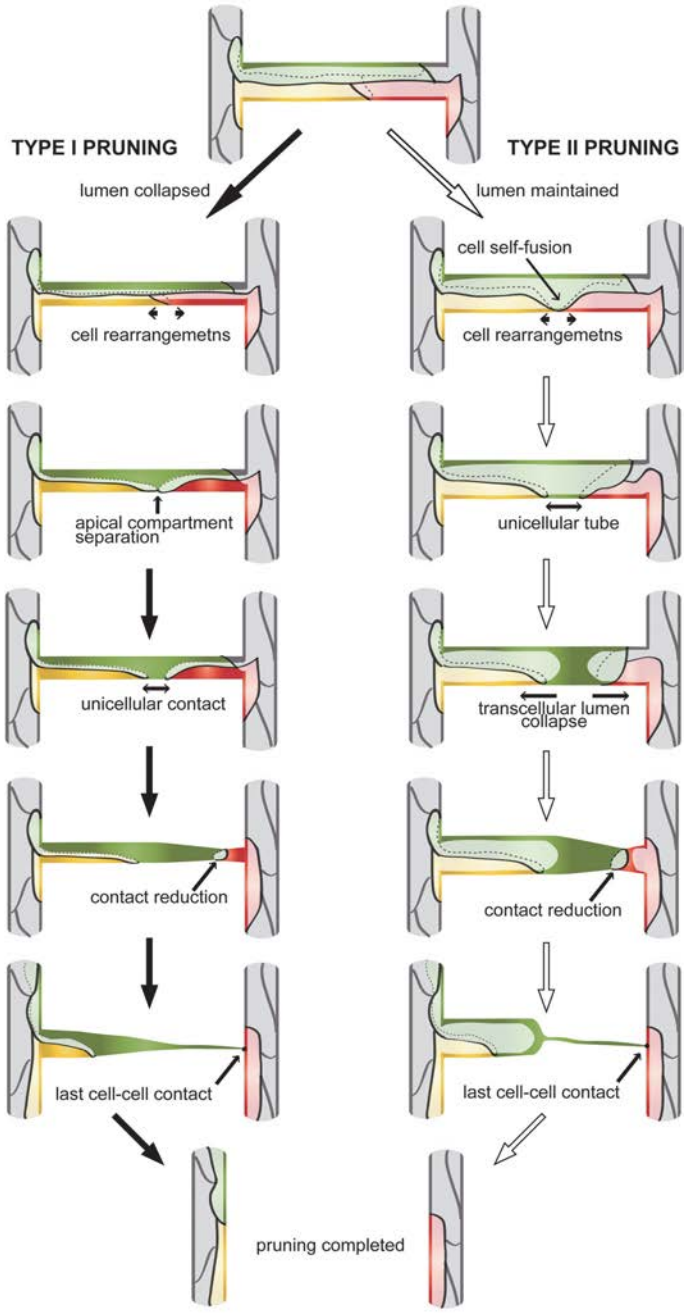

Figure 1.7: **Cell behaviour during vascular pruning.** Multicellular tubes suffer different cellular rearrangements during pruning depend on the presence or absence of lumen. Type I pruning: lumen collapses before cell rearrangements ad then, EC rearrange and form an unicellular tube that regress to completely resolve the last connection. Type II pruning: the lumen is maintained while ECs suffer rearrangements that lead to a lumenized unicellular tube. Transcellular lumen collapses in the unicellular tube, and form two separate luminal compartments. The last cell reduces its contact to one of the major branches and culminating in detachment. (Adapted from Lenard et al., 2015)

pruning can be trigger under low VEGF and under low blood flow. After a decrease in the withdrawal of survival factors as VEGF, vessels can suffer regression by EC apoptosis or by intussusception regression resulting in decreased vessel number and decreased flow to tissues subtended by the regressing vasculature (Ricard and Simons, 2015). However, recently it has been described that small vessels can be pruned by reabsorption of ECs into the remaining vasculature independently of EC apoptosis. In this case, the local blood flow changes promote vascular regression driven by EC migration (Kochhan et al., 2013). Franco and collaborators described a mechanism by which local decrease of flow induces a change in the orientation of the ECs that promotes their migration against the direction of the flow to be reabsorbed in vessels with high flow. This study proposed a four step model inverse to the anastomosis process: branch selection, lumen collapse, EC retraction and detachment (Franco et al., 2015b). In parallel, Lenard et al. described in detail the cellular mechanism of blood vessels pruning in zebrafish subintestinal vein (SIV) using high resolution time-lapse microscopy. Similar as the process of anastomosis, pruning occurs via two cellular mechanism depending on the state of vessel perfusion during the process (Lenard et al., 2015). In type I pruning, the first step is lumen collapse followed by EC migration towards the neighbouring vessels together with EC rearrangements (**Figure 1.7**). This type of pruning resembles the mechanism of prunning described by Franco et al. in zebrafish ISVs and retinal vasculature in mice, in which the lumen disruption is the first step. On the other hand, in type II, the vessel undergoes EC rearrangements until turn into a unicellular tube. Then, the lumen collapse and the cell body moved towards one of the major neighbouring vessels (**Figure 1.7**). Therefore, the presence or absence of flow determine the mode of pruning and particularly the sequence of lumen collapse and EC rearrangements (Lenard et al., 2015). Under low flow, pruning is driven by EC migration and EC rearrangements that results in decreased total vessel area and increased average blood flow. In this case, pruning happens without the loss of luminal integrity and without reduction in the total endothelial mass (Ricard and Simons, 2015).

Numerous signalling pathways have been implicated in the control of the vessel pruning. They are summarised in the **Figure 1.8** and reviewed in (Korn

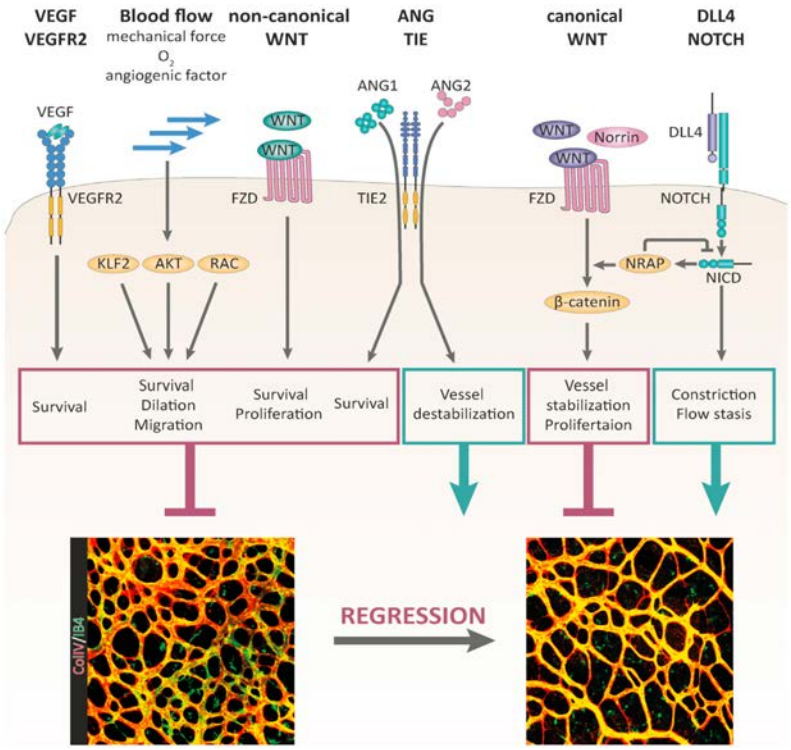

Figure 1.8: **Control of vessel pruning and regression.** Summary of the signalling pathways involve in the regulation of vascular pruning. Among others VEGF/VEGFR2 signalling, non-canonical WNT signalling, and blood flow-induced signalling serve as critical maintenance factors of the vasculature that are involved in the control of vessel regression. On the other hand, Dll4/ Notch signalling could promote constriction and flow stasis. Ang/Tie signalling acts in a context dependent manner: through Ang1 stimulation promotes EC survival whereas Ang2 destabilizes the vascular network, favouring vessel regression in the absence of survival factor activity (Adapted from Korn and Augustin, 2015).

and Augustin, 2015). However, the role and fate that the mural cells acquired during this process is still unclear.

1.2.2.8 Vascular quiescence

Finally, once vessels have supplied oxygen and nutrients to the demanding tissues, external VEGF expression will be reduced and the endothelial oxygen sensors will be inactivated, leading to a shift in the endothelial behaviour towards a quiescent phenotype (Potente et al., 2011). Nonetheless, even at this point ECs decelerate their proliferation and blood vessels are mature and prevented from sprouting, they still need to undergo survival properties to guarantee their integrity. Blood flow itself is already an important factor for keeping ECs quiescent but also other molecules determine this endothelial phenotype. It has been described that the endothelial release of VEGF can act as a survival factor due to the activation of pro-survival pathways such as the phosphatidylinositol-3-kinase (PI3K) signalling cascade (Warren and Iruela-Arispe, 2010). Thus, VEGF expression in blood vessels prevents ECs from being apoptotic and from disrupting vessel integrity. Ang1/Tie2 promote cell survival, which is essential for the maintenance of vascular quiescence by suppressing mediators of the apoptotic pathway (Augustin et al., 2009). Fibroblast growth factors (FGFs) helps maintaining vessel quiescence and survival by stabilizing EC-EC junctions (Beenken and Mohammadi, 2009). Furthermore, the blood flow of established blood vessels act itself as an anti-apoptotic factor for the ECs.

1.3 Animal models of angiogenesis

Despite their anatomical differences, vertebrates share similar developmental programs that give rise to the cardiovascular system. The postnatal mouse retina and the embryonic zebrafish have been intensively used to study angiogenesis.

1.3.1 Postnatal angiogenesis in early mouse retina

Mouse retina is a powerful *in vivo* model because it allows a deeply study of the vascular development. It is possible to visualize at high resolution EC

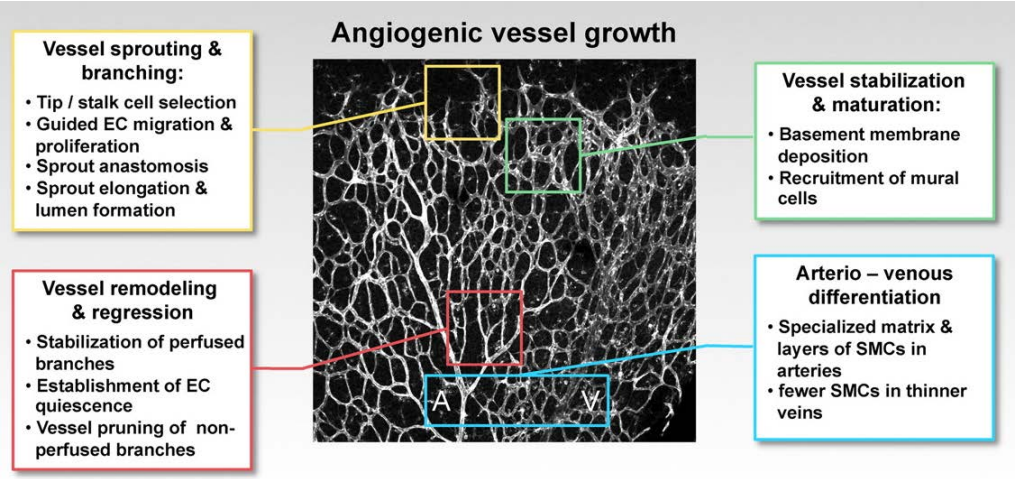

Figure 1.9: **Mouse retina as model to study angiogenesis.** Visualization of the different steps of the angiogenic vessel morphogenesis that can be studied in the mouse retina at the same time. Mouse retinas at postnatal day 5 stained for an endothelial marker. A indicates artery; V, vein. (Modified and adapted from Oellerich and Potente, 2012)

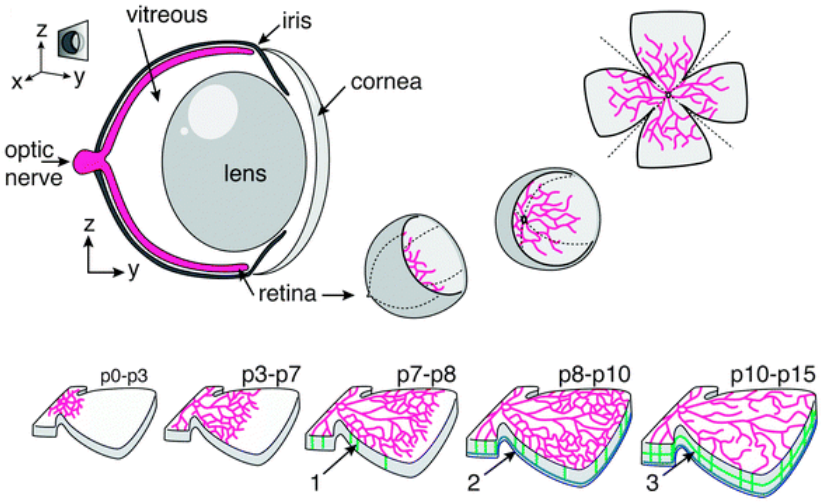

Figure 1.10: **Scheme of postnatal mouse retinas extraction and vasculature growing.** On the top: conceptual sketch of the retina and its vasculature. On the bottom: schematic sketch of the developmental stages during retinal angiogenesis. Sprouting is initiated from the optic nerve and proceeds to cover the entire retina around P8, followed by subsequent remodelling and maturation of the superficial plexus. (modified and adapted from Milde et al., 2013)

proliferation, sprouting, perivascular cell recruitment, vessel remodelling and maturation **(Figure 1.9)**.

Initially, during the embryonic development the hyaloid vasculature supplies the inner part of the eye with oxygen and nutrient but after birth the hyaloid vasculature regresses and is replaced by the retinal vasculature in mice. The retinal vasculature is formed by sprouting angiogenesis following a pre-existing astrocyte plexus. Astrocytes under hypoxia strongly express vascular endothelial growth factor (VEGF-A) that induce EC migration toward the hypoxic region whereas astrocytes express less VEGF-A in already vascularized areas. This gradient of VEGF-A allows the vascularization of the retina radially, from the nerve optic to the periphery of the retina. This primary vasculature reaches the periphery of the retinas around the first week after the birth (postnatal day 8, P8) and contains both arteries and veins that enter and exit through the optic nerve. Until this moment, the retinal vasculature has growth in a two-dimensions plane making possible to observe easily the different stage of the vascular development. At P7 vessels in the periphery are less mature and we can visualize the sprouting of new vessels whereas in the central area vessels are suffering remodelling and maturation (Gariano and Gardner, 2005; Milde et al., 2013).

From postnatal day 7, new angiogenic sprouts emerge from the primary vascular plexus into deeper retinal layers within 2 weeks forming a three inter-connected and parallel vessel networks in the nerve fibre layer and the inner-plexiform and outer-plexiform layers. The retinal vasculature becomes fully mature in mice at 6 weeks of age. This process starts in the centre of the retina and expands towards the periphery and is governed by transient expression of VEGF in somatas located in the inner nuclear layer (INL). However, the cellular and molecular mechanism that induce and guide this process is not well described yet. It is known that is independent of retinal astrocytes (Milde et al., 2013). All the steps of the vascular growing in the retina are shown schematically in the **Figure 1.10**.

The major limitation of this model is that vessels are visualized by snapshots of retinal vascular development and it is therefore difficult to appreciate the dynamics of certain processes, which would be only uncovered by live imaging methods

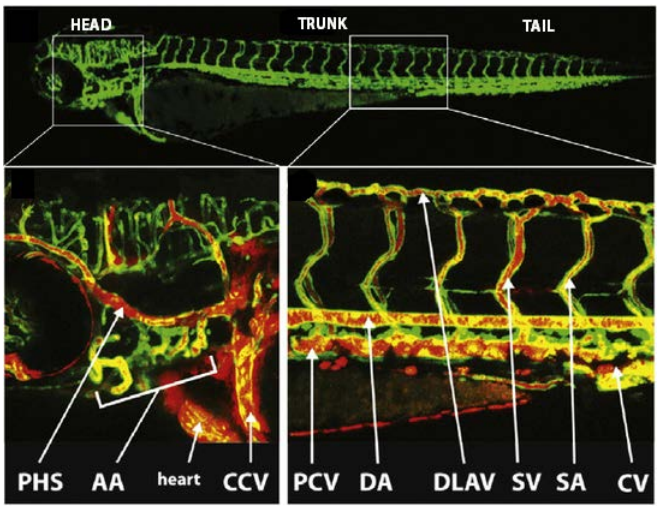

Figure 1.11: **The vascular system in fish embryos.** Visualization of the vasculature in a 3-day-old zebrafish embryo with the transgenic reporter (TG:flk1:EGFP in green) and by microangiography using quantum dots (red). Indicated vessels: Aaortic arches (AA), caudal vein (CV), common cardinal vein (CCV), dorsal aorta (DA), posterior cardinal vein (PCV), primary head sinus (PHS), segmental artery (SA or SeA) and segmental vein (SV or SeV). (Modified and adapted from Ellertsdóttir et al., 2010)

that are not yet available for this model. However, this model allows the study of different steps of the angiogenic process because there is a spatial separation. Process such as sprouting of new vessels and anastomosis are taking place in the growing front and arterial-venous differentiation and vessel regression in the more proximal vasculature allowing the study of different events in the same retina. In addition, the inducible control of gene deletion specifically in vessels using the iCre-LoxP strategy and the easy delivery of drugs in the pups place the retina as the prototypical vascular network for evaluation of transgenic mice and for pharmacological testing and intervention (Pitulescu et al., 2010).

1.3.2 Zebrafish embryos

The use of the zebrafish as vertebrate model to study vascular development has been spread over the last decade. Zebrafish is a vertebrate model with a closed circulatory system that conserve to high degree the development and physiology of blood vessels and the molecular mechanism underlying vessel formation to those in humans and other high vertebrates (Isogai et al., 2001; Gore et al., 2012) **(Figure 1.11)**. Furthermore, this model provides several advantage as its rapid development and short generation time, high number of

offspring, genetic amenability and relative low maintenance costs. Zebrafish embryos develop externally following fertilization which makes them easy to be manipulated, and present optical transparency that allows high-resolution optical imaging of blood vessels. The first technique to analyse vessels in zebrafish was the microangiography that consisted in introduction by injection of fluorescent dyes into the heart of the fish and then, observe perfused vessels and blood flow over time with confocal microscopy (Weinstein et al., 1995). The handicap of this model is that do not allow to see non perfused vessels The generation of transgenic zebrafish that express fluorescent protein specifically in blood vessels overcome that limitation. This molecular tool together with high-resolution time lapse imaging analysis make this model excellent to understand thoroughly the dynamic formation of blood vessels.

The vasculature develops early in the embryo and already at 24 hpf (hours post fertilization) heart beat begins and the first blood cells can be seen travelling along the anterior-posterior axis. The tail vasculature is simple, yet stereotypically patterned, and it forms a complete circulatory network at a very early embryonic stage, before 48 hpf.

First, by vasculogenesis the first blood vessels are formed in the embryo, the dorsal aorta (DA) and the posterior cardinal vein (PCV) around 16 hpf. Then, around 22hpf, primary angiogenic sprouts emerge bilaterally from the dorsal aorta, independently of the blood flow. These primary sprouts called intersegmental arteries (SeAs) and grow dorsally between the somites and notochord and then between the somites and neural tube, tracking along vertical myotomal boundaries. The SeAs extend until the dorsolateral roof of the neural tube (at approximately 28 hpf) and bifurcate into two major branches (T-shape) that turn caudally and rostrally to anastomose with ipsilateral sprouts and form two independent bilateral dorsolateral anastomotic vessels (DLAVs) (Isogai et al., 2003). DLAV plexus formation requires both circulatory flow and VEGF signalling (Zygmunt et al., 2012). Approximately from 36hpf a secondary set of vascular sprouts arise from the the posterior cardinal veins (PCV) and half of them make a connection with the adjacent SeA, linking the posterior cardinal vein to the primary vascular network, forming the intersegmental veins (SeVs) (Isogai et al., 2003).

Both SeAs and SeVs define the intersegmental vessels (ISVs). All the process is schematised in the **Figure 1.12**. This vascular bed has been extensively used to analyse sprouting angiogenesis in zebrafish because the patterned character of ISVs makes them a very useful model to observe the same event repeated multiple times in one embryo. In addition, there are several alternative sprouting models that develop later as communicating vessels (CMV), the posterior cerebral vein (PCeV) and the palatocerebral artery (PLA) (Lenard et al., 2013).

Although the study of angiogenesis in ISVs has some experimental advantages, there are other aspects that make difficult to extrapolate the results into other vessels types. Differentially from mouse retinas or other vascular beds, during ISV formation the tip cell fuses to other two tip cells from neighbouring ISVs, forming a T-shape. Also, the ISVs sprout and fuse very early on, almost simultaneously with the onset of blood circulation, meaning that in some ISVs the fusion process and initial lumen formation take place in the presence of a very weak or no blood pressure, whereas in vessels forming at later stages are subjected to relatively strong flow which influences the formation of the network. Also differentially after tip fusion and DLAV formation no additional angiogenic branches are formed compared to other vascular beds.

1.4 Molecular regulators of the vascular signalling

Several signalling pathways are involved in the regulation of the vascular development. However, among all, two major signalling pathways play critical roles in angiogenesis, the VEGF / VEGFR and Notch signalling pathways, which will be described in greater detail in the following sections. Besides, other signalling pathways, such as the PDGF-B / PDGFR-B, the Ephrin / Eph, the Semaphorins / Plexins, the Netrins / Unc5b, the TGF-β, or the PI3K, have been shown to be crucial in the control of different phases of the vascular growth.

1.4.1 VEGFs and their receptors

The VEGF family consist of VEGF-A, VEGF-B, VEGF-C, VEGF-D, placenta growth factor (PlGF), parapoxvirus VEGF-E and snake venom VEGF-F that

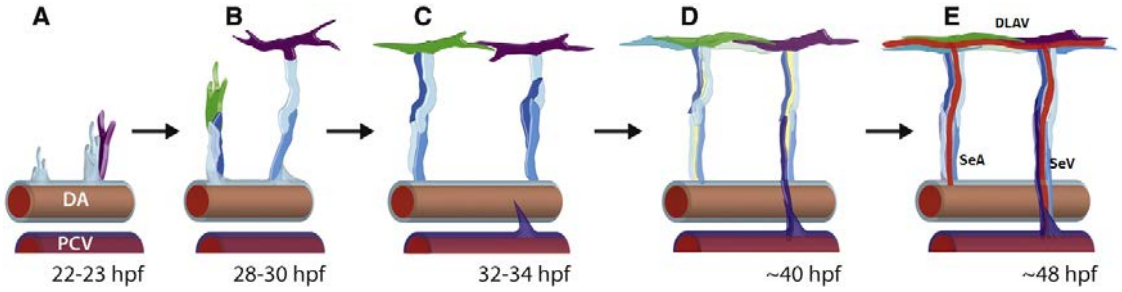

Figure 1.12: **Morphogenetic events that lead to formation of intersegmental vessels (ISVs) and DLAV in the zebrafish trunk.** Two neighbouring sprouts are depicted as representative examples. **(A)** At 22 hpf primary angiogenic sprouts emerge from the dorsal aoirta (DA) and grow along the somite boundaries up to the dorsal roof of the neural tube **(B)**. Sprouts are omposed between 2 ad 4 cells in these stages, that are stabilized by interendothelial junctions. **(C)** Tip cells extend protrusions to their anterior and posterior neighbours to establish connections (T-shape). **(D)** Further cell rearrangements and cell divisions lead to formation of a continuous apical surface that may surround initial luminal spaces (yellow). At around 32 hpf, secondary angiogenic sprouts emerge from the PCV **(C)**. **(D,E)** Some of them connect with the already formed segmental arteries (SeAs) which becomes segmental veins (SeVs), or generate a group of lymphatic cells, called parachordal lymphangioblasts (not shown). At 48hpf, ISVs and DLAV are fully formed and carry blood flow. (Modified and adapted from Ellertsdóttir et al., 2010)

have crucial roles in the formation, function and maintenance of the blood and lymphatic vessels during health and disease. VEGFs are secreted glycoproteins that exert their function through the binding and activation of VEGFRs. There are three VEGF receptors, VEGFR-1 (Flt1), VEGFR-2 (Flk1), and VEGFR-3 (Flt4). The receptors show an overlapping but distinct expression pattern. Upon ligand binding the receptor undergo homo- or heterodimerization and auto- or transphosphorylation of tyrosine residues, resulting in the recruitment of intracellular signalling mediators with Src-homology-2 (SH2) or phosphotyrosine binding domains, and therefore, activating distinct downstream signalling pathways. VEGFs also bind to VEGFs co-receptors as neuropilin NRP1 and NRP2 and to heparan sulfate proteoglycans (HSPGs). Summarised in **Figure 1.13**.

VEGF/VEGFR signalling is tightly regulated at different levels: receptor expression levels, the availability and affinities for binding of its different ligands, the presence of VEGF-binding co-receptors, non-VEGF-binding auxiliary proteins and inactivating tyrosine phosphatases, the rate of receptor cellular uptake, extent of degradation and speed of recycling. Furthermore, VEGFR endocytosis and

trafficking regulate the specificity as well as the duration and amplitude of the signalling output (Simons et al., 2016).

VEGF-A ligand binds to and activates both VEGFR-1 (Flt-1) and VEGFR-2 (KDR/Flk-1), mostly expressed in ECs, promoting angiogenesis, vascular permeability, cell migration, and the expression of several genes. VEGF-A is essential for embryonic development, and homozygous or heterozygous deletion of VEGF-A results in embryonic lethality (Carmeliet et al., 1996; Ferrara et al., 1996). VEGFR-1 has a higher affinity for VEGF-A than VEGFR-2, however its tyrosine kinase activity is approximately 10-fold weaker than VEGFR-2 activity. VEGF-A promotes cell migration, proliferation and survival through VEFGR-2 activation. Mice lacking this gene die in early embryonic stages due to loss of vascular development (Shalaby et al., 1995). However, VEGFR-1 acts as a sink for VEGF-A, to control the mechanism of sprout formation and prevent hypersprouting. Loss of function of VEGFR-1 leads to extensive sprouting and vasculature disorganization and it is also embryonic lethal (Fong et al., 1995). This suggests that the two receptors control vessel outgrowth through antagonistic interactions.

On the other hand, VEGFR-3 is expressed in endothelial cells until E16.5 when its expression is almost restricted to lymphatic vessels (also found neuronal progenitors, macrophages and osteoblasts). However, VEGFR-3 expression is also re-induced in the tip cell of angiogenic sprouts, veins and blood capillaries during angiogenesis. VEGFR-3 can be activated by unprocessed VEGF-C and VEGF-D, whereas proteolytically processed ligands bind to both VEGFR-2 and VEGFR-3 with high affinity. (Simons et al., 2016). Upon VEGF-C or VEGF-A stimulation VEGFR-3 can also form complexes with VEGFR-2 (Nilsson et al., 2010; Dixelius, 2003). Both constitutive deletion of VEGFR-3 and blocking VEGFR-3 using monoclonal antibodies in mice lead to a decrease in sprouting angiogenesis, with less vascular density and decreased proliferation of ECs (Dumont, 1998; Tammela et al., 2008). However, controversially, endothelial specific deletion of VEGFR-3 leads to the opposite vascular phenotype, where there is an increase in EC number and vascular density (Tammela et al., 2011). Tammela et al. proposed that VEGFR-3 has ligand-dependent and ligand-

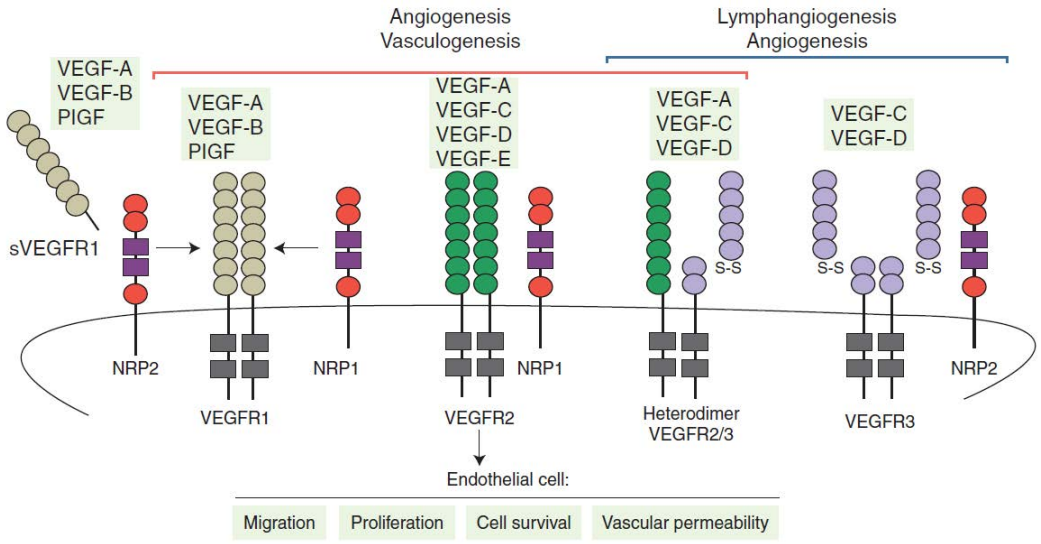

Figure 1.13: **Receptor-binding specificity of VEGF family members.** Schematic diagram that shows the interaction between the different VEGF ligands (VEGF-A, -B, -C, -D, -E, and PlGF) and their tyrosine kinase receptors, VEGFR-1, VEGFR-2, and VEGFR-3. The co-receptors NRP1 or NRP2 are also shown. VEGFR-1 and VEGFR-2 activation is important in the regulation of both the vasculogenesis and angiogenesis. On the other hand, VEGFR-3 activation as homodimer or heterodimer (with VEGFR-2) regulates lymphangiogenesis and embryonic angiogenesis. (Modified and adapted from Blanco and Gerhardt, 2012)

independent functions. Phosphorylation of VEGFR-3 could still occur *in vivo* in the presence of blocking antibodies or the absence of the ligand, by the ECM and mediated by Src, that could only be eliminated by genetic deletion of the receptor. However, in this case, Src produces a different phosphorylation pattern compared to the one induced by the ligand activation of VEGFR-3 (Galvagni et al., 2010). Furthermore, deletion of VEGF-C and VEGF-D does not recapitulate VEGFR-3$^{-/-}$ phenotype suggesting that VEGFR-3 ligand-dependent function is dispensable during the embryonic development (Haiko et al., 2008). On the other hand, Tammela et al. described a VEGF-C-dependent function of VEGFR-3 that acts increasing Notch signalling by receptor tyrosine kinase activation and thus restricts angiogenesis at sites of EC anastomoses (Tammela et al., 2011). It is clear that VEGFR-3 plays a role in the correct development of the vasculature but it is still unknown how VEGFR-3 exerts its functions. It is also important to take in consideration that VEGFR-3 can heterodimerize with VEGFR-2 and may play a role in angiogenesis by modulating VEGFR-2-mediated signals (Zhang et al., 2010).

1.4.2 Notch signalling

Notch signalling is a conserved pathway that regulates cell fate specification, growth and differentiation during the embryonic development, tissue homoeostasis, and the maintenance of stem cell in adults (Kopan and Ilagan, 2009). In mammals, there are four Notch receptors (Notch1, Notch2, Notch3 and Notch4) and five ligands named Jagged1, Jagged2, Delta-like (Dll)1, Dll3 and Dll4. The pathway is activated when a signal-sending cell expressing a Notch ligand physically interacts with a signal-receiving cell expressing a Notch receptor leading to several proteolytic cleavage of the receptor. The last cleavage is triggered by the γ-secretase complex that releases the Notch intracellular domain (NICD) that translocates to the nucleus. Once in the nucleus, NICD forms a complex with the RBP-Jk protein, a sequence-specific DNA binding protein, activating the Notch transcriptional machinery that modulates the expression of multiple genes as Hairy/enhancer of split (HES), HES-related proteins (HEY/HRT/HERP) family genes and also Dll4 gene (Iso et al., 2003). This signalling mechanism is known as the “canonical Notch pathway”.

Notch1 and Notch4 receptors and Dll, Dll4 and Jagged1 ligands are expressed in ECs. Many studies modulating the expression of the different Notch components in mice and zebrafish have revealed that this pathway has an essential role in angiogenesis regulating different steps of the angiogenic process (reviewed in Roca and Adams, 2007).

During angiogenic expansion, reduced Dll4 expression or Notch inhibition by different strategies promotes sprouting, branching, and filopodia formation (Hellström et al., 2007; Suchting et al., 2007; Benedito et al., 2012). In contrast, activation of Notch signalling leads to the opposite vascular phenotype (Hellström et al., 2007). It has been described that VEGF signalling induces Dll4 expression, and in turn, Dll4 (from signal-emitting cell) stimulates Notch signalling in the adjacent cell (signal-receiving cell) restricting the angiogenic behaviour of neighbouring EC and thereby establishing an adequate ratio between tip and stalk cells (described in **1.2.2.1.1**) (reviewed in Benedito and Hellström, 2013). However, apart from Dll4, Jagged1 ligand is also involved in angiogenesis. These two ligands show a different pattern of expression that varies spatially

and temporally. Dll4 is found up-regulated in tip cell, whereas Jagged1 ligand is strongly expressed in stalk cells upon Notch activation. Furthermore, Fringe-mediated posttranslational glycosilation of the Notch receptor modules Notch responses to the ligands. Benedito et al. showed that Fringe enhances Notch receptor affinity to bind Dll4 but reduced Jagged1signalling ability. Consequently, Jagged1 negatively regulates Notch activity because antagonizes Dll4-Notch signalling. The enhanced Jagged1 production in stalk cells competitively interferes with the ability of Dll4 expressed by stalk cells to activate Notch in tip cells and, as a consequence, augments the differential Notch activity. Therefore, Dll4 and Jagged1 ligands present an opposite function in postnatal sprouting angiogenesis (Benedito et al., 2009).

On the other hand, Notch signalling has also been involved in the regulation of arteriovenous specification in blood vessels (Lawson et al., 2001; Quillien et al., 2014) and arteriogenesis in adults (Limbourg et al., 2007; Domenga, 2004), controls EC proliferation and regulates the maintenance of endothelial cell quiescence (Phng et al., 2009; Ehling et al., 2013; Kerr et al., 2016; Serra et al., 2015).

1.5 PI3K signalling pathway

1.5.1 The core pathway

The PI3K signalling network plays critical roles in nearly all aspects of cell and tissue biology having not only a relevant role from a physiological point of view but also in several pathologies such as human cancer, diabetes and ageing. PI3K signalling regulates cell growth, proliferation, differentiation, motility, survival, and intracellular trafficking. PI3Ks work as master regulators situated in the crossroad between extracellular signals (growth factors, cytokines ad other cues) and intracellular signals that end in different cellular functions (Vanhaesebroeck et al., 2010). PI3Ks are characterized for phosphorylate the 3-hydroxyl group of the inositol ring of different phosphatidylinositol (PtdIns) lipid substrates. There are three possible lipid substrates of PI3Ks: PtdIns(PI), PtdIns(4)P (PIP) and PtdIns(4,5)P_2 (PIP_2) that can be respectively converted into PtdIns(3)P,

PtdIns(3,4)P_2 and PtdIns(3,4,5)P_3 (PIP_3). These 3-phosphoinositides coordinate the localization and function of multiple effector proteins, which bind these lipids through specific lipid-binding domains such as FYVE and a subset of phox homology (PX) and pleckstrin homology (PH) domains triggering cell signalling events, protein-protein interactions and directional vesicular trafficking. The relatively low phosphoinositide-binding affinity of these domains in combination with 3-phosphoinositide phosphatase activities, permits highly reversible effector localization and responses (Jean and Kiger, 2014). PI3Ks are divided into three classes (class I, class II and class III) based on their structure, substrate preference, distribution, mechanism of activation and functions (**Figure 1.14**). *C.elegans* and *Drosophila melanogaster* present only one isoform per class while yeasts only have a class III PI3K.

Class I PI3Ks subfamily comprises four members in vertebrates and works as heterodimers consisting of a p110 catalytic subunit and a regulatory subunit. Furthermore, PI3Ks class I can be divided into class IA and class IB, depending on their ability to bind the p85-type of regulatory subunit (Graupera and Potente, 2013). Class IA is composed of a p110α, p110β or p110δ catalytic subunit bind to a p85-type regulatory subunit (p85α, its splicing variants p55α and p50α, p85β or p55γ). On the other hand, class IB consists of p110γ isoform binds to p101 or p87 regulatory subunit. p110δ and p110γ expression is manly enriched in immune cells whereas p110α and p110β are ubiquitous. Furthermore, they also present isoform-specific cell-type and context-dependent requirements. Class I PI3K is mainly characterized by their catalytic activity but there is growing evidence of kinase-independent scaffolding roles at least for p110γ and p110β (Jean and Kiger, 2014).

Class II PI3K is made up of three single isoforms in vertebrates, PI3K-C2α, PI3K-C2β and PI3K-C2γ not binding to any regulatory subunit. PI3K-C2α and PI3K-C2β are broadly expressed while PI3K-C2γ expression is limited to the liver, prostate and breast tissues. This class presents additional domains that suggests that class II PI3K proteins could interact with clatrin-coated vesicles. These enzymes generate PtdIns(3)P *in vivo* and also PtdIns(3,4)P_2 *in vitro* (**Figure 1.14**).

Finally, a single class III PI3K is conserved in all eukaryotes, called vacuolar

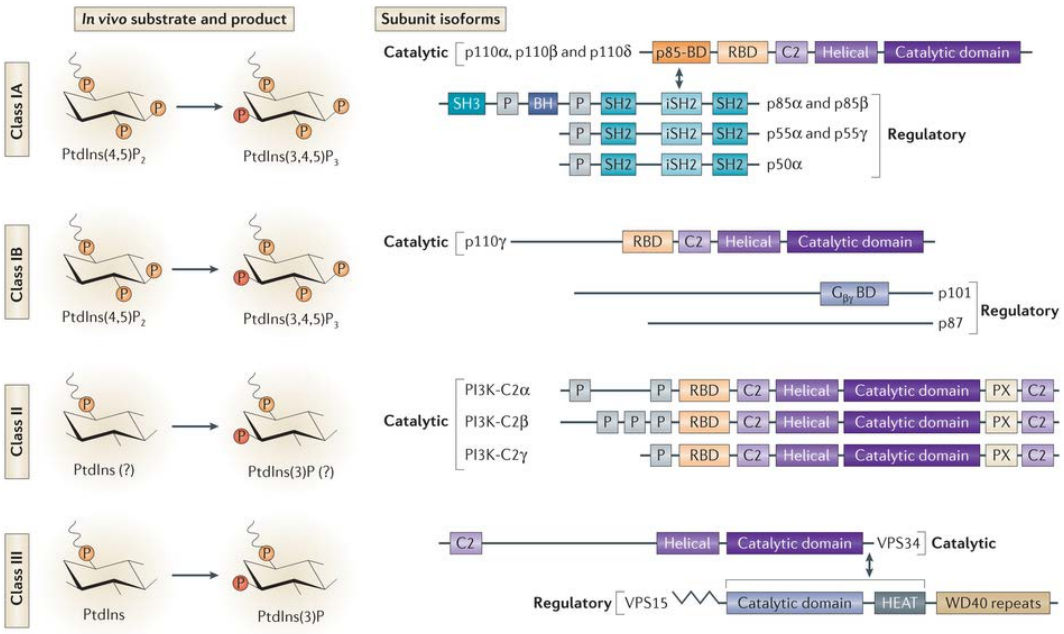

Figure 1.14: **The members of the phosphoinositide 3-kinase (PI3K) family.** Class IA PI3Ks are heterdimers formed by catalytic isoforms (p110α, p110β and p110δ) and p85 regulatory isoforms (p85α, p85β , p55α, p55γ and p50α). Catalytic isoforms present a p85-binding domain (p85-BD), a RAS-binding domain (RBD), a helical domain and a catalytic domain whereas p85 regulatory isoforms have an inter-SH2 (iSH2) domain that binds to class IA catalytic subunits, flanked by SH2 domains that bind to phosphorylated YXXM motifs. The longer isoforms, p85α and p85β, also present an amino-terminal SH3 and a breakpoint cluster homology (BH) domains. Class IB PI3Ks are heterodimers of a p110γ catalytic subunit and a p101 or p87 regulatory subunit. The p110γ subunit has an RBD, a helical domain and a catalytic domain. The domain structures of p101 and p87 are not fully known, but a carboxy-terminal region of p101 has been shown to bind to Gβγ subunits. Class II PI3Ks are monomers with only a single catalytic subunit that presents divergent N-terminus followed by a Ras binding domain (RasBD), C2 domain, helical domain, and catalytic domain with PX and C2 domains at the C-termini. VPS34 (the only class III PI3K) has helical and catalytic domains and forms constitutive heterodimer with the myristoylated, membrane-associated VPS15 protein. (Adapted from Thorpe et al., 2014)

protein sorting 34 (Vps34). This protein binds to the adaptor protein Vps15 (which is myristoylated) regulating the intracellular membrane localization of Vps34 and its activity. Vps34 has as lipid substrate PtdIns, generating PtdIns(3)P and, principally, it is involved in vesicle trafficking and autophagy (Vanhaesebroeck et al., 2010) (**Figure 1.14**).

1.5.2 Class I PI3-kinases

Class I PI3Ks are the best understood among the three classes of PI3Ks. Class I PI3Ks mediate signalling mainly downstream of receptors tyrosine kinases

(RTKs), G-protein-coupled-receptors (GPCRs) and small GTPases as Ras. Upon their activation, cytosolic class I PI3K heterodimers are recruited to the plasma membrane where they generate PtdIns(3,4,5)P_3 (PIP_3) and indirectly, PtdIns(3,4)P_2. PIP_3 is mainly generated at the plasma membrane, although it might also be presented in endosomes and the nucleus (Lindsay et al., 2006). Although all class I PI3Ks produce the same lipid they differ in their expression patterns, modes of activation and physiological function (Vanhaesebroeck et al., 2010)) (**Figure 1.15**). p85 regulatory proteins present Src homology 2 (SH2) domains, which are able to bind to phosphorylated Tyr-X-X-M (YXXM) motif in Tyr kinase receptors and membrane-associated proteins, and in this way, activate and bring the p110α, p110δ and probably p110β into contact with their lipid substrate. Most class I PI3K subunits might also be activated by GPCRs, either directly through Gβγ protein subunits (in the case of p110β and p110γ) (Dbouk et al., 2012) or indirectly, for example through Rho family GTPases as Rac or Cdc42 (Fritsch et al., 2013). Another important mechanism of PI3K activation involves the small GTPase Ras, that activates p110α and p110γ (**Figure 1.15**). Notably, Ras binds to the p110 catalytic subunit directly and independently of the p85 adaptor (Castellano and Downward, 2011). PTEN phosphatase is responsible for dephosphorylates PIP_3 at the plasma membrane and thereby inhibits PI3K-mediated signals (Hopkins et al., 2014).

1.5.2.1 Functions of the regulatory subunits of class I PI3Ks

In class IA PI3Ks, p85 regulatory subunits provide at least three functions to the p110 catalytic isoforms: to stabilize the catalytic subunit avoiding its degradation, to maintain inactivate p110 activity in the basal state and to allow the recruitment of the heterodimer to phosphorilated Tyr (pTyr) in receptors tyrosine kinase (RTK) and adaptors proteins through their SH2 domains. In addition to this, p85α regulatory protein can be phosphorylated and ubiquitinated, modifications that can have an impact on its regulation (Mellor et al., 2012). Moreover, some studies suggest that p85 may exist in excess of p110. Preferentially p85 binds to p110 and, once saturated, free p85 binds other partners that negatively regulate PI3K signalling (Mauvais-Jarvis et al., 2002; Ueki et al., 2002)(reviewed in Mellor et al.,

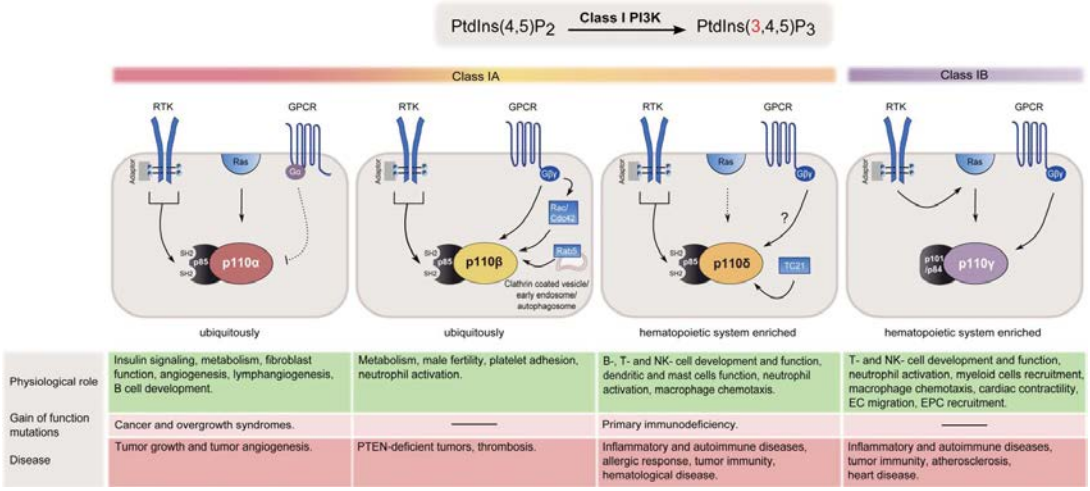

Figure 1.15: **Expression patterns, modes of activation, and physiological and pathophysiological roles of class I PI3K isoforms.** p110α and p110β are ubiquitously expressed, in contrast to p110δ and p110γ, which are enriched in leukocytes. p110α and p110δ are preferentially activated by RTKs, whereas p110β and p110γ are activated by GPCRs. Each of the class I catalytic isoforms contains a Ras-binding domain (RBD). p110α, p110δ, and p110γ interact with Ras although a physiological role of this interaction has only been reported for p110α and p110γ. The RBD of p110δ preferentially interacts with the small G protein TC21. p110β does not bind to Ras but interacts with the Rho subfamily GTPases Rac and Cdc42. p110β also binds to the GTP-bound Rab5 and regulates receptor-mediated endocytosis and autophagy independent of its kinase activity. (Adapted from Soler et al., 2015)

2012). Heterozygous p85α or p85β mice present increased sensitivity to insulin through PI3K signalling (Luo and Cantley, 2005) and partial silencing p85α and p85β by miRNAs in zebrafish also results in increased PI3K activity (Nicoli et al., 2012; Fish et al., 2008). Two models have emerged to describe the negative regulation of PI3K signalling by p85: (1) the existence of a free pool of p85 that competes with the heterodimer p85-p110 for binding to pTyr residues in the activated receptors and (2) p85 regulatory subunits bind to PTEN enhancing its phosphatase activity, and therefore, counterbalance PI3K signalling (Mellor et al., 2012). Geering et al. showed that there is an equimolar relationship between levels of p85 and p110, and that monomeric p85 is unstable, thus questioning the existence of pools of free p85α and suggesting that p85 can decrease cellular PI3K lipid levels through mechanisms that are independent of its capacity to compete for pTyr docking sites (Geering et al., 2007). In this line, it has been shown that p85α can form homodimers that bind to PTEN increasing its stability by inhibiting its ubiquitination (Cheung et al., 2015). All these data provide evidence that p85 levels modulate the output of PI3K signalling. On the other hand, p85 subunits also present PI3K independent functions. For example, p85α is involved in the spatial control of cytosolic division independently of PI3K activity (García et al., 2006).

p101 and p87 regulatory subunits of class IB PI3K have distinct tissue distribution and are important for the relay of signals by Gβγ and Ras to p110γ. p101-p110γ heterodimers generate PIP_3 in the plasma membrane that is rapidly endocitosed to motile, microtubule-associated vesicle compared to the PIP_3 generated by p87-p110γ heterodimer (Vanhaesebroeck et al., 2010).

The field has experienced progress in understanding the specific role of each regulatory subunit. There is some evidence suggesting that the regulatory subunits present a differential binding to receptors (Xia and Serrero, 1999; Inukai et al., 2001), to p110 isoforms (González-García and Carrera, 2012) and tissue-dependent expression (Geering et al., 2007) but many questions remain unanswered.

1.5.2.2 Class I PI3K signalling transduction

PIP_3 is the lipid generated by class I PI3Ks. PIP_3 acts as second messenger activating several downstream signalling pathways that regulate several cellular functions. PIP_3 propagates intracellular signalling by a direct binding to proteins with PH domains recruiting them to the plasma membrane (Vanhaesebroeck et al., 2010). Akt is the major effector of class I PI3Ks (abbreviated from here on as PI3Ks). The Akt family consists of three isoforms: Akt-1, Akt-2 and Akt-3. Recent studies of Akt isoform-specific knockout mice suggest that Akt signalling diversity might in part be due to different functions of the three Akt family members (Zhou et al., 2006; Dummler and Hemmings, 2007) although there is some overlap (or compensation) among the isoforms. Akt1 and Akt2 seem to be ubiquitously expressed, whereas the expression of Akt3 is more restricted with predominance toward heart, kidney, brain, testes, lung, and skeletal muscle. All the Akt isoforms contain an N-terminal PH domain for phospholipid binding, followed by a short linker domain, a catalytic domain and a C-terminal regulatory tail domain (Hanada et al., 2004). Through its PH domain, Akt binds to the PIP_3 allowing its activation by the upstream kinase called phosphoinositide-dependent kinase 1(PDK1), which is recruited to the membrane by its biding to PIP_3 and, thereby phosphorylates Akt in the kinase domain (Thr308). However to fully activate Akt activity additional phosphorylation on Ser473 by mammalian target of rapamycin complex 2 (mTORC2) is needed (Sarbassov et al., 2005). Activated Akt can move to the cytoplasm and nucleus (Wang and Brattain, 2006), where it phosphorylates, activates or inhibits different downstream targets to regulate several cellular processes. In the literature, more than 100 non-redundant substrates of Akt have been identified. The **Figure 1.16** contains a summary of the principal Akt effectors and their function in the cell.

Briefly, Akt enhances the **survival** of cells by blocking the function of proapoptotic proteins and processes. Akt negatively regulates proteins as BAD and inhibits the expression of BH3-only proteins as BIM through effects on transcription factors, such as FoxO and p53. Furthermore, MDM2 is also phosphorilated by Akt and negatively regulates p53 function as tumour suppressor protein responsible for cell-cycle arrest and apoptosis. Akt activity also promotes

cell growth through the activation of the mammalian target of rapamycin (mTOR) complex 1 (mTORC-1). Activated Akt can phosphorylate the tuberous sclerosis complex 2 (TSC-2), which is a tumour suppressor complex that acts as a negative regulator of mTORC-1 signalling (Inoki et al., 2002)). Akt also controls **cell growth** through the prolin-rich Akt subtrate of 40kDa (PRAS40) a negative regulator of mTORC1 signalling. The Akt-mTORC-1 pathway is known to regulate cellular growth, protein synthesis and autophagy. Activation of the mTORC1 target, S6 kinase, negatively feeds back to decrease PI3K activation.

Akt activation can also stimulate **proliferation** through multiple downstream targets affecting cell-cycle regulation. Akt negatively regulates the cyclin-dependent kinase inhibitors $p21^{Cip1/WAF1}$ and $p27^{Kip1}$. Akt-dependent phosphorylation on GSK3, TSC2, and PRAS40, is also likely to drive cell proliferation through regulation of the stability and synthesis of proteins involved in cell-cycle entry. In a cell context-depend manner, Akt signalling regulates **nutrient uptake and metabolism**. Akt activation leads to Glut4 translocation to the plasma membrane putatively through Rab-GAP AS160 and PIKfyve substrates. Akt-dependent activation of mTORC1 can contribute to HIFα-dependent Glut1 regulation, as well. Glucose uptake is controlled by the regulation of Glu1 and Glu4 by Akt. It also regulates glucose and lipid metabolism in the cell. Akt activation increases glycolisis rate, phosphorylation on GSK3 by Akt allows glycogen synthase activation. Lipid production is enhanced by Akt activation, which promotes Sterol regulatory element-binding protein (SREBP) stability. FoxO1 inhibition by Akt contributes to glucose homoeostasis (Manning and Cantley, 2007).

There are many studies that have linked Akt activity and cell **migration**; however, the complete molecular mechanism involved is still unknown. In some contexts, Akt activity promotes cell migration contributing to actin polymerization or actin filament stabilization. Akt not only phosphorylates some substrates related with migration and invasion as APE/girdin, filamin A or NHE1, but can also contribute negatively to cell motility. Akt1 can phosphorylate palladin which leads to F-actin bundles disruption. Similarly, phosphorylation on TSC2 can attenuate migration impairing F-actin assembly. On the other hand, Akt can

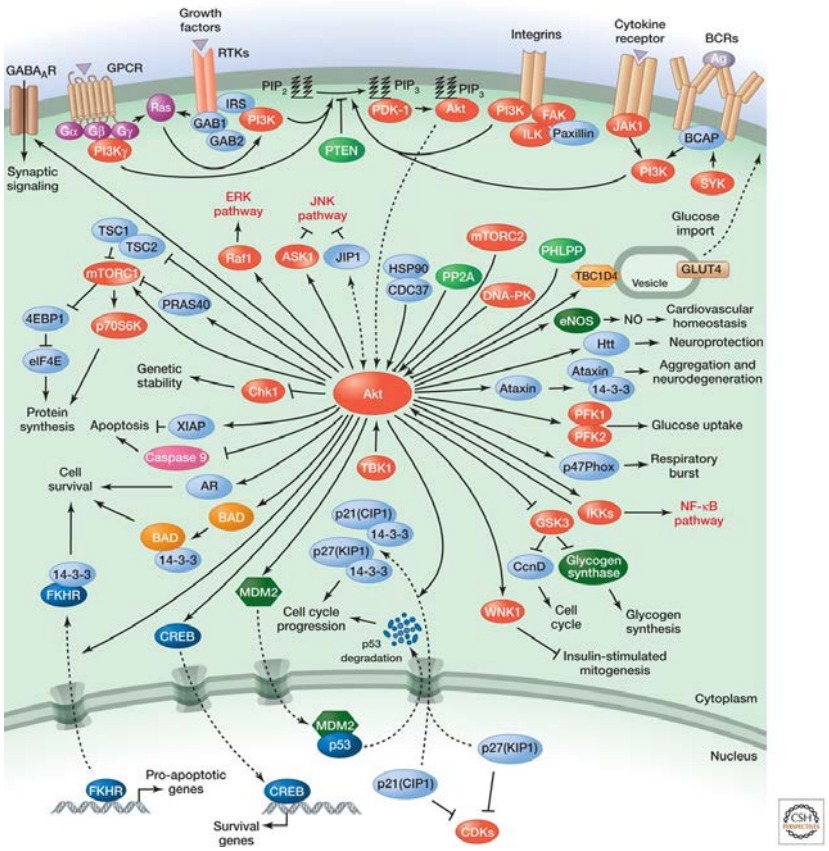

Figure 1.16: **Akt as the main effector of PI3Ks.** Schematic representation of Akt downstream effectors and the cellular functions regulated by them. Akt binds to PIP_3 through its PH domain and is thereby phosphorylated at Thr308 by PDK1. To fully activation, mTORC2 phosphorylates Akt at Ser473. (Adapted from Hemmings and Restuccia, 2012)

control migration mediating crosstalk with other signalling pathways such as VEGFR/eNOS, Ephrin receptor tyrosin kinases (Ehp), ACAP1/ARP6-β1-integrin recycling (Xue and Hemmings, 2013).

Beyond Akt, other PI3K effectors with PH domains have been identified. PI3Ks regulate small-GTPases as Rac, Ras, Rho and Arf through the regulation of their GEFs and GAPs. Their activation is PI3K isoform-selective and cell-type dependent comparing to a more universal activation of Akt. Moreover, there are several adaptor proteins that present a PH domain as GAB1, GAB2, TAPP1or DAPP to bind to PIP_3, however it is still unknown how they drive PI3K function.

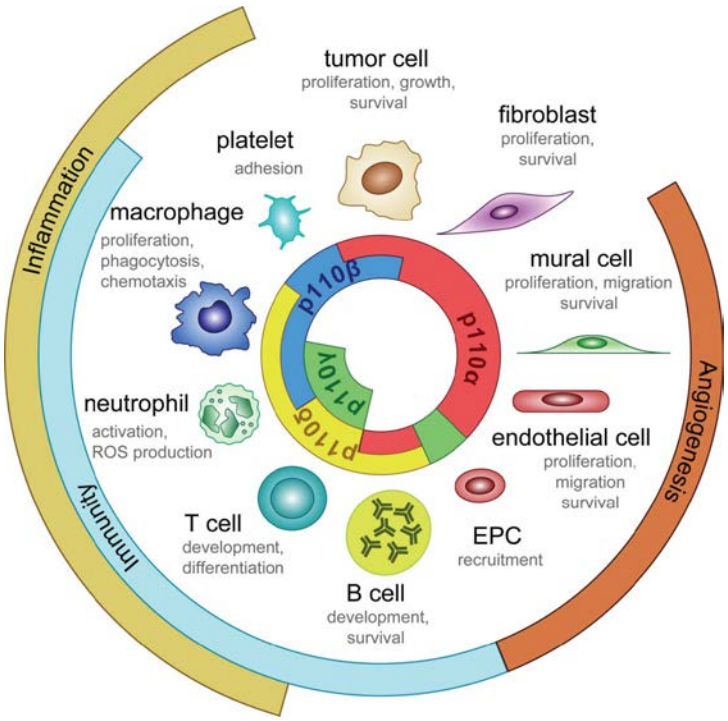

Figure 1.17: **Isoform-specific roles of class I PI3Ks.** This illustration shows the cell-autonomous roles of class I PI3K isoforms in normal physiology and cancer. (Adapted from Soler et al., 2015)

1.5.3 PI3Ks in angiogenesis

The first evidence that PI3K signalling regulates angiogenesis *in vivo* was supported by studies in which wortmannin inhibited angiogenesis in a chick embryo chorioallantoic membrane system (Oikawa and Shimamura, 1996). Since them, numerous studies have revealed that PI3K signalling pathway regulates angiogenesis in a pleiotropic way, from all cell types involved in vessels growth. Not only is PI3K signalling required in endothelial cells for proper vascular development, but also in mural cells, macrophages, and immune cells (**Figure 1.17**). In addition, PI3K signalling in tumour cells has an impact on angiogenesis (Soler et al., 2015). I will focus on PI3K functions in endothelial cells. The most extensively investigated PI3Ks have been class I PI3Ks but recently studies have shown that class II PI3Ks also regulate vascular morphogenesis.

1.5.3.1 Class IA PI3Ks in endothelial cells

In endothelial cells, class I PI3Ks signal downstream of many cell surface receptors (VEGFR1-3, TIE-1/2, EGFR1-2, PDGFR-b, ERBB1-4, among others)

that are activated by growth factors, cytokines or biophysical signals (VEGFA, VEGFC, angiopogetin (Ang)1, Ang2, VE-cadherin, Dll4, and ephrins, among others). Through the activation of this central signalling axis PI3K regulates endothelial cell proliferation and survival, angiogenic sprouting and vessel growth, maturation, and permeability. Nonetheless, the regulation of the entire axis is not well-known yet. When, by what and how PI3K signalling exerts its function needs to be studied in depth (Graupera and Potente, 2013).

Different studies have been done to characterize the specific roles and functions of the different PI3K isoforms. Individual deletion of different members of class IA heteroenzymes showed that they are required for early embryonic development (Bi et al., 1999, 2002; Fruman et al., 2000). Studies in mice and zebrafish have revealed specific functions of class IA PI3K in vascular development. In mice, endothelial-specific loss of p85 regulatory subunits (p85α and p85β) leads to defects in vascular integrity and embryos die at E11.5 showing that class IA PI3K regulates vessel integrity *in vivo* (Yuan et al., 2008). Ubiquitous deletion of p110α-PI3K catalytic subunit also points to its function in angiogenesis because these embryos show growth retardation and angiogenesis defects at mid-gestation, dying at E10.5 (Lelievre, 2005; Bi et al., 1999). Regardless, full depletion of p110α leads to the up-regulation of p85 which acts as dominant negative on all p110, making it difficult to understand whether the phenotype is a consequence of the p110α deletion or of the p85 up-regulation (Bi et al., 1999).

Subsequently, Graupera and colleges studied selectivity among the class IA PI3K catalytic isoforms and their mechanism of action (Graupera et al., 2008). On one hand, they generated knock-in mice for the different catalytic p110 isoforms, carrying a germ-line mutation in the DFG motif of the p110 ATP binding site, leading to the expression of inactive p110 protein (kinase-dead p110 protein). On the other hand, they inactivated each p110 isoform specifically in endothelial cells during embryonic development. Interestingly, this study showed a surprising degree of isoform selectively among the class IA PI3K members in developmental angiogenesis. Only ubiquitous and endothelial-cell specific inactivation of p110α led to severe defects in angiogenic sprouting and vascular remodelling and, as a consequence, embryos died before E12.5. On the other hand, p110β and p110δ

mutants were viable and did not present vascular defects. They described that only the p110α isoform is required in a cell-autonomous manner in ECs and solely drives VEGF-A signalling. Furthermore, p110α controls EC migration through the positively regulation of RhoA-GTPase activity. Inactivation of p110α in ECs impairs proper EC migration but not EC survival or proliferation (Graupera et al., 2008).

Other investigations corroborated the specific role of p110α in controlling ECs migration during vascular formation. Herbert et al. studied the formation of the caudal vein from angioblast segregation of the dorsal aorta (DA) in zebrafish embryos. Using both a board-spectrum or a p110α specific inhibitor, it was shown that ventral sprouting from the DA was impaired. The number of angioblasts was not affected, but cells were retained in the DA (Herbert et al., 2009). It is only the exposure of embryos to p110 isoform specific inhibitors at concentrations that inhibits p110α blocked vein morphogenesis. Therefore, Herbert et al. proposed that the activation of p110α-PI3K via VEGFR-C/VEGFR-3 promotes the migration of “venous” angioblasts from the DA to form the caudal vein. This process is also regulated by the Efnb2-Ephb4 bidirectional signalling (Herbert et al., 2009).

In zebrafish, regulation of p85 levels by microRNA (miRs) contributes to proper EC functionality. miR-221 induces tip cell proliferation through the down-regulation of cyclin dependent kinase inhibitor 1b (cdkn1b) and acts as modulator of VEGF-C/VEGFR-3(Flt4)/PI3K signalling axis by reducing p85α levels promoting tip cell migration. Inactivation of PI3K activity pharmacologically or the overexpression of p85α significantly decrease ISV length and cell number, without changes in EC proliferation (Nicoli et al., 2012). On the other hand, miR-126 regulates several aspects of the EC biology such as cell migration, organization of the cytoskeleton, capillary network stability, and cell survival. This is accomplished partially through the promotion of the VEGF-A / VEGFR-2 / PI3K signalling pathway by repressing p85β expression (Fish et al., 2008).

1.5.3.1.1 Inputs of class IA PI3Ks in ECs

There are several studies showing that PI3K signalling can be activated downstream of many different signals, however, their specific contribution *in vivo*

during sprouting angiogenesis is still not well known. It has been described that both VEGFR-1 and VEGFR-2 can bind to the p85 regulatory subunit of PI3K inducing its activation (Dayanir, 2001; Cunningham et al., 1995). Specifically in ECs it has been shown that VEGF-A / VEGFR-2 activation drives SFKs activation which in turn engages Axl, and consequently promoting the ligand-independent autophosphorylation of Axl at YXXM motif. The SH2 domains of p85 can bind to this motif and activate PI3K. VEGF-A activation regulates EC migration, permeability and tube formation through Axl and thereby associates with PI3K and activates Akt (Ruan and Kazlauskas, 2012). *In vitro* studies in lymphatic endothelial cells (LECs) showed a direct association between VEGFR-3 and PI3K subunit although the lack of a p85-binding motif in the cytoplasmatic tail of VEGFR-3 suggests an indirect interaction (Coso et al., 2012), and the stimulation with VEGF-C and VEGF-D ligands activates PI3K signalling (Coso et al., 2012; Makinen, 2001). Furthermore, several *in vivo* studies suggest a role in vascular development to the VEGF-C /VEFGR-3 / PI3K signalling axis (Tammela et al., 2011; Herbert et al., 2009; Nicoli et al., 2012). However, whether VEGFR-2 / VEGFR-3 heterodimers contribute to PI3K activation *in vivo* has not been evaluated yet, nor has their role in physiology.

PI3K signalling can be activated by Ras, as well. Mutant mice in which the interaction between p110α and Ras is blocked do not present vascular defects but the activation of Akt is impaired. These mice present lymphatic defects similar to heterozygous VEGF-C knock-out mouse, suggesting that Ras-p110α interaction could be necessary to drive VEGF-C / VEGFR-3 / PI3K signalling in lymphatic cells whereas in blood vessels VEGFR3-dependent activation of PI3K signalling should occur through a different molecular mechanism independent of Ras (Gupta et al., 2007).

The angiopoietin (Ang) ligands-Tie receptors signalling is essential during embryonic vessel assembly and maturation, and also controls vascular homoeostasis in adults (reviewed in Augustin et al., 2009). Activation of Tie2 receptor by its ligand Ang1 can activate PI3K signalling by the binding of p85 subunit to the activated receptor (Jones et al., 1999). Ang2 acts as antagonist of Ang1, favouring vessel destabilization. Ang1/Tie2 signalling in resting ECs

through the PI3K/Akt signalling controls ECs survival (Papapetropoulos, 2000) and also regulates vessel stability, promoting a negative-feedback loop on EC Ang2 production (Daly, 2004). Furthermore, it has been demonstrated that PI3K is not only downstream of Tie2 but also regulates its expression (Lelievre, 2005). On the other hand, in no-resting ECs Ang1/Tie2 signalling regulates in minor manner several aspects of the angiogenic cascade as EC migration possibly through the activation of PI3K signalling (Augustin et al., 2009).

PI3K signalling has also been found to be activated downstream of VE-cadherin. p85 subunit of PI3K may bind to the phosphorylated form of VE-cadherin (Hudry-Clergeon, 2005). Upon clustering of VE-cadherin, PI3K is activated and signals through the nucleus via FoxO1 and β-catenin transcription factors, to maintain endothelial features (Taddei et al., 2008). It has also been shown that VEGF-A promotes EC survival through the formation of a VE-cadherin / β-catenin / PI3K / VEGFR-2 complex (Carmeliet et al., 1999). However, the adaptor protein that allows the binding of p85 to VE-cadherin is unknown.

1.5.3.1.2 Outputs of class IA PI3K in ECs

As previously mentioned, class I PI3Ks generate the PIP_3 lipid that coordinates the localization and function of multiple effector proteins with a PH domain. One of those proteins is Akt, which plays important roles in both physiological and pathological angiogenesis through its activity in both ECs and cells producing angiogenic signals such as tumour cells (**Figure 1.18**). PI3K/Akt signalling pathway is activated downstream of VEGFR-2. VEGFR-2 traps the complex p110-p85 via the tyrosine kinase receptor Axl and through Akt1 activates endothelial nitric oxide (NO) syntase (eNOS) producing NO (Ruan and Kazlauskas, 2012). NO stimulates vasodilation, vascular remodelling and angiogenesis. In addition, Akt signalling in ECs or non-ECs increases the production of the hypoxia inducible factor α (HIF-1α and HIF-2α) that stimulates angiogenesis inducing VEGF expression and secretion. Genetic loss of Akt1 substantially impairs ischemia-induced arteriogenesis and VEGF-induced postnatal angiogenesis, as well as wound, inflammation, and VEGF-induced vascular permeability (Yang et al., 2003; Chen et al., 2005a; Ackah et al., 2005). However, the ubiquitous

absence of Akt1 is not embryonic-lethal, implying that additional isoforms, such as Akt2, may compensate for the loss of Akt1. Postnatal endothelial-specific deletion of Akt1 confers significant retinal vascular defects while Akt2 appears to play a minimal role in vascular development, because double endothelial-specific deletion of Akt1 and Akt2 in mice does not display obvious exacerbation of the $Akt1^{i\Delta EC}$ phenotype (Lee et al., 2014b). In contrast, endothelial specific deletion of Akt in adults results in impaired vessel perfusion and severe tissue dysfunction due to the loss of mural cells and deterioration of the basement membrane. Thus, Akt in quiescence vessels is required for sustained Jagged1/Notch signalling, vascular stability and homoeostasis. Akt's function in established vasculature is distinct from developmental or postnatal vascular growth or remodelling (Kerr et al., 2016).

PI3K signalling inhibits Forkhead box O (FoxO) transcription factors (FoxO1, FoxO3, and FoxO4) through Akt-mediated phosphorylation leading to their nuclear exclusion (**Figure 1.18**). FoxO1 activity is negatively regulated by VEGF, Ang1, and shear stress through activation of PI3K/Akt signalling. FoxOs are critical regulators of vessel formation. FoxO1 and FoxO3 control endothelial sprout formation and migration *in vitro*. FoxO3a deficiency increased eNOS expression and enhanced vessel formation and maturation (Potente et al., 2005). FoxO1 regulates vessel growth, maintenance (survival, quiescence, barrier function), and remodelling. A primary role of FoxO1 in the endothelium is to feed back and activate Akt/mTORC1, thus sensitizing cells to the effect of VEGF (Dharaneeswaran et al., 2014). Apart from that, FoxO1 also promotes endothelial quiescence by antagonizing MYC, which leads to a coordinated reduction in the proliferative and metabolic activity of ECs, thereby ensuring efficient nutrient and oxygen delivery (Wilhelm et al., 2016) (**Figure 1.19**).

Arap3 was identified as PIP_3 binding partner (Krugmann et al., 2002) and is a PI3K- and Rap-regulated GAP (guanosine triphosphatase (GTPase)-activating protein) for the small GTPases RhoA and Arf6. PIP_3 drives the recruitment of Arap3 to the plasma membrane, bringing it into the vicinity of its activator, Rap-GTP, and its substrates, RhoA-GTP and Arf6-GTP (Krugmann et al., 2004) (**Figure 1.18**). In mice, ubiquitous and endothelial-specific deletion of Arap3

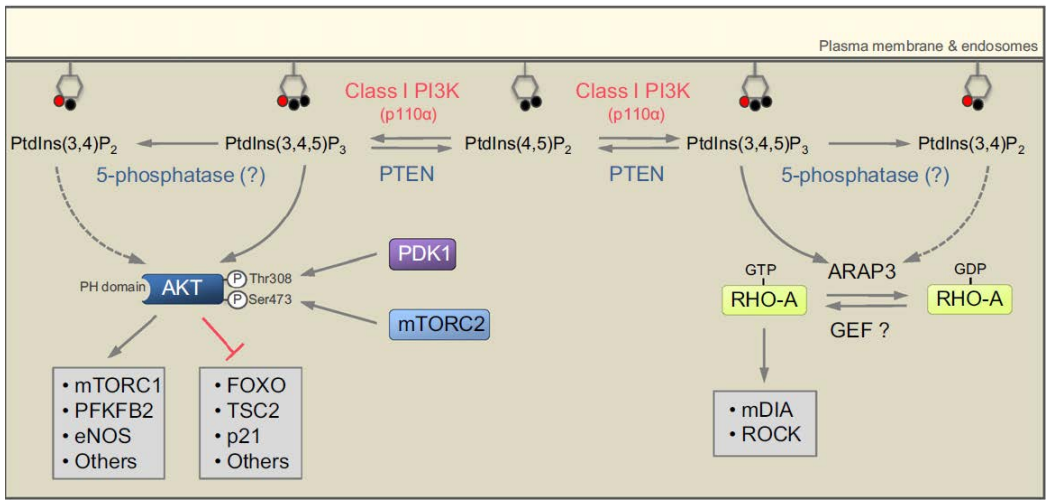

Figure 1.18: **Signalling pathways regulated by class I PI3Ks in ECs.** (Adapted from Graupera and Potente, 2013)

and mutated Arap3 protein (knock-in point mutations that interrupt its binding to PIP_3) leads to defective embryonic angiogenesis similar to p110α loss-of-function mice and to embryonic lethality. *In vitro*, knocking-down Arap3 by RNAi leads to a decrease in the global amount of RhoA-GTP under normal growing conditions. However, Arap3-depleted cells experience a greater increase in RhoA-GTP in response to VEGF compared to control ECs. Taking into account that PI3K activity generates a localized increase of PIP_3 in the membrane, measuring total amount of the GTPases underestimates any local change in PI3K / Arap3 signalling responsible for proper EC functionality (Gambardella et al., 2010). Surprisingly, in zebrafish, the overall blood vasculature appeared normal in Arap3a (isoform expressed in the vasculature) zebrafish morphants, but present numerous lymphatic vascular defects (Kartopawiro et al., 2014). Vascular analysis was poorly address at 48 hpf making it possible to overlook some early blood vascular minor defects. Curiously, Arap3 mice and zebrafish phenotypes present a similar behaviour with VEGFR-3 phenotypes. VEGFR3-null mice present vascular defects whereas VEGFR-3 morphants and mutants present lymphatic vascular defects (Dumont, 1998; Hogan et al., 2009).

An *in vitro* study identified p110α protein as key regulator in the assembly of a VE-cadherin signalling complex. p110α acts upstream of Pyk2 regulating its autophosphorylation and its association with VE-cadherin and also regulates Rac activity putatively via recruitment of the Rac GEF Tiam-1 to the VE-cadherin

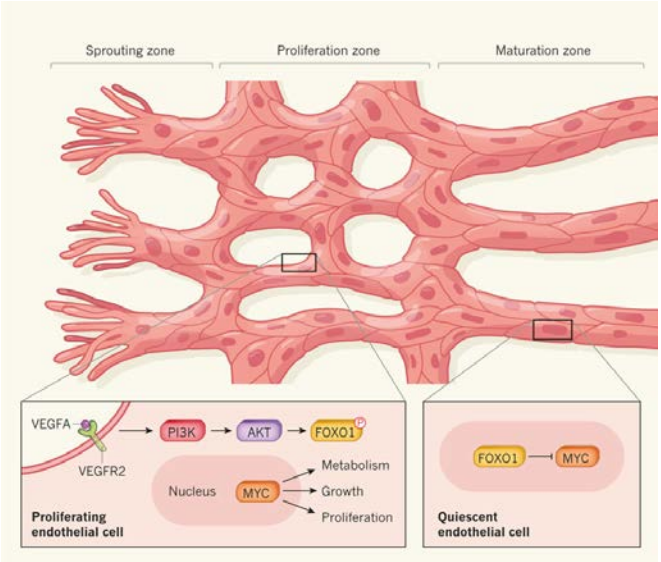

Figure 1.19: **FoxO1 and MYC in angiogenesis.** Upon growth factor stimulation, FoxO1 is phosphorylated through the activity of PI3K/Akt signalling pathway, being located in the cytoplasm. MYC remains in the nucleus favouring cell metabolism, growth and proliferation. In more mature vessels, the growth factor signalling decreases, and therefore, unphosphorylated FoxO1 is translocated to the nucleus and inhibits MYC which leads to EC quiescence. (Adapted from Betsholtz, 2016)

complex. In the end, they show that p110α isoform controls endothelial cell barrier function and leukocyte TEM by the regulation of cell–cell contacts in ECs (Cain et al., 2010).

1.5.3.1.3 Regulation of PI3K activity by the lipid phosphatase PTEN in ECs

The main activity of PTEN is to dephosphorylate the lipid phosphatidylinositol 3,4,5-trisphosphate (PIP_3) at the 3´-position antagonizing PI3K signalling (**Figure 1.18**). The balance between PI3K and PTEN activity largely determines the intracellular levels of PIP_3 and downstream activity, therefore ensuring proper EC functionality. Deletion of PTEN, specifically in ECs, has a dramatic impact on embryonic development. Tie2-CrePten$^{flox/flox}$ mice die before embryonic day 11.5 (E11.5) due to bleeding and cardiac failure caused by impaired recruitment of pericytes and vascular smooth muscle cells to blood vessels, and of cardiomyocytes to the endocardium (Hamada et al., 2005). In addition, loss of PTEN increases the levels of pro-angiogneic factors enhancing EC proliferation and growth. These results suggested that PIP_3 not only regulated ECs migration, but also cell cycle progression during vessel growth although any PI3K catalytic

isoform has been related to EC proliferation until now. However, a recent study in which Serra et al. inactivated PTEN postnatally in ECs to avoid embryonic lethality has revealed that PTEN not only has PI3K-dependent function, but PI3K-indepedent nuclear functions, as well. Furthermore, they showed that Dll4/Notch signalling arrests stalk cell proliferation by inducing expression of PTEN. Therefore, PTEN deletion in ECs unbalances stalk cell numbers leading to an aberrant dense vasculature. PTEN is required for stalk cells' proliferative arrest during vessel development (Serra et al., 2015).

Zebrafish embryos lacking functional PTEN ($Ptena^{-/-}Ptenb^{-/-}$) display increased angiogenesis together with elevated pAKT and Vegfaa levels. Treatment with the PI3K inhibitor LY294002 rescues the vasculature hyperbranching phenotype indicating that these defects were caused by enhanced PI3K/Akt signalling (Choorapoikayil et al., 2013). Another study highlights the "lipid" phosphatase activity of PTEN during angiogenesis regulating PI3K signalling. Only the re-introduction of wild-type-PTEN or mutant-PTEN that retained lipid phosphatase activity can rescue the hyperbraching of ISVs generated by the loss of PTEN. Nevertheless, the "protein" phosphatase activity of PTEN is not necessary during angiogenesis (Stumpf and den Hertog, 2016). Most PTEN molecules are held in the cytosol in a closed conformation by intramolecular interactions between the C-terminal tail and core region. Dephosphorylation of the tail opens the conformation and enhances its dual localization (membrane and nuclear) and enzymatic activity (Nguyen et al., 2015). Expression of the open conformation human PTEN (PTEN QMA) or PTENb K13R (which enhances the accumulation of Ptenb at the cell membrane) in PTEN loss of function zebrafish embryos not only rescues the hyperbranching phenotype, but also generates stalled vessel (some ISVs do not connect to the DLAV.). Expression of PTENb K13R and PTEN QMA also induces stalled vessels and development defects in wild-type embryos. Stumpf and den Hertog showed that increased PTEN localization in the membranes causes excessive activity of PTEN towards PIP_3 and therefore decreases VEGF / VEGFR signalling pathway leading to stalled vessels (Stumpf and den Hertog, 2016).

1.5.3.2 Class II PI3Ks in ECs

Class II PI3Ks are monomers that are predominantly localized in intracellular membranes and produce mainly PtdIns(3)P *in vivo*. There are three members of the class II PI3K subfamily: PI3K-C2α, PI3K-C2β and PI3KCγ (Vanhaesebroeck et al., 2010). Until now, only PI3K-C2α has been involved in vascular morphogenesis *in vivo*. PI3K-C2α specifically localized in endosomes, the trans-Golgi and clatrin-coated vesicles and is highly express in endothelial cells. Constitutive ubiquitous and endothelial-specific deletion of PI3K-C2α leads to embryonic lethality due to severe defects in sprouting angiogenesis and vascular maturation. Differentially of class I PI3Ks, at the cellular level, PI3K-C2α is not only essential for EC migration, proliferation and survival but also in endosomal RhoA activation and in vesicular trafficking, regulating VE-cadherin trafficking to the membrane, VE-cadherin assembly at the cell-cell junction and internalization of activated VEGFR2. Thus, C2α is important in neovascularization and in the maintenance of the vascular integrity in quiescent vasculature (Yoshioka et al., 2012; Biswas et al., 2013).

1.5.4 Class I PI3Ks in pathology

PI3K / Akt / mTOR signalling pathway is one of the most frequently dysregulated pathways in cancer. Oncogenic PI3K signalling is derived from activating mutations in p110α catalytic subunit (PIK3CA gene) together with PIK3CA amplification, PTEN loss, AKT mutations, RTK amplification and KRAS mutations (Thorpe et al., 2014; Massacesi et al., 2016). For this reason, PI3K has been a very attractive pathway to target for cancer therapy. However, PI3K inhibitors have only shown slight efficacy in solid tumours as single therapy and also, have shown on-target effects, intrinsic and acquired drug resistance, and tolerability. Upon blocking of the pathway, a compensatory effect from other pathways allows the survival, proliferation and dissemination of cancer cells. Nowadays, several PI3K inhibitors are under clinical investigation, including pan-PI3K inhibitors (targeting all four isoforms of class I PI3K) and isoform-selective inhibitor. PI3K inhibitors are also under investigation in combination with different agents, to

avoid target-on effects due to negative feedback loops of the signalling axis and its crosstalk with other signalling pathways, and therefore, improve the clinical outcome. To date, many studies point to the use of PI3K inhibitors to target cancer stroma and, indirectly, influence tumour development and dissemination, specifically by targeting the vasculature and the immune system. For example, recently, a p110δ isoform-specific inhibitor has been approved to use for treatment of human B cell malignancies such as chronic lymphocytic leukaemia (CLL) (Brown et al., 2014). In the next section the effect of PI3K inhibitors as anti-angiogenic therapy will be described.

Somatic mutations in p110α (PIK3CA) and other members of the PI3K signalling pathway have been found in common cancers, but recently also in a spectrum of congenital or early-childhood-onset human overgrowth disorders as LM, VM, KTS, FAVA, and CLOVES (Kurek et al., 2012; Luks et al., 2015; Limaye et al., 2015). In particular, somatic gain-on-function mutations in PIK3CA have been found in venous malformations (Limaye et al., 2015). Surprisingly, PIK3CA mutations are similar to the ones found in cancer, suggesting that the context in which the mutation appears determines its role in disease. Due to the lethality, no germ-line mutations in PIK3CA were found in adult humans but are acquired post-zygotically. In the last two years evidence has increased that PI3K inhibitors can be useful for treating these diseases, providing an important update on the clinical development of PI3K pathway inhibitors (Roy et al., 2015; Castillo et al., 2016; Castel et al., 2016). Promising treatment with BYL719, a p110α-specific inhibitor or mTOR inhibitors (everolimus or rapamycin) effectively induces reduction of venous malformation (VM) volume and reduces proliferation (Castillo et al., 2016; Castel et al., 2016), reflecting the sensitivity that ECs have to p110α activity and reinforcing the importance of this protein in the vascular bed. Over-activation of p110α ubiquitously, or specifically in ECs, is embryonic lethal by E10.5 due to severe defects in vascular remodelling and angiogenesis in the developing embryo (Hare et al., 2015; Castel et al., 2016). $PIK3CA^{H1047R}$ mouse embryos present impairment in the formation of small vessels, failure in the remodelling of the primitive vasculature and enlargement of the vessels of the yolk sac. They also present a dramatic increase in VEGF levels, and also

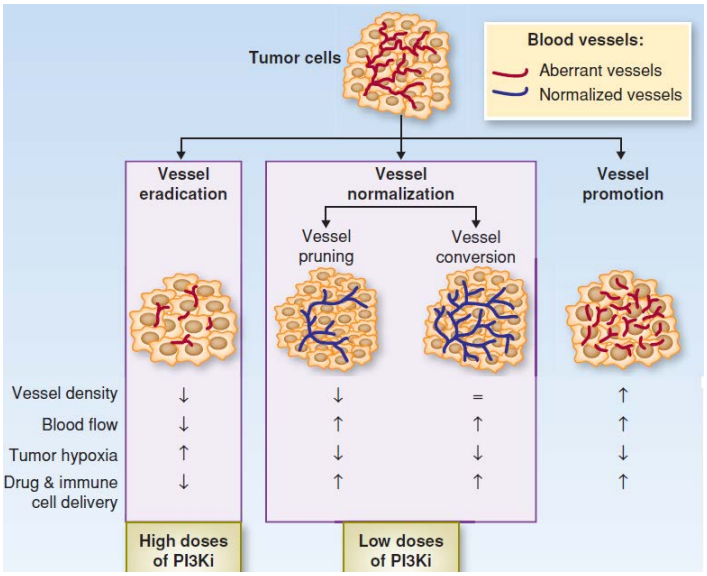

Figure 1.20: **Vascular targeting strategies in cancer with PI3K inhibitors.** (Modified and adapted from Okkenhaug et al., 2016)

in VEGF receptors NRP1, NRP2 and VEGFR-2 expression (Hare et al., 2015). On the other hand, postnatal expression of PIK3CA^{H1047R} in ECs results in retinal vascular hyperplasia together with increased EC proliferation. No differences in the number and length of sprouts were found suggesting no defects in the process of formation of new sprouts. However, endothelial hyperplasia did not present proper mural coverage and ECs lose arteriovenous markers (Castillo et al., 2016). Interestingly, this study has helped to understand the mechanical features that could be favouring the development of VMs upon p110α over-activation.

1.5.5 Targeting class I PI3Ks as anti-angiogenic therapy

Knowing the importance that PI3K signalling acquired in ECs prompted researchers to think that the blockage of this signalling pathway can be used as anti-angiogenic therapy. Furthermore, vascular development in physiological and pathological conditions requires the cooperation between endothelial cells and other cells types in which PI3K activity has also been described as playing a role (**Figure 1.17**). Therefore, using PI3K inhibitors to target the tumour vasculature can have an impact on tumour growth and dissemination. Unfortunately, the impact of PI3K inhibition on tumour angiogenesis in the clinic has not been examined. Preclinical studies have shown that the inactivation of PI3K/Akt/mTOR

signalling pathway leads to anti-angiogenic effects (Soler et al., 2015). This effect is explained by the impact of the drug on the cancer cells, on the ECs and on other stromal cells. The effect of PI3K inhibition on tumour vasculature is heterogeneous and depends mostly on the dose, but also partly on the genetic background. High doses of PI3K inhibitors reduce vessel function, independently of the vessel number, and therefore enhance intra-tumour hypoxia. However, in the end, increased hypoxia can accelerate tumour dissemination and metastasis and reduced functionality of the vessels, which implies reduced chemotherapy delivery to the tumour. There are also tumours with an intrinsic or acquired resistance to vessel pruning. These preclinical results were not very promising. Luckily, recent studies have suggested that PI3K treatment should be administrated in low doses that improve vascular functionality ("normalization" of the tumoural vasculature), and in this way, allow better drug delivery to the tumour and immunotherapy. Furthermore, target-off and target-on effects decrease due to reduced doses of the inhibitor being a more tolerable therapy (Soler et al., 2015; Okkenhaug et al., 2016). Schema of the different strategies in **Figure 1.20**.

To date, many studies try to elucidate whether it is better to use pan-PI3K inhibitors or isoform-specific inhibitors to target tumour stroma. No difference in the effect on tumour vasculature between the use of pan-PI3K or p110α-specific inhibitors has been found (Soler et al., 2016), however, the use of p110δ-specific or p110γ-specific inhibitors has shown decreased in tumour growth due to their role as immunomodulators in cancer, regulating T-cell responses and the myeloid cell compartment respectively (Okkenhaug et al., 2016).

1.6 Cytoskeleton

The cytoskeleton acts in several key functions of cell physiology, such as mitosis, cell division, volume control, cell stiffness, cell polarity, and extracellular matrix patterning, promoting tissue development and differentiation. Several intracellular and extracellular signals are received, integrated and transmitted by the cytoskeleton. Most of these cues signal through the lipid bilayer to the cytoskeleton, making membrane-cytoskeleton interactions essential for understanding how cytoskeletal remodelling is integrated throughout cells and

tissues. There are three cytoskeletal subsystems: actin, microtubules, and intermediate filaments. The cytoskeletal networks are essential for ensuring both the mechanical stability and dynamic shape changes of cells integrating various signals received at the membrane, and facilitating distinct functions in response (Bezanilla et al., 2015).

1.6.1 Actomyosin contractility: partners and regulation

Many cellular processes such as cell migration, shape changes, adhesion dynamics, endo- and exo-cytosis, and cytokinesis depend on interactions between actin filaments and myosin. In non-muscle cells, actin filaments and myosin form more disorganized and dynamic contractile networks.

Actin is approximately 5-15% of the total protein in endothelial cells. The actin cytoskeleton is a highly dynamic structure, and undergoes polymerization and depolymerization based on cellular demand. The actin organization and thus the signal transduction events in ECs can be different depending on the vascular bed and the type of vessel. Actin monomers (G-actin) polymerize to form actin filaments (F-actin). Actin polymerization need two sequential processes, nucleation and elongation. Otherwise, F-actin depolymerizes primary due to hydrolysis of bound ATP into ADP, resulting in loss of binding affinity between adjacent monomers. Numerous actin-binding proteins are responsible for the induction and regulation of the balance between G-actin and F-actin. F-actin can be lying just beneath the membrane (cortical actin) or extended throughout the cell cytoplasm forming actomyosin bundles needed to induce cell contraction (stress fibres) and thus, generate a centripetal tension that counteracts the centrifugal tension establish by the cortical actin rim. Both cell-cell and cell-matrix adhesion complexes are associated with F-actin fibres (Prasain and Stevens, 2009).

Non-muscle myosin II (NMII) is a actin-binding protein that has actin cross-linking and contractile properties and is regulated by the phosphorylation of its light and heavy chains (**Figure 1.21**). Mammalian cells express up to three isoforms of NM II (NM IIA, IIB, and IIC), each of which possesses distinct biophysical properties, and supports unique, as well as redundant, cellular functions. NMII is a hexamer that consists of two homodimerized heavy chains (NMHC), two

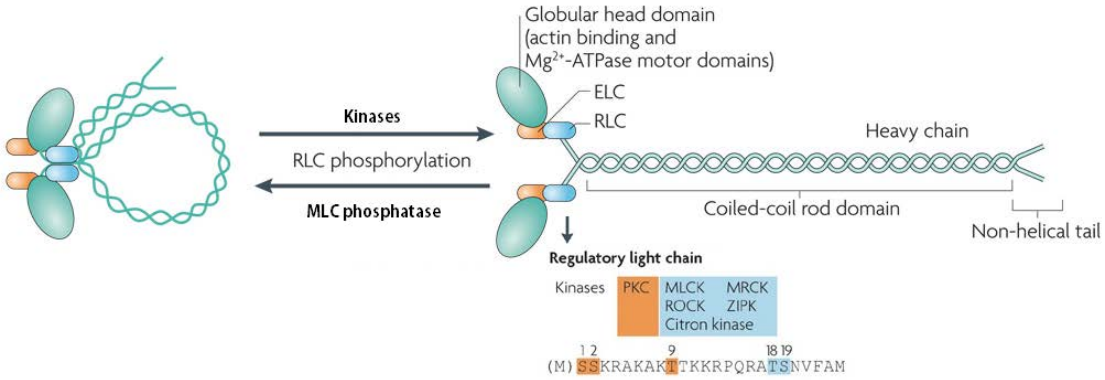

Figure 1.21: **Structure of non-muscle myosin II and its regulation.** NMII forms a dimer through interactions between the α-helical coiled-coil rod domains. The globular head domain contains the actin-binding regions and the enzymatic Mg2+-ATPase motor domains. The essential light chains (ELCs) and the regulatory light chains (RLCs) bind to the heavy chains at the lever arms that link the head and rod domains. In the absence of RLC phosphorylation, NMII forms a compact molecule through a head to tail interaction. This results in an assembly-incompetent form (left) that is unable to associate with other NMII dimers. On RLC phosphorylation, NMII becomes an assembly-competent form (right). Multiple kinases, including myosin light chain kinase (MLCK), Rho-associated, coiled coil-containing kinase (ROCK), citron kinase, myotonic dystrophy kinase-related CDC42-binding kinase (MRCK) and leucine zipper interacting kinase (ZIPK) can phosphorylate the regulatory light chain (RLC, also known as MLC) of NM II on Ser19 or on Thr18 and Ser19 to activate it. Protein kinase C (PKC) can phosphorylate the RLC on Ser1, Ser2 and Thr9 to inhibit NMII. MLC phosphatase de-phosphorylate RLC on Ser19 and Thr18. (Modified and adapted from Vicente-Manzanares et al., 2009)

regulatory light chains (RLC, normally called MLC), and two essential light chains (ELC). The motor activity, which allows myosin to move filamentous actin, is due to the ATPase activity that resides in the head domain of the heavy chain. Motor activity is induced by phosphorylation of the regulatory light chains. The heavy chain can also be regulated by post-translational modification of the tail domain, a region that is required for the assembly of multimeric myosin filaments (Vicente-Manzanares et al., 2009). NM-II activity and assembly state are tightly regulated. Mainly NMII activity is regulated by the reversible phosphorylation of the RLC. Phosphorylation of RLC in the residues S19 and T18 activates the enzymatic activity facilitating the filament assembly and thus, actomyosin-mediated contractility. Multiple kinases regulated by different upstream signals are able to phosphorylate the RLC (**Figure 1.21**). The most studied ones are non-muscle myosin light chain kinase (nmMLCK) and Rho-associated, coiled coil-containing kinase (ROCK), but also myotonic dystrophy kinase-related CDC42-binding kinase (MRCK; also known as CDC42BP), leucine zipper interacting kinase (ZIPK; also known as DAPK3), citron kinase (CK) and p21-associated kinase (PAK) have been described to phosphorylate RLC. Myosin light chain kinase (MLCK) and ZIPK activities are Ca2+/calmodulin influx dependent, ROCK, PAK, MRCK and CK are activated by Rho-GTPases and MRCK is Cdc42-GTPase dependent. In some cell types, ROCK and MLCK play distinct roles in the spatial regulation of RLC phosphorylation, MLCK is required to form cortical actin bundles, whereas activation by ROCK favours the assembly of stress fibres in the centre of cells (Totsukawa et al., 2000). Although Rac and Cdc42 signalling can promote RLC phosphorylation, they generally regulate actin polymerization, being RhoA-GTPase through ROCK the major cause for driving the formation of actomyosin filament bundles.

On the contrary, the **myosin light chain (MLC) phosphatase** (MLCP) is responsible for inactivating NMII by dephosphorylating RLC. MLCP is a trimeric heteroenzyme composed of a catalytic PP1c subunit, an associated regulatory targeting subunit (MYPT1, also known as PPP1R12A), and a smaller subunit, M20, of unknown function. PPIc exerts the catalytic function led by the MYPT regulation. MYPT1 have a RVxF motif near to the N-terminus to bind PP1c

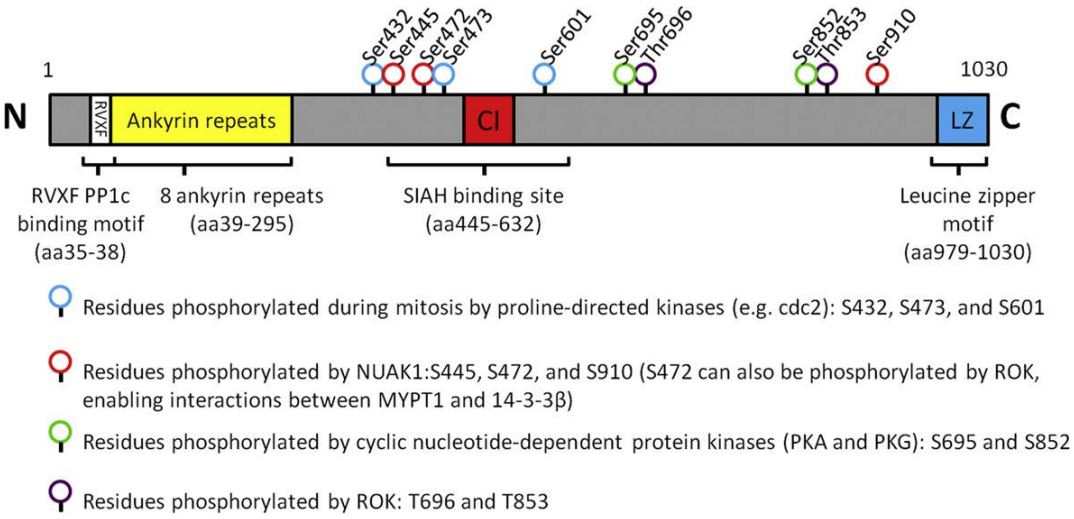

Figure 1.22: **MYPT1 regulatory subunit of MLC phosphatase complex.** Schematic representation of human MYPT1, highlighting the known phosphorylation sites. (Grassie et al., 2011)

catalytic subunit. The ankyrin repeat domain forms an interactive platform for binding to a variety of proteins, including the substrate phosphorylated myosin. The MYPT1-myosin interaction localizes PP1c in proximity to its substrate. The principal mechanism of regulation of MYPT functions involves phosphorylation within this central region by a variety of protein serine/threonine kinases (**Figure 1.22**). ROCK not only activates NMII activity by direct phosphorylation on RLC but also indirectly by the phosphorylation of MYPT1 regulatory subunit on T697 and T855 residues, thus, promoting dissociation of MYPT from myosin and decrease MLCP activity. In cell detachment, it has been described that activated NUAK1 interacts directly with MYPT1 and subsequently phosphorylates MYPT1 at S445, S472 and S910 (Zagorska et al., 2010). NUAK1-dependent phosphorylation of MYPT1 results in binding of 14-3-3β and suppression of MLCP activity. The C-terminal half of MYPT1 contains binding sites for M20, RhoA-GTP, acidic phospholipids and arachidonic acid which functions are less known.

The **myosin phosphatase-Rho interacting protein** (mRIP or p116 RIP) is a protein that interacts with the MYPT protein of the MLCP complex and

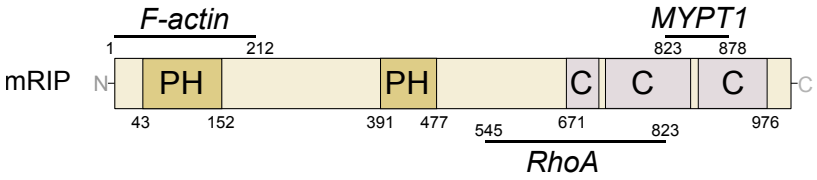

Figure 1.23: **mRIP protein.** Schematic representations of the 1024-amino-acid mRIP, with the pleckstrin homology domains (PH) and coiled-coiled domains (C), as well as minimal regions for actin binding (F-actin, amino acids 1–212) (Mulder et al., 2003), MYPT binding (amino acids 823–878) and RhoA-GTP (Surks et al., 2003), indicated.

participates in the recruitment of MLCP to dephosphorylate MLC on actomyosin fibers (**Figure 1.23**). mRIP binds directly to the leucine zipper domain in the C-terminus of the MYPT1. mRIP localizes MLCP to the actomyosin fibres by direct binding to the actin fibres, enhancing RLC dephosphorylation. It is controversial, whether mRIP is only acting as a scaffolding protein bringing close MLCP to the actomyosin fibres or also modifies its activity. Conversely, NUAK2-mRIP association inhibits fibre disassembly and MYPT1-mediated RLC dephosphorylation. NUAK2 acts as part of a positive-feedback loop contributing to actin stress fibre maintenance independently of its catalytic function (Vallenius et al., 2011). *In vitro*, mRIP can bind to the small GTPase RhoA acting as a GTPase-activating protein. Cytosolic GTP-bound RhoA interacts with mRIP, resulting in the acceleration of GTP hydrolysis. Inactivation of RhoA/ROCK signalling by mRIP also contributes to the increase in MLCP activity, thus reducing myosin phosphorylation in HeLa cells (Koga and Ikebe, 2004; Surks et al., 2005). mRIP protein also presents two PH domains not well studied yet.

2 Objectives

Class I PI3K signalling is required in a cell-autonomous manner in endothelial cells (ECs) for proper blood vessel growth. Although ECs express all class I PI3K isoforms, only the catalytic subunit p110α is required for vascular development and remodelling. However, little is known about the role of p110α-PI3K signalling in the different steps of vascular morphogenesis. Both the constitutive ubiquitous and constitutive endothelial-specific p110α mutant mice showed embryonic lethality. Therefore, we use an inducible system or pharmacological inhibition to determine the specific role that p110α-PI3K exerts in the sprouting angiogenic process, in particular, in endothelial cell contractility regulation. To reach this objective we have set up the following specific aims:

1. Study the relevance of the endothelial p110α-PI3K activity in vessel patterning during sprouting angiogenesis in postnatal mouse retinas and zebrafish embryos.

2. To identify molecular players downstream of endothelial p110α-PI3K signalling regulating physiological sprouting angiogenesis.

3 Methods and Materials

3.1 Mouse experiments

3.1.1 Mouse care

Mice were kept in individually ventilated cages and cared for according to the guidelines and legislation of the Catalan Departament d' Agricultura, Ramaderia i Pesca, with procedures accepted by the Ethics Committees of IDIBELL-CEEA.

3.1.2 Mouse models

To investigate the inactivation of p110α in ECs we used different transgenic mice available in the laboratory (**Figure.3.1**).

- **p110α^{D933A} mice:** These mice present a germline mutation in the ATP-binding site that change DFG motif to a AFG motif (knock-in strategy). This point mutation inactivates p110α kinase function but p110α^{D933A} protein is not degraded. In contrast to gene deletion, this approach preserves signalling complex stoichiometry and avoids possible compensation from other p110 isoforms (Foukas et al., 2006). Homozygous p110α$^{D933A/D933A}$ mice die at embryonic day 10 while heterozygous p110α$^{WT/D933A}$ mice are viable and just present a slight retardation in the vascular development that overcomes. Adult p110α$^{WT/D933A}$ mice show similar vasculature compared to wild-type mice.

- **p110α$^{Flox/Flox}$ mice:** In an attempt to circumvent the embryonic lethality exhibited by p110α homozygous mutants (Graupera et al., 2008), we have used a tamoxifen-inducible endothelial Cre line, Pdfgb-iCreER^{T2} transgenic mouse line (Claxton et al., 2008), in which the Cre is only active in endothelial cells after 4-OH tamoxifen administration crossed with p110α$^{flox/flox}$ mouse (Graupera et al., 2008). In this case, we can deplete p110α specifically in ECs postnatally by 4-OH tamoxifen administration (knock-out strategy). With this model we would expect to have full deletion of p110α; however,

Mouse line	Description	Source
p110α^{D933A}	*Pi3kca* knock-in mouse (carrying a germline mutation in the DFG motif of the p110α ATP binding site) that express a kinase-dead p110α^{D933A} protein. Homozygous lethal at E10.5. It is viable in heterozygosity.	(Foukas et al., 2006)
p110α$^{flox/flox}$	*Pi3kca* conditional knock-out mouse.	(Graupera et al., 2008)
p110α$^{flox/D933A}$	One *Pi3kca* allele is carried the germiline mutation in DGF motif of the of the p110α ATP binding site that express a kinase-dead p110α^{D933A} protein. Second *Pi3kca* allele is floxed.	In this study
Pdgfb-iCreER^{T2}	Tamoxifen-inducible Cre recombinase expression under Pdgfb endothelial specific promoter	(Claxton et al., 2008)
Rosa26-R-LacZ	Expression of *LacZ* gene after Cre-recombinase activity.	(Soriano, 1999)

Table 3.1: Mouse lines

total deletion of p110α will depend on the efficiency of recombination and the absence of p110α protein could lead to possible compensations by the other PI3K members.

- **p110α$^{Flox/D933A}$ mice:** For the majority of the experiments of this work we have used Pdgfb-iCreER^{T2} ;p110α$^{flox/D933A}$ mice. This model presents one allele with p110α floxed and the other allele with the constitutive kinase-death mutation D933A and the expression of iCreER^{T2} specifically in ECs. After 4-OH tamoxifen administration we obtained a Pdgfb-iCreER^{T2} ;p110α$^{i\Delta EC/D933A}$ mice, where only inactive p110α^{D933A} protein is expressed. The advantage of this model is that we get full inactivation of p110α without changes in the the signalling complex stoichiometry and without compensations from other PI3K family members.

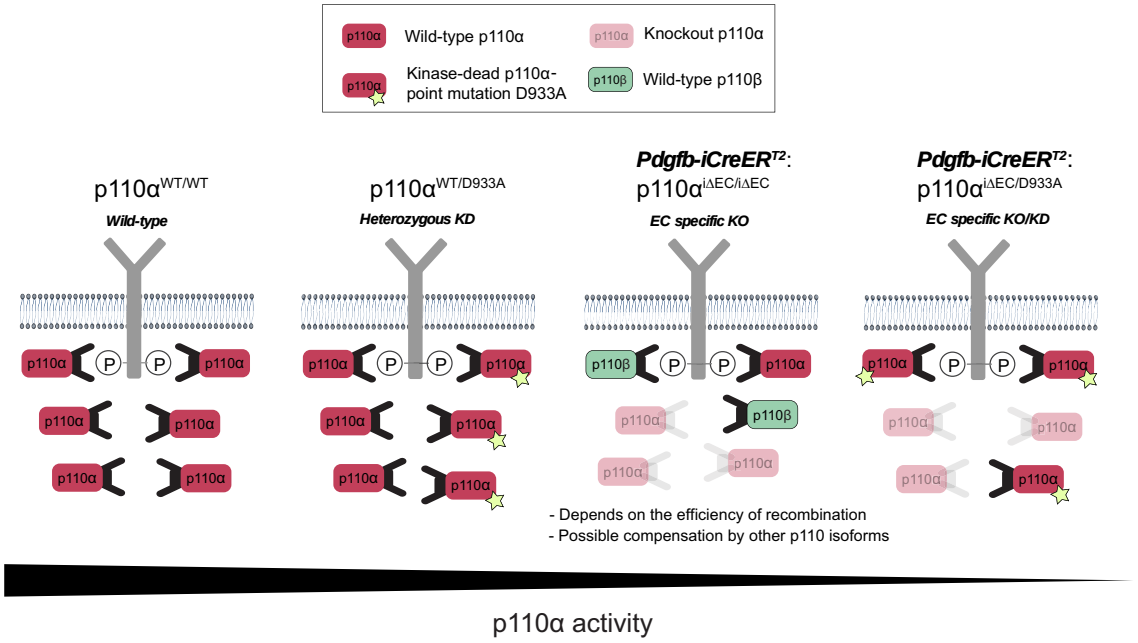

Figure 3.1: **Schematic representation of the mode of action of the different genetic strategies**

For experiments, breeding were set up between $p110\alpha^{flox/D933A}$ mice and Pdgfb-iCreER^{T2} ; $p110\alpha^{flox/flox}$ mice obtaining as offspring the principal transgenic mice models used in this thesis work: $p110\alpha^{flox/flox}$ (referred as Control), $p110\alpha^{flox/D933A}$ (referred as heterozygous), Pdgfb-iCreER^{T2} ; $p110\alpha^{flox/flox}$ (also referred as EC specific inducible knock-out) and Pdgfb-iCreER^{T2} ; $p110\alpha^{flox/D933A}$ (principal model of study). Pdgfb-iCreER^{T2} transgenic mice incorporate Cre recombinase protein fused to the mutant form of the human estrogen receptor (ER^{T2}) that is insensitive to estrogen but is responsible to the artificial ligand 4-OH tamoxifen. CreER^{T2} is expressed under the endothelial-specific promoter Pdgfb. Hence, Cre-mediated recombination and deletion of floxed p110α can be induced in endothelial cells expressing Pdgfb upon 4-OH tamoxifen administration. As consequence, in the absence of 4-OH tamoxifen, the iCreER^{T2} protein remains in the cell cytoplasm sequestrated by the heat shock protein 90 (Hsp90), whereas, in presence of 4-OH tamoxifen, the iCreER^{T2} is translocated to the nucleus to mediate loxP-specific recombination events. In the absence of Cre-ER^{T2}, upon 4-OH tamoxifen administration floxed p110α can not be recombined and $p110\alpha^{flox/flox}$ mice is used as control.

Gen	PCR type & Primers	Program	Type
p110α	PCR type II ma36: CCTAAGCCC TTAAAGCCTTAC ma47:ACTGCCATGC AGTGGAGAAGCC	1. 94ºC 3 min 2. 94ºC 30 s 3. 65ºC 30 s 4. 72ºC 30 s 5. 2-4 for 39 cicles 6. 72ºC 7 min 7- 16ºC- hold	II
pdgfb-iCreER^{T2}	PCR type I EGFP_3UTR_FW: 5'-CCAGCCGCCGTCGCAACT-3' EGFP_3UTR_RV : 5-'GCCGCCGGGATCACTCTCG-3' IL-2 FW: 5'-CTAGGCCACAGAATTGAAAGATCT-3' IL-2 RV: 5'- GTAGGTGGAAATTCTAGCATCATCC-3'	1-94ºC - 4min 2- 94ºC - 30sec 3- 57.5ºC - 45sec 4- 72ºC - 1min 5- From 2 to 4 x 34 cycles 6- 72ºC - 5min 7- 16ºC- hold	I
Rosa26-R	PCR type I R1:5'-AAAGTCGCTCTGAGTTGTTAT-3' R2: 5'-GCGAAGAGTTTGTCCTCAACC-3' R3: 5'-GGAGCGGGAGAAATGGATATG-3'	1-94ºC - 2min 2- 94ºC - 30sec 3- 50ºC - 30sec 4- 72ºC - 40sec 5- From 2 to 4 x 40 cycles 6- 72ºC - 5min 7. 16ºC - hold	I

Table 3.2: PCR conditions and primers

3.1.3 Mouse genotyping

3.1.3.1 Tissue digestion

New born mice were weaned once they turned 3-weeks old. Upon weaning tail biopsies were kept for genotyping. Tissue was lysated with 600 µl of 50 mM NaOH (Sigma). Samples were incubated at 100ºC for 15 min and were vortexed and kept at room temperature (RT) until they reached 50-70ºC. To neutralize the samples, 100 µl of 1M Tris HCl pH 7.4 (Sigma) were added to each sample. Samples were vortexed, centrifuged at maximum speed for 1 min and kept at 4ºC until samples were processed for DNA amplification.

3.1.3.2 PCR

Polymerase chain reactions (PCR) were performed using two different protocols referred as PCR reaction I and PCR reaction II. **Table 3.2**

- PCR reaction I (to a final volume of 30 µl): 2 µl DNA sample, 15.75 µl H_2O, 3 µl $MgCl_2$ 15mM (diluted from $MgCl_2$ 50 mM Ecogen, #MG-110C), 3 µl of 10X reaction buffer without Mg (Ecogen), 3 µl of 10M primer pool (forward+reverse), 3 µl dNTPs and 0.35 µl Ecotaq DNA polymerase (Ecogen, #BT-314106).
- PCR reaction II (to a final volume of 25 µl): 1.5 µl DNA sample, 15.875 µl H_2O, 2.5 µl 10X Titanium taq reaction buffer, 2.5 µl of 10 M primer pool (forward+reverse), 2.5 µl dNTPs and 0.125 µl 50X titanium taq polymerase (Clontech, #K1915- y).

Mastercycler (Eppendorf) was used to perform PCRs. PCR reactions were then separated on a 2% agarose (Sigma) gel diluted in TAE buffer 1X (from a TAE 50X stock: 242 g Tris base (Sigma), 57.1 ml acetic acid glacial (Panreac) and 100ml EDTA 0.5 M pH8 (Gibco, #15575) in dH_2O) with ethidium bromide (Sigma).

3.1.4 Pharmacological treatments in mouse

3.1.4.1 Induction of Cre mediated gene deletion

Cre activity and gene deletion were induced by intraperitoneal injections of 4-OH tamoxifen (Sigma, #H7904). 25 mg of 4-OH tamoxifen powder were dissolved in ethanol to obtain a working solution of 10mg/ml. The solution was aliquoted under sterile conditions and stored at -20ºC. New born mice were injected at specific postnatal days with 25 µg/pup/day of 4-OH tamoxifen. Remarkably, 4-OH tamoxifen solution needed to be previously homogenized to avoid precipitates. A Hamilton syringe (Hamilton Company, #80087) was used for injection. Pups derived from Pdgfb-iCreER^{T2} ;p110α$^{Flox/Flox}$ / p110α$^{flox/D933A}$ breedings were injected with 4-OH tamoxifen at postnatal days 1 (P1) and P2 and tissue of interest was collected at P6, P7, P10 or P15.

Name of the inhibitor	Specificity	Concentration used	KI: Inhibitory Constant
GDC-0326 from Genentech	p110α	1 μM *in vitro*	0.2 nM p110α, 133 nM p110β, 20 nM p110δ i 51 nM p110γ
Y-27632 from Calbiochem	ROCK1	10μM *in vitro*; 30mg/kg *in vivo*	140 μM ROCK1
VX-680 from Selleck	pan-Aurora kinase	50mg/kg *in vivo*	0.6 nM Aurora A Less potent towards Aurora B/ C

Table 3.3: Inhibitors used *in vivo* and *in vitro* and their inhibitory constant

3.1.4.2 Aurora kinases inhibition through VX-680 injection

VX-680 (Tozasertib) was bought from Selleck (Selleck #1048, **Table 3.3**) and was resuspended in DMSO to generate a working solution of 7.5 mg/ml. Half of a wild-type litter was injected subcutaneously at P6 (6 pm) and P7 (10 am) with 50 mg kg^{-1} of VX-680 (20 μl of 7.5 mg/ml working solution). Same volume of DMSO was injected to the other half of the litter to obtain the control condition. Retinas were isolated at P7 (6 pm) for analysis.

3.1.4.3 ROCK inhibition through Y-27632 injection

ROCK inhibitor, Y-27632 (Calbiochem, 688000, **Table 3.3**), was resuspended in DMSO to generate a working solution of 4.5 mg/ml. Half of the litter was injected intraperitoneally at P6 (6 pm) and P7 (10 am) with 30 mg kg^{-1} of Y-27632 (20 μl of 4.5 mg/ml working solution). Same volume of DMSO was injected to the other half of the litter to obtain the control condition. Retinas were isolated at P7 (2 pm) for analysis.

3.1.5 Postnatal mouse retina isolation and staining

3.1.5.1 Eyes extraction and retina isolation

Pups were sacrificed by decapitation and eyes were quickly removed using scissors and forceps. Eyes were fixed in a solution of 4% paraformaldehyde (PFA, Sigma, #15.812-7) in phosphate-buffered saline (PBS) for 45 min at 4ºC. Then eyes were washed in PBS followed by dissection of retinas. The procedure of retina isolation was done with the help of a binocular dissecting microscope (Carl Zeiss). Briefly, eyes were collected in a clean culture dish filled with PBS and the cornea was incised with the help of a needle. Using micro-scissors (Fine Science Tools, #15000-10), the cornea was cut and removed. Next, the iris was also removed using two forceps (Fine Science Tools, #11252-00) and the outer layer of the eye, the sclera and the pigmented retina layer started to be separated. The outer layer should be dissected carefully, in small increments, to avoid damaging the retina layer beneath. At this point, the lens and the vitrous humor, which appear as a single jelly-like structure need to be removed. Finally, the hyaloids vessels were carefully detached from the inner side of the eye using fine movements. Isolated retinas were fixed for 1h at 4ºC and were kept in PBS at 4ºC until they were processed for immunofluorescence (IF). Procedure details are shown in **Figure 3.2.**

3.1.5.2 Staining of whole-mount retinas

3.1.5.2.1 Immunofluorescence staining with primary antibodies

Retinas were blocked with permeabilization buffer (1% bovine serum albumin (BSA, Sigma), 0.3% Triton X-100 in PBS) ON at 4ºC with gentle rocking. Then, retinas were incubated with primary antibodies in appropriate dilutions (**Table 3.4**) in permeabilization buffer ON at 4ºC with gentle rocking. The following day, primary antibodies were removed and retinas were washed 3 times (10 min each) with PBT buffer (0,1% Tween-20 in PBS). Retinas were further incubated 30min at RT in Pblec buffer (1% Triton X-100, 1 mM $CaCl_2$, 1 mM $MgCl_2$and 1 mM $MnCl_2$ in PBS pH6.8) and then, they were incubated ON at 4ºC or 2h at RT

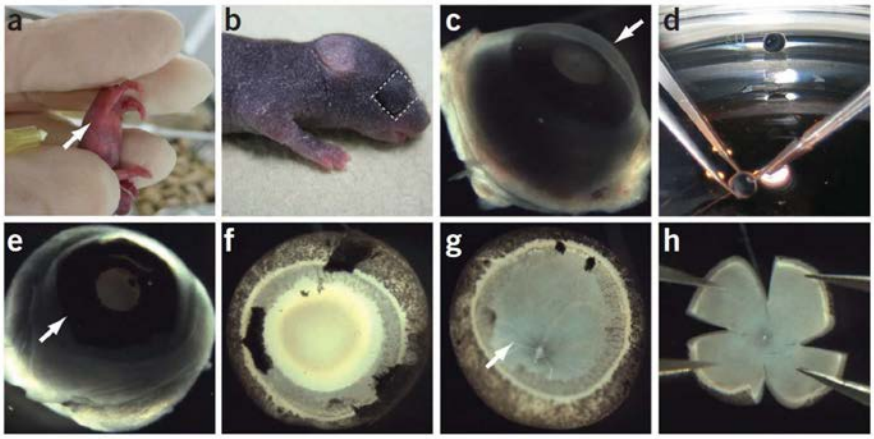

Figure 3.2: **Tamoxifen injection, eye isolation and retina dissection**. a, Intragastric tamoxifen injection in a P1 and P2 mouse pup. b, Image showing where to make the incisions around the eye of the pup. c, Dissected eyeball from a P6, P7, P10 or P15 pup. Arrow points to the cornea surface. d, Overview of cornea dissection. e, Eyeball without cornea. Arrow indicates dissected cornea. f, Image showing eye without sclera, choroid, cornea layers, pigmented layers and without the iris. g, Dissected eye without lens. Arrow shows hyaloid vessels. h, Retina with four radial incisions. Figure modified from (Pitulescu et al., 2010).

with the appropriate dilution of secondary antibodies (**Table 3.5**). Conjugated isolectin-B4 and phalloidin were added together with the secondary antibodies in the appropriate dilution (**Table 3.4**). Then, retinas were washed 3 times, 10 min each with PBT. After antibody staining, retinas were post-fixed in 4% PFA for 5min. It the end, between 4-5 incision were made in the retinas to flat-mounted them on glass slides using Mowiol (Calbiochem, #475904) with DAKO (Sigma) as mounting medium. All the incubation were done in 2 ml tubes (Eppedorf).

3.1.5.2.2 *In vivo* proliferation assay by Edu detection

EdU is a syntetic analogue of thymidine, and therefore, it can be incorporated into DNA during S phase. The Click-iT EdU Imaging Kit (Invitrogen, #C10337 and #C10340) was used for EdU injection and detection. To determine the number of proliferating ECs in the growing retinal vasculature, pups were injected intraperitoneally with 60 µl of component A from the kit (diluted to 0.5 mg/ml in 50% DMSO: 50% PBS) 2h before they were sacrificed for retina extraction as described in **section 3.1.5**. Then, the reaction for EdU detection was performed following the instructions the Click-iT Imaging Kit. Briefly, each pair of retinas were

incubated for 1h at RT with gentle rocking in 100 µl of EdU detection solution (8,6 µl of 10X Click-iT EdU reaction buffer in 77,4 µl of H_20 (component D), 4 µl of CuSO4 (component E), l µl of 10X azyde-conjugated Alexa-Fluor in 9 µl of H_20 (component F) and 0,24 µl of alexa 633 (component B)). Retinas were washed twice with PBS and then, they were incubated with permeabilization buffer ON at 4ºC with gentle rocking. Thereafter, retinas were incubated in appropriate dilution of Erg 1,2,3 antibody (**Table 3.4**) in permeabilization buffer ON at 4ºC with gentle rocking. The day after, retinas were washed 3 times with PBT at RT, followed by 30 min incubation with Pblec buffer at RT. Secondary antibody against Erg1,2,3 and isolectin-B4 were incubated ON agitating at 4ºC in appropriate dilutions (**Table 3.5**). Retinas were washed 3 times (10 min each) with PBT and post-fixed for 5 minutes with 4% PFA at RT. Finally, they were flat-mounted on glass slides using Mowiol with DAKO. Quantification of proliferative ECs was done as detailed in **3.1.7.6.**

3.1.5.2.3 β-gal staining to test recombination efficiency

For β-gal staining, eyes were fixed in 1% PFA in PBS for 45min. Retinas were dissected as described in **section 3.1.5**. Upon isolation, retinas were fixed for 1h in 1% PFA and then they were washed once in PBS. Retinas were incubated in detergent rinse (0.1M phosphate buffer pH 7.3, 2 mM $MgCl_2$, 0.01% sodium deoxycholate and 0.02% Nonidet P-40) twice for 20min each time at RT. Then, retinas were incubated in β-gal staining solution (containing 0.1M phosphate buffer pH 7.3, 2 mM $MgCl_2$, 0.01% sodium deoxycholate, 0.02% nonidet P-40, 5mM potassiumferricyanide, 5 mM potassiumferrocyanide and 1mg/ml X-gal (5-bromo-chloro-indolyl-galactopyranoside, Roche, #10703729001)) at 37ºC for 1h with gentle rocking. After the incubation, retinas were washed twice (20min each time) in detergent rinse and once in PBS for 10 min. Finally, retinas were post-fixed in 4% PFA for 10 min at RT and flat-mounted on glass slides using Mowiol with DAKO.

Antibody	Conj	Host	Dilution	Company	Catalogue #
VE-cadherin	-	Rat	1:50	BD Bioscience	555289
Erg 1,2,3	-	Rabbit	1:100	Santa Cruz	sc-353
Erg 1,2,3	-	Rabbit	1:400	Abcam	ab92513
pS19-MLC	-	Rabbit	1:100 retinas; 1:200 cells	Rockland	600-401-416
pS19T18-MLC	-	Rabbit	1:100	Cell Signalling	3674
ICAM-2	-	Rat	1:100	BD Pharmingen	553326
p-S6	-	Rabbit	1:100	Cell Signalling	2215S
Par-3	-	Rabbit	1:100	Millipore	07-330
Collagen IV	-	Rabbit	1:50	Millipore	AB756P
Cleavege caspase-3	-	Rabbit	1:100	Cell Signalling	9664
β-catenin	-	Mouse	1:200	BD Bioscience	610153
Isolectin GS-IB4	488	-	1:300	Mol. probes	I21411
Isolectin GS-IB4	568	-	1:300	Mol. probes	I21412
Isolectin GS-IB4	647	-	1:300	Mol. probes	I32450
Phalloidin	568	-	1:400	Mol. probes	A12380
Phalloidin	647	-	1:400	Mol. probes	A22287

Table 3.4: List of primary antibodies used for immunofluorescence in mouse retinas or cultured cells

Antibody	Conjugated	Dilution	Company	Catalogue #
Goat anti-rabbit	Alexa Fluor 488	1:300	Invitrogen	A11008
Goat anti-rabbit	Alexa Fluor 568	1:300	Invitrogen	A11011
Donkey anti-rabbit	Alexa Fluor 647	1:300	Invitrogen	A31573
Goat anti-rat	Alexa Fluor 488	1:300	Invitrogen	A11006
Goat anti-rat	Alexa Fluor 568	1:300	Invitrogen	A11077
Goat anti-rat	Alexa Fluor 633	1:300	Invitrogen	A21094
Goat anti-mouse	Alexa Fluor 488	1:300	Invitrogen	A11001
Goat anti-mouse	Alexa Fluor 568	1:300	Invitrogen	A21236
Goat anti-mouse	Alexa Fluor 633	1:300	Invitrogen	A-11031

Table 3.5: List of secondary antibodies used for immunofluorescence in mouse retinas or cultured cells

3.1.5.2.4 Senescence detection in mouse retinas

Senescence Detection Kit from Calbiochem was used to detect cell senescence (Calbiochem, QIA117). Eyes and retinas were isolated from P15 pups as has been described in **section 3.1.5**. Differently, the fixation after the isolation of the retinas was done with 0,5ml of Fixative Solution from the kit at RT for 15min. Then, retinas were washed twice with 1ml 1X PBS. Subsequently, 0,5 ml of Staining Solution MIX was added to the tube (470 µl Staining solution, 5 µl Staining supplement, ad 25 µl of 20mg/ml X-gal in DMF) and retinas were incubated at 37ºC ON. The following day, retinas were washed with PBS and fixed for 10 min with 4% PFA. Then, they were further incubated 30 min at RT in Pblec buffer (1% Triton X-100, 1mM $CaCl_2$, 1mM $MgCl_2$and 1mM $MnCl_2$ in PBS pH6.8) and incubated ON at 4ºC or 2h at RT with the appropriate dilution conjugated isolectinB4 to also visualize the vasculature.

3.1.5.3 Real-time PCR

3.1.5.3.1 RNA isolation

For total RNA isolation of retinas, pups were culled by decapitation, eyes were removed and without being fixed, retinas were isolated freshly as described in

Gene	Reference
HPRT	Mm00446968_m1
CDH-5	Mm00486938_m1
Hes-1	Mm01342805_m1
Hey-1	Mm00468865_m1
Dll4	Mm00446968_m1

Table 3.6: Primers used for qRT-PCR using TaqMan Gene Expression Assay

section 3.1.5. Upon isolation, retinas were quickly snapped frozen in dry ice and were processed for RNA extraction using the RNeasy Plus Kit (Qiagen) as recommended by manufacturer. RNA was eluted in a final volume of 30µl and quantified using NanoDrop 1000 (Thermo Scientific).

3.1.5.3.2 cDNA synthesis

cDNA was produced from 0.5 g of RNA using the High Capacity cDNA Reverse Transcription Kit (Applied Biosystems) following the protocol recommended by manufacturer.

3.1.5.3.3 Relative quantitative PCR

TaqMan Gene Expression Assays developed by Applied Biosystems were used for relative quantitative PCR (qPCR) experiments to compare differences in gene expression of Dll4, Hey1 and Hes1 between different animals of different genotypes. PCR was carried out in TaqMan Universal PCR Master Mix (Applied Biosystems) using Applied Biosystems 7900HT sequence detection system. Gene expression was normalized to the endogenous control HPRT and VE-cadherin (CDH-5), and an average ΔCt value was calculated for each animal. See **Table 3.6** for FAM/TAMRA primers used from Applied Biosystems.

3.1.6 Confocal imaging

Leica TCS SP5 confocal microscope was used. Images were taken with objectives: 10x, 20x, 40x (oil) and 63x (oil) objectives. All images are maximal

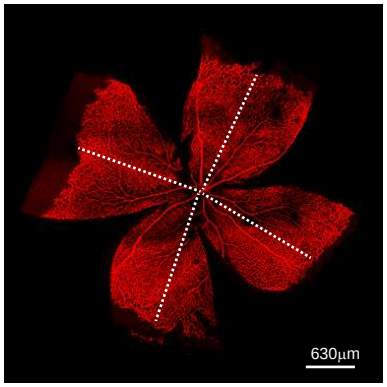

Figure 3.3: **Quantification of radial expansion.**

z-stack projections (unless specified otherwise). Images were processed using Volocity, Fiji and Adobe Photoshop CS5. Only images in **Figure 4.3.C** were taken with the Nikon microscopy 801.

3.1.7 Methods used for quantifying vessel features

Image processing and analysis was performed using the ImageJ, Fiji and the Adobe Photoshop CS5 software.

3.1.7.1 Radial expansion

The migratory length of the vascular plexus was analysed by measuring the total length of the retinal vasculature from the optic nerve towards the retinal periphery (**Figure 3.3**). Four measurements were made from each retina. The average distance of vessel migration per retina was used in comparisons between animals of different genotypes. Images for the radial expansion quantification were taken with the 4x objective of the Nikon 801 microscope.

3.1.7.2 Vascular branching

The number of branch points per field of $10^4 \mu m^2$ behind the vascular sprouting front or in the capillary area were quantified as shown in **Figure 3.4**. Six images of the sprouting front or of the capillary area were taken from each retina and, at least five retinas per genotype were analysed. Quantified images were taken with the 40x objective.

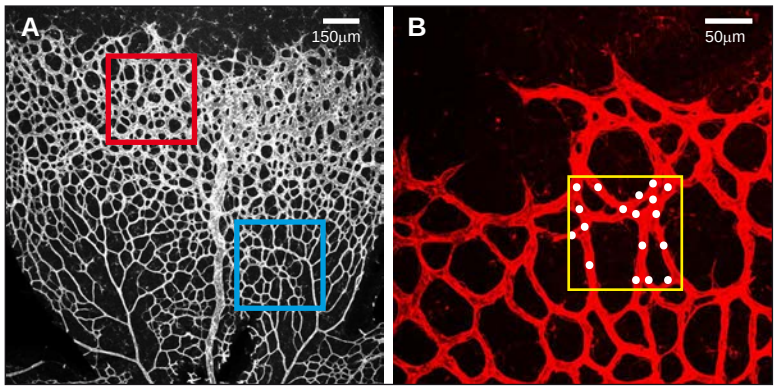

Figure 3.4: **Quantification of vessel density. (A)** Vessel density was analysed in the sprouting front (red box) and in the inner retina (blue box). **(B)** The number of branching point were quantified in six field of $10^4 \mu m^2$ per retina as shown the yellow box.

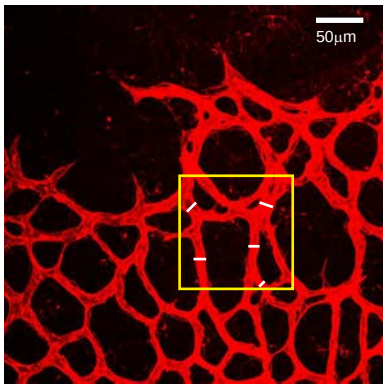

Figure 3.5: **Quantification of vessel width in mouse retinas.** The width of five representative branches were quantified in a field of $10^4 \mu m^2$per image.

3.1.7.3 Vessel width

A visual field of $10^4 \mu m^2$ was determined behind the vascular sprouting front of images taken with the 40x objective. Vessel width (µm) was determined using ImageJ software with the proper scale set up (**Figure 3.5**). Six images of the sprouting front were taken from each retina and vessel width of five representative branches were quantified per image, and at least four retinas per genotype were analysed.

3.1.7.4 Number of sprouts

The number of sprouts was expressed as number of sprouts per 100µm of the perimeter of the sprouting front. For this, the total vessel length of the sprouting front was determined using images taken with the 40x objective with the proper

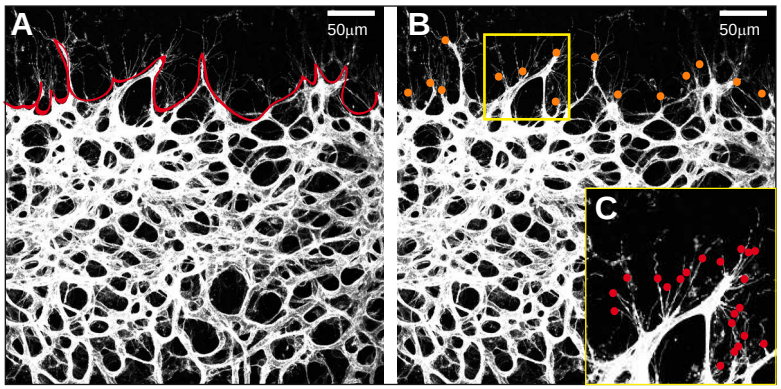

Figure 3.6: **Quantification of the number of sprouts and filopodia in the sprouting front. (A)** The perimeter of the sprouting front was measured with the proper scale set up in 40x images. Then, the number of sprout **(B)** and filopodia **(C)** were quantified as shown and divided by the length of the sprouting front.

scale set up, as shown in **Figure 3.6**. Thereafter, the number of sprouts present throughout the sprouting membrane was quantified. Six images of the sprouting front were taken from each retina and at least nine retinas per genotype were analysed. Graphs represent the number of sprout in 100 µm of sprouting front.

3.1.7.5 Filopodia quantification

The number of filopodia in the perimeter of the sprouting front was quantified (**Figure 3.6**). The number of filopodia/100µm distance was plotted. Six images of the sprouting front were taken from each retina and at least nine retinas per genotype were analysed.

3.1.7.6 Quantification of ECs nuclei

The number of nuclei stained with Erg1,2,3 was counted in a visual field of 10^4 μm^2 determined behind the vascular sprouting front of images at 40x (**Figure 3.7, green square)**. Six images of the sprouting front were taken from each retina.

3.1.7.7 Quantification of proliferative ECs

A field of 200x200 µm (**Figure 3.7 , yellow square**) was determined behind the vascular sprouting front of images taken with the 40x objective from retinas stained for EdU, Erg1,2,3 and isolectin-B4. The number of Edu^+ (green)- Erg^+(red) divided

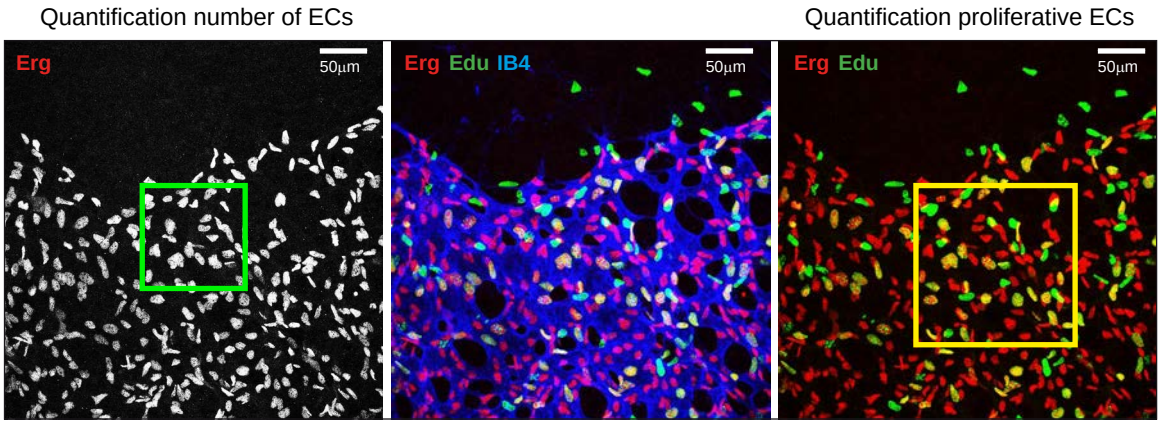

Figure 3.7: **Quantification of EC nuclei and EC proliferation in mouse retina.**

by the total number of Erg^+ EC nuclei within this visual field of 200x200 µm was represented as % of proliferative ECs. Six images of the sprouting front were taken from each retina.

3.1.7.8 Quantification of phalloidin and pS19-MLC staining intensity in the retinal vasculature

The quantification was done using the Image J software in images taken with the 40x objective and proper scale set up. I quantified total intensity of the corresponding staining (phalloidin or p-MLC) over the isolectin-B4 positive area as shown in **Figure 3.8**. For that, first I splitted channels from maximal z-stack projections. From maximal z-stack projections, the isolectin-B4 channel was used to establish the vascular area by setting a manual threshold to have a binary image. Isolectin-B4 positive area was used as template to measure the intensity of the other channels (phalloidin and p-MLC) in this area. Area and integrated density parameters were measured. Then, to calculate the corrected total fluorescence (CTF) the following formula was used:

- CTF = Integrated Density – (Area selected for Isolectin-B4 positivity x Mean fluorescence of background readings).

The background readings were taken from three areas close to the vasculature but negative for isolectin-IB4. The average of the CTF of different retinas is the value represented in the graphs named as integrated density.

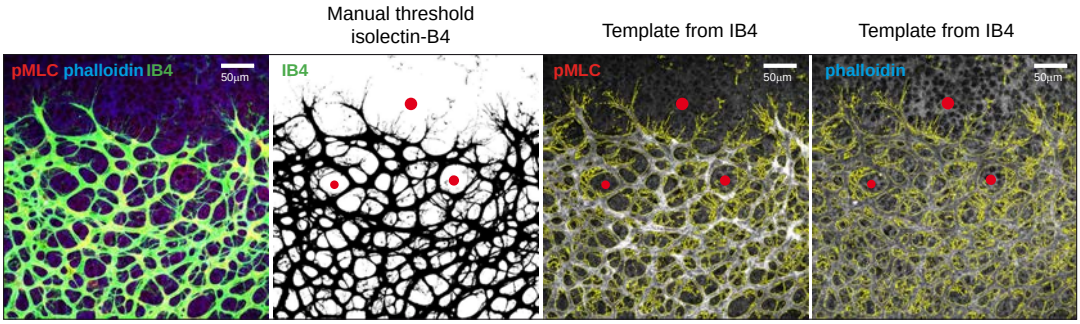

Figure 3.8: **Quantification of the staining intensity in the retinal vasculature.** Red dots represent areas used for measuring the background

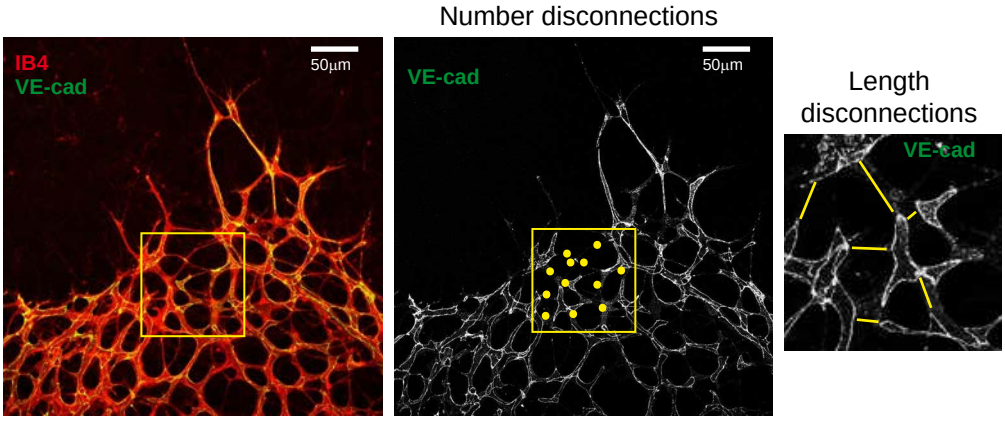

Figure 3.9: **Quantification of VE-cadherin staining.** Yellow dots indicate branch points negative for VE-cadherin staining. Yellow lines indicate how was measured the distance between two branches without VE-cadherin staining.

3.1.7.9 Quantification VE-cadherin and ICAM-2 staining

First, a visual field of $10^4 \mu m^2$ was determined behind the vascular sprouting front of images taken with the 40x objective. To quantify the number of VE-cadherin disconnections, there was counted the number of branch points (Isolectin-B4 positive) negative for VE-cadherin staining (**Figure 3.9**). To quantify the length of the vessel without VE-cadherin staining, the distance between two points positive for VE-cadherin was measured in proper scale images as shown in **Figure 3.9**.

Similarly, to quantify the number of lumen disconnections, there was counted the number of branch points (Isolectin-B4 positive) negative for ICAM-2 staining.

3.2 Cell culturing

3.2.1 Culturing of HEKs

Human embryonic kidney cells 293 (HEKs) were cultured in DMEM (Lonza) containing 10% FBS (Gibco) and 1% P/S.

3.2.1.1 Specific inhibition of p110α with the GDC-0326 inhibitor

HEKs were seeded and treated with 1μM GDC-0326 inhibitor (from a stock solution of 1,5 mM in DMSO, Genentech) or DMSO for 48h hours.

3.2.1.2 Immunoprecipitation of MYPT in HEKs

Immunoprecipitations were performed using MYPT1 antibody (**Table 3.9**) covalently coupled to protein G-Sepharose (GE Healthcare, #17-0618-01) (1 μg of antibody per 1 μl of beads) with a dimethyl pimelimidate cross-linking procedure. Cells treated with DMSO or GDC-0326 for 48h were lysed with IP buffer (50 mM Tris pH 8.0, 150 mM NaCl, 0,1% SDS, 1% NP40, 0,5% sodium deoxycolate,1 mM pepstatin A, 1 M leupeptin, 10 g/ml TLCK, 1 mM PMSF, 50 mM NaF, 1 mM $NaVO_3$ and 1 μM okadaic acid) and clarified by centrifugation at max. speed for 15 min at 4 °C. Cell lysate (1 mg) was incubated with 5 μg of coupled antibody for 1 hour at 4°C. Immunoprecipitates were washed four times with IP buffer and resuspended in 1X SDS Sample Buffer. Immunoprecipitates and cell lysates (50 μg) were subjected to electrophoresis on a 8% polyacrylamide gel and transferred to nitrocellulose membranes. For sheep antibodies, the membranes were incubated for 30 min with TBS-T containing 10% (w/v) skimmed milk. The membranes were then immunoblotted in 5% (w/v) skimmed milk in TBS-T with the MYPT primary antibody (1 μg/ml) overnight at 4°C. The incubation with phosphospecific MYPT sheep antibody was performed with the addition of 10 μg/ml of a dephosphopeptide variant of the antigen used to raise the antibody (**Table 3.9**). Commercial antibodies were used as indicated in **Table 3.9**.

3.2.2 Culturing of mouse lung endothelial cells (mLECs)

3.2.2.1 Endothelial cell isolation from mouse lungs

3.2.2.1.1 Tissue digestion

Mice of the respective genotypes were sacrificed by cervical dislocation and their lungs were removed and kept in ice cold Hank's balanced salt solution (Gibco) containing 1% penicillin/streptomycin (P/S, Gibco). Once in the cell culture primary hood, lungs were minced with a scalpel. Then, lung pieces were poured through a 40 µm cell strainer, placed on a 50 ml Falcon tube, to remove blood constituents. Tissue pieces were digested in 5ml 4U/ml of dispase II (Gibco, #17105-041) for 1h at 37ºC. Thereafter, the suspension containing lung pieces was homogenized by pippetting up and down to release single cells from the tissue pieces. Then, DMEM (Lonza, #BE12-604F) containing 10% of inactivated FBS (Gibco, #10270-106) and 1% P/S was added to the cell suspension and the homogenate was filtered through a 40 µm cell strainer, placed on a 50ml. A pellet containing mouse cells was obtained by centrifugation (5min 1200rpm). The pellet was washed twice with PBS/BSA (PBS containing 0.5% BSA (diluted from PAA, #K11-022), performing a 5 min centrifugation (1200rpm) after every wash.

3.2.2.1.2 First selection

The resulting cell pellet from the last centrifugation was re-suspended in 100µl of PBS/BSA. Previously, we have prepared magnetic beads coated with VE-cadherin (BD Pharmigen, #555289) used to isolate specifically endothelial cells from the lung homogenate. 6µl/lung of magnetic beads were placed into a 1.5ml eppendorf and were washed five times with PBS/BSA using a Dynal magnet (Dynal, MCP-S). After the last wash, magnetic beads were re-suspended in 6µl of PBS/BSA and finally, 1.25µl/lung of VE-cadherin antibody were added. The mixture of magnetic beads and VE-cadherin was incubated 1h at RT with gentle shaking. Magnetic beads were then washed four times with PBS/BSA using a magnet for cell separation. Then, 100 µl of PBS/BSA were added into the eppendorf and the mixture was homogenized and transferred to incubate with

the 100 µl of cell suspension for 30 min at RT. Then, magnetic beads were washed four times with PBS/BSA using a magnet for cell separation. After the final wash, magnetic beads coupled with ECs were re-suspended in F-12 complete medium containing: DMEM F-12 (Gibco, #21041-025), supplemented with 20% of inactivated FBS (Gibco, #10270-106), 4 ml of endothelial cell growth factor (Promocell, #C-30140) and 1% P/S. Then, the suspension was seeded on 12-well culture dishes coated with 0.5% gelatine (Sigma) in sterile H_2O (this moment is considered as passage 0 (P0)). The following day, the wells were carefully washed twice with PBS/BSA and F-12 complete medium was replaced. Medium was changed every second day.

3.2.2.1.3 Second selection

Once the cells had been in culture for 7 days, they were re-purified by removing the culture medium and incubating the cells for 1h with a solution containing VE-cadherin antibody-coated magnetic beads (prepared as described in **3.2.2.1.2**). After 1h of incubation at RT, cells were trypsinized and centrifuged for 5 min at 1200 rpm. Then, the pellet was washed three times with PBS/BSA and finally re-suspended in DMEN F-12 complete medium. Cells were seeded on 12-well culture dishes coated with 0.5% gelatine in sterile H_2O. The following day, the wells were carefully washed twice with PBS/BSA and DMEN F-12 complete medium was replaced. From here on, cells were cultured and splitted following standard procedures, always guaranteeing a confluence of at least 70% and never exceeding from passage 5.

3.2.2.2 Induction of gene deletion in mLECs carrying Cre recombinase

Induction of gene deletion *in vitro* was done in mLECs isolated from Pdgfb-iCreER^{T2} ;p110α$^{flox/flox}$ and Pdgfb-iCreER^{T2} ; p110α$^{flox/D933A}$ mice. mLECs from p110α $^{Flox/Flox}$ mice were used as control. Once cells were sufficiently amplified, they were treated with 1µM 4-OH tamoxifen (Sigma, #H7904) or ethanol (Emsure). To asses the time point in which p110α protein is completely depleted after the induction of gen recombination, Pdgfb-iCreER^{T2} ;p110α$^{flox/flox}$ mLECs were

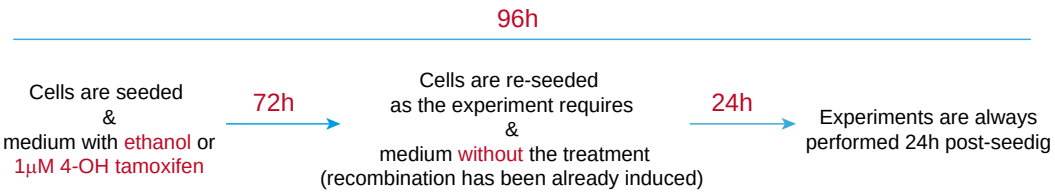

Figure 3.10: **Workflow scheme of culturing p110α$^{flox/flox}$ and Pdgfb-iCreER^{T2}; p110α$^{flox/D933A}$ mLECs for experiment.**

treated with ethanol (vehicle) or 1µM 4-OH tamoxifen. The medium was replaced every second day, until the desired time point was reached. Pdgfb-iCreER^{T2};p110α$^{flox/D933A}$ mLECs were always treated for 96h. Normally, p110α $^{Flox/Flox}$ mLECs treated with 1µM 4-OH tamoxifen were used as control (referenced in the text as control). For experiments, cells were seeded and treated for 72h. These cells were re-seeding for experiment (without adding treatment), and experiments were performed 24h after. Procedure summarized in **Figure 3.10**.

3.2.2.3 Pharmacological treatments

3.2.2.3.1 Specific inhibition of p110α isoform using the GDC-0326 inhibitor

mLECs isolated from wild-type mice were seeded and treated with 1µM GDC-0326 inhibitor (from a stock solution of 1,5 mM in DMSO, Genentech, **Table 3.3**) or DMSO for 48h.

3.2.2.3.2 Inhibition of ROCK using the Y-27632 inhibitor

mLECs were treated with 10 µM ROCK inhibitor, Y-27632 (Calbiochem, 688000, stock solution of 50 mM, **Table 3.3**) or DMSO (vehicle) for 10min or 30min.

3.2.2.4 Immunofluorescence of cultured mLECs

MLECs were seeded on cover-slips in 6-well plates (3 cover-slip per well) coated with 0.5% gelatine. After 24h, cells were washed once with PBS (containing calcium and magnesium, LONZA) and fixed in 4% PFA for 15min at RT. Then, cells were washed three times with PBS and permeabilised in 0.1% Triton X-100 in PBS for 30min at RT. Next, cells were incubated in blocking solution (3%

BSA, 5% goat serum, 0.1% Triton X-100 in PBS) for 1h at RT. Cover-slips were removed from the culturing plate and were incubated in the appropriate dilution of primary antibodies (**Table 3.4**) in blocking solution ON at 4ºC in a wet chamber (40µl of antibody solution were used for each cover-slip). The following day, cover-slips were washed three times (5min each) with PBS at RT (shaking) and were incubated in the appropriate dilution of secondary antibody or conjugated probes (**Table 3.5**) in PBS for 1-2h at RT in a wet chamber (40µl of antibody solution were used for each cover-slip). Three washes (5min each) with PBS were performed, adding 1µg/ml of 4',6-diamidino-2-phenylindole (DAPI, Molecular Probes) in the last one. Cover-slips were mounted on microscope slides using Mowiol as mounting medium.

3.2.2.4.1 Quantification of phalloidin and p-MLC staining intensity in mLECs

The quantification was done using the Image J software in images taken with the 63x objective and proper scale set up. Total intensity of phalloidin or p-MLC/cell was quantified using the junctional staining of β-catenin to select individual mECs (Area C1). Using the enlarge command two concentric areas were drawn in each cell (distance of -2.5µm (Area C2) and -7.5µm (Area 3 C3) from the junctional β-catenin positive staining). CTF was calculated as explained in **3.1.7.8**. For measuring **total levels**: CTF from C1 areas were used as templates to measure total intensity of phalloidin or p-MLC staining in individual mECs. For measuring **subcortical levels**: CTF from C2 area - CTF from C3 area was calculated in individual mECs. The background readings were taking from three areas close to the cells. The average of the CTF of 5 cells per image, and minimum 6 images per genotype and treatment were used for the quantification. **Figure 3.11.**

3.2.2.5 Ki-67 proliferation marker immunofluorescence

Ki-67 is a cellular marker for proliferation. It is considered to be present during all active phases of cell cycle (G1, S, G2 and mitosis), but it is absent in resting cells (G0). Ki-67 is an excellent marker to determine the growth fraction of a

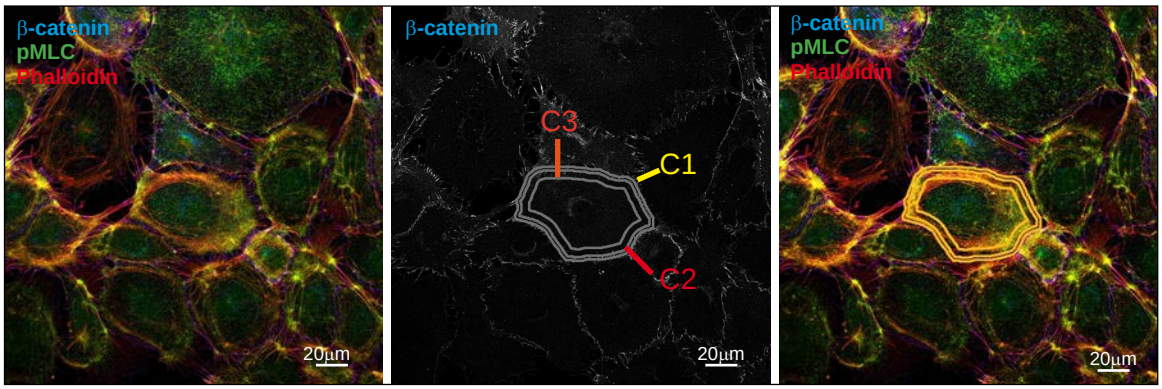

Figure 3.11: **Quantification of the intensity of the phalloidin and p-MLC immunostaining in mLECs**

given cell population. The primary antibody used was purchased from Thermo Scientific (#RM-9106-S1) and was used at 1:50 dilution. Secondary antibody used was Alexa Fluor goat anti-rabbit 488 at 1:200 dilution (Invitrogen, #A-11008). Immunofluorescence was visualized with a Nikon microscope 801 (40X lens). For analysis, the number of Ki-67 positive ECs per field was rectified by the total number of ECs present at the field. A minimum of 100 cells per condition were used for analysis.

3.2.2.6 Senescence detection in cultured mLECs

mLECs were seeding in cover-slips in 12-well plates. Senescence Detection Kit from Calbiochem was used to detect cell senescence (Calbiochem, #QIA117). First, culture medium was removed and cells were washed with 1ml of 1X PBS. Then, mLECs were fixed with 0,5 ml of Fixative Solution from the kit at RT for 15 min. Cells were washed twice with 1ml 1X PBS. Subsequently, 0,5 ml of Staining Solution MIX was added to each well (470 µl Staining solution, 5 µl Staining supplement, ad 25 µl of 20mg/ml X-gal in DMF) and fixed cells were incubated at 37ºC ON. Cell were washed one with 1X PBS with Dapi. Cover-slips were mounted on microscope slides using Mowiol as mounting medium. The Nikon microscope 801 was used for visualization.

Target	Target sequences (SMARTpool)	Reference
mouse mRIP	GAUCAUCAGUGGGUGGUUA-GGAAAUGGCAGCGACGAUU-GGAUGGUGGUCGGAAAGUA-GCAAGUGUCAGAACUGCUU-	# M-058568-00-0005, Dharmacon
mouse MYPT	GAACGAGACUUGCGUAUGU-AAGAAUAGUUCGAUCAAUG-CGACAUCAAUUACGCCAAU-UCGGCAAGGUGUUGAUAUA-	# M-063177-02-0005, Dharmacon
Non-targeting	UAGCGACUAAACACAUCAA-UAAGGCUAUGAAGAGAUAC-AUGUAUUGGCCUGUAUUAG-AUGAACGUGAAUUGCUCAA-	# D-001206-13-05, Dharmacon

Table 3.7: siGENOME SMART pool siRNA target sequences

3.2.2.7 siRNA transfection

Wild-type mLECs were washed once with PBS and then, DMEN F-12 complete medium without antibiotics was added to the cells for 2h. Then, solution A (493 µl of optimen (GIBCO) + 7,5 µl of siRNA oligomer 20 µM (Dharmacon)) and solution B (493 µl of optimen + 7,5µl of lipofectamine RNAi Max (Thermo Fisher Scientific)) were prepared and incubated for 5min at RT in separated tubes. Subsequently, solution B was added to solution A and incubated for 20 min at RT. Then, cell were trypsinized, centrifuge, and resuspended in DMEN F-12 complete without antibiotics to have 750.000 cells/ 500µL. 750.000 cells were seeded onto 1ml of optimen per well in 6 well-plates (final vol. per well: 1.5 ml). The medium was changed the day after. Then, after 48h, transfected cells were seeded on cover-slips in 6-well plates (3 cover-slip per well) coated with 0.5% gelatine. The following day, cells were fixed for immunofluoresce assays or lysed for western blotting (72h post-transfection). siRNA oligomers are shown in **Table 3.7**.

3.2.2.8 Pull-down assays to detect Rho activity

3.2.2.8.1 Preparation of the GST-fusion protein/sepharose 4B beads

First, 150µl of glutathione-sepharose-4B resin (GE healthcare, #17-0756-01) was washed three times (4ºC 1000rpm) with 150µl of TBS with 10 mM $MgCl_2$, 1 mM PMSF and 1 mM DTT and keeped in ice (volume per condition). Then, lyophilized pellet from E-coli bacterias that expressed the GST-rhotekin-RBD fusion protein (courtesy of Jaime Millán) was incubated with 1 ml TBS with 10mM $MgCl_2$, 1 mM PMSF and 1 mM DTT and sonicated on ice, 10 times, 1min each, 20A in an eppendorf. Then, 1% Triton-X-100 was added and tubes were incubated with rocking for 30min at 4ºC. Then, tubes were centrifuged at maximum speed for 20 min at 4ºC and the supernatant was mixed and incubated at 4ºC for 1h with the glutathione-sepharose-4B resin that was previously washed. Subsequently, resin was washed three times with TBS with 10 mM MgCl2 , 1 mM PMSF and 1 mM DTT (4ºC 1000 rpm) and kept on ice until being used.

3.2.2.8.2 Cell lysate for pull-down assay

mLECs were cultured in 10cm culture dish coated with 0.5% gelatin and treated with ethanol and with 1 µM 4-OH tamoxifen for 96h. Then, cells were washed with cold PBS (with $Ca^{2+}Mg^{2+}$) and scraped and lysed on ice with 500 µl of the following lysis buffer A (50 mM Tris-HCL pH 7.5, 1 mM EDTA, 500 mM NaCl, 10 mM $MgCl_2$, 1% triton-X-100, 0,5 M sodium deoxycolate, 0,1% SDS, 10% glicerol, 1 mM PMSF, 1 mM DTT, 0,2 mM Na_3VO_4, 1 mM NaF, 1 µg/ml aprotinin, 1 µg/ml leupeptin, 1 µg/ml pepstatin and 0,5% 2-mercaptoethanol). From now on all the step have to be done at 4ºC. Lysates were transferred to a cold eppendorf and subjected to centrifugation for 10min at 10000g at 4ºC. Then, we kept 30µl of total cell lysate as control of total protein and we added 1X SDS sample buffer. The rest of the supernatant volume was subjected to pull-down assay to analyse active, GTP-loaded RhoGTPases.

3.2.2.8.3 Pull-down assay

Supernatant was added to the resin (previously prepared as indicated above) and incubated for 1h at 4ºC in a rotary shaker. Then, resin was washed four times with cold lysis buffer A. After the washing, bound proteins were solubilized by the addition of 35 µl of 1X SDS sample buffer, followed by separation on 12.5% SDS-PAGE gels and Western blotting for RhoA and RhoC (**Table 3.9**). These last steps are explained in more detail in following sections.

3.3 Protein extraction and Western immunoblotting

3.3.1 Protein lysis and sample processing

For Western blot analysis, mLECs or HEKs were lysed with lysis buffer B (150 mM NaCl, 1mM EDTA, 50 mM Tris-HCl pH 7.4 and 1% Triton X-100 in H_2O) supplemented with 1mM DTT, 2 mg/ml aprotinin, 1 mM pepstatin A, 1 M leupeptin, 10 g/ml TLCK, 1 mM PMSF, 50 mM NaF, 1 mM $NaVO_3$ and 1 µM okadaic acid. Lysates were collected in a 1.5ml eppendorf and were kept on ice for 15min. Then, lysates were centrifuged for 15min, at maximum speed at 4ºC. Supernatants were collected in new ice-cold 1.5ml eppendorfs and were kept frozen at -80ºC until processed for experiment. The protein content of the samples was quantified using the BCA protein assay kit (Pierce) following the instructions recommended by the manufacturer. Protein samples were then diluted in sample buffer 4X (250 mM Tris-HCl pH 6.8, 40% glycerol, 8% SDS, 0.04% bromophenol blue and 250mM DTT in H_2O) in a proportion of 3 volumes of protein sample: 1 volume of 4X SDS sample buffer. Samples were heated at 100ºC for 5min and spinned for 30sec to recover all the volume.

3.3.2 Protein electrophoresis and membrane transference

Samples were resolved on 8%, 10% or 12,5% SDS poli-acrylamide gels. SDS-PAGE gels were composed of a stacking part (4% acrylamide, 125mM Tris-HCl pH 6.8, 0.4% SDS, 0.1% ammonium persulfate (APS) and 0.1% tetrametiletilendiamina (TEMED) in H_2O) and a resolution part (10% acrylamide,

Product	Company-Catalogue #
DL-Dithiothreitol (DTT)	Sigma ; #D0632
Aprotinin	Sigma ; #A6279
Pepstatin A	Sigma ; #P4265
Leupeptin	Sigma ; #L2884
Na-p-tosyl-L-lysine chloromethyl ketone (TLCK)	Sigma ; #T7254
Phenylmethylsulfonylfluoride (PMSF)	Sigma ; #P7626
Sodium fluoride (NaF)	Sigma ; #S7920
Sodium orthovanadate (NaVO3)	Sigma ; #S6508
Okadaic acid	Cayman Chemical Company; #10011490
2-mercaptoethanol	Sigma ; #M3148

Table 3.8: Reducing agents, phosphatase and protease inhibitors used for the different lysis buffers

375mM Tris-HCl pH8.8/0.4% SDS, 0.1% APS and 0.1% TEMED in H_2O). Samples were runned for 1- 2h at 130V with running buffer 1X (25mM Tris, 192 mM glycine and 0.1% SDS in H_2O). Thereafter, proteins separated in the acrylamide gels were transferred generally onto PVDF membranes (Roche) previously activated in methanol (Emsure). For the detection of MYPT was used nitrocellulose membranes (Roche). Gel to membrane transference was performed at 4ºC at 250 mA for 2h in Transfer buffer 1X (25mM Tris, 192mM glycine and 20% methanol). After transference, membranes were washed for 5min in 1X TBS (For 500mL of TBS 10x: 6g Tris, 43.85 g NaCl, pH7.5) containing 0.05% Tween (referred as TBS-T). Membranes were then incubated for 1h at RT with TBS-T containing 5% of milk. Membranes were washed twice (5min each time) with TBS-T and incubated ON at 4ºC with incubation solution (2% BSA in TBS-T with 0.02% sodium azide) containing the desired primary antibody at the appropriate dilution. **Table 3.9** details primary antibodies used for immunoblotting. The following day, membranes were washed three times (10min each) with TBS-T and were incubated for 1h at RT with 5% milk in TBS-T containing the

Primary antibody	Host	Dilution	Company	Catalogue #
VE-cadherin	Goat	1:500	Santa cruz	sc-6458
β-actin	Mouse	1:50000	Abcam	49900
p-Akt	Rabbit	1:2000	Cell Signalling	4060
t-AKT	Rabbit	1:2000	Cell signalling	9272
p110α	Mouse	1/10	monoclonal clone U3A	
p110β	Rabbit	1/200	Santa Cruz	sc-602
mRIP	Rabbit	1:1000	Cell Signalling Technology	14396
pS445-MYPT	Sheep	1 µg/ml	Ubiquigent	68-0043-100
MYPT1 non-phosphorylated peptide	-	10µg/ml	Ubiquigent	68-1004-001
t-MYPT1	Sheep	1 µg/ml	Ubiquigent	68-0041-100
pS19-MLC	Rabbit	1:2000	Rockland	600-401-416
RhoA (26C4)	Mouse	1:200	Santa Cruz	sc-418
RhoC (D40E4)	Rabbit	1:500	Cell signalling	3430
pan-p85	Rabbit	1:2000	Upstate	06-195

Table 3.9: Primary antibodies used for immunoblotting

appropriate dilution of secondary antibodies (**Table 3.10**). Upon incubation with secondary antibody, membranes were washed three times (10min each) with TBS-T and protein detection was performed by enhanced chemiluminescence (ECL) following the protocol described in **Table 3.1**1. Quantification of band intensities by densitometry was carried out using the Image J software.

3.4 Phosphoproteomic screening

3.4.1 Preparation of the sample

Mouse lung endothelial cells were isolated from p110α$^{flox/flox}$ (control) and Pdgfb-iCreER^{T2} ; p110α$^{flox/D933A}$ mice following the instructions described in **3.2.2.1**.

Secondary antibody	Host	Dilution	Company	Catalogue #
Anti-Rabbit HRP	Swine	1:5000	Dako	P 0399
Anti-Sheep HRP	Rabbit	1:5000	Dako	P 0163
Anti-Mouse HRP	Rabbit	1:5000	Dako	P 0260
Anti-Goat HRP	Rabbit	1:5000	Dako	P 0160

Table 3.10: Secondary antibodies used for immunoblotting

Solution A	Solution B
5 mL 1 M Tris pH 8.5 45 mL H_2O 110 µL 90 mM acid cumaric (Sigma) 250 µL 250 mM luminol (Sigma)	100 µL H_2O_2 30% 900 µL H_2O
Solutions A and B need to be mixed following the proportion 1mL (A) + 3 µL (B)	

Table 3.11: ECL composition

These cell were treated with ethanol for 24h and with 1μM 4-OH tamoxifen for 24h and for 96h. Cells were washed twice with cold PBS containing protease ad phosphatase inhibitors. Then, cells were lysated with a specific lysis buffer C (1 ml was composed of 9779 μl of 8 M Urea in 20 mM HEPES, pH 8.0, 100 μl of 100mM Na_3VO_4 , 20 μl of 500 mM NaF, 1 μl of 1 M β-glycerolphosphate and 100 μl of 250 mM $Na_2H_2P_2O_7$. Scrape cells and transfer to a eppendorf. Then, cell suspension was sonicated at 20% intensity for 10sec, rested for 10sec and repeated two further times. Tubes were immersed in ice to ensure that heat generated by sonication does not adversely affect phosphoprotein content. Then, cell suspension was centrifuged at 20,000g for 10min at 4ºC. Supernatant was recovered to a 1.5 ml eppendorf protein Lo-bind tube and BCA assay was performed. Then, lysates were immediately snap frozen in dry ice and sent to Dr. Pedro Cutillas laboratory for the phosphorpoteomic analysis by **Dr. Pedro Casado Izquierdo**.

3.4.2 Titanium dioxide affinity purification (TiO_2)

Phosphopeptide enrichment was performed using a TiO_2 protocol as described in Wilkes et al., 2015.

3.4.3 Nanoflow-liquid chromatography tandem mass spectrometry (LC-MS/MS)

For LC-MS/MS analysis, dried phosphopeptide extracts were resuspended in 20 μL of 0.1% TFA (5% ACN) containing 20 $fmol.\mu L^{-1}$ enolase digest (Waters, Manchester, UK). Then it was followed the protocol described in (Wilkes et al., 2015), but the Thermo Scientific Q Exactive Hybrid Quadrupole-Orbitrap Mass Spectromete was used instead of the Orbitrap - Velos mass spectrometer (Thermo Fisher Scientific).

3.4.4 Identification and quantification of phosphopeptides

For phosphopeptide identification, the Mascot server version 2.3. Mascot Distiller version 2 was used to analyze the MS data. Then, the protocol described in Wilkes

et al., 2015 was followed to have the final results.

3.4.5 Statistical analysis of the phosphoproteomic assay

All the statistical analysis were performed by two tail unpair t-test comparing Pdgfb-iCreER^{T2} ; p110α$^{flox/D933A}$ mLECs vs. p110α$^{flox/flox}$ mLECs.

3.5 Zebrafish experiments

All the experiment in zebrafish embryos were done by me during my secondment in Dr. Markus Affolter laboratory, in the Biozentrum, Basel.

3.5.1 General care

Zebrafish were maintained as previously described (Westerfield, 2007). All experiments were performed in accordance with federal guidelines and were approved by the Kantonales Veterinaramt of Kanton BaselStadt.

3.5.2 Zebrafish transgenic lines

Transgenic lines used in my thesis detailed in **Table 3.12**.

Genotype	Source	To visualize
Tg(flia:EGFP)^{y1}	(Lawson and Weinstein, 2002)	ECs
Tg(kdrl:mCherry-CAAX)	(Fujita et al., 2011)	EC membrane
Tg(UAS:EGFP-UCHD)^{ubs18}	Sauteur et al. (2014)	Actin
Tg(kdrl:EGFPnls)^{ubs1}	(Blum et al., 2008)	EC Nuclei
Tg(kdrl:EGFP)^{s843}	(Jin, 2005)	ECs

Table 3.12: Transgenic zebrafish embryos. From Markus Affolter laboratory (Biozetrum, Basel)

3.5.3 Morpholino injections

The microinjection needles were pooled using Sutter Instrument.Co. The needles were filled using a micro loader tip (Eppendorf) and to open the needle its end was

Morpholino	Dose/ embryo	Sequence	Source
p110α-ATG	20ng	TCTTGGAGGCATGATTTGTAATCCT	From this work, Gene tools
p110α-splice	20ng	GCTGCCAAAGTTTAAAGTCTTACCA	From this work, Gene tools
p53	10ng	GCGCCATTGCTTTGCAAGAATTG	Gene tools
standard control	20ng	CCTCTTACCTCAGTTACAATTTATA	Gene tools

Table 3.13: Morpholino oligomers sequences

broken with forceps. Plates for injections were prepared pouring hot 1% agarose-Egg water into a Petri dish. Then, a striated mould was inserted to create slots where put the eggs. After solidification of the agarose, the mould was removed and Petri dish was store at 4ºC with Egg water on top to prevent from drying until being used.

Antisense oligonucleotides (MO, Gene Tools, **Table 3.13**) were diluted in DEPC water containing 0,2% phenol red. The standard control oligonucleotide offered by Gene tool was used as control. Standard control MO should not target or have significant biology activity in zebrafish. A mix of 20 ng of standard control-MO with 10 ng p53-morpholino or a mix of 20 ng p110α-MO with 10 ng of p53-MO were injected into 1-2-cell stage zebrafish embryos.

3.5.4 GDC-0326 treatment in zebrafish embryos

Dechorionated zebrafish embryos were treated with DMSO (vehicle) or 20 μM, 50 μM or 100 μM GDC-0326 inhibitor in Egg water containing 1X PTU solution (to inhibit pigmentation). The treatment was performed as follows: 10 embryos/well in 6well plates (that were previously incubated ON with 1X PBS to avoid the attachment of the embryos to the plastic) The medium was changed every 4h until embryos were mounted for confocal microscopy. The fluorescence positive embryos were selected using a Leica MZ FLIII fluorescent

stereomicroscope for presence of red or/and green fluorescence. Selected embryos were anaesthetized using tricaine and mounted in a 35 mm glass bottom petri dish (0.17 mm, MatTek), using 0.7% low melting agarose (Sigma) containing 0.01% tricaine, 0,003% PTU and the corresponding concentration of GDC-0326 inhibitor.

3.5.5 Prepare zebrafish embryos for Western immunoblotting

The cells forming the embryo proper constitute only a minor volume of the embryo compared to the large yolk cell. The abundance of yolk proteins interferes with any proteomic application that intends to target the cells of the embryo proper. To avoid this we subjected embryos to a deyolking protocol. Dechorionated embryos were collected in a 1.5 ml tube filled with 1 ml deyolking buffer (55 mM NaCl, 1,8 mM KCl and 1,25 mM $NaHCO_3$). By pipetting with a narrow tip the yolk sac was disrupted (200 µl tip, Sarstedt 70.760.502). The embryos were shaken for 5 min at 1100 rpm to dissolve the yolk (Thermomixer, Eppendorf). Cells were pelleted at 300g for 30sec and the supernatant discarded. Two additional wash steps were performed by adding 1 ml of wash buffer (110 mM NaCl, 3.5 mM KCl, 2.7 mM $CaCl_2$, 10 mM Tris/Cl pH8.5), shaking 2 min at 1100 rpm and pelletting the cells as before. The samples were frozen in liquid nitrogen or processed directly for protein extraction as explained in section 3.3.1.

3.5.6 Immunofluorescence in whole-mount zebrafish embryos

Dechorionated zebrafish embryos from 27-38 hpf were fixed in 2% paraformaldehyde in PBS-T at 4ºC ON in 2 ml tube (10-50 embryos per tube). After fixation embryos were washed four times (5min each) in PBST. Permeabilization of the embryos was done by the incubation with 0.5 % Triton-X-100 in PBST at RT for 15-30 min with shaking. Embryos were incubated in 1 ml of Blocking Buffer at 4°C ON with shaking. Then, embryos were incubated in 500µl of the appropriate dilution of primary antibody in Blocking Buffer at 4°C overnight (**Table 3.14**). Embryos were washed in PBST minimum 6 times over 3 hours. Embryos were incubated in 500 µl of the appropriate dilution of secondary antibody in Blocking Buffer at 4°C ON (**Table 3.14**). Embryos were washed in

PBST at 4°C ON with shaking.

Antibody	Dilution	Host	Company
VE-cadherin	1:200	Rabbit anti-zebrafish	H. G. Belting
ZO-1	1:100	Mouse anti-human	Zymed
Alexa 568	1:1000	Goat anti-rabbit	Invitrogen
Alexa 633	1:1000	Goat anti-mouse	Invitrogen

Table 3.14: Primary and secondary antibodies used for immunofluorescence in whole-mount zebrafish embryos

3.5.7 Confocal microscopy

3.5.7.1 Fixed embryos for confocal imaging

After completion of the immunostaining procedure, the embryos were kept in PBST at 4 °C. To mount the embryos for confocal imaging of the trunk vasculature the heads were detached with forceps and discard, whereas the other part was mounted in a 35 mm glass bottom petri dish (0.17 mm, MatTek), using 0.7% low melting agarose (Sigma). Images were taken with the Leica SP5 confocal microscope using a 10x air, 20x air and 40x water immersion objectives with a frame size of 1024x512 pixels. All images are maximal z-stack projections.

3.5.7.2 Time-lapse movies of living embryos

For time lapse imaging of living embryos, the embryos older than 24 hpf were kept in 1X PTU solution to inhibit pigmentation. The fluorescence positive embryos were selected using a Leica MZ FLIII fluorescent stereomicroscope for presence of red and green fluorescence. Selected embryos were anaesthetized using tricaine and mounted in a 35 mm glass bottom petri dish (0.17 mm, MatTek), using 0.7% low melting agarose (Sigma) containing 0.01% tricaine and 1X PTU. All movies were taken with a Leica SP5 confocal microscope using a 40x water immersion objective with a frame size of 1024x512 pixels. Stacks were taken every 10 min. All images are maximal z-stack projections.

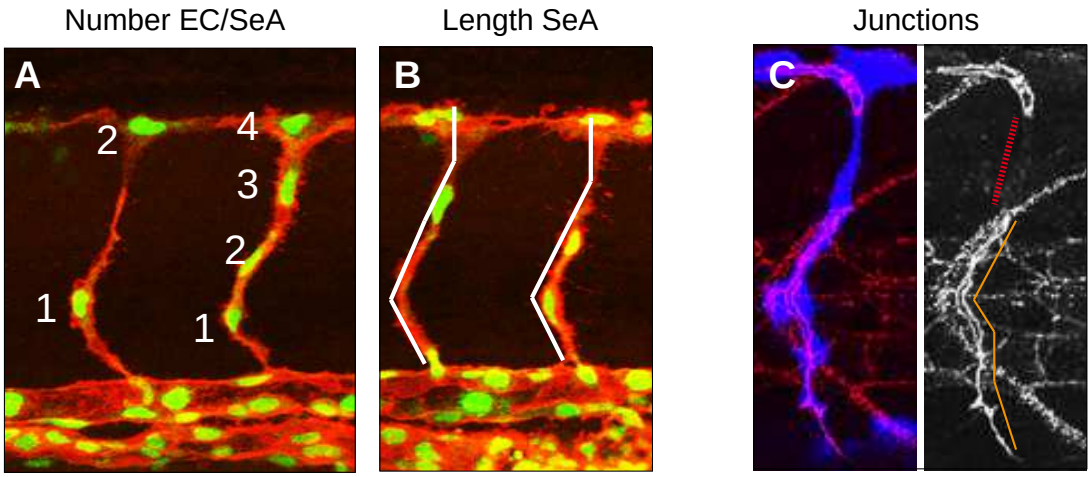

Figure 3.12: **Quantification of vessel features in zebrafish embryos. (A)** Quantification EC number per SeA. **(B)** Quantification of the length of the SeA starting from the dorsal aorta. **(C)** Quantification of the length of the junction starting from the DA following the junctional staining (orange line) and quantification of the length of the disconnection (no junctional staining, red punctuate line).

3.5.8 Methods used for quantifying vessel features in zebrafish embryos

Quantification of the different vascular parameters in zebrafish embryos was done as indicated in **Figure 3.12**. Images were taken at 40x water immersion objective, and there were quantified five SeAs per embryo. Only flat-mounted embryos were selected for quantification avoiding crooked ones.

3.6 Statistical analysis

Statistical analysis was performed by nonparametric Mann Whitney's test using Prism 5 (GraphPad Software Inc.) unless indicated otherwise. In all figures across the manuscript, errors bars are standard error of the mean. In all cases *, $P < 0.05$; **, $P < 0.01$; and ***, $P < 0.001$ were considered statistically significant.

4 Results

4.1 p110α PI3-kinase activity during sprouting angiogenesis.

p110α activity is essential for vascular development during the embryonic period (Graupera et al., 2008), therefore, our first aim was to study its specific contribution during sprouting angiogenesis. We first studied p110α expression in the retinal vasculature throughout the angiogenic process. By western blotting we showed that at postnatal day 3 (P3) and P6, when the sprouting process takes place, p110α protein level was higher than at P15, when vessels remodel and mature (**Figure 4.1.A**). Next, we wondered whether an increase in p110α protein level correlated with an increase in its activity. To test that, we performed an immunostaining of pS6, as read out of PI3K activity, in wild-type retinas at P6 and P15. At P6 we noticed a strong immunostaining of pS6 specifically in the sprouting front of the vasculature (**Figure 4.1.B**) whereas at P15 pS6 staining was undetectable (**Figure 4.1.C**). All these data indicate that there is an increase in p110α protein level that correlates with an increase in its activity specifically during sprouting angiogenesis.

4.2 Unrevealing p110α functions in the process of sprouting angiogenesis.

Until now, progress in the understanding of how p110α regulates sprouting angiogenesis has been hampered by the embryonic lethality that exhibits both the ubiquitous and endothelial-specific p110α knockout mice. Given that p110α is essential during embryonic vascular development we decided to use an inducible system in mouse and pharmacological and genetic approaches in zebrafish embryos to gain insight into the role of p110α in the sprouting angiogenesis.

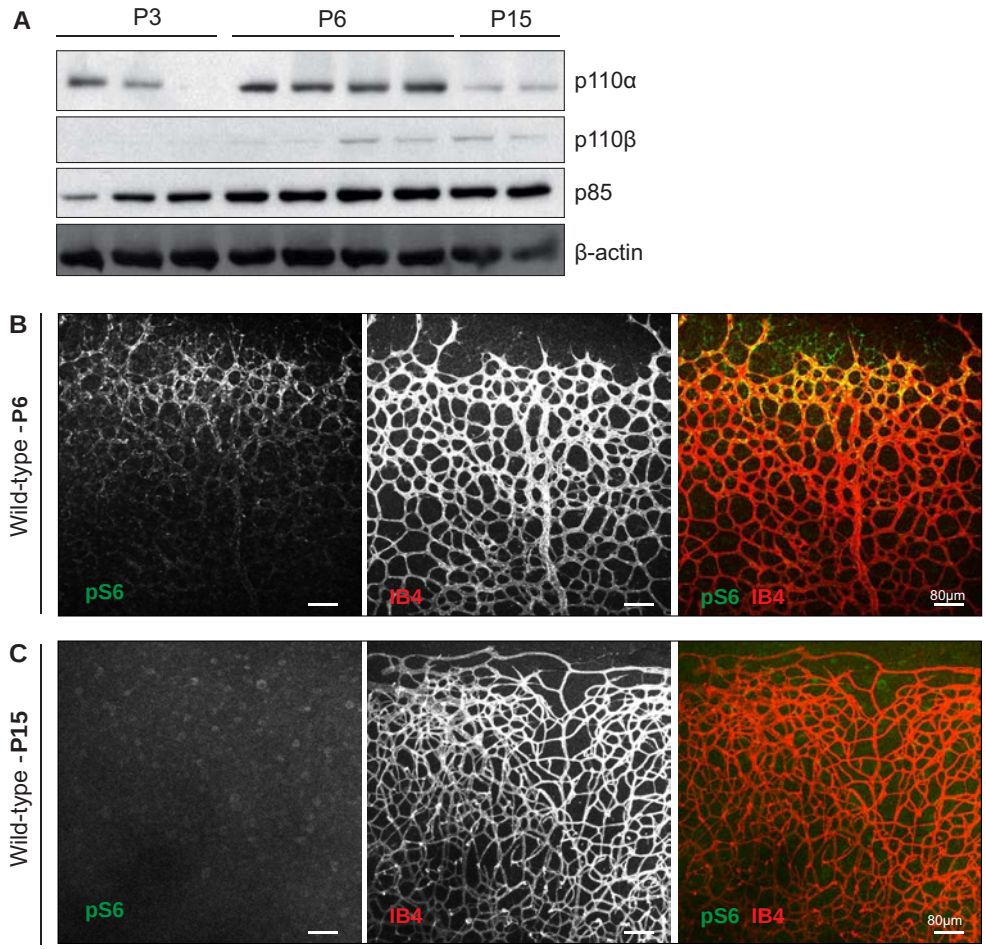

Figure 4.1: **p110α activity is upregulated during sprouting angiogenesis. (A)** Immunoblotting analysis of indicated antibodies in homogenates from wild-type retinas at P3, P6 and P15. **(B,C)** Whole-mount retinas stained for isolectin-IB4 (red) and pS6 (green) at P6 **(B)** and P15 **(C)**.

4.2.1 Endothelial p110α can be selectively inactivated upon 4-OH tamoxifen injection in newborn Pdgfb-iCreER^{T2} ;p110α$^{flox/flox}$ mice

Next, we aimed to establish a mouse model in order to study p110α inactivation specifically in ECs avoiding embryonic lethality. We crossed p110α$^{flox/flox}$ mice onto Pdgfb-iCreER^{T2} mice, that express 4-OH tamoxifen-inducible Cre specifically in ECs. First, we analysed when p110α protein is effectively depleted and deleted in ECs after 4-OH tamoxifen administration. To answer that question, we isolated mouse lung endothelial cells (mLECs) from p110α$^{flox/flox}$ and Pdgfb-iCreER^{T2};p110α$^{flox/flox}$ mice. After obtaining a pure culture of ECs, we induced p110α recombination *in vitro* by the administration of 4-OH tamoxifen in the culture media. We observed that in Pdgfb-iCreER^{T2};p110α$^{i\Delta EC/i\Delta EC}$ mLECs p110α protein

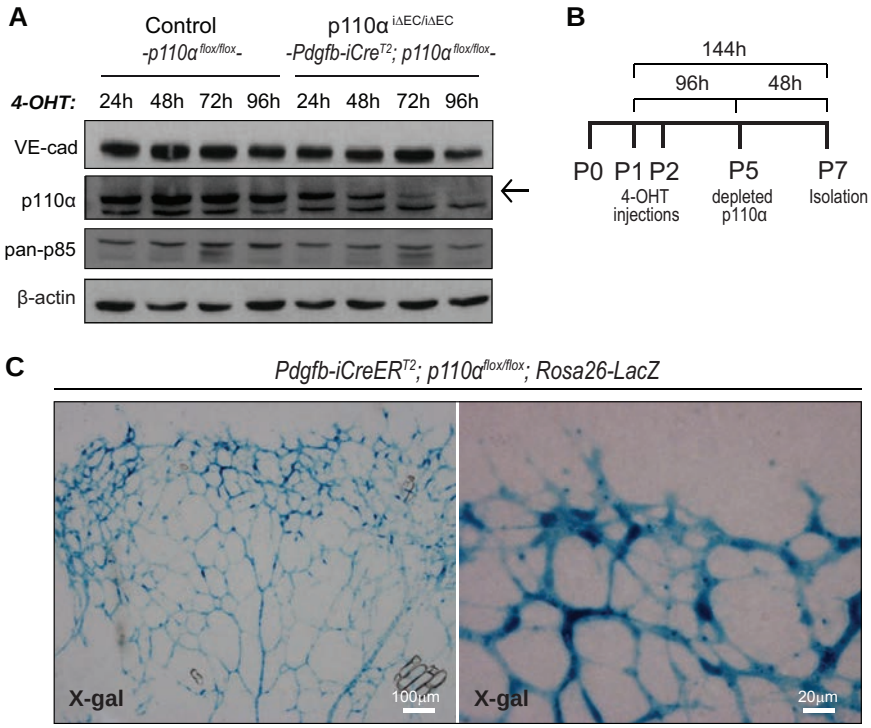

Figure 4.2: **Efficient induction of p110α deletion specifically in ECs upon 4-OH tamoxifen treatment. (A)** Western blotting of the indicated antibodies in mLECs isolated from p110α$^{flox/flox}$ mice and Pdgfb-iCreER^{T2};p110α$^{flox/flox}$ mice that were treated with 4-OH tamoxifen for 24h, 48h, 72h, and 96h. **(B)** Followed protocol to induce endothelial-cell specific p110α deletion in pups. **(C)** Cre expression detected by X-gal staining (blue) in P7 retinas of Pdgfb-iCreER^{T2};p110α$^{flox/flox}$;Rosa26R-LacZ pups after 4-OH tamoxifen injections at P1 and P2.

level decreased over time, being almost undetectable after 96h. In contrast, p110α$^{flox/flox}$ derived from mice not carrying iCreER^{T2} (used as control), p110α protein level was maintained upon 4-OH tamoxifen administration. We determined that at least 96h were needed to degrade the remaining p110α protein after the induction of the recombination (**Figure 4.2.A**).

Given that it takes 96h to fully deplete p110α in ECs, we induced gene recombination *in vivo* at P1 and P2 and isolated retinas to study postnatal angiogenesis at P7. By this time point 48h had passed since fully p110α protein depletion (**Figure 4.2.B**). We confirmed the effective recombination of p110α floxed gene by crossbreeding Pdgfb-iCreER^{T2};p110α$^{flox/flox}$ mice with Rosa26-LacZ reporter strain. In this case, upon 4-OH tamoxifen administration not only was p110α deleted in ECs, but LacZ gene was also expressed. By adding 5-bromo-4-chloro-3-indoul-β-D-galactopiranoside (X-gal) we detected β-galactosidase activity in the cells that have carried out recombination. We

observed that at P7 p110α$^{i\Delta EC/i\Delta EC}$ retinal vasculature presented LacZ expression after 4-OH tamoxifen administration (**Figure 4.2.C**).

4.2.2 Small amount of p110α can support angiogenesis to some degree.

In order to establish the best model to study p110α inactivation in mouse ECs we used several transgenic mouse models available in the lab (presented in **section 3.1.2**). These mouse models allowed us to study p110α dose-dependent inactivation defects. We injected 4-OH tamoxifen at P1 and P2 and analysed the retinal vascular pattern at P7 and P10. First, we used heterozygous knock-in p110α$^{WT/D933A}$ mice in which one allele constitutively expresses a kinase death form of p110α (p110α^{D933A}), leading to counteract p110α activity by 50% with no compensation from other isoforms (Foukas et al., 2006). Second, we used Pdgfb-iCreER^{T2};p110α$^{i\Delta EC/i\Delta EC}$ mouse in which upon 4-OH tamoxifen administration p110α in completely delete in ECs. Although this approach allows selective targeting in ECs, it has been proven *in vitro* that complete deletion of p110α leads to compensation by other isoforms (data not shown). Third, we have used the Pdgfb-iCreER^{T2} ;p110α$^{i\Delta EC/D933A}$ mouse, that combines one allele floxed and the other expresses p110α^{D933A} kinase-death protein, and therefore, maintains the signalling complex stoichiometry avoiding deregulation of PI3-kinase signalling components due to the expression of 50% of p110α kinase-death protein. The only limitation was that the p110α$^{WT/D933A}$ mutation is constitutive in every cell of the mouse. To discern that the phenotype obtained was not due to the reduction of p110α activity in the body but in the endothelial cells we also used heterozygous p110α$^{WT/D933A}$ mouse as a control model.

First, we measured the expansion of the vascular plexus to the periphery of the retina at P7 (**Figure 4.3.A,B**). No changes in heterozygous p110α$^{WT/D933A}$ mice compared to control (p110α$^{flox/flox}$) littermates were detected suggesting that 50% of p110α activity is sufficient to support retinal angiogenesis. In contrast, inactivation of p110α activity in p110α$^{i\Delta EC/i\Delta EC}$ and p110α$^{i\Delta EC/D933A}$ pups significantly reduced the growth of the vascular plexus to the retinal periphery (**Figure 4.3.A,B**). Analysis at P10 revealed a p110α dose-dependent delay in the radial expansion (**Figure 4.3.C**). In control and heterozygous p110α$^{WT/D933A}$

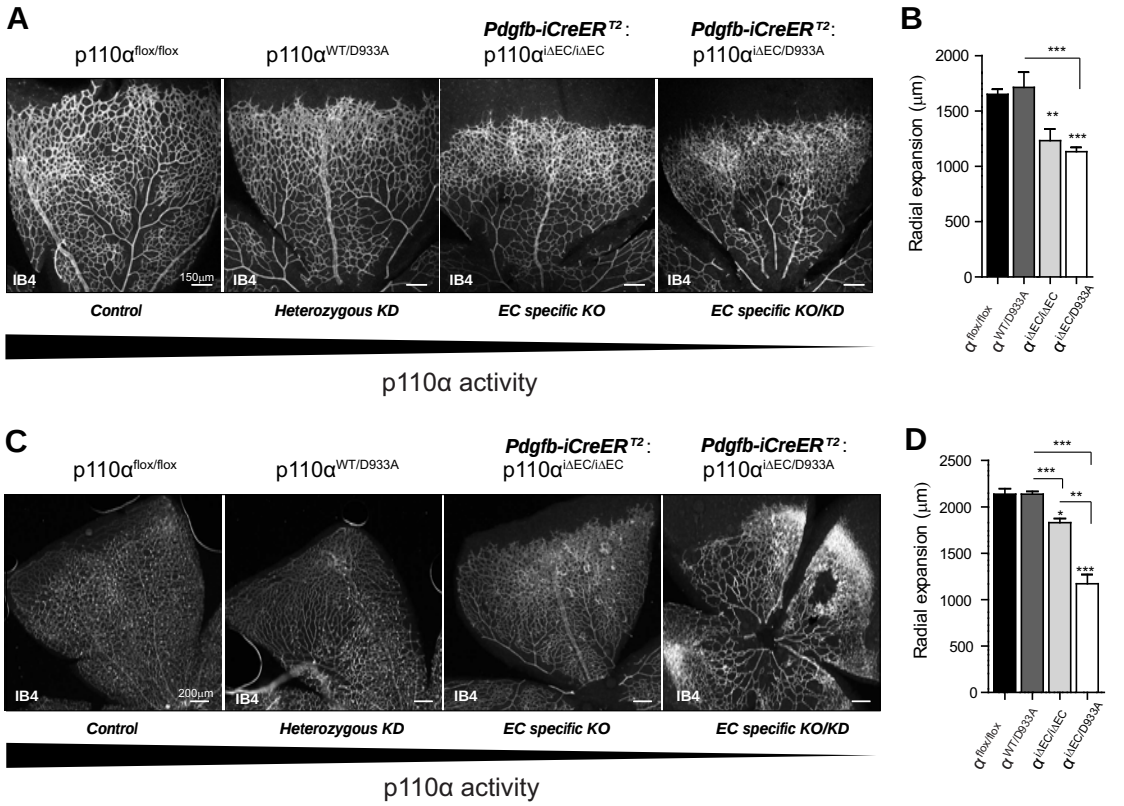

Figure 4.3: **Small amount of p110α can support angiogenesis to some degree.** **(A)** Whole-mount of P7 retinas injected with 4-OH tamoxifen at P1 and P2 and stained with isolectin-B4. **(B)** Quantification of radial expansion of blood vessels in P7 retinas of respective genotypes. n ≥ 4 retinas for each genotype except for p110α$^{i\Delta EC/i\Delta EC}$ n=2 retinas. **(C)** Whole-mount of P10 retinas injected with 4-OH tamoxifen at P1 and P2 and stained with isolectin-B4. **(D)** Quantification of the radial expansion of the vascular plexus in P10 retinas of respective genotypes. n ≥ 3 retinas for each genotype. Error bars are SEM. * P<0.05 ** P<0.01 ***P<0.001 were considered statistically significant. Statistical analysis was performed by Student's test.

littermates, the formation of the primary vascular plexus covering the surface of the retina was complete and sprouting of new vessels into the deeper layers of the retina to form a tridimensional plexus proceeded normally (slight delay in the heterozygous pup overcame with the time, data not shown) (**Figure 4.3.C,D**). Instead, p110α$^{i\Delta EC/i\Delta EC}$ pups showed a significant delay in the expansion of the vascular plexus that was even more dramatic in p110α$^{i\Delta EC/D933A}$ littermates. In fact, the radial expansion at P7 and P10 of p110α$^{i\Delta EC/D933A}$ retinas was similar (**Figure 4.3.B,D**), suggesting that total inactivation of p110α activity results in EC migration arrest. Differences observed between p110α$^{i\Delta EC/i\Delta EC}$ and p110α$^{i\Delta EC/D933A}$ pups could be due to recombination efficiency and/or possible compensations of other p110s in the p110α$^{i\Delta EC/i\Delta EC}$ mice. Hence, we decided to establish as a model of work the p110α$^{i\Delta EC/D933A}$ mouse.

4.2.3 p110α activity is efficiently decreased in p110α$^{i\Delta EC/D933A}$ ECs.

Next, we assessed whether p110α inactivation led to the reduction of PI3-kinase signalling in P7 control and p110α$^{i\Delta EC/D933A}$ retinas stained for pS6. While control retinas showed an enrichment of pS6 staining in the vascular sprouting front, p110α$^{i\Delta EC/D933A}$ retinas exhibited decreased immunostaining in this area (**Figure 4.4.A,B**). Then, we aimed to validate this observation *in vitro*. Pre-treatment with ethanol and 4-OH tamoxifen of p110α$^{flox/flox}$ mLECs (in the absence of the iCreER^{T2} expression) modifies neither p110α expression nor pAkt levels. On the other hand, Pdgfbi-CreER^{T2} ;p110α$^{flox/D933A}$ mLECs treated with ethanol showed decreased pAKT levels, which rely on the 50% of p110α^{D933A} kinase-death protein, whereas those mLECs treated with 4-OH tamoxifen showed halved p110α levels and almost undetectable levels of pAkt (**Figure 4.4.C**). These data demonstrate that inactivation of p110α in ECs both *in vivo* and *in vitro* results in an impairment of PI3-kinase signalling.

4.2.4 Mice deficient in p110α PI3-kinase activity exhibit retinal vasculature defects.

The analysis of p110α$^{i\Delta EC/D933A}$ retinas showed several abnormalities beyond the extension of the plexus (**Figure 4.3, Figure 4.5**). We decided to focus our

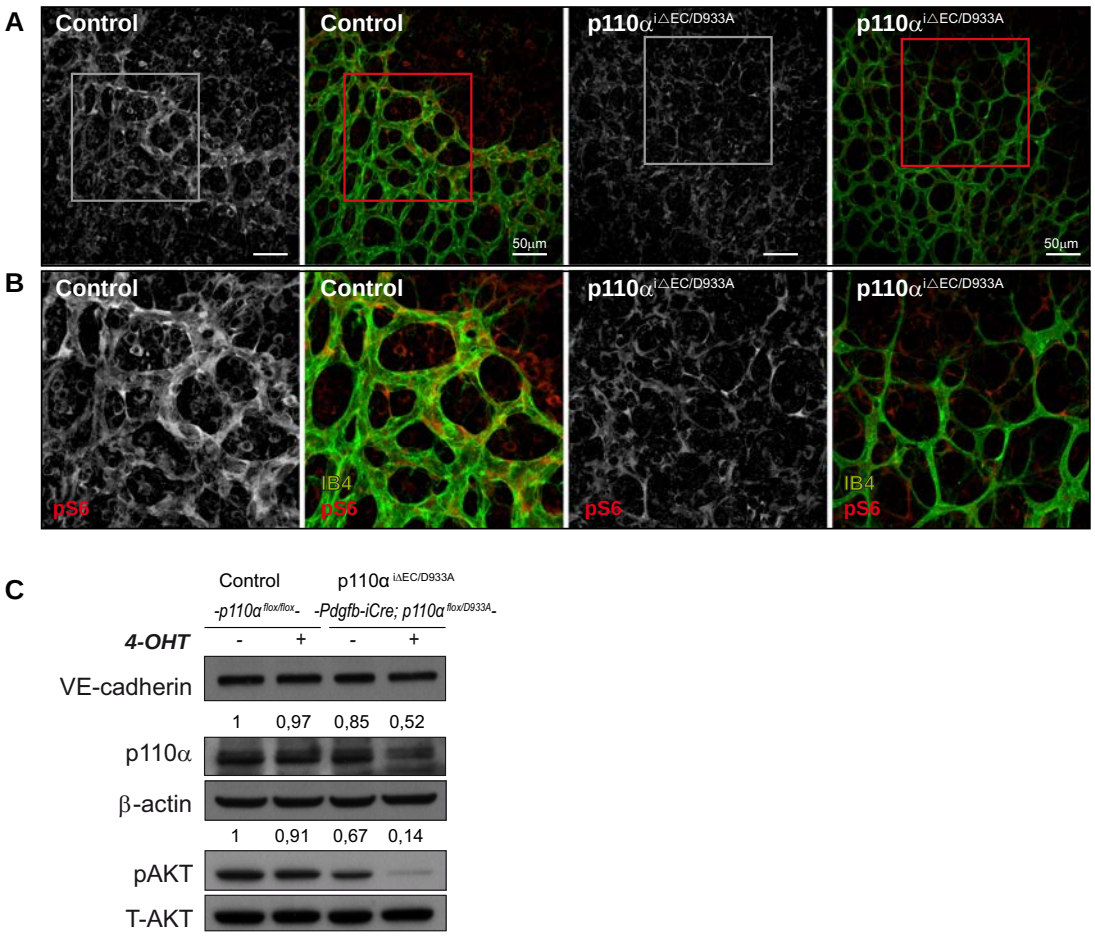

Figure 4.4: **p110α activity efficiently decreased upon p110α inactivation in ECs. (A)** Whole-mount control and p110α$^{i\Delta EC/D933A}$ retinas from P6 littermates stained with isolectin-B4 (green) for vessels and with anti-pS6 antibody (red) as readout of p110α activity. 4-OH tamoxifen administration was done at P1 and P2. **(B)** High magnification images from the selected frames to highlight the decrease of pS6 staining upon p110α inactivation specifically in ECs. **(C)** Western blotting of the indicated antibodies in mLECs isolated from p110α$^{flox/flox}$ mice and Pdgfb-iCreER^{T2};p110α$^{flox/D933A}$ mice and treated for 96h with ethanol (vehicle) or 4-OH tamoxifen. Three independent experiments were done.

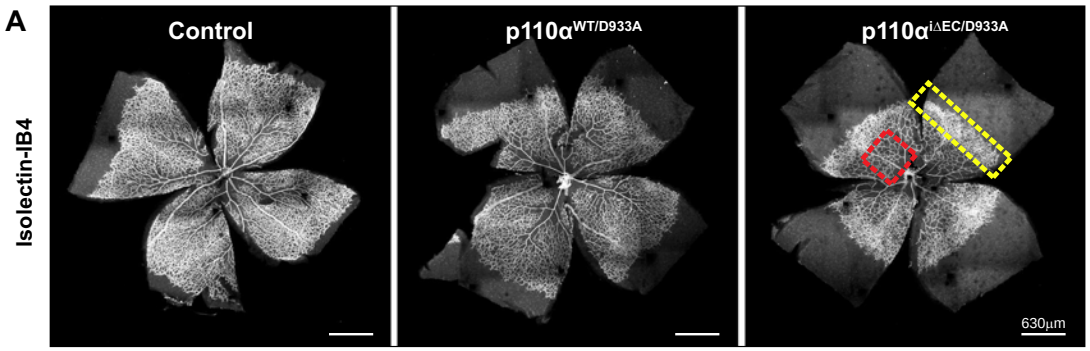

Figure 4.5: **Overview images of retinal vessels defects in p110α-deficient mice.** Whole-mount retinas of control, p110α$^{flox/D933A}$ and p110α$^{i\Delta EC/D933A}$ at P7 stained with isolectin-B4 after 4-OH tamoxifen administration at P1 and P2. Yellow islet highlights sprouting defects while red islet highlights vascular defects in the remodelling part.

analysis at P7 before the complete migration arrest has occurred. Intriguing, p110α$^{i\Delta EC/D933A}$ retinas showed opposite changes in the vascular density between the sprouting front and the capillary region (**Figure 4.5**). On one hand, there was a significant increase in the number of vascular branches in p110α$^{i\Delta EC/D933A}$ retinas compared to control and heterozygous littermates in the migrating vascular front (**Figure 4.6.A-C, A'-C', D**). Interestingly, although there were more branches in p110α$^{i\Delta EC/D933A}$ retinas they were significantly thinner (**Figure 4.6.C,C', E**). On the other hand, a reduction in vessel density was observed in the more mature plexus of the retinal vasculature (**Figure 4.7**). Taken together, these data allow us to conclude that inactivation of p110α in ECs have different consequences in the sprouting front than in the capillary area suggesting that p110α could be regulating different steps of angiogenesis.

Given that PI3K signalling is enriched in the sprouting front and p110α inactivation results in a strong phenotype in that area, we decided to focus our study on the sprouting front. By taking high magnification images, we examined whether the increase in the number of narrow vascular structures could be due to increased endothelial sprouting activity. By counting the number of sprouts and filopodia in the perimeter of the sprouting front, no changes in the formation of sprouts and filopodia were observed (**Figure 4.8**). However, the inner part of the angiogenic front showed multidirectional hypersprouting with tip-like cells growing above the vascular plane (**Figure 4.8.A",B"**). Due to tridimensionality, it was difficult to quantify the number of both sprouts and filopodia. Z-stacks of

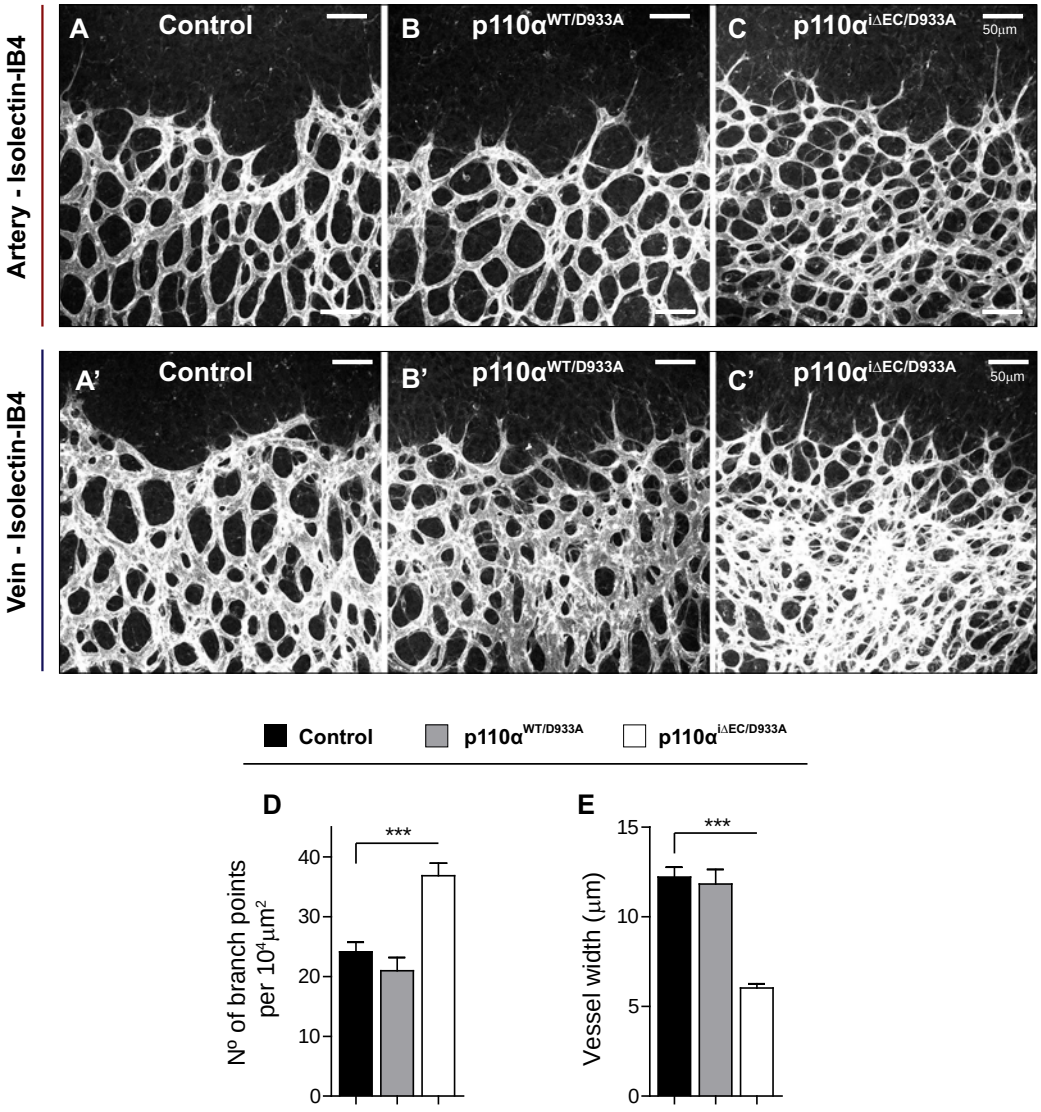

Figure 4.6: **p110α inactivation leads to increased vascular density with thinner vascular structures in the sprouting front.** Whole-mount visualization of arteries **(A, B, C)** and veins **(A', B', C')** by Isolectin-B4 staining of control, p110α$^{flox/D933A}$ and p110α$^{i\Delta EC/D933A}$ littermate retinas respectively at P7. 4-OH tamoxifen injections were performed at P1 and P2. **(D)** Quantification of the number of branch points in the sprouting front area. n = 12 retinas for control, n = 4 retinas for p110α$^{flox/D933A}$ and n = 15 retinas for p110α$^{i\Delta EC/D933A}$ **(E)** Quantification of vessel width. n = 6 retinas for control and p110α$^{i\Delta EC/D933A}$ and n = 4 retinas for p110α$^{flox/D933A}$. Error bars are SEM. ***P<0.001 was considered statistically significant. Statistical analysis was performed by non-parametric Mann-Whitney test.

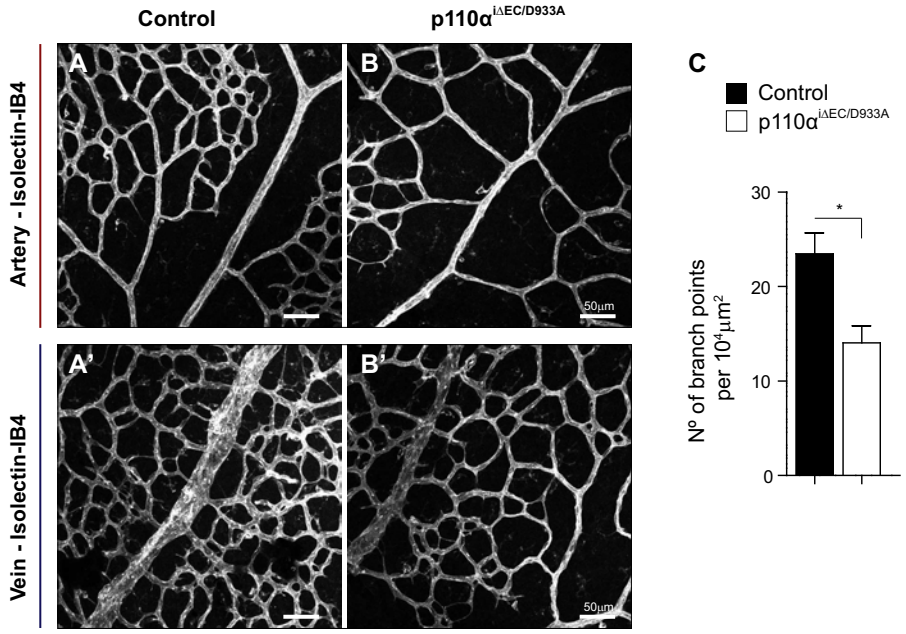

Figure 4.7: **p110α inactivation leads to decreased vessel density in the remodelling plexus.** Whole-mount visualization of arteries **(A,B)** and veins **(A',B')** in the inner retina by isolectin-B4 staining of control and p110α$^{i\Delta EC/D933A}$ littermate retinas respectively at P7. 4-OH tamoxifen injections were performed at P1 and P2. **(C)** Quantification of the number of branch points in the remodelling plexus area. n ≥ 5 retinas for each genotype. Error bars are SEM. *P<0.05 was considered statistically significant. Statistical analysis was performed by non-parametric Mann-Whitney test.

the retinal vasculature showed that, while in control retinas the vascular plexus was developed in 2-dimensions, in p110α$^{i\Delta EC/D933A}$ retinas the sprouts did not grow to the the periphery of the retina but in multiple layers (**Figure 4.9**). This phenotype was further enhanced at P9 (**Figure 4.10**) indicating that although p110α$^{i\Delta EC/D933A}$ ECs fail to migrate towards the periphery they continue emitting multiple protrusions. Altogether, these results suggest that p110α$^{i\Delta EC/D933A}$ retinal vessels maintain a highly dynamic formation of new sprouts what can be explained by different possibilities: p110α$^{i\Delta EC/D933A}$ ECs do not receive the inhibitory Notch signal (tip-stalk selection fails) or p110α$^{i\Delta EC/D933A}$ ECs fail to establish new stable connections, and therefore do not terminate tip cell fate. It is already known that p110α is important in EC migration (Graupera et al., 2008; Nicoli et al., 2012), but how p110α-inactivated ECs continue in a "pro-angiogenic" state is not known.

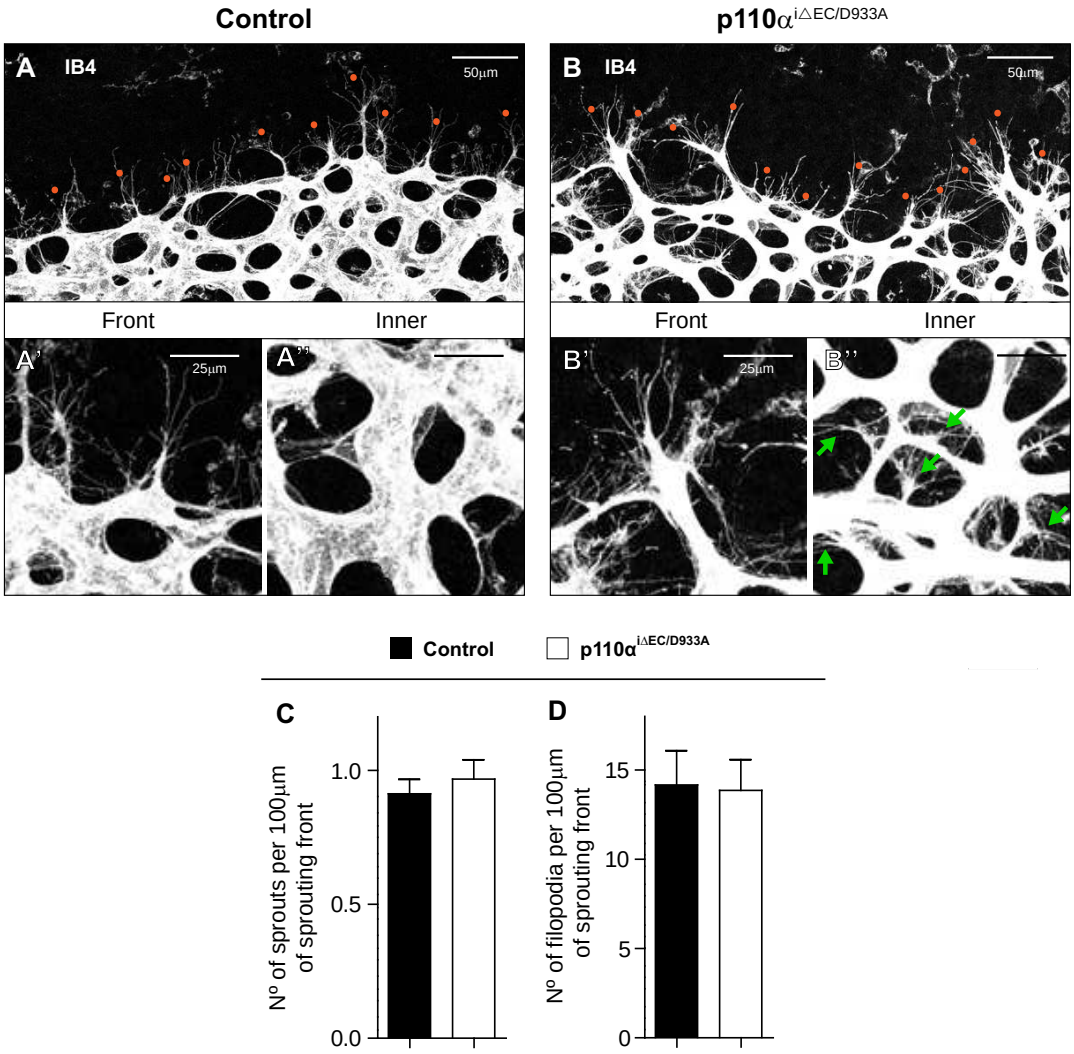

Figure 4.8: **p110α inactivation leads to the appearance of unusual sprouts and filopodia in the inner retina without changes in the leading sprouts number.** Isolectin-B4 immunostaining was performed in control **(A, A', A'')** and p110α$^{i\Delta EC/D933A}$ **(B, B', B'')** retinas at P7. 4-OH tamoxifen injections were performed at P1 and P2. **(A', B')** Zoom of vascular sprouts in the growing front of respective genotypes. **(A''', B''')** Zoom of the vasculature in the inner part of the growing front of respective genotypes. Green arrows in **B''** point at unusual sprouts with filopodia in the inner retina that appear when p110α is inactivated. **(C)** Quantification of the number of sprouts in the sprouting front **(orange dots, A, B)**. **(D)** Quantification of filopodia in the sprouting front. n ≥ 9 retinas for each genotype. Error bars are SEM. Statistical analysis was performed by non-parametric Mann-Whitney test.

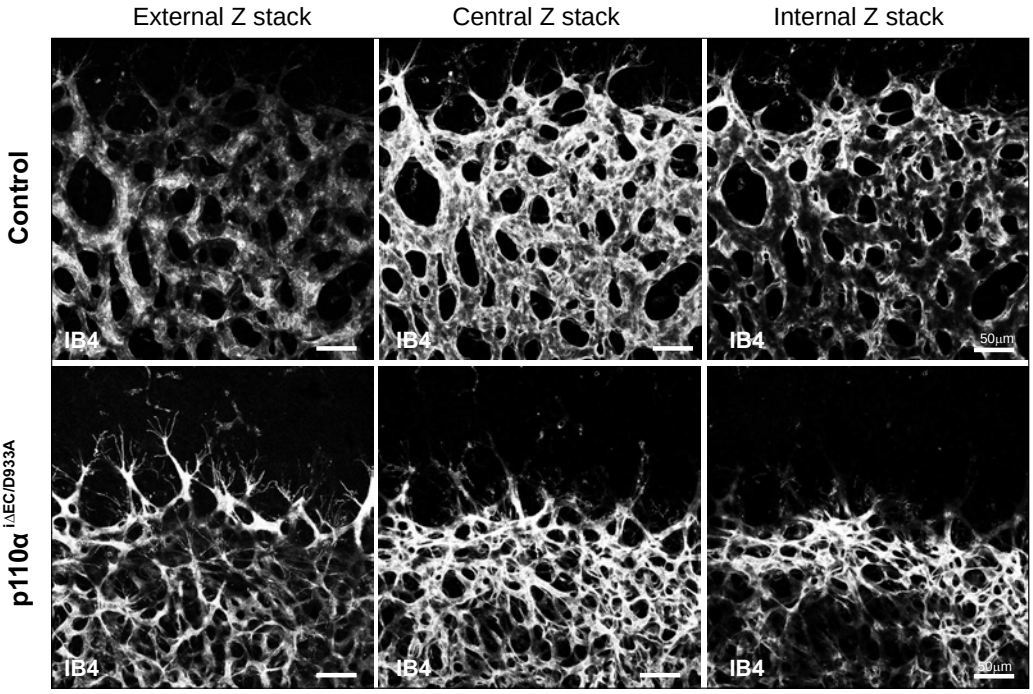

Figure 4.9: **Loss of p110α activity results in the formation of aberrant sprouts no restricted to 2D plexus generating a immature 3D vascular plexus.** Different Z-stacks from confocal images of control and p110α$^{i\Delta EC/D933A}$ retinal vessels visualized by isolectin-B4 staining. Injections were performed at P1 and P2 and retinas were isolated at P7.

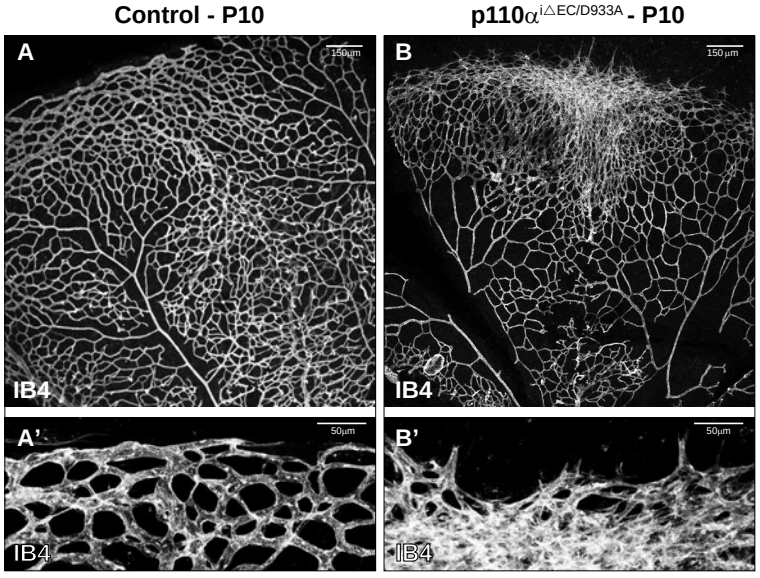

Figure 4.10: **Retinal vascular defects associated with p110α inactivation in ECs are maintained and increased in time. (A,A',B,B')** Confocal images of P10 control and p110α$^{i\Delta EC/D933A}$ retinal vessels visualized by isoletin-B4 staining. **(A',B')** High magnification images of the sprouting front where the exacerbated angiogenic defects appear.

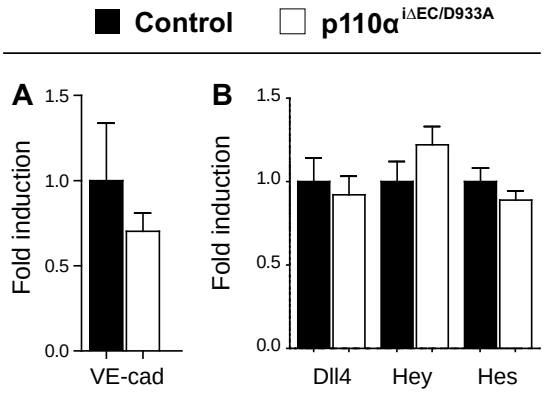

Figure 4.11: **p110α inactivation does not affect Notch target genes transcription. (A,B)** Quantitative-PCR analysis of VE-cadherin, Dll4, Hey1 and Hes1 in P7 control and p110α$^{i\Delta EC/D933A}$ retinal homogenates. The data was normalized first with endogenous control HPRT **(A)**, and then with VE-cadherin (vascular marker) to compensate for decreased EC numbers in p110α$^{i\Delta EC/D933A}$ pups **(B)**. 4-OH tamoxifen injections were performed at P1 and P2. n=8 retinas per genotype. Error bars are SEM. Statistical analysis was performed by non-parametric Mann-Whitney test.

4.2.4.1 p110α activity does not control tip-stalk selection.

As tip/stalk cell selection is mediated by Dll4/Notch lateral inhibition we tested whether Dll4/Notch signalling was impaired upon p110α inactivation. No changes in the transcriptional expression levels of the canonical Notch target genes (Hes1 and Hey1) and the Notch ligand Dll4 were detected between control and p110α$^{i\Delta EC/D933A}$ retinas (**Figure 4.11**) suggesting that p110α inactivation *in vivo* does not affect Notch signalling. However, immunostaining for Dll4 revealed an increase in Dll4 protein levels in p110α$^{i\Delta EC/D933A}$ retinas compared to control littermates (**Figure 4.12.A**). Using another tip cell marker, ESM-1, we confirmed that upon p110α inactivation there was an increase in the number of tip cells all over the multidirectional hypersprouting front (**Figure 4.12.B**). All these data suggest that p110α-PI3K signalling is not required for tip/stalk selection but it may play a key role on terminating/resolving the tip cell fate.

4.2.4.2 Loss of p110α activity results in decreased endothelial cell proliferation.

Next, we quantified the number of ECs per field using the endothelial nuclei marker Erg1,2,3 in P7 mouse retinas (**Figure 4.13.A,B**). In this regard, there was

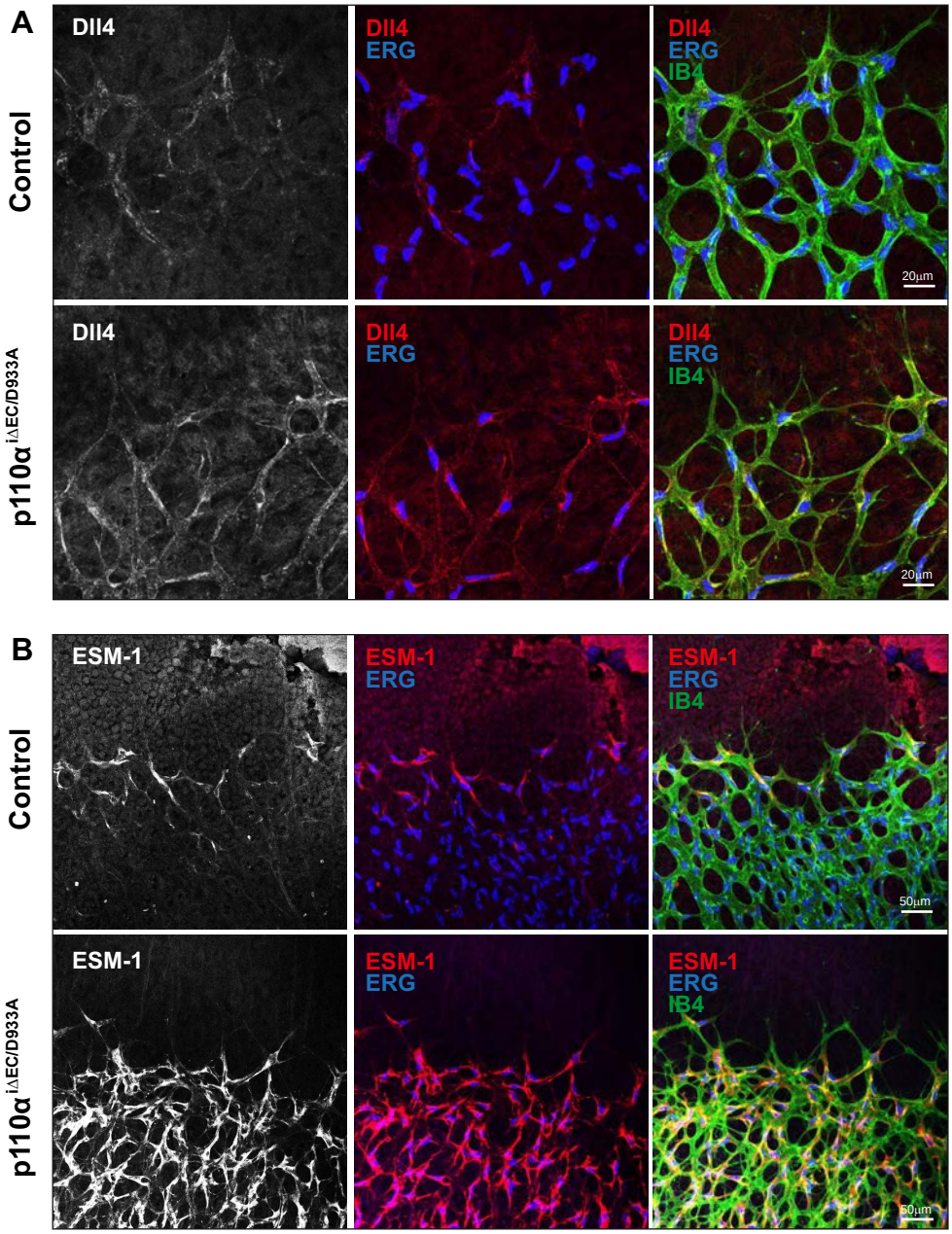

Figure 4.12: **Tip cell markers are increased in p110α$^{i\Delta EC/D933A}$ retinas.** Confocal images of P7 control and p110α$^{i\Delta EC/D933A}$ retinas stained for **(A)** Dll4 (red) or **(B)** ESM-1 (red) tip cell markers. Erg staining (blue) was used to visualized EC nuclei and Isoelctin-B4 (green) to visualize endothelial vessels.

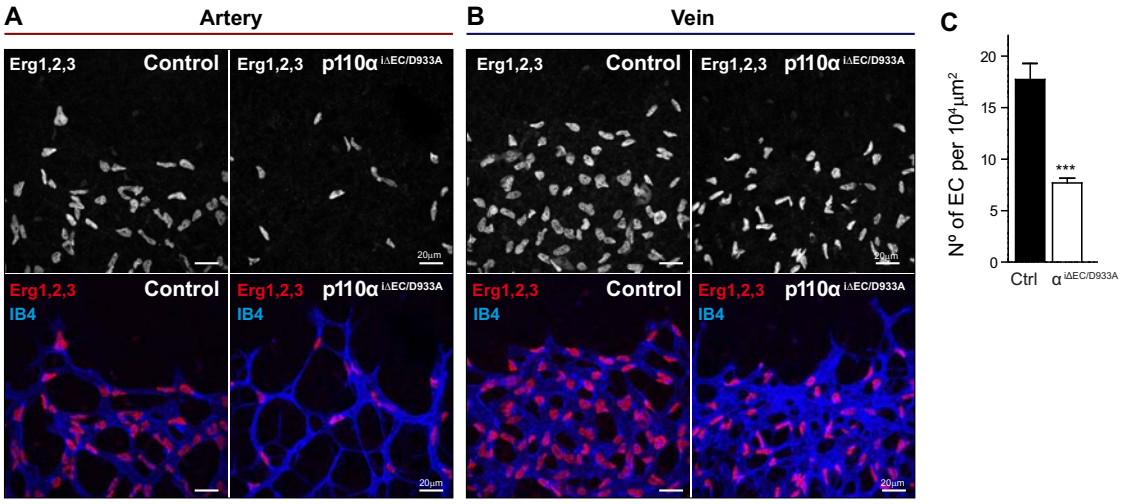

Figure 4.13: **Loss of p110α activity decreases EC numbers in the sprouting front.** Confocal images of arteries **(A)** and veins **(B)** of P7 control and p110α$^{i\Delta EC/D933A}$ retinas stained for isolectin-B4 (blue) and for the endothelial nuclear marker Erg1,2,3 (red). 4-OH tamoxifen injections were performed at P1 and P2. **(C)** Quantification of endothelial cell number in $10^4 \mu m^2$ shows decreased number of EC in p110α$^{i\Delta EC/D933A}$ retinal vasculature. n ≥ 7 retinas for each genotype. Error bars are SEM. ***P<0.001 was considered statistically significant. Statistical analysis was performed by Mann-Whitney test.

a significant decrease in the number of ECs in p110α$^{i\Delta EC/D933A}$ retinas compared to control littermates, indicating that a hypersprouting phenotype does not always correlate with an increase in ECs. Thus, we wondered whether p110α$^{i\Delta EC/D933A}$ vascular phenotype could be a consequence of increased cell death or of reduced cell proliferation. Staining with cleaved caspase-3 to evaluate EC apoptosis showed no differences between control and p110α$^{i\Delta EC/D933A}$ retinas neither at P7 (**Figure 4.14.A,B**) nor at P10 (**Figure 4.14.C**). Secondly, we evaluated EC proliferation in mouse retinas by injecting the pups with EdU (it detects the S-phase of the cell cycle by incorporating the nucleoside analog uridine into newly synthesized DNA) and performed a triple staining for EdU, isolectin-B4 and Erg1,2,3. p110α$^{i\Delta EC/D933A}$ retinas showed a dramatic reduction of proliferative ECs compared to control littermates (**Figure 4.15.A,B**). We also studied the proliferative behaviour of control and p110α$^{i\Delta EC/D933A}$ mLECs *in vitro*. KI67, a proliferation marker, showed that the p110α$^{i\Delta EC/D933A}$ mLECs presented a lower proliferation rate than control mLECs (**Figure 4.15.C,D**).

The significant decrease in endothelial cell proliferation supports an explanation for the decrease in the number of ECs. However, we wondered whether p110α loss-of-function phenotype was a direct consequence of the

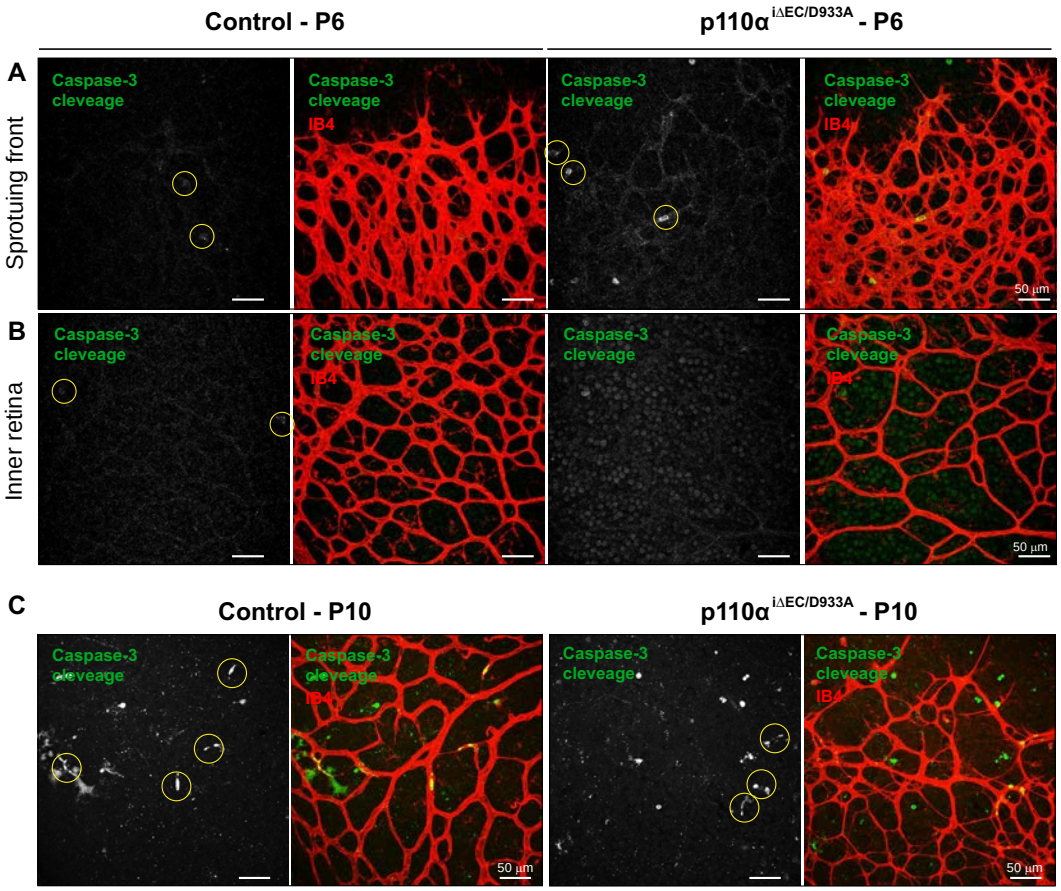

Figure 4.14: **Decreased number of ECs in p110α inactivated-retinas is not due to an increase in EC apoptosis. (A-C)** Whole-mount control and p110α$^{i\Delta EC/D933A}$ retinas stained for cleaved caspase-3 (green, marker of apoptosis) and Isolectin-B4 (red) at P6 **(A,B)** and P10 **(C)**. 4-OH tamoxifen injections were performed at P1 and P2. Yellow rings point Caspase-3 cleavage-positive cells.

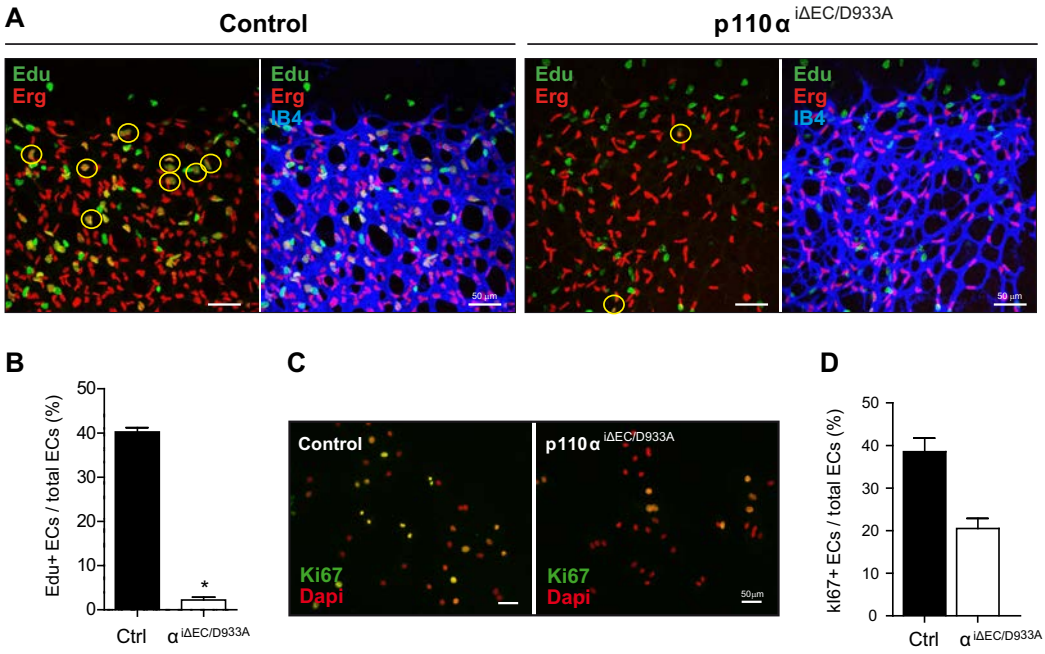

Figure 4.15: **p110α-PI3K signalling is required for endothelial cell proliferation.** **(A)** Whole-mount of control and p110α$^{i\Delta EC/D933A}$ retinas at P7 previously injected with 4-OH tamoxifen at P1 and P2 and injected with EdU 2h before isolation. Retinas were stained for isolectin-B4 (blue), Erg (red) and EdU (green). Yellow rings highlight EC nuclei positive for EdU. **(B)** Quantification of EdU positive cells per total number of endothelial cells (Erg-positive) showed a dramatic decrease in endothelial cell proliferation. n=4 retinas per genotype. **(C)** Ki67 (green) and Dapi (red) immunofluorescence in control and p110α$^{i\Delta EC/D933A}$ mouse lung endothelial cells (mLECs) treated 96h with 4-OH tamoxifen. **(D)** Quantification of the percentage of proliferative ECs. n=2 independent experiments. Error bars are SEM. *P<0.05 was considered statistically significant. Statistical analysis was performed by Mann-Whitney test.

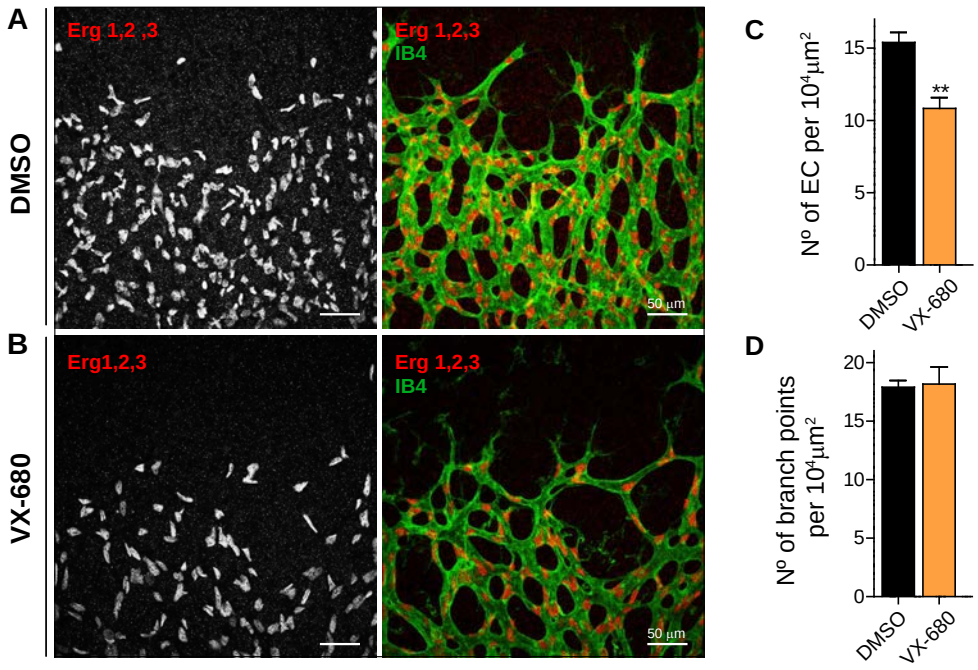

Figure 4.16: **Inhibition of proliferation does not reproduce the loss of p110α activity in retinal vasculature. (A)** Confocal images of P7 retinas of wild-type mice treated with DMSO (vehicle) or Aurora kinase inhibitor (VX-680) at P6 and P7. Retinas were stained for Erg (Red) and Isolectin-B4 (Green). **(B)** Quantification of EC number and **(C)** branch points in $10^4 \mu m^2$ in DMSO and VX-680 treated retinas. n ≥ 6 per treatment. Error bars are SEM. **P<0.01 was considered statistically significant. Statistical analysis was performed by Mann-Whitney test.

diminution in EC proliferation or p110α inhibition alters other cell functions, such as cell shape, which could result in an aberrant proliferation rate. Therefore, we inhibited proliferation *in vivo* to confirm whether a decrease in ECs led to a similar vascular phenotype. We used a specific inhibitor against the Aurora kinase A (VX-680), that is a protein implicated in cell cycle progression, and we observed a decrease in EC numbers without defects in branching and vessel structure (**Figure 4.16.A-D**). These data suggest that the decrease in proliferation showed in p110α$^{i\Delta EC/D933A}$ retinas is a consequence (or at least not the main cause) of the defects in p110α$^{i\Delta EC/D933A}$ retinal vasculature.

4.2.4.3 Long-term inactivation of p110α leads to senescent vessels.

Since apoptosis in ECs was not increased in p110α$^{i\Delta EC/D933A}$ retinas at P10, when vascular defects were very severe, we wondered whether there was an increase in EC senescence that might help to prevents the growth of

damaged or stressed cells. Staining of P15 control and p110α$^{i\Delta EC/D933A}$ retinas for senescence-associated β-galactosidase (SAβG) activity showed that whereas control retinas were completely negative for SAβG staining, p110α$^{i\Delta EC/D933A}$ retinas exhibited SAβG signal all over the vasculature (**Figure 4.17.A**). p110α$^{i\Delta EC/D933A}$ mLECs also showed an increase in SAβG staining compared to controls and p110α heterozygous mLECs (**Figure 4.17.B,C**). Conversely, neither control nor p110α$^{i\Delta EC/D933A}$ retinas at P7, when vascular defects were less severe, showed SAβG activity (data not shown). Furthermore, short-term inhibition of p110α activity with a specific inhibitor did not promote EC senescence *in vitro* (data not shown). All these data suggested that the appearance of the cellular senescence was in response to long-term p110α inactivation.

4.2.5 Inactivation of p110α in zebrafish embryos leads to the abnormal formation of ISVs.

Next, we used the zebrafish model not only as a complementary approach to validate the results obtained in the murine model, but also because zebrafish (ZF) embryos allows us to study angiogenesis in a more dynamic way. We used two different approaches to inhibit p110α: a pharmacological approach using a newly developed small molecule inhibitor with selectivity for p110α (GDC-0326) which blocks its activity, and a genetic approach using morpholino oligonucleotides (MO) that block protein translation.

First, we set up the optimal concentration of the GDC-0326 to completely block PI3K signalling in zebrafish embryos. Sprouting of segmental arteries (SeAs) start around 22 hours-post fertilization, therefore we initiated the treatment at 20 hpf in order to inactivate p110α before the beginning of the sprouting of SeAs and without affecting vasculogenesis. Zebrafish embryos were treated with vehicle (DMSO) or different concentrations of GDC-0326 (20 μM, 50 μM and 100 μM) for 2h, 4h and 8h. While zebrafish embryos treated with 20 μM GDC-0326 showed partial reduction of pAKT levels, embryos treated with 50 μM or 100 μM showed efficient reduction of p-Akt levels for a longer time (**Figure 4.18**). Thus, following experiments were done using 50 μM and 100 μM concentrations of GDC-0326. We detected that embryos treated with GDC-0326 and exposed to time lapse

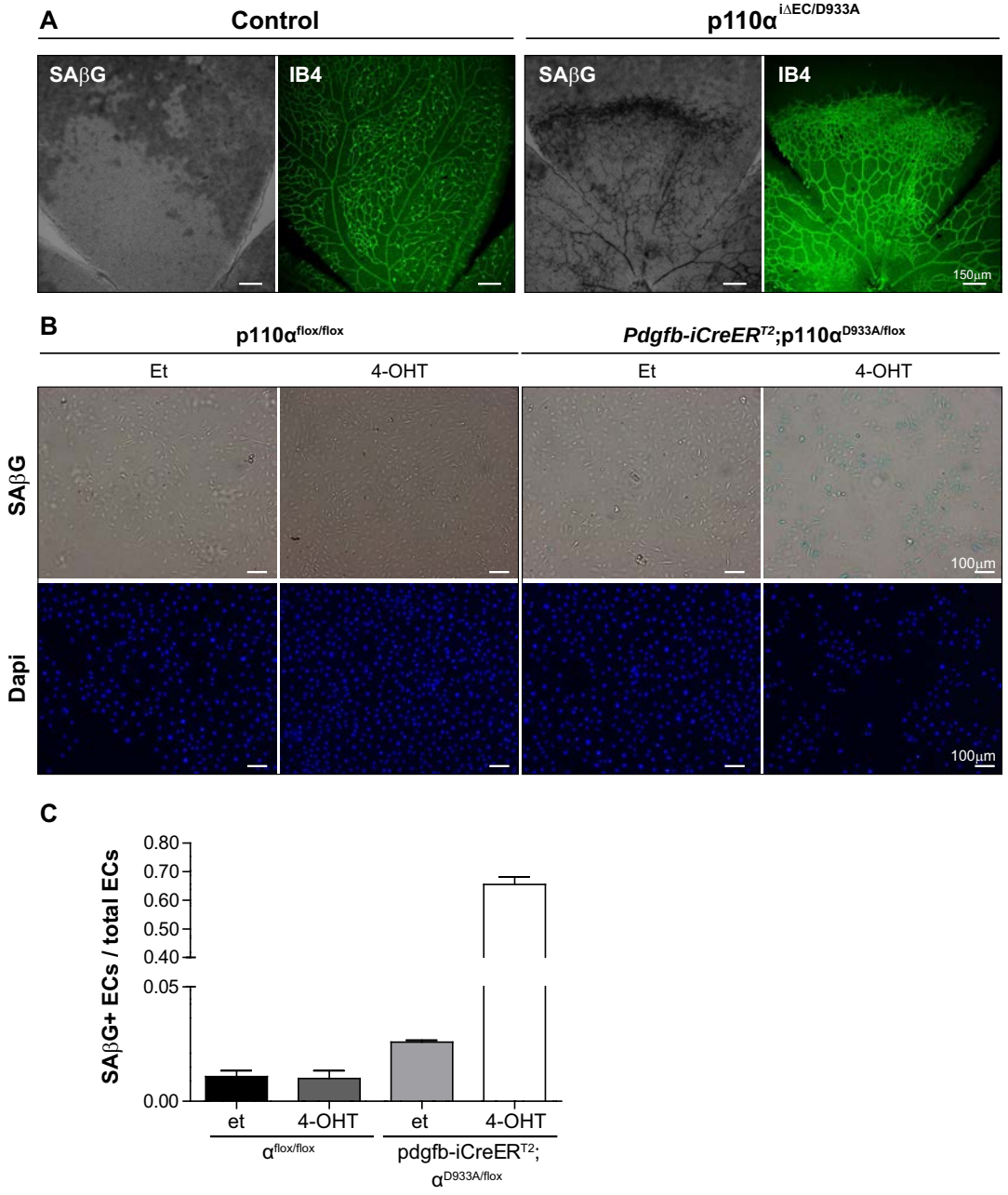

Figure 4.17: **Sustained inactivation of p110α leads to endothelial cell senescence.** **(A)** Whole mount control and p110α$^{i\Delta EC/D933A}$ retinas at P15 stained for SAβG and isoletin-B4. **(B)** SAβG and DAPI immunofluorescence in control and p110α$^{i\Delta EC/D933A}$ mouse lung endothelial cells (mLECs) treated 96h with ethanol or 4-OH tamoxifen. **(C)** Quantification of the percentage of SAβG positive cells. n = 2 independent experiments.Error bars are SEM.

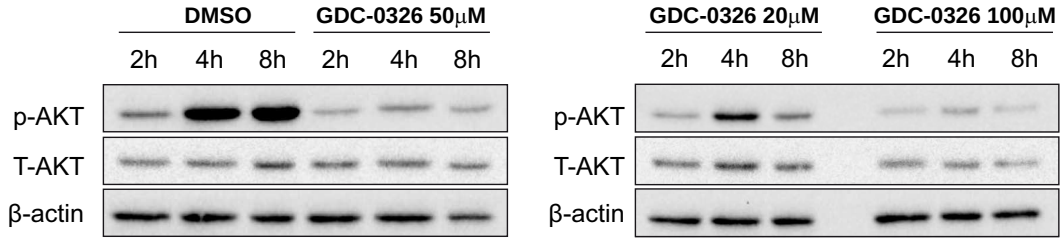

Figure 4.18: **PI3K activity increases during ISV formation and p110α-PI3K specific inhibition is sufficient to decrease PI3K activity in zebrafish embryos.** Wild-type sibling zebrafish embryos were treated with DMSO, 20 μM, 50 μM and 100 μM GDC-0326 at 20 hpf for 2h, 4h and 8h followed by immunoblotting with p-AKT, as PI3K activity read out, T-AKT and β-actin.

microscopy analysis presented a dramatic increase in cell apoptosis that led to zebrafish embryonic death (data not shown). To overcome unspecified off-target effects, we thus performed experiments in a p53 knock-down background by injecting at 2-cell stage p53-morpholino (Nicoli et al., 2012). In this experimental condition, p110α-inhibited embryos were still alive after time-lapse analysis (data not shown).

On the other hand, we tested a p110α translational morpholino (MO), designed to bind to the start codon sequence and thus, disrupting protein translation. In the same line, to avoid unspecified off-target effects and embryonic lethality, standard control-MO or p110α-MO were co-injected with a p53-MO into 2-4 cell stage ZF embryos. Western blotting analysis revealed that p110α-MO led to a 80% reduction in p110α protein level compared to control MO at 27 hpf (**Figure 4.19**). Nevertheless, p110α depletion did not result in decreased pAKT level. These results suggest that low levels of p110α are sufficient to sustain PI3K activity. Moreover, we can not rule out that compensation by other p110 isoforms sustain activation of Akt in p110α-morphants. Although the morpholino approach was not the best option for studying the protein function, we have used it as a second model to validate the results obtained with the p110α inhibitor.

In order to have a initial picture of p110α function in zebrafish vessel development, we treated Tg(kdrl:EGFP) transgenic embryos with DMSO, 50 μM GDC-0326 and 100 μM GDC-0326 from 20 hpf and analysed the vasculature at 32 hpf and 48 hpf. At 32 hpf, control embryos have developed SeAs that extended dorsally between somites boundaries on both sides of the notochord and

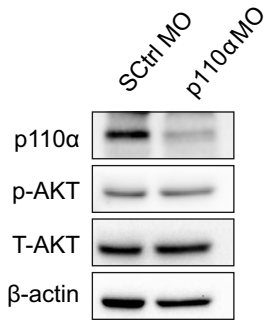

Figure 4.19: **p110α morpholino decreases p110α protein level but not p-AKT level.** Wild-type sibling zebrafish embryos were injected at 2-cell stage with 20 ng of Standard Control MO and 20 ng of p110α morpholino and subjected to immunoblotting with p-AKT (as PI3K activity read out),T-AKT and β-actin (as loading control.) at 27 hpf.

have anastomosed with adjacent SeAs to form the dorsal longitudinal anastomotic vessel (DLAV) (**Figure 4.20**). Instead, inactivation of p110α resulted in an abnormal morphology of the SeAs and DLAV. We observed vessel disconnections between the SeA and the DLAV and within the DLAV (**Figure 4.20**). At 48 hpf, segmental veins (SeVs) have connected to primary SeAs to form the intersegmental veins (ISVs) in control embryos. In contrast, GDC-0326 treated embryos displayed an aberrant formation of the ISVs and maintained the vessel disconnections already seen at 32 hpf (**Figure 4.21**, **yellow asterisks**). Vascular defects were more predominant in 100 μM GDC-0326 treated embryos than in 50 μM GDC-0326 treated ones, suggesting that higher concentrations of drug resulted in greater PI3K signalling inhibition or toxic side-effects (**Figure 4.20, Figure 4.21**).

Next, to visualize EC nuclei and EC membrane we used Tg (kdrl:EGFPnls)^{ubs1}; Tg (kdrl:mCherry-CAAX)^{S916} transgenic embryos treated with DMSO, 50 μM and 100 μM GDC-0326 from 22 hpf. In control embryos, SeAs have arrived to the dorsal part of the axis and the tip cell of the sprouts have started to establish contacts between them to form the DLAV at 27 hpf. Instead, the outgrowth of the SeAs was significantly reduced in GDC-0326 treated embryo (**Figure 4.22.A,C,F,H)**. By 33 hpf (**Figure 4.22.B,C**) and 38 hpf (**Figure 4.22.G,H**), the majority of the SeAs in GDC-0326 treated embryos were extended until the dorsal part and form the DLAV, but there were some that remained disconnected. Furthermore, the length of the SeAs was reduced in GDC-0326 treated embryos at these time-points. By measuring only the length of the SeAs that reached the

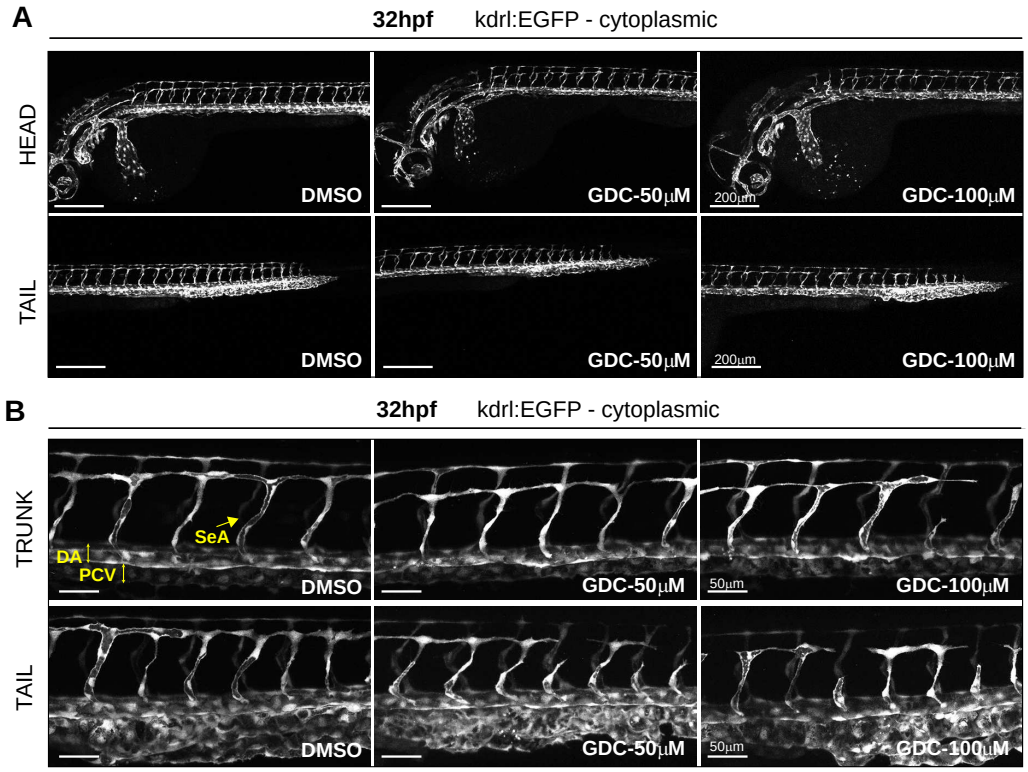

Figure 4.20: **p110α activity is required for SeAs growth in zebrafish embryos. (A,B)** Tg(kdrl:EGFP) zebrafish treated with DMSO (vehicle), 50 μM GDC-0326 and 100 μM GDC-0326 from 22 hpf and analysed at 32 hpf. **(A)** Confocal images show an overview of the zebrafish embryo vasculature upon each treatment. **(B)** High magnification images of each treatment. DA, dorsal aorta. PCV, caudal vein. SeA, segmental artery.

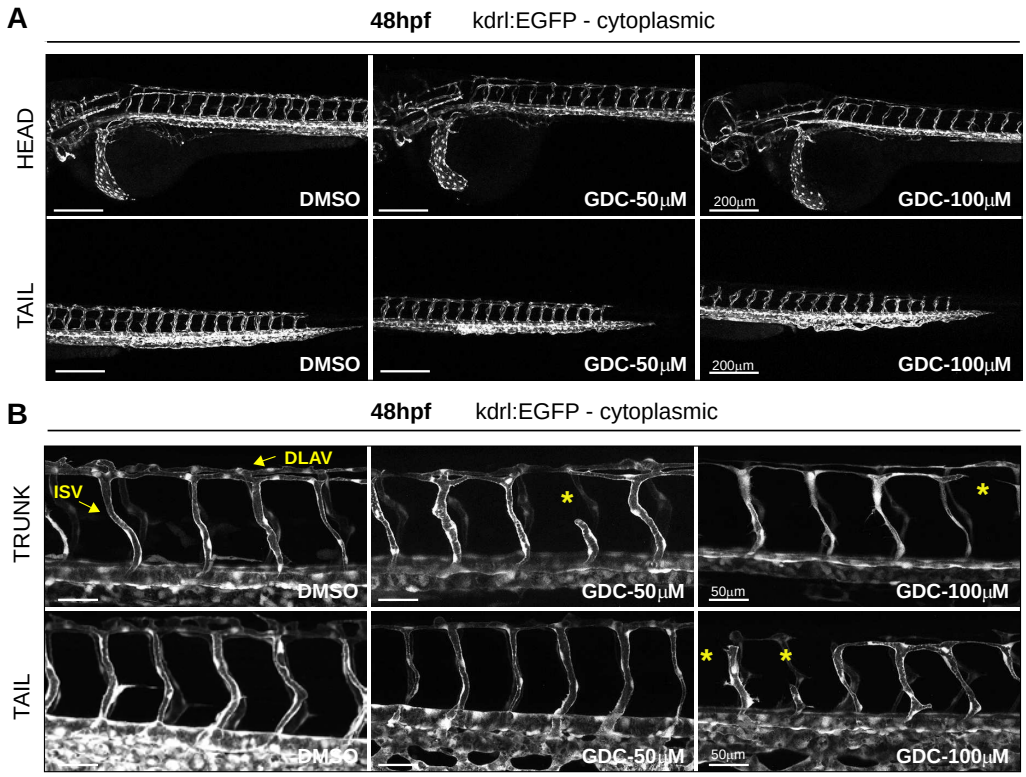

Figure 4.21: **Inactivation of p110α activity in zebrafish embryos results in disconnected ISVs at 48 hpf. (A,B)** Tg(kdrl:EGFP) zebrafish treated with DMSO (vehicle), 50 μM GDC-0326 and 100 μM GDC-0326 from 22 hpf and analysed at 48 hpf. **(A)** Confocal images show an overview of the zebrafish embryo vasculature upon each treatment. **(B)** High magnification images of each treatment. ISV, intersegmental vessels. DLAV, dorsal longitudinal anastomotic vessel.

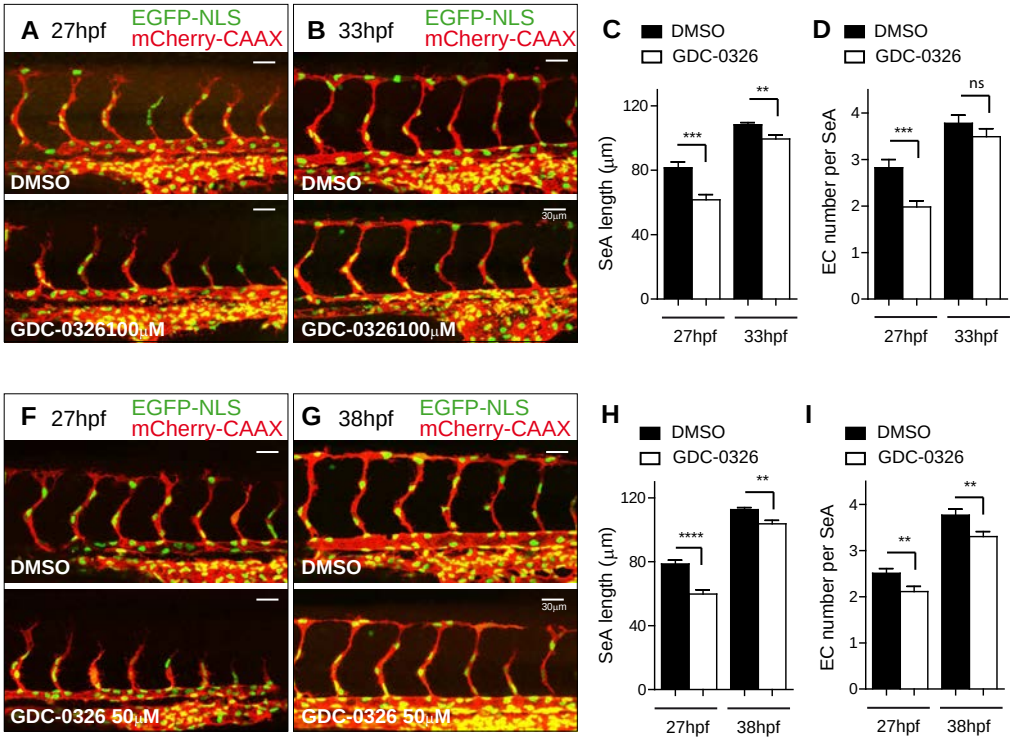

Figure 4.22: **Inactivation of p110α activity leads to a decrease in SeAs length and in EC numbers. (A,B,F,G)** Tg(kdrl:EGFPnls)^{ubs1} ; Tg(kdrl:mCherry-CAAX^{S916}) transgenic embryos treated from 22hpf with vehicle (DMSO), 50μM and 100μM GDC-0326 and fixed **(A,F)** at 27hpf , **(B)** at 33 hpf and **(G)** at 38 hpf. **(C,H)** Quantification of the length of the segmental arteries (SeAs), n ≥ 52 SeAs per treatment. **(D,I)** Quantification of EC nuclei per SeA, n ≥ 56 SeAs per treatment. Error bars are SEM. **P<0.01 and ***P<0.001 were considered statistically significant. Statistical analysis was performed by nonparametric Mann-Whitney test.

dorsal part and formed the DLAV, we did not observe differences between DMSO and GDC-0326 treated embryos, indicating that the phenotype observed upon p110α inactivation was not due to the reduction on the size of the zebrafish embryo (**Figure 4.23.A**). Therefore, p110α inactivation specifically leads to a delay in the outgrowth of the SeAs. Similarly to mouse retinas, inactivation of p110α led to a reduced number of EC nuclei (**Figure 4.22.A,B,D-G,I**).

Analysis of p110α-morphants also showed a delay in the outgrowth of the SeAs and DLAV formation compared to standard control-morphants (**Figure 4.24.A,B**). Time-lapse analysis of Tg(kdrl:EGFPnls)^{ubs1} ; Tg(kdrl:mCherry-CAAX^{S916}) transgenic embryos showed that the extension of the SeAs was slower in p110α-morphant (**Figure 4.25**). At 27 hpf, the number of EC nuclei per SeA was not different between standard control- and p110α-morphants (**Figure 4.25.A,B,D**), but the outgrowth of the SeAs was reduced in the p110α-

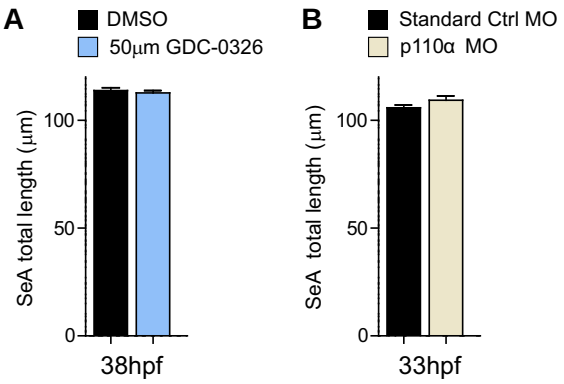

Figure 4.23: **No differences in zebrafish embryos size upon p110α inactivation. (A,B)** Quantification of the length of the SeAs that have already started to form DLAVs. **(A)** At 38 hpf in wild-type sibling zebrafish embryos treated with vehicle or 50 μM GDC from 22 hpf. **(B)** At 33 hpf in wild-type sibling zebrafish embryos injected at 2-cell stage with 20 ng of Standard Control morpholino and 20 ng of p110α morpholino. n ≥ 24 SeAs per treatment. Error bars are SEM. Statistical analysis was performed by Mann-Whitney test.

morphans (**Figure 4.25.A-C**). This result showed that the defects in the SeAs elongation were not dependent on the number of ECs. At 33 hpf, p110α-morphans maintained the delay in the outgrowth of the SeAs but also showed a decrease in the number of nuclei per SeAs compared to control-morphants (**Figure 4.25.D**). The fact that p110α-morphants exhibited first defects in the outgrowth of the SeAs (27 hpf) and at later stages arose a decrease in EC nuclei (33 hpf) reinforced previous observations suggesting that the decrease in the number of ECs was a consequence, and not the main cause, of the phenotype observed upon p110α inactivation (Nicoli et al., 2012) (**Figure 4.16, Figure 4.25**). We also quantified the length of the SeAs that arrived to the dorsal part and formed the DLAV to ensure that the decrease in the outgrowth of the SeAs observed in p110α-morphant was not a consequence of smaller embryos-size (**Figure 4.23.B**).

Taken together, our data suggest that p110α is required in ECs to ensure the proper outgrowth of the SeAs and anastomosis of adjacent SeAs to form the DLAV in zebrafish embryos.

4.2.6 p110α inhibition results in the emergence of spindly vascular structures formed by single ECs.

Sprout outgrowth is a dynamic process which requires the coordination of migration and proliferation of endothelial cells and relies on cell rearrangements.

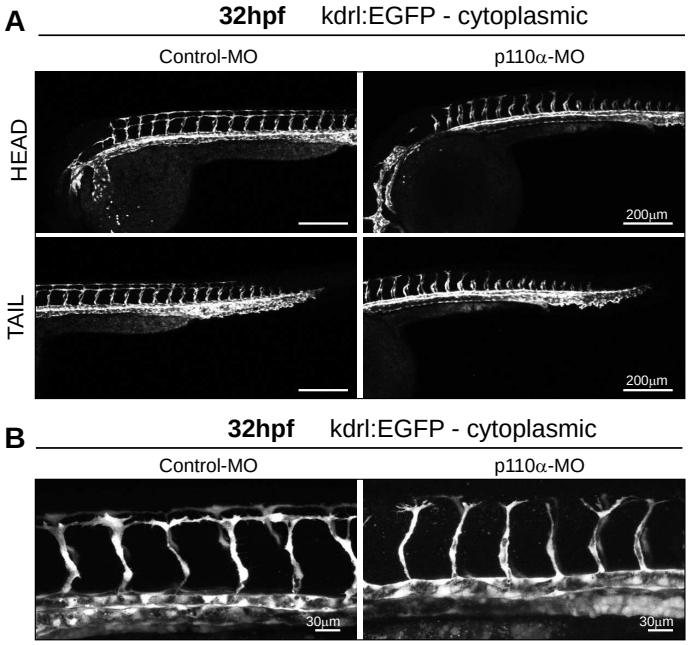

Figure 4.24: **Knock-down of p110α in zebrafish embryos results in defective SeA and DLAV formation at 32hpf. (A,B)** Wild-type sibling Tg(kdrl:EGFP) zebrafish embryos were injected at 2-cell stage with 20ng of Standard control morpholino and 20ng of p110α morpholino and analysed at 32hpf. **(A)** Confocal images show an overview of the zebrafish embryo vasculature upon each treatment. **(B)** High magnification images of the trunk.

To better understand EC behaviour upon p110α inactivation we stained both mouse retinas and zebrafish embryos with junctional markers. Co-staining of VE-cadherin, main component of adherens junctions, and isolectin-B4 showed that vessels were composed of several ECs that contact each other at several points, forming multicellular tubes in control retinas (**Figure 4.26.A,A'**). On contrary, p110α$^{i\Delta EC/D933A}$ retinas showed an increase in vascular branches negative for VE-cadherin and also appeared either in isolated rings or single-dots structures, reflecting that vascular tubes were composed of single cells or few ECs only connected by a small surface area (**Figure 4.26.B,B', asterisks**). The length of VE-cadherin-negative vascular branches was longer in p110α$^{i\Delta EC/D933A}$ retinas compared to control retinas (**Figure 4.26.C**). These data suggest that retinal vascular branches in p110α$^{i\Delta EC/D933A}$ retinas are mostly composed of very elongated single ECs that extend multiple protrusions connected by a small surface. High magnification images showed that in control retinas there were both linear and serrated VE-cadherin stainings with abundant endocytic VE-cadherin (**Figure 4.26.A', yellow and green arrows respectively**), while in p110α$^{i\Delta EC/D933A}$

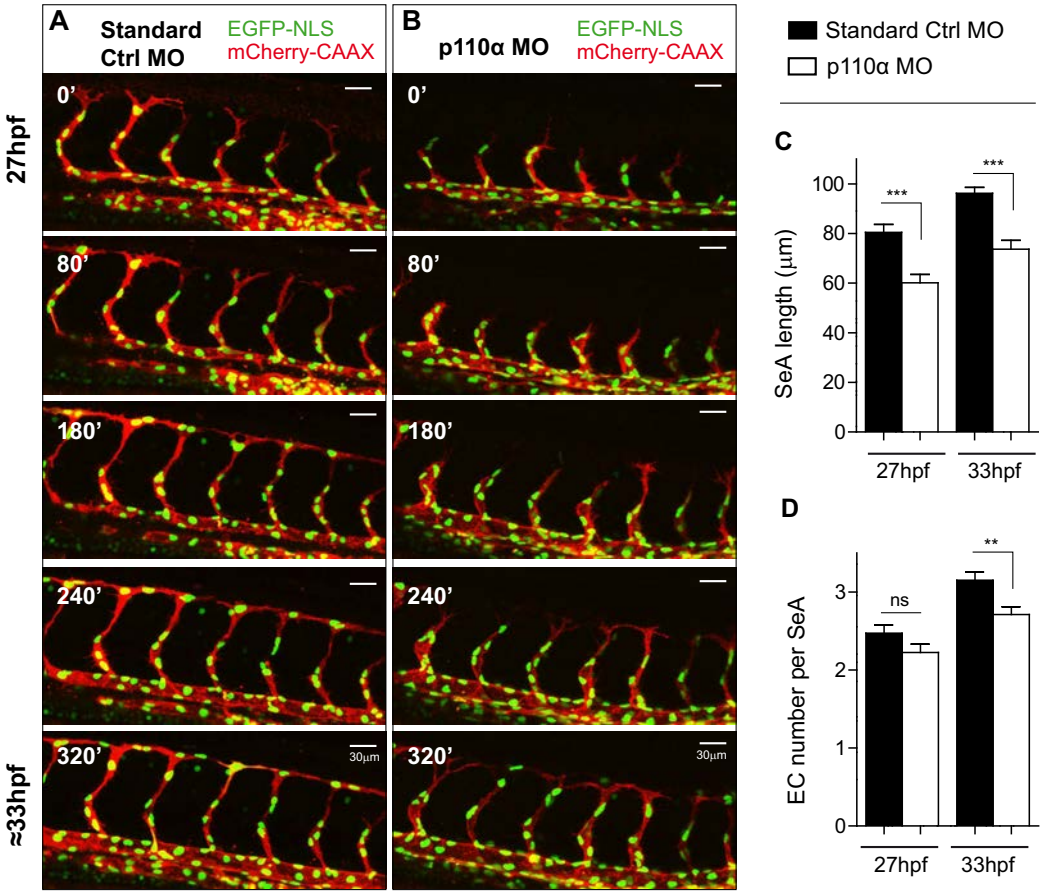

Figure 4.25: **p110α-morphants show decreased length of the SeAs and reduced number of ECs per SeA at 33 hpf.** Confocal still images of time-lapse movies of control-MO **(A)** and p110α-MO **(B)** injected at 2-cell stage in transgenic Tg(kdrl:EGFPnls)^{ubs1} ; Tg(kdrl:mCherry-CAAX)^{S916} embryos. **(C)** Quantification of SeA length, n ≥ 39 SeAs per treatment. **(D)** Quantification of EC nuclei per SeA, n ≥ 77 SeAs per treatment. Error bars are SEM. **P<0.01 and ***P<0.001 were considered statistically significant. Statistical analysis was performed by non-parametric Mann-Whitney test.

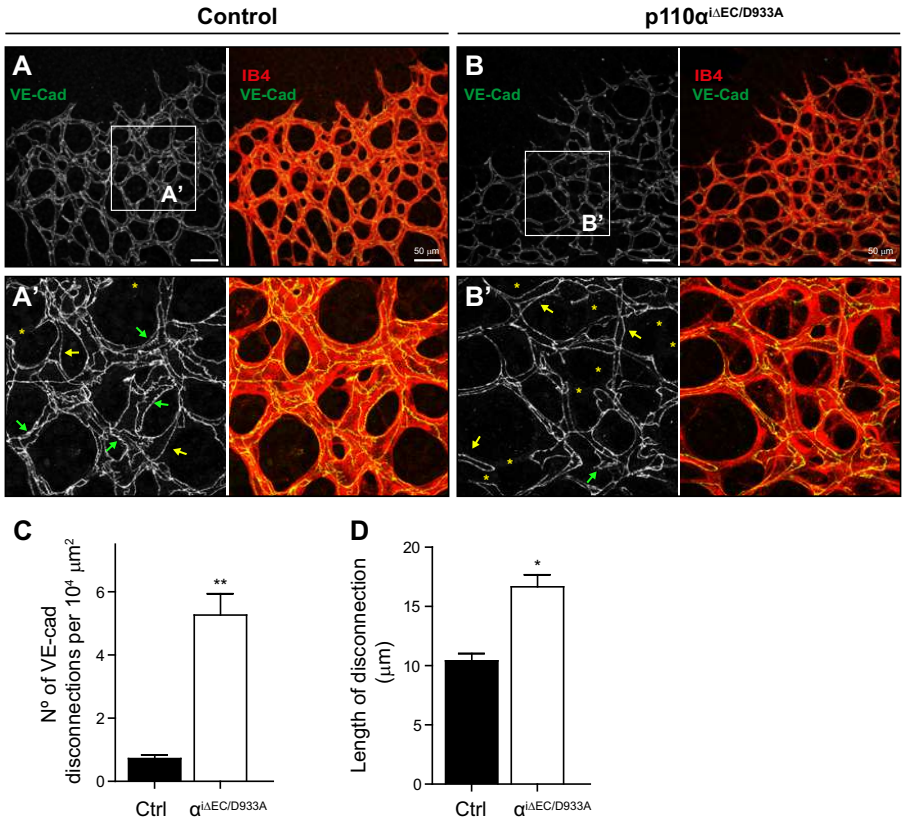

Figure 4.26: **p110α inactivation in ECs lead to the appearance of spindly vascular structures formed by single ECs. (A,B)** Confocal images of control and p110α$^{i\Delta EC/D933A}$ retinas stained for VE-cadherin (green, marker of adherens junctions) and Isolectin-B4 (red) at P7. **(A',B')** High magnification images of respective genotypes. Green arrows highlight serrated junctions and yellow arrows highlight linear junctions. Asterisks point at branches formed by single cells (VE-cadherin-negative). **(C)** Quantification of the number of vascular structures negative for VE-cadherin. **(D)** Quantification of the length of the vascular structures negative for VE-cadherin. n≥6 retinas per genotype. Error bars are SEM. *P<0.05 and **P<0.001 were considered statistically significant. Statistical analysis was performed by Mann-Whitney test.

retinas most of the VE-cadherin staining was linear (**Figure 4.26.B', yellow arrows**). This altered pattern of the staining further supports a defect in EC migration and intercalation upon p110α inactivation (Bentley et al., 2014).

Likewise, EC junctional distribution was also altered in zebrafish embryos upon p110α inactivation. We stained for ZO-1, marker of tight junctions, the transgenic tg(fli:EGFP)^{y1} embryos treated with DMSO and 50 μM GDC-0326. Control embryos showed elongated cell junctions over the SeA axis representing the longitudinal expansion of ECs to form multicellular vascular tubes (**Figure 4.27.A,E, punctuate lines**). In contrast, GDC-0326 treated embryos showed shorter and discontinuous ZO-1 staining in the ventral area, where sprouts start

to grow (**Figure 4.27.B,E, discontinuous white lines**). These data suggested that upon p110α inactivation ECs were stuck to the base and, in turn, impaired the outgrowth of the sprout. Similar to p110α$^{i\Delta EC/D933A}$ mouse retinas, the lack of junctional staining in the dorsal region of the SeA axis was more frequent and longer in GDC-0326 treated embryos (**Figure 4.27.C,D**) suggesting that this part of the SeAs were composed of single ECs. Genetic inactivation of p110α in zebrafish embryos led to similar junctional defects (**Figure 4.28**). All these data suggest that upon p110α inactivation stalk cells are not able to rearrange properly to elongate the SeAs and, as a consequence, leading cells were forced to stretch in order to contact other endothelial cells and form the DLAV.

4.2.7 p110α inactivation alters EC polarity and lumen formation leading to non-functional vessels.

Normally, retinal vessels are composed of several ECs leading to multicellular lumenazed vessel. We stained vessels for ICAM-2, a marker of apical membrane, to visualise the vessel lumen and detect whether the aberrant vasculature that appears after p110α inactivation is still functional. While in control retinas the majority of tubes were positive for ICAM-2, suggesting well-lumenazed vessels, p110α$^{i\Delta EC/D933A}$ retinas showed isolated ICAM-2 positive areas with an aberrant distribution of isolated vesicle or balloon-like structures (**Figure 4.29.A,B**). Interestingly, the narrow vascular structures, positive for isolectin-B4, were negative for ICAM-2, indicating that these vascular structures were not functional (**Figure 4.29.C**). The cell polarity proteins Par3 and Par6 are required for establishing apico-basal polarity, lumen formation and are thought to be present in the AMIS complex during the stabilization of new EC contacts. As we have observed defects in the distribution of the apical ICAM-2 protein we wondered whether endothelial cells lose polarity after p110α inactivation. Co-staining for Par3, ICAM-2 and Isolectin-B4 in P7 control and p110α$^{i\Delta EC/D933A}$ retinas showed that, while in control Par3 was localized in the apical membrane, inactivation of p110α disrupted its localization and some small ICAM-2 positive isolated aggregates appeared along the vessel (**Figure 4.30**). Therefore, p110α inactivation alters EC polarity, generating a non-functional vasculature.

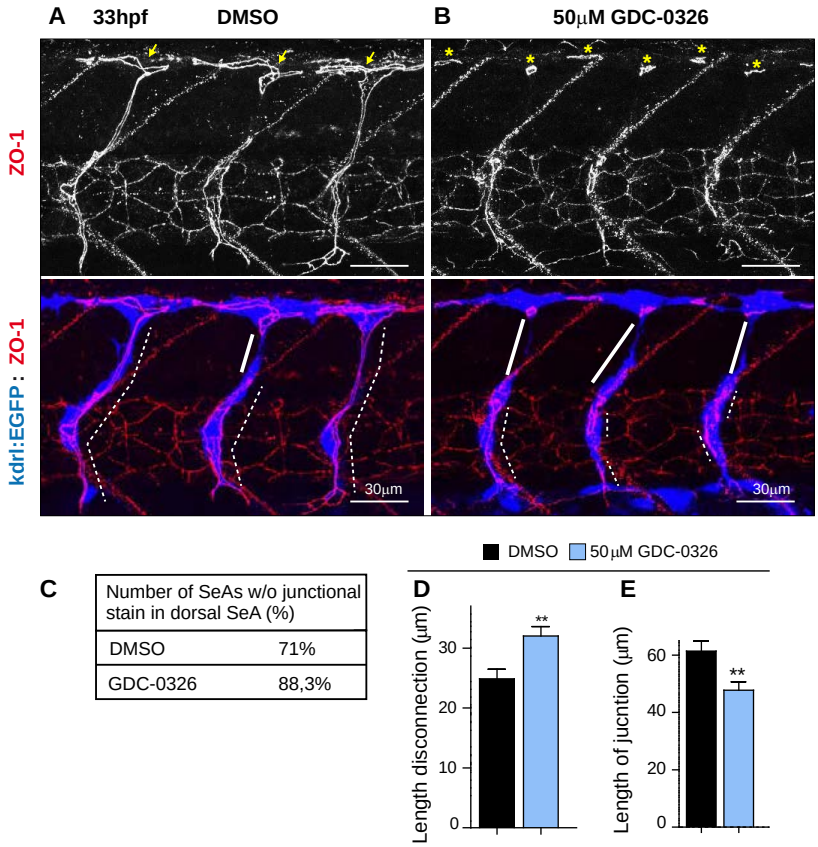

Figure 4.27: **p110α inactivation in zebrafish embryos leads to a failure in cell rearrangements and to a reduction in the cell-cell interface during sprout outgrowth.** **(A,B)** Lateral views of SeAs in DMSO **(A)** and 50 µM GDC-0326 **(B)** treated transgenic Tg(kdrl:EGFP)^{S843}(blue) zebrafish embryos stained for ZO-1 (red, tight junctions) at around 33 hpf. In p110α-inactivated embryos, the dorsal part of the SeA shows longer distances without any junctional ZO-1 staining. It is demarcated by the white lines in **A** and **B** and quantified in **(D)**; n ≥ 54 SeAs per genotype. **(E)** The length of the ventral part of the SeA with continuous ZO-1 staining (white punctuate lines in **A** and **B**) was measured and found to be significantly shorter in p110α-inactivated embryos showing an impairment in EC intercalation ; n ≥ 68 SeAs per genotype. Error bars are SEM. **P<0.01 was considered statistically significant. Statistical analysis was performed by Mann-Whitney test.

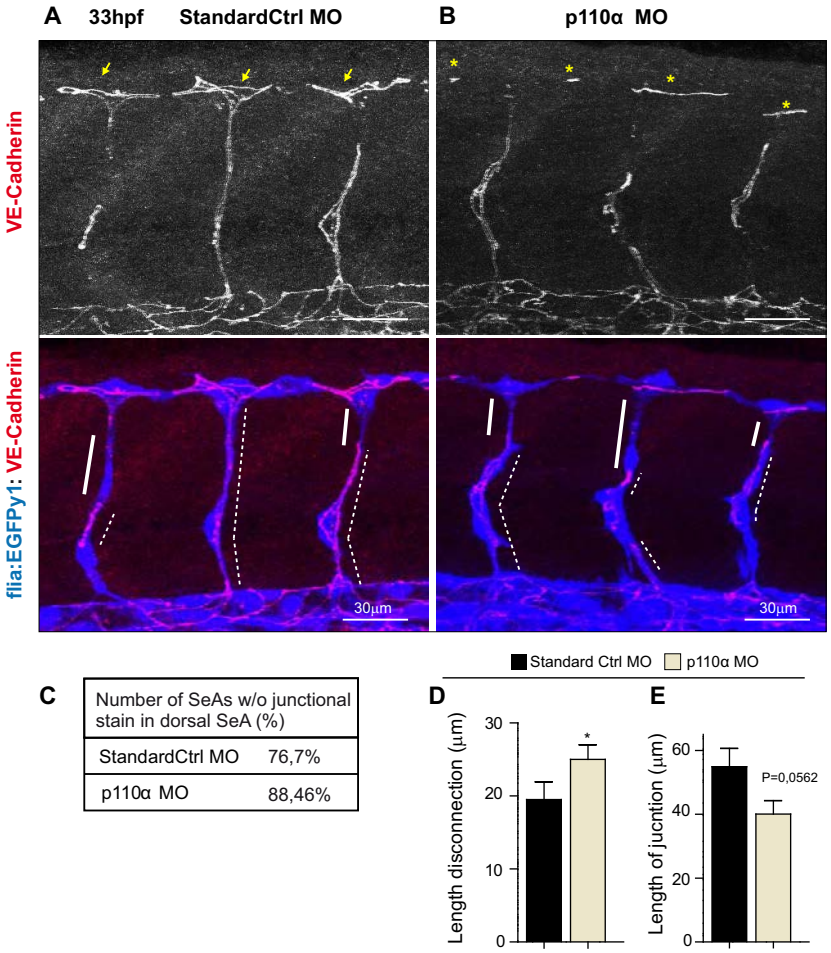

Figure 4.28: **p110α-morphants showed a failure in cell rearrangements and a reduction in the cell-cell interface during sprout outgrowth. (A,B)** Lateral views of SeAs in standard control **(A)** and p110α **(B)** morphants of transgenic Tg(fli:EGFP)^{y1}(blue) zebrafish embryos stained for VE-cadherin (red, adherens junctions) at around 33hpf. In p110α-inactivated embryos, the dorsal part of the SeA shows longer distances without any junctional VE-cadherin staining. It is demarcated by the white lines in **A** and **B** and quantified in **(D)** ; n ≥ 22 SeAs per genotype. **(E)** The length of the ventral part of the SeAs with continuous VE-cadherin staining (white punctuate lines **A** and **B**) was measured and found to be significantly shorter in p110α-inactivated embryos showing an impairment in EC intercalation. n ≥ 24 SeAs per genotype. Error bars are SEM. *P<0.05 was considered statistically significant. Statistical analysis was performed by Mann-Whitney test.

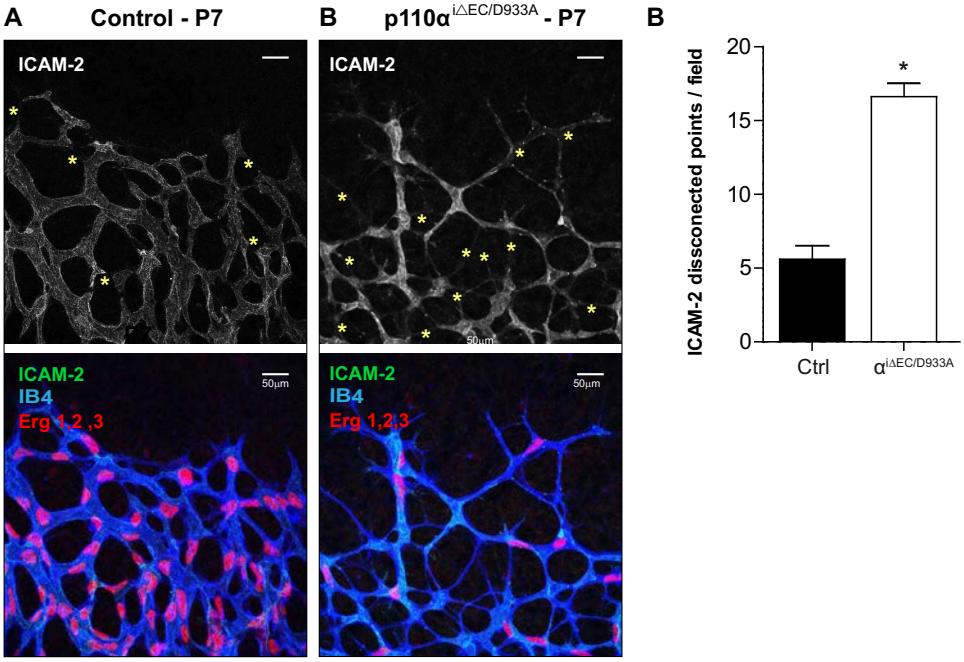

Figure 4.29: **p110α inactivation leads to a non-well lumenized vasculature. (A,B)** Confocal images of control **(A)** and p110α$^{i\Delta EC/D933A}$ **(B)** littermate retinas stained for ICAM-2 (green, apical membrane marker), Erg1,2,3 (red) and Isolectin-B4 (red, vasculature) at P7. **(C)** Quantification of vascular branches negative for ICAM-2. Yellow asterisks highlight alumenized vascular structures. n = 4 retinas per genotype. Error bars are SEM. *P<0.05 was considered statistically significant. Statistical analysis was performed by Mann-Whitney test.

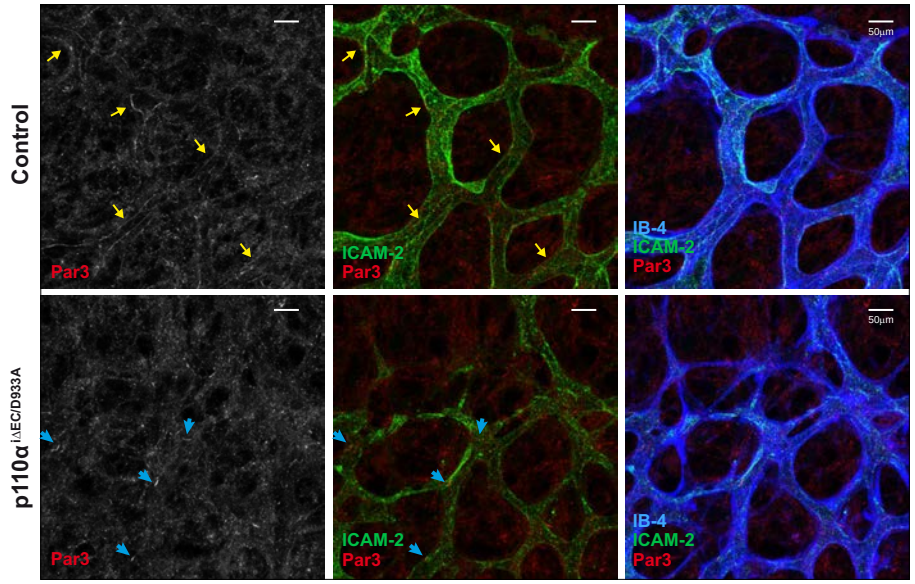

Figure 4.30: **Loss of apico-basal polarity in ECs upon p110α inactivation. (A,B)** Confocal images of control **(A)** and p110α$^{i\Delta EC/D933A}$ **(B)** littermate retinas at P7 stained for ICAM-2 (green, apical membrane marker), polarity factor Par3 (red) and isolectin-B4 (red, vasculature). Arrows highlight Par3 staining.

4.2.8 Failure in the stabilization of new EC contacts upon p110α inactivation.

Our data have shown that inactivation of p110α leads to aberrant endothelial cell migration, rearrangements and the formation of new functional vessels. All these observations suggested that p110α activity could be regulating endothelial cell-to-cell contacts. Considering that junctional stability between ECs is critical in regulating sprouting angiogenesis and vessel homoeostasis, we next investigated the role of p110α in the stabilization of new endothelial cell-to-cell contacts.

To test that, first we studied the effect of p110α inactivation on the early anastomosis process in zebrafish embryos. We performed time-lapse experiments using UCHD-EGFP in the presence of membrane CAAX- mCherry transgene, to visualize both actin and EC membrane. Embryos were treated with DMSO or with 50 μM GDC-0326 and subjected to time-lapse analysis at 30hpf for 6 hours. We compared SeAs of similar elongation at 30 hpf from control (**Figure 4.31**) and GDC-0326 (**Figure 4.32**) treated embryos. In control embryos, we observed that two angiogenic sprouts from neighbouring SeAs contact each other and fuse to give rise to a lumenized dorsal longitudinal anastomotic vessel (DLAV) (**Figure 4.31**). However, in GDC-0326 treated embryos, the first connection between adjacent SeAs did not progress to form a lumenized DLAV. Instead, ECs retracted and left behind a gap between SeAs (**Figure 4.32**).

In order to discern whether this failure in EC junctional stabilization during anastomosis could be due to the previous defects found during the outgrowth of the SeA, or p110α activity specifically controls this process, we treated embryos from 27 hpf for 3h, ones the SeAs have almost arrived to the dorsal part. As previously seen, later inactivation of p110α also resulted in a lack of contacts stabilization between neighbouring sprouts and the retraction of tip cells (**Figure 4.33**).

These data suggested that p110α inactivation is required for the stabilization of new EC contacts during the early anastomosis process. In this line, confocal images of the EC junctions in control embryos showed stretched EC junctions in the DLAV (growing of the junctional ring) to give rise to a multicellular DLAV (**yellow arrows, Figure 4.27.A, Figure 4.28.A**). However, DLAV of p110α

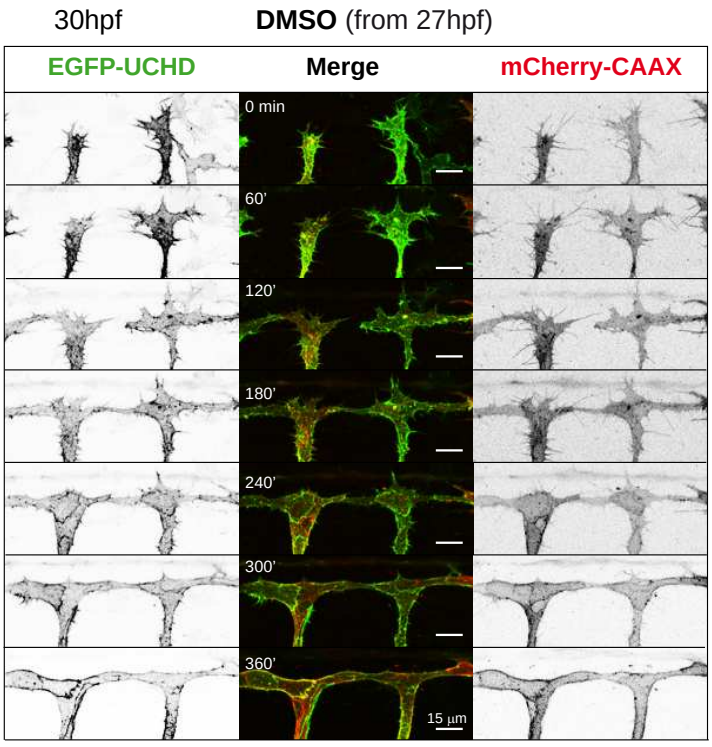

Figure 4.31: **Early anastomosis steps in control zebrafish embryos.** Confocal still pictures from a time-lapse movie (starting at 30 hpf) showing lateral views of SeA morphogenesis in transgenic Tg(UAS:EGFP-UCHD)^{ubs3}; (kdrl:mCherry-CAAX)^{S916} embryos treated with DMSO (vehicle) from 27 hpf. EC membrane is visualized in red and the actin cytoskeleton is visualized by F-actin binding domain of utrophin in green.

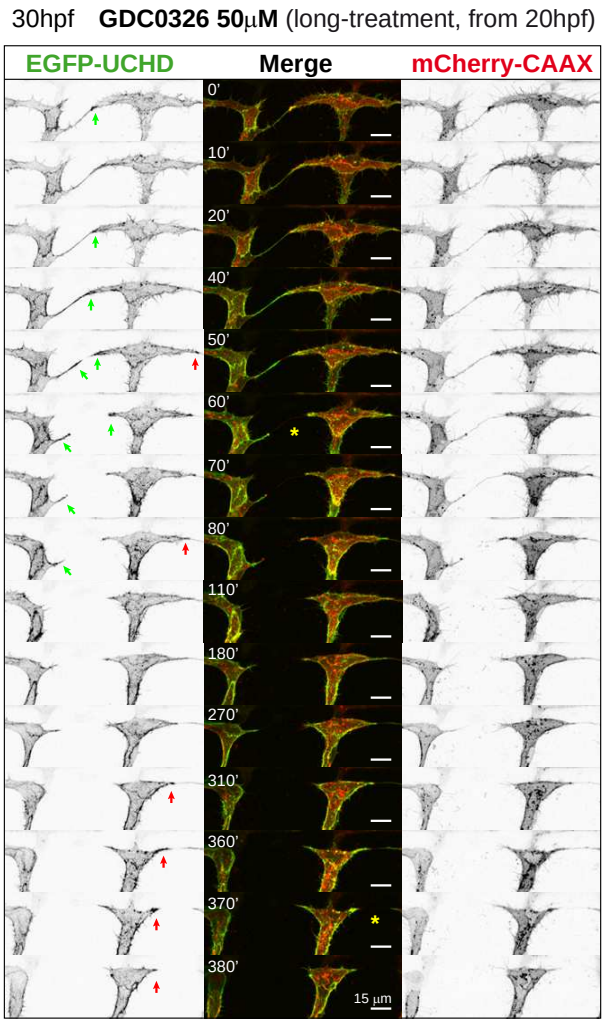

Figure 4.32: **p110α-inactivated ECs fail to stabilise nascent cell connections during anastomosis in zebrafish embryos.** Confocal still pictures from a time-lapse movie (starting at 30 hpf) showing lateral views of SeA morphogenesis in transgenic Tg(UAS:EGFP-UCHD)^{ubs3}; (kdrl:mCherry-CAAX)^{S916} embryos treated with 50 μM GDC-0326 from 20 hpf. EC membrane is visualized in red and the actin cytoskeleton is visualized by F-actin binding domain of utrophin in green. Red and green arrows highlight an increase in actin in "the tip" of the leading cells. We observed that upon p110α inactivation there was a initial inefficient contact that ends with the retraction of the leading ECs and the formation of a discontinuous DLAV.

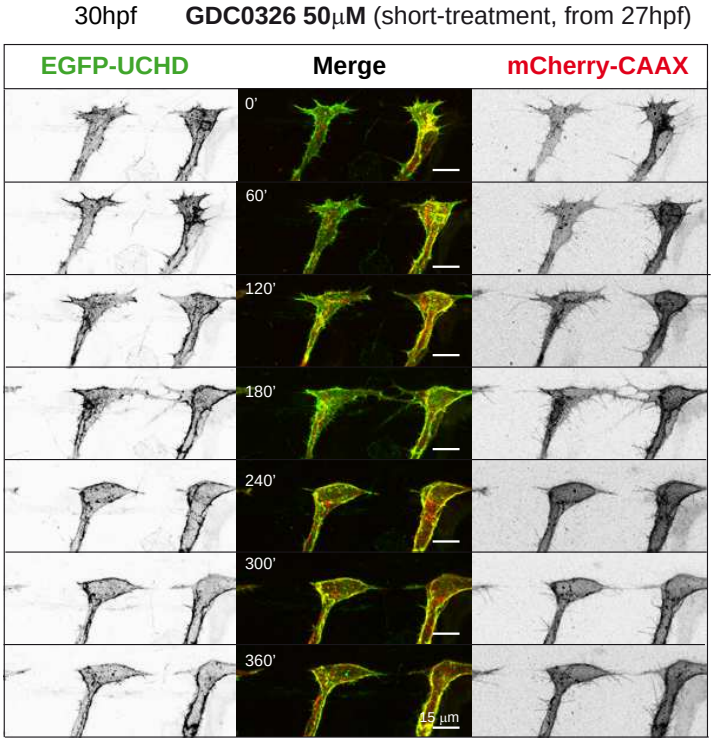

Figure 4.33: **Upon short p110α-inhibitor treatment ECs fail to contact and stabilise nascent cell connections during anastomosis.** Confocal still pictures from a time-lapse movie (starting at 30 hpf) showing lateral views of SeA morphogenesis in transgenic Tg(UAS:EGFP-UCHD)^{ubs3}; (kdrl:mCherry-CAAX)^{S916} embryos treated with 50 μM GDC-0326 from 27 hpf. EC membrane is visualized in red and the actin cytoskeleton is visualized by F-actin binding domain of utrophin in green. We observed that upon p110α inactivation there was an initial inefficient contact that ends with the retraction of the tip ECs and the foramtion of a discontinuous DLAV.

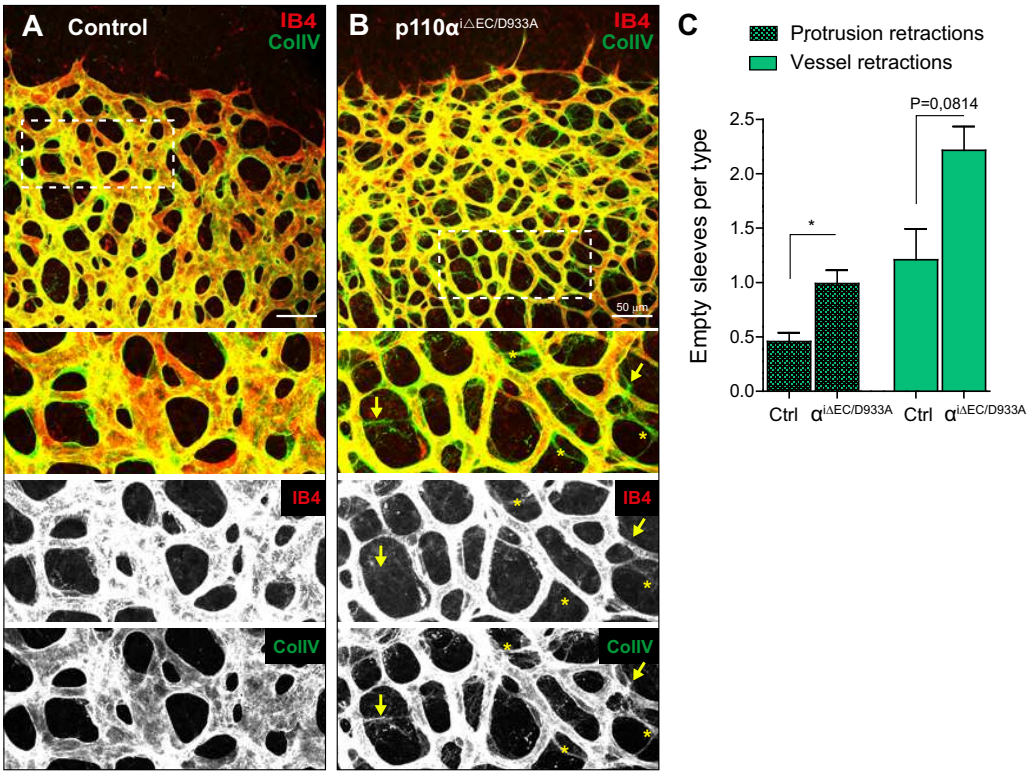

Figure 4.34: **Loss of p110α leads to instability of sprout fusion points. (A,B)** Confocal images of control **(A)** and p110α$^{i\Delta EC/D933A}$ **(B)** littermate retinas stained for Collagen IV (green, ECM marker) and Isolectin-B4 (red, vasculature) at P7. **(C)** Quantification of ColIV^{+}IB-4^{-} areas (empty sleeves) divided by type. Yellow asterisks in **B** point to *vessel retractions* and arrows in **B** point to *protrusion retractions*. n = 4 retinas per genotype. Error bars are SEM. *P<0.05 was considered statistically significant. Statistical analysis was performed by Mann-Whitney test.

inactivated embryos showed small junctional rings that seem not to stretch to form a continuous contact surface and therefore, a multicellular DLAV. (**yellow asterisks, 4.27.B, Figure 4.28.B**). We conclude that p110α plays a role in coordinating the anastomosis process in the early steps and, as well as during SeAs outgrowth, allows the growing of the junctional ring to form multicellular tubes.

To further validate an increase in tip cell retraction upon p110α inactivation, we stained control and p110α$^{i\Delta EC/D933A}$ retinas for ColIV, a basement membrane component that is synthesized and secreted by endothelial cells as they mature. At the sprouting vascular front of control retinas, collagen IV (ColIV) regularly co-localize with endothelial isolectin-B4 staining except for the tip cells (**Figure 4.34.A**). However, during the process of vessel pruning, empty basement sleeves often remain after endothelial cells have regressed. Therefore, empty

ColIV sleeves indicate the previous existence of vessels that have regressed. We distinguished two types of retraction based on ColIV deposition: *vessel retraction*, called to ColIV deposition that connects two remained vessels (normal during pruning) (**Figure 4.34.B, yellow asterisks**) and *protrusion retraction* called to ColIV deposition connected only to one vessel (that could reflect both a vascular retraction prior to connecting to other vessel or prior to have time to deposit ColIV) (**Figure 4.34.B, yellow arrows**). Analysis of ColIV staining at the sprouting front of control and p110α$^{i\Delta EC/D933A}$ retinas showed an increment of both types of retraction but significantly of *protrusion retractions* (**Figure 4.34.A-C**) indicating that upon p110α inactivation in the sprouting area there is highly dynamic extension and retraction of vasculature structures that fail to stabilize new sprout fusion contacts and therefore, fail to form new functional vessels. In line with zebrafish time-lapses, this result confirms that p110α inactivation leads to defects in anastomosis and, in consequence, ECs maintain a angiogenic-like state sending multiple inefficient protrusion.

4.2.9 p110α activity controls actomyosin contractility in endothelial cells during sprouting angiogenesis

Given that p110α$^{i\Delta EC/D933A}$ ECs present defects in migration and in junctional stabilization, we decided to study possible defects in cytoskeleton dynamics. For this purpose, retinas were stained with phalloidin to visualize F-actin. Unexpectedly, we observed an increase in F-actin level in p110α$^{i\Delta EC/D933A}$ retinal vasculature (**Figure 4.35.A-D**). High magnification images showed that there were more and thicker fibres of F-actin in ECs upon p110α inactivation (**Figure 4.35.C**). Next, we tested the contractility state by using phosphorylated myosin light chain (p-MLC) staining. In line with the phallodin staining, there was a dramatic increase in p-MLC levels in p110α$^{i\Delta EC/D933A}$ retinas compared to control ones (**Figure 4.36.A-D**). *In vivo* analysis of actin cytoskeleton has shown that p110α inactivation leads to the increase in actomyosin contractility.

To gain insight into the regulation of actomyosin contractility, we studied control and p110α$^{i\Delta EC/D933A}$ mLECs in basal conditions. Co-staining of F-actin and p-MLC confirmed that inactivation of p110α in ECs results in increase

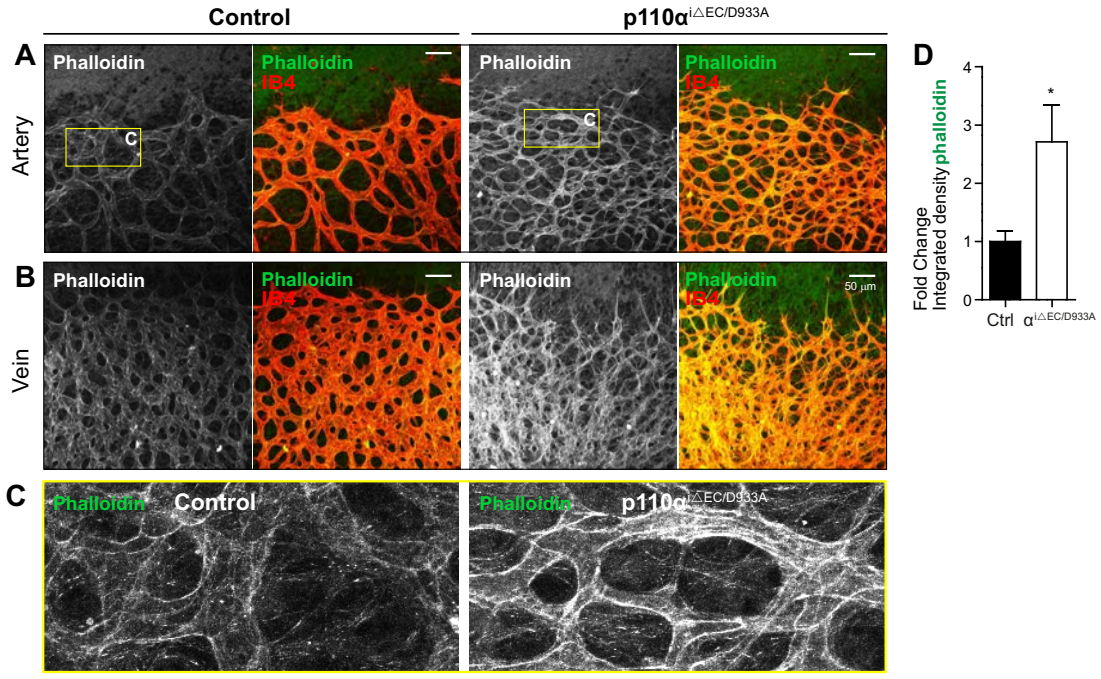

Figure 4.35: **p110α inactivation leads to increased F-actin levels in ECs.** Confocal images of arteries **(A)** and veins **(B)** of P7control and p110α$^{i\Delta EC/D933A}$ retinas stained with isolectin-B4 and phalloidin. **(C)** Zoom of **A** highlighting the change in the localization of the phalloidin staining between conditions. **(D)** Quantification of the intensity per vascular area (integrated density) of phalloidin staining. n = 6 retinas per genotype. Error bars are SEM. *P<0.05 was considered statistically significant. Statistical analysis was performed by Mann-Whitney test.

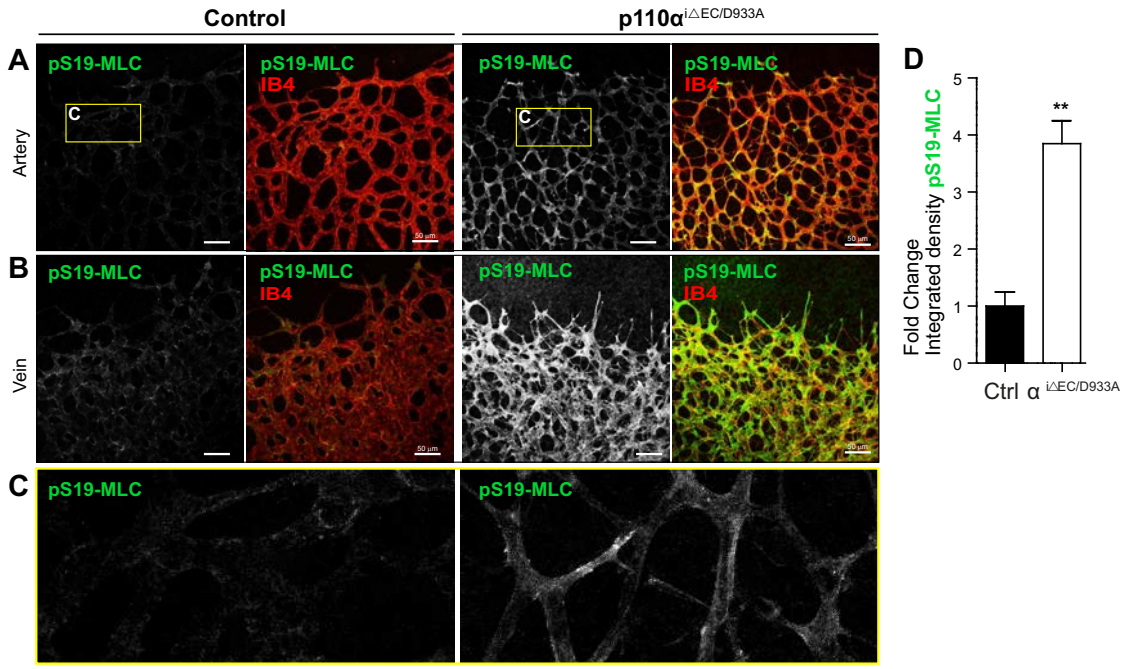

Figure 4.36: **p110α inactivation leads to increased p-MLC levels in ECs.** Confocal images of arteries **(A)** and veins **(B)** of P7control and p110α$^{i\Delta EC/D933A}$ retinas stained for Isolectin-B4 and pS19-MLC. **(C)** Zoom of **A** highlighting the p-MLC staining between conditions. **(D)** Quantification of the intensity per vascular area of pS19-MLC staining. n ≥ 5 retinas for each genotype. Error bars are SEM. **P<0.01 was considered statistically significant. Statistical analysis was performed by Mann-Whitney test.

actomyosin contractility (**Figure 4.37.A,B, C)**. Interestingly, there was a change in the localization of the staining. Control mLECs presented stress fibres across the cytoplasm of the cell whereas in p110α$^{i\Delta EC/D933A}$ mLECs F-actin and p-MLC were enriched at the subjunctional region of p110α$^{i\Delta EC/D933A}$ mLECs (**Figure 4.37.A',B', D)**. A similar pattern was observed with the double phospho-MLC staining (Thr18/Ser19) (**Figure 4.38**). By western blotting, we confirmed the increase in p-MLC level upon both, genetic (**Figure 4.39**) and pharmacological (**Figure 4.40**) inactivation of p110α.

Altogether we found that p110α negatively regulates actomyosin contractility. Actomyosin contractility is critical for the regulation of the actin cytoskeleton, cell-substrate adhesion, cell shape, cell–cell contacts and migration. In the absence of p110α activity, many of these features which were affected prompted us to study how p110α regulates actomyosin contractility and therefore the angiogenic process.

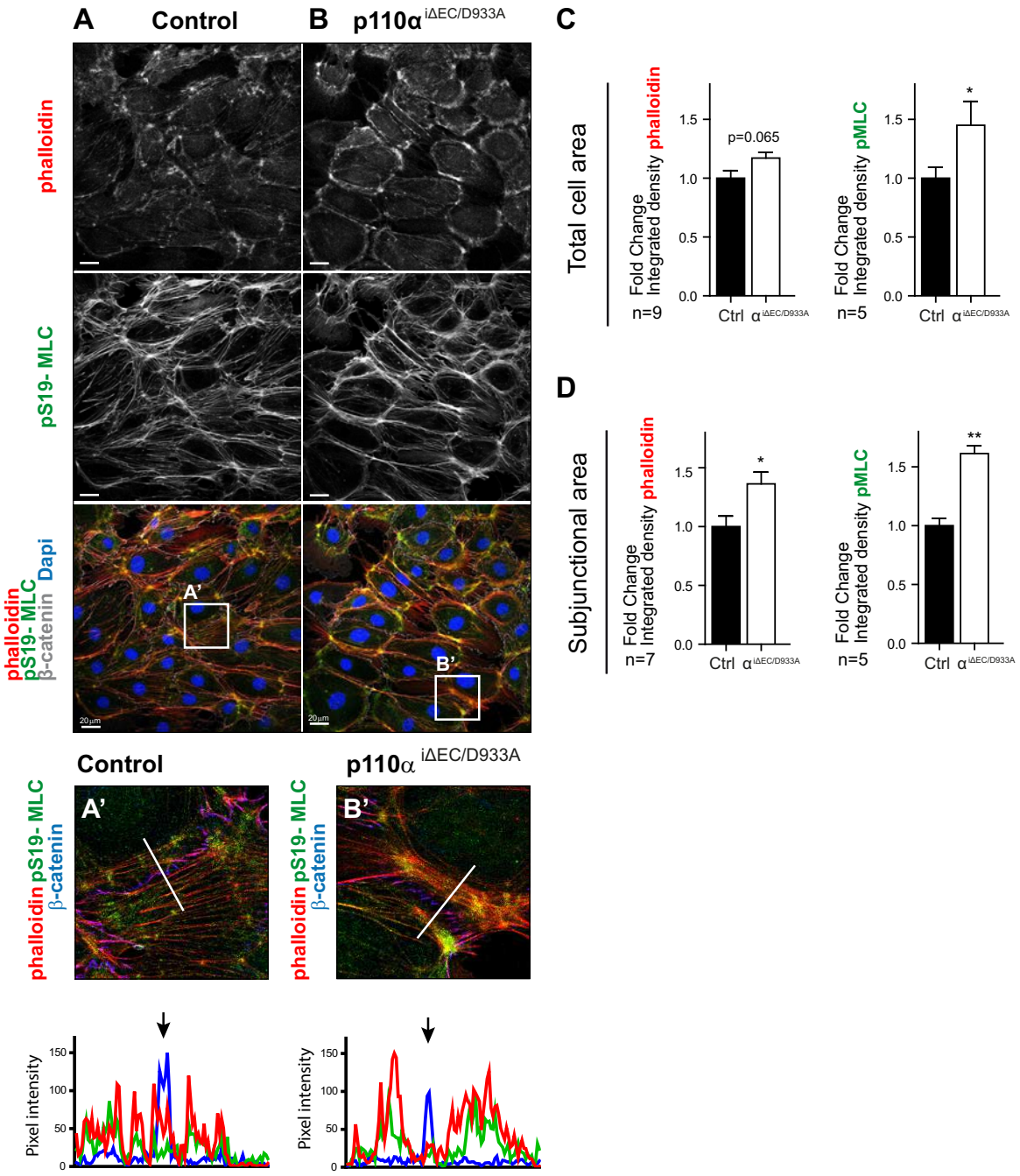

Figure 4.37: ***In vitro* inactivation of p110α leads to increased subcortical actomyosin contractility in mLECs.** **(A,B)** Confocal images of pS19-MLC (green), phalloidin (red), β-catenin (grey) and DAPI (blue) immunofluorescence in Control and p110α$^{\Delta iEC/D933A}$ mouse lung endothelial cells (mLECs). **(A'-B')** Zoom of **A** and **B** highlighting the change in the localization of the phalloidin and pS19-MLC staining between conditions. Accompanying fluorescence intensities along the depicted lines showing that the distribution of p-MLC (green), F-actin (red) and β-catenin (blue) in the different conditions. Black arrows indicate the localization of the junction. Quantification of signal intensities was done in ImageJ by applying a single ROI to multiple colour channels in the same image and extracting the plot profile. **(C)** Quantification of phalloidin and pS19-MLC intensity per cell area. **(D)** Quantification of the phalloidin and pS19-MLC intensity in the subjunctional area. Error bars are SEM. *P<0.05 and **P<0.01 were considered statistically significant. n means independent experiments. Statistical analysis was performed by Mann-Whitney test.

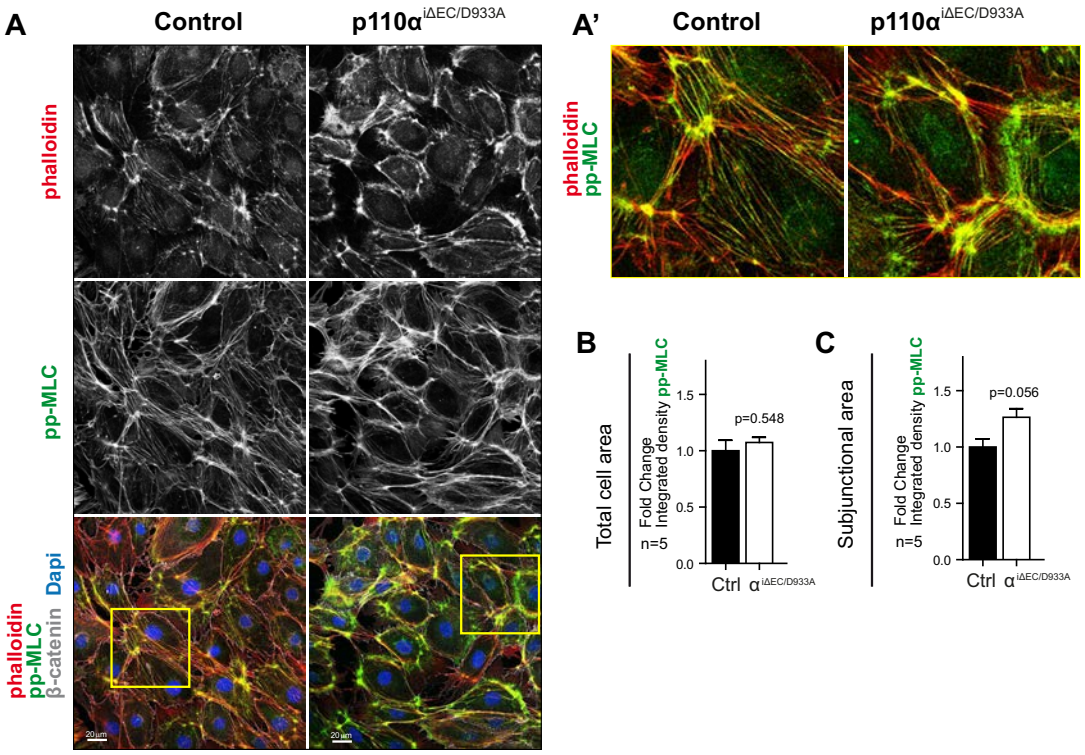

Figure 4.38: ***In vitro* inactivation of p110α leads to increased subcortical pp-MLC in mLECs.** **(A)** Confocal images of pThr18S19-MLC (pp-MLC,green), phalloidin (red), β-catenin (grey) and DAPI (blue) immunofluorescence in Control and p110α$^{\Delta iEC/D933A}$ mouse lung endothelial cells (mLECs). **(A')** Zoom of **A** highlighting the change in the localization of the phalloidin and pp-MLC staining between conditions. **(B)** Quantification of pp-MLC intensity per cell area. **(C)** Quantification of the pp-MLC intensity in a subjunctional area. Error bars are SEM. n means independent experiments. Statistical analysis was performed by Mann-Whitney test.

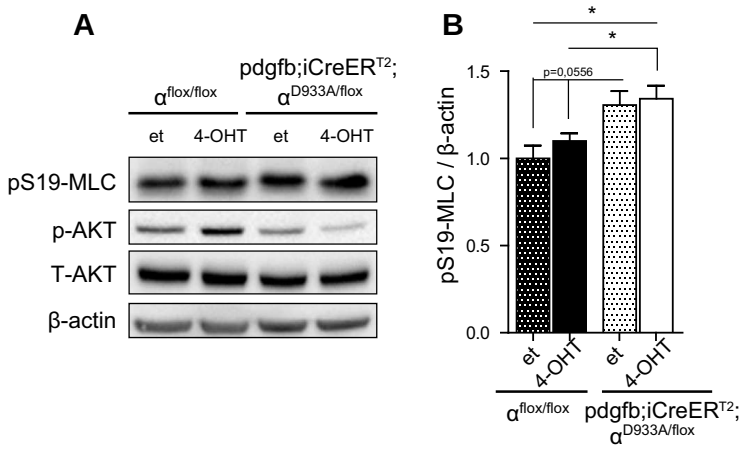

Figure 4.39: **Inactivation of p110α *in vitro* leads to increased in p-MLC levels.** **(A)** p110α$^{flox/flox}$ and pdgfb-iCreER^{T2};p110α$^{flox/D933A}$ mouse lung endothelial cells (mLECs) were treated with ethanol and 4-OH tamoxifen for 96h and subjected to immunoblotting with pS19-MLC, p-AKT, T-AKT and β-actin antibodies. **(B)** Quantification of the relative immunoreactivity of pS19-MLC protein normalized to β-actin of three independent experiments. Error bars are SEM. *P<0.05 was considered statistically significant. Statistical analysis was performed by Mann-Whitney test.

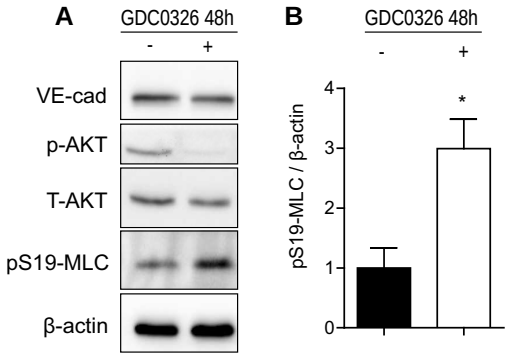

Figure 4.40: **Pharmacological inactivation of p110α *in vitro* leads to increased p-MLC levels. (A)** Wild-type mouse lung endothelial cells (mLECs) were treated with DMSO (vehicle) and GDC-0326 for 48h and subjected to immunoblotting with VE-cadherin, pS19-MLC, p-AKT, T-AKT and β-actin antibodies. **(B)** Quantification of the relative immunoreactivity of pS19-MLC protein normalized to β-actin of three independent experiments. Error bars are SEM. *P<0.05 was considered statistically significant. Statistical analysis was performed by Mann-Whitney test.

4.2.9.1 Establishing a link between p110α-PI3K and RhoA/ROCK signalling.

RhoA/ROCK signalling increases MLC phosphorylation, leading to cell contraction. The PI3K pathway has been shown to regulate RhoA activity but by distinct ways. Data from our group showed that heterozygous inactivation of p110α impaired activation of RhoA upon FBS stimulation (Graupera et al., 2008), whereas Gambardella et al. showed that Arap3 (a GAP of RhoA GTPase and effector of PI3K in ECs) deletion favours RhoA activation upon VEGF stimulation (Gambardella et al., 2010). To explore the mechanism by which p110α regulates MLC phosphorylation in retinal vasculature we monitored the activity of RhoA- and RhoC-GTPases in control and p110α inactivated mLECs. No changes in their activity (GTP-bound) were detected upon p110α inactivation in basal growing conditions (**Figure 4.41**). From our data we could hypothesise two explanations: (1) p110α-PI3K activity controls instead of Rho-ROCK activity their localization or (2) increased p-MLC subcortical level upon p110α inactivation is independent of RhoA/ROCK signalling.

First, we assessed whether an increase in subcortical p-MLC was due to increased RhoA/ROCK activity at the cortical region. To date no phosphorylation-specific antibodies have been reported for active forms of ROCK, restricting information on the spatial activation of this kinase. Therefore, we approached

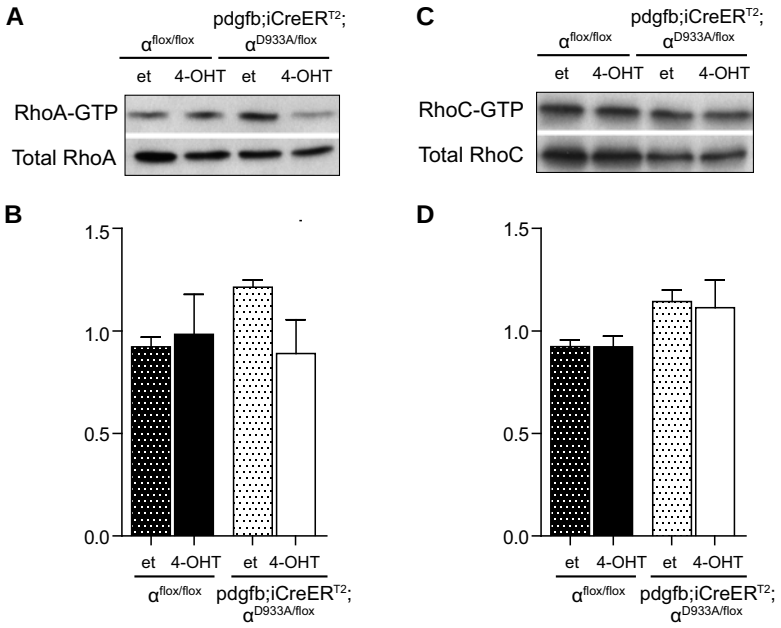

Figure 4.41: **p110α inactivation in ECs does not affect Rho-GTPase state.** Activation of RhoA **(A,B)** or RhoC **(C,D)** in basal conditions in p110α$^{Flox/Flox}$ and Pdgfb-iCreER^{T2} ;p110α$^{D933A/Flox}$ mLECs treated with ethanol or 4-OH tamoxifen for 96h. **(B,C)** Quantification of RhoA- and RhoC-GTP form respectively in three independent experiments are shown. Error bars are SEM. Statistical analysis was performed by Mann-Whitney test.

using a selective ROCK kinase inhibitor, Y-27632, in the *in vivo* and the *in vitro* models. We expected that if p110α$^{i\Delta EC/D933A}$ phenotype was RhoA/ROCK-dependent, we should observe a partial or total rescue of the phenotype upon ROCK inhibition. Blocking of ROCK in both control and p110α$^{i\Delta EC/D933A}$ retinas led to the reduction in the p-MLC levels but greater levels in control retinas (**Figure 4.42.A-E)**. Furthermore, there was no rescue in p110α$^{i\Delta EC/D933A}$ retinas after ROCK inhibitor treatment showed by the quantification of different vascular parameters affected by p110α inactivation as branching number (**Figure 4.42.F**), vessel width (**Figure 4.42.G**) or EC numbers (**Figure 4.42.H**).

Similarly, we observed that ROCK inhibitor efficiently decreased p-MLC level and disassembled actin stress fibres in control mLECs (**Figure 4.43.A-A", B-B", Figure 4.44.A,B**). Conversely, the decrease in p-MLC and phalloidin levels was less prominent in p110α$^{i\Delta EC/D933A}$ mLECs (**Figure 4.43.C-C", D-D", Figure 4.44.A,B**) and subcortical actin remained assembled after the treatment (**Figure 4.43.C-C",D-D"**). Accompanying fluorescence intensities along the depicted lines reflect the effect of ROCK inhibition on the distribution of the actomyosin fibres (**Figure 4.43.B'-B", D-D"**). We also corroborated that by immunoblotting. We

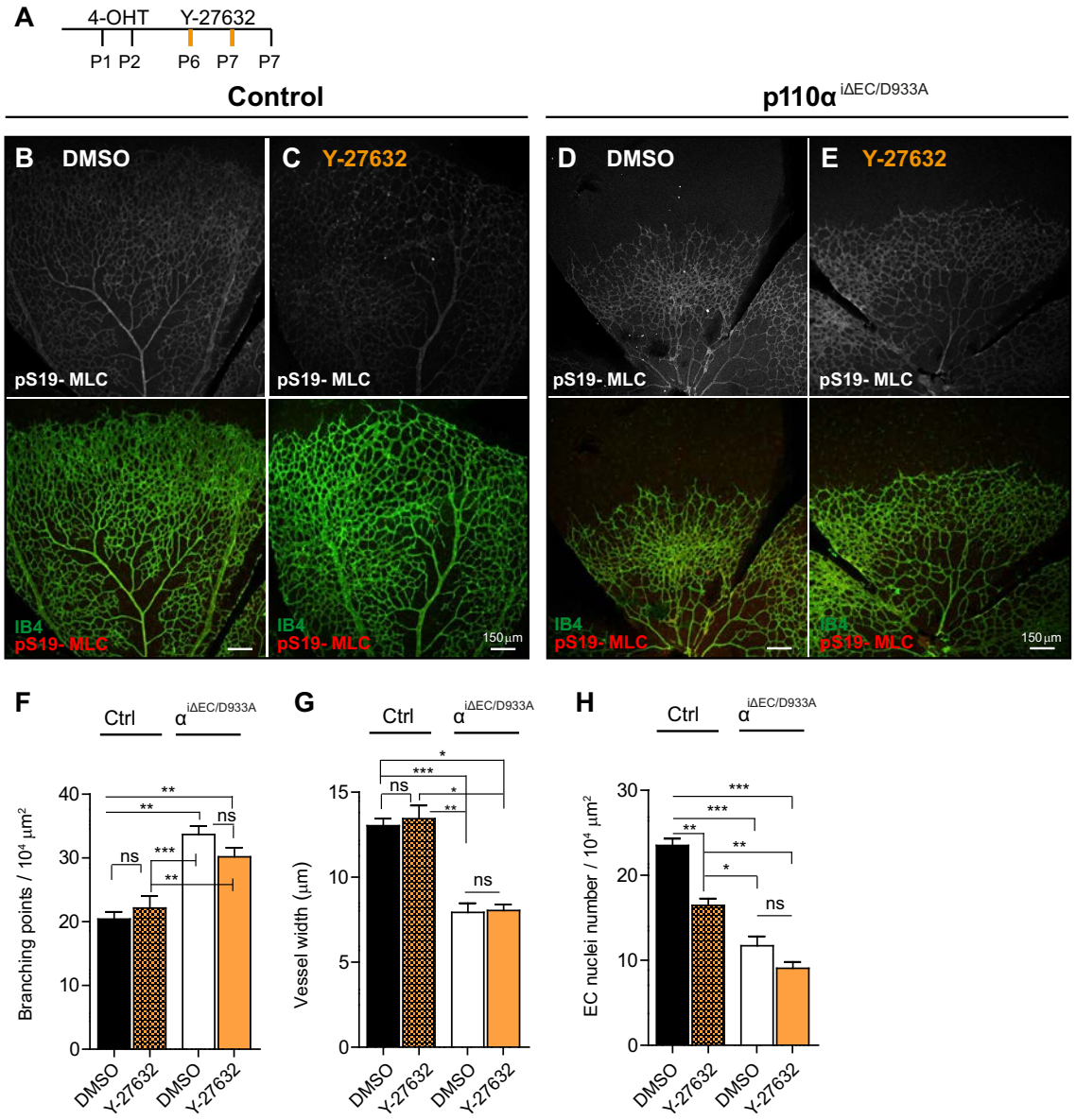

Figure 4.42: **p110α does not regulate actomyosin contractility through RhoA/ROCK signalling pathway *in vivo*.** **(A)** Schematic representation of drugs administration.Whole-mount control **(B,C)** and p110α$^{i\Delta EC/D933A}$retinas **(D,E)** treated with DMSO or Y-27632 (ROCK inhibitor) at P6 and P7 and isolated at P7. pSer19-MLC (red) and Isolecin-B4 (green) staining were performed. **(F-H)** Quantitative analysis of the retinas shown in **(B-E)**, n≥5 retinas per genotype-treatment. **(F)** Number of branch points per unit area. **(G)** Vessel width. **(H)** Endothelial cell nuclei number. Error bars are SEM. *P<0.05,**P<0.01 and ***P<0.001 were considered statistically significant. Statistical analysis was performed by non-parametric Mann-Whitney test. (falta en las grafiscas todas las estdisticas)

observed that upon ROCK inhibition control mLECs decreased p-MLC level almost by half, while p110α$^{i\Delta EC/D933A}$ mLECs exhibited just a slight decrease in p-MLC (**Figure 4.44.C**). As previously shown (Yang and Kim, 2012), p-AKT level increased upon ROCK inactivation via PTEN (**Figure 4.44.C**). Altogether, our data show that upon p110α inactivation ROCK inhibition partially decreases p-MLC levels but it doesn't disassemble subcortical F-actin fibres, suggesting that the increase in subcortical actomyosin contractility is RhoA/ROCK-independent.

.

4.2.9.2 Looking for new p110α-PI3K effectors in ECs by a phospho-proteomic screening

To gain insights into the molecular mechanisms that are affected by p110α inactivation in EC and lead to an increase in actomyosin contractility, we performed a phospho-proteomic screening. Changes in the phosphorylation status can alter many aspects of protein biology, including their localization, protein-protein interactions, stability, and enzymatic activity (Manning et al., 2002). This analysis was performed in collaboration with Dr. Pedro Cutillas (Barts Cancer Institute, London). For that, we established two groups (p110α$^{flox/flox}$ mLECs vs. Pdgfb-iCreER^{T2} p110α$^{flox/D933A}$ mLECs) with 3 experimental conditions in each group: ethanol treatment for 24h (basal conditions), 4-OH tamoxifen treatment for 24h (detect acute changes) and 4-OH tamoxifen treatment for 96h (the time required to completely deplete p110α protein produced by the flox allele and, therefore, achieve complete inactivation) that were analysed using a quantitative LC-MS/MS phosphoproteomics workflow (**Figure 4.45.A**). We identified 6,836 putative phosphorylation sites.

We analysed data by also comparing Pdgfb-iCreER^{T2};p110α$^{flox/D933A}$ mLECs vs. p110α$^{flox/flox}$ mLECs (control) within the different conditions **(Figure 4.45.A)**. Based on a two-tailed Student's t test ($P < 0.05$), the abundance of 259 phosphopeptides was differentially altered (elevated or reduced) when half of the p110α protein was inactivated (ethanol treatment: p110α$^{flox/D933A}$ vs. p110α$^{flox/flox}$). However, we focused our attention specifically on the phosphopetides that changed after 96h of 4-OH tamoxifen, when complete inactivation of p110α

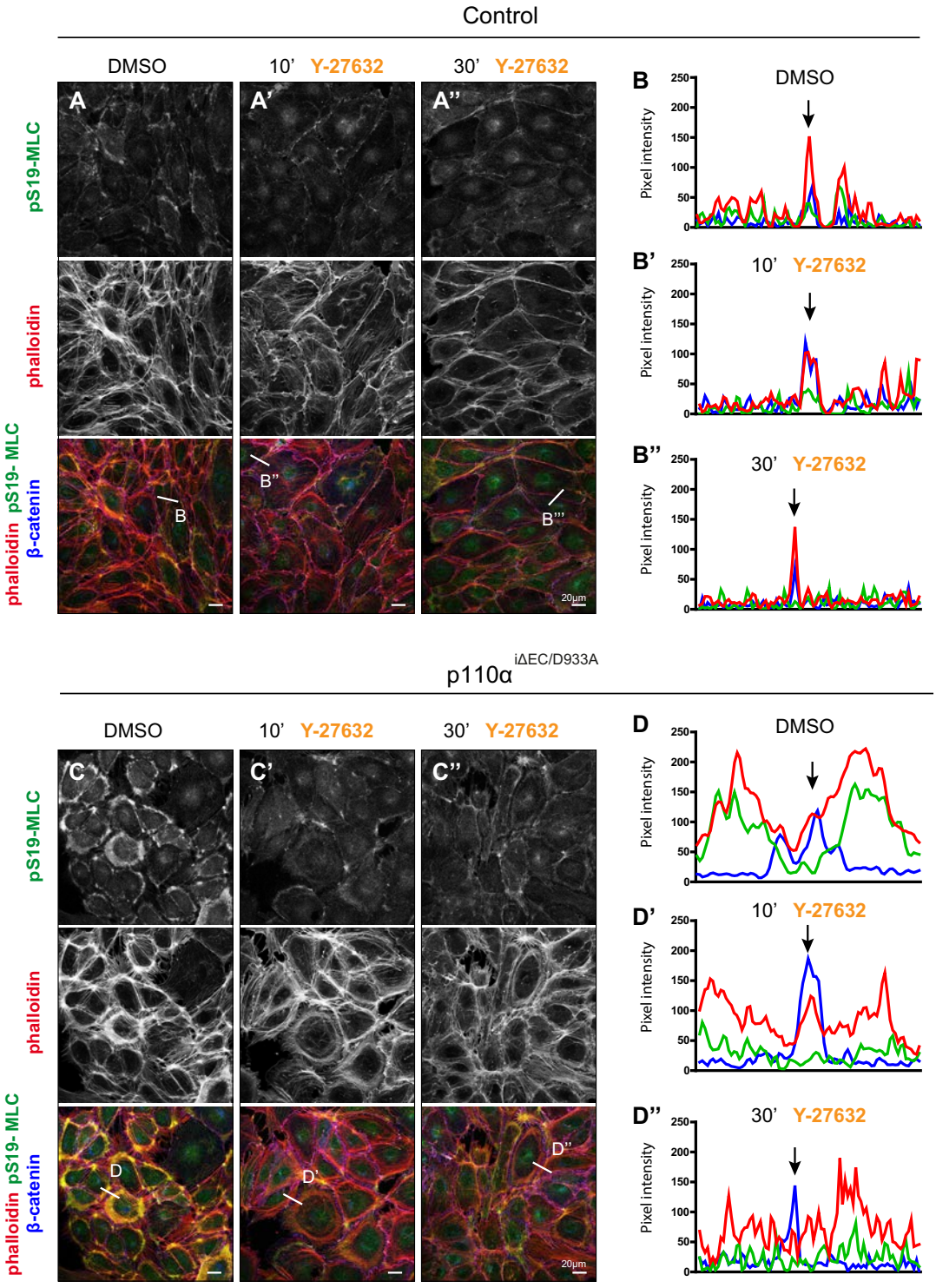

Figure 4.43: **p110α does not regulate actomyosin contractility through RhoA/ROCK activity *in vitro*. (A-A")** Confocal images of S19-MLC (green), phalloidin (red), β-catenin (blue) immunofluorescence in control mLECs treated with DMSO for 30' **(A)** and with Y-27632 (ROCK inhibitor) for 10' **(A')** or 30' **(A"). (C-C")** Confocal images of S19-MLC (green), phalloidin (red), β-catenin (blue) immunofluorescence in p110α$^{i\Delta EC/D933A}$ mLECs treated with DMSO for 30' **(C)** and with Y-27632 (ROCK inhibitor) for 10' **(C')** or 30' **(C"). (B-B";D-D")** Accompanying fluorescence intensities along the depicted lines showing that the distribution of p-MLC (green), F-actin (red) and β-catenin (blue) in the different conditions. Black arrows indicate the localization of the junction. **B-B"** refer to the depicted lines in **A-A"** and **D-D"** refer to the depicted lines in **C-C".**

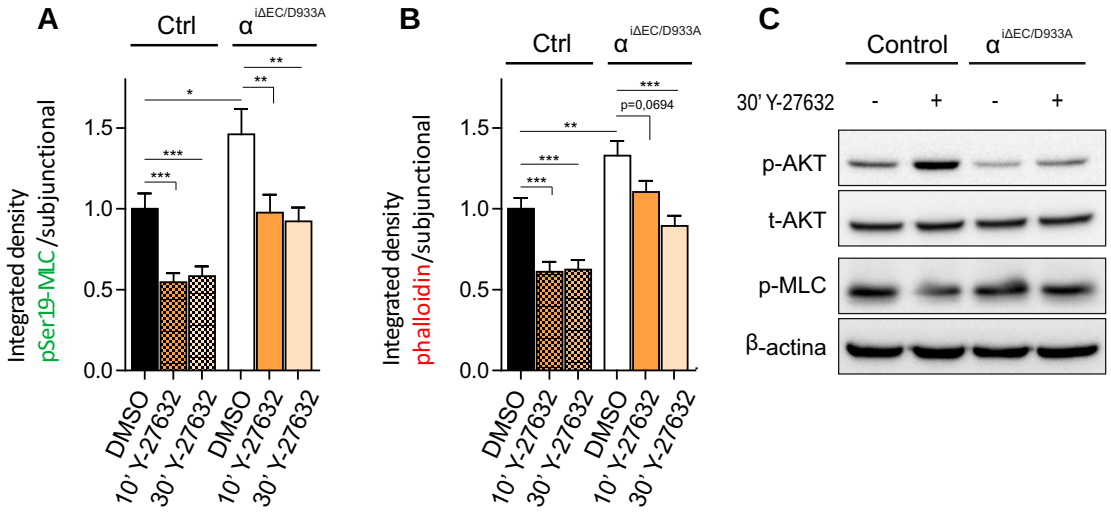

Figure 4.44: **p110α inactivation partially protects ECs from ROCK inhibitor effects.** Quantification of the pSer19 **(A)** and phalloidin **(B)** intensity in a selected subjunctional area of control and p110α$^{i\Delta EC/D933A}$ mLECs treated with DMSO for 30' and with Y-27632 (ROCK inhibitor) for 10' and 30". n≥28 images of at least three independent experiments. **(C)** Control and p110α$^{i\Delta EC/D933A}$ mLECs were treated with DMSO (-) or Y-27632 (+) for 30' and subjected to immunoblotting with p-AKT, T-AKT, pS19-MLC and β-actin antibodies. n=3 independent experiments. Error bars are SEM. *P<0.05, **P<0.01 and ***P<0.001 were considered statistically significant. Statistical analysis was performed by Mann-Whitney test.

was achieved. In this condition, 245 phosphopeptides were differentially altered (**Figure 4.45.B**). We represented the results using volcano plots that enable a visual identification of the phosphopeptides that display significant changes (**Figure 4.45.C**).

Surprisingly, no phosphopeptides of AKT protein, the principal effector of p110α, were detected by the mass spectrometry. However, by running a bioinformatic analysis based on the detected phosphorylations (KSAE) we identified that the kinase activity of Akt1 and mTOR (kinases activated downstream PI3K signalling) were decreased upon p110α inactivation (**Figure 4.46.A**). Among others, we selected the altered phosphopeptides from cytoskeleton-related proteins in order to find a molecular mechanism that may explain p110α loss of function phenotype in ECs. Interestingly, we found proteins related to the myosin light chain phosphatase (MLCP), to the cdc42-Rac1 signalling pathway, to the EC junctions and focal adhesions and also to other components of the cytoskeleton such as filament intermediates and the microtubules (**Figure 4.46.B**).

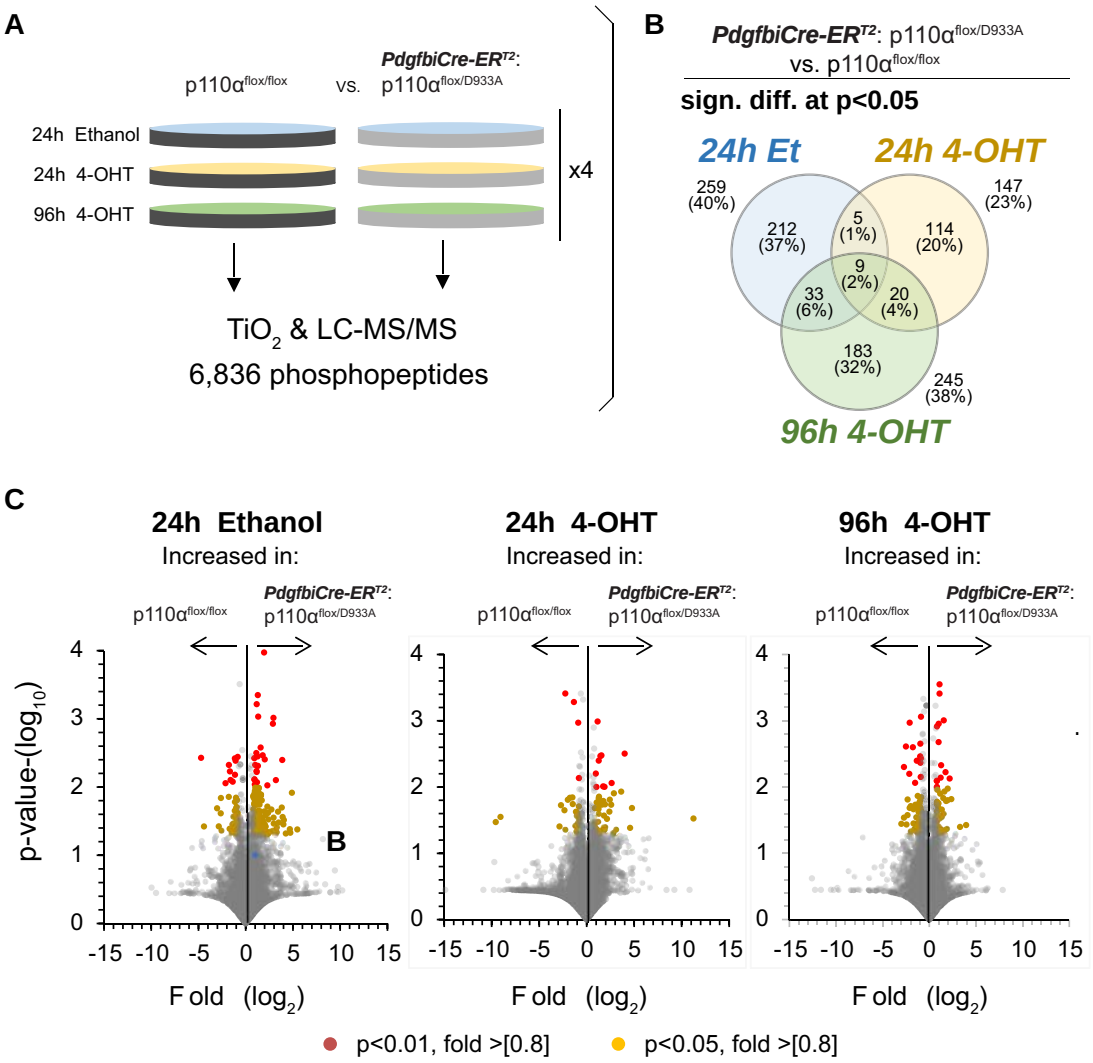

Figure 4.45: **Phosphoproteomic screening upon p110α inactivation in mLECs. (A)** Schematic illustrates the phosphoproteomic approach followed. Phosphorylated peptides were enriched by TiO_2 and identified and quantified by LC-MS/MS. **(B)** Venn diagram shows the phosphopeptides identified in the phosphoproteomic experiment that changed for each condition with statistical significance of p<0.05. **(C)** Volcano plots indicate significantly altered phosphoproteins identified in the screening. The Y axis represented negative log_{10} of p-value (highly significant appearing towards the top of the plot) and in the X axis was the log_2 of the fold change between $p110\alpha^{flox/flox}$ mLECs and Pdgfb-iCreER^{T2} ;$p110\alpha^{flox/D933A}$ mLECs treated with ethanol , 4-OH tamoxifen for 24h and 4-OH tamoxifen for 96h. Red and yellow dots represented the phosphopetides that showed high statistical significance (p<0.01 and 0.05, respectively) together with a fold change > 0.8. Four biological replicates were analysed for each condition (24 samples). Statistical analysis was performed by two-tailed Student's t test.

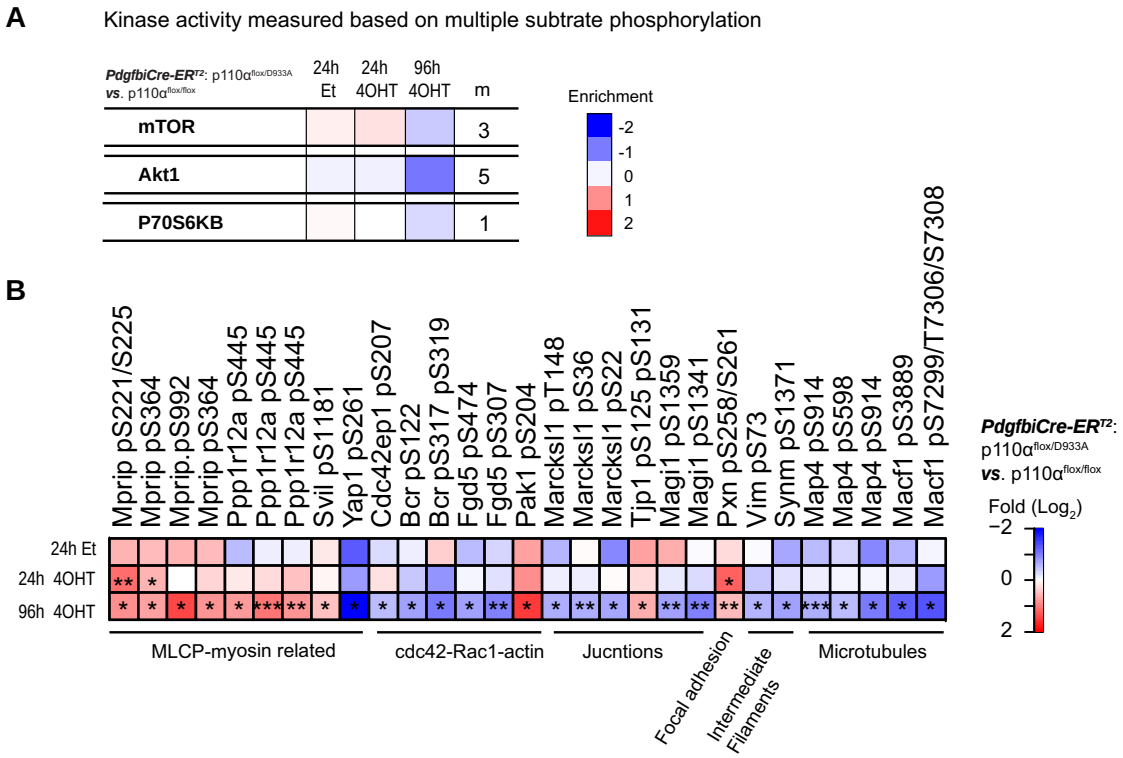

Figure 4.46: **Phosphoproteomic analysis reveals a larger population of cytoskeleton related proteins that change their phospho-state upon p110α inactivation.** (A) Kinase activity estimation of PI3K downstream kinases based on kinase substrates from our phosphoprotemic analysis. The heatmap scale indicates fold change. (B) Heatmap representation of the selected phosphorylated peptides related with cytoskeleton dynamics identified in the phosphoproteomic screening. *P<0.05, **P<0.01 and ***P<0.001 were considered statistically significant. Statistical analysis was performed by two-tailed Student's t test.

In concordance with our previous data, phosphopeptides from myosin light chain (MLC) protein showed an increase in pSer19 and pThr18 upon p110α inactivation albeit the difference was not significant (data not shown). Two critical proteins of the regulation of actomyosin contractility were identified: (1) Protein Phosphatase 1 Regulatory Subunit 12A (PPP1R12A, also called MYPT1) and (2) Myosin Phosphatase Rho Interacting Protein (Mprip, also called mRIP). For both target we identified an increase in their phosphorylation state upon p110α inactivation (**Figure 4.46.B**).

4.2.9.2.1 Role of MYPT downstream of p110α-PI3K signalling pathway — *Preliminary*

MYPT1 is the regulatory subunit of the MLC phosphatase complex (MLCP) which is responsible for dephosphorylating MLC and, as result, decreasing actomyosin contractility. We detected a significant increase in the phosphorylation on S445 upon p110α inactivation (**Figure 4.46.B**). Zagorska et al. recently identified that an increase in the pS445 of MYPT1 promotes its binding to 14-3-3, and in turn, attenuates MLCP activity. First, we validated the increase in pS445-MYPT levels by western blotting when p110α activity was inactivated in mLECs. We observed that pSer445 levels increased in p110α$^{i\Delta EC/D933A}$ mLECs compared to control mLECs (same conditions used in the phosphoproteomic assay) (**Figure 4.47.A,B**). In addition, we tested whether pharmacological inactivation of p110α reproduced this pattern in wild-type mLECs and in other non-endothelial model as HEKs. Wild-type mLECs (**Figure 4.47.C,D**) and HEK-293 cells (**Figure 4.47.E,F**) were treated with DMSO and GDC-0326 for 48h revealing that pharmacological inactivation of p110α also leads to an increase in pS445-MYPT levels.

As pS445 has been described as an inhibitory phosphorylation, to explore the biological role of the change in the phosphorylation state of MYPT1, we knocked down MYPT1 using siRNA in wild-type mLECs. We transfected cells with control siRNA and MYPT1 siRNA and 72h after we evaluated the efficiency of siRNA silencing by western blotting (**Figure 4.48.A,B**). Then, phalloidin and p-MLC immunofluorescence staining were performed to analyse whether knock-

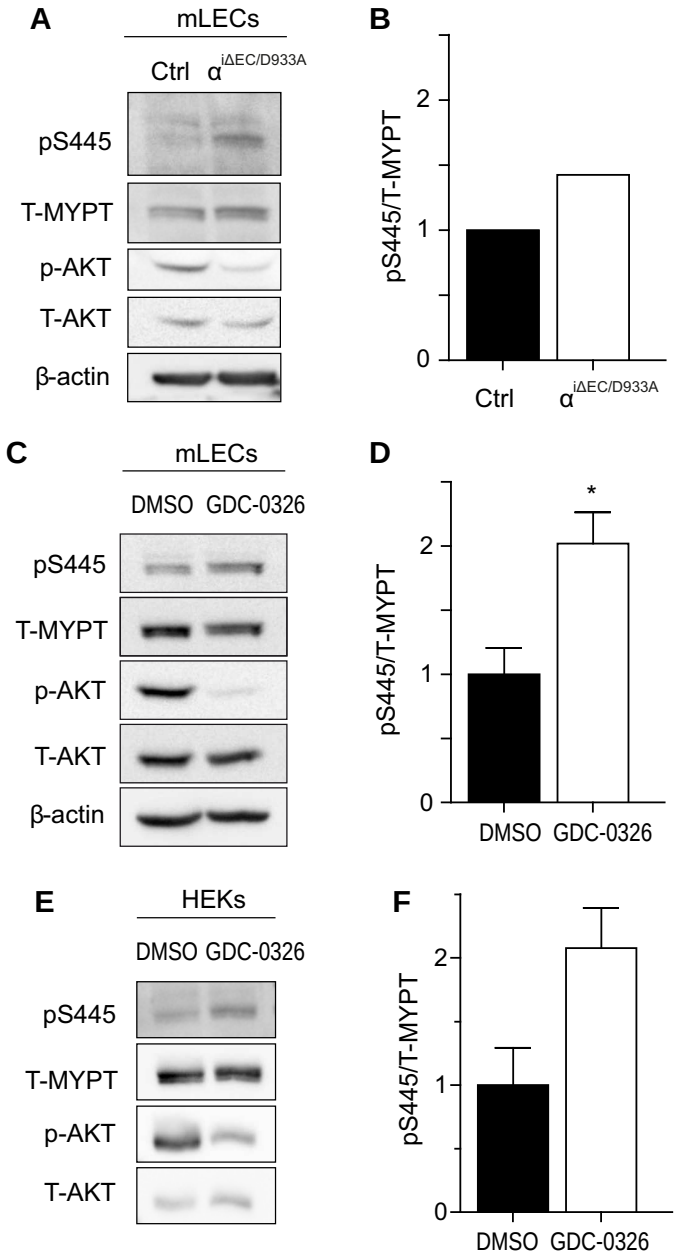

Figure 4.47: **Inactivation of p110α leads to an increase in the phosphorylation of MYPT on S445. (A)** p110α$^{flox/flox}$ (control) and Pdgfb-iCreER^{T2};p110α$^{flox/D933A}$ mLECs were treated with 4-OH tamoxifen for 96h and subjected to immunoblotting with pS445-MYPT, T-MYPT, p-AKT, T-AKT and β-actin antibodies. One independent experiment. **(B)** Quantification of the relative immunoreactivity of pS445 protein normalized to total MYPT of **A**. Four independent experiments.**(C)** Wild-type mouse lung endothelial cells (mLECs) were treated with DMSO (vehicle) and GDC-0326 for 48h and subjected to immunoblotting with pS445-MYPT, T-MYPT, p-AKT, T-AKT and β-actin antibodies. **(D)** Quantification of the relative immunoreactivity of pS445 protein normalized to total MYPT of **C**. Four independent experiments. **(D)** HEKs were treated with DMSO (vehicle) and GDC-0326 for 48h and subjected to immunoblotting with pS445-MYPT, T-MYPT, p-AKT and T-AKT antibodies. **(E)** Quantification of the relative immunoreactivity of pS445 protein normalized to total MYPT of **E**. Two independent experiments. Error bars are SEM. *P<0,05 was considered statistically significant. Statistical analysis was performed by Mann-Whitney test

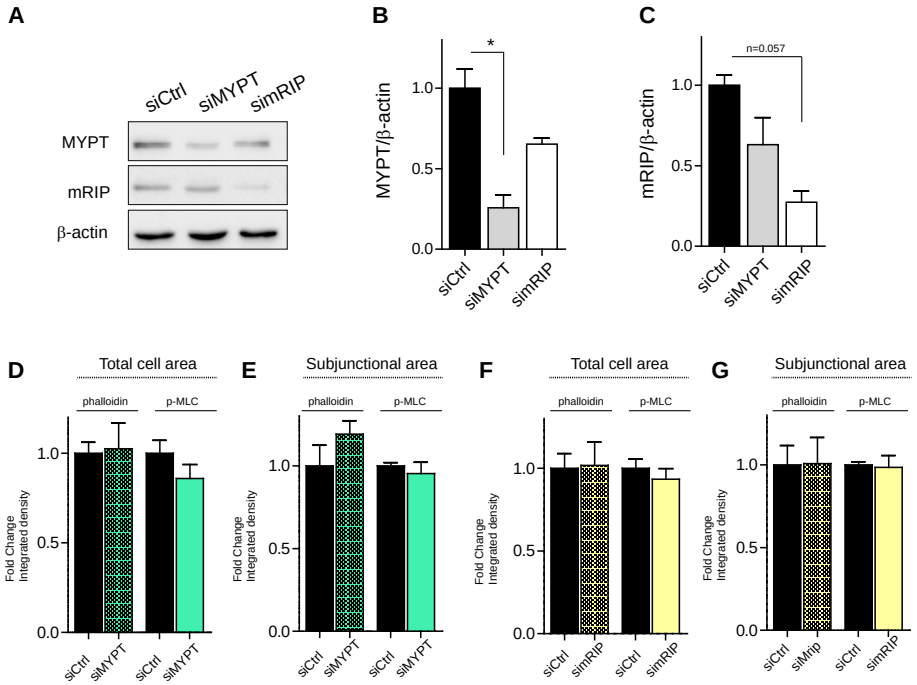

Figure 4.48: **Down-regulation of MYPT and mRIP protein levels do not affect actomyosin contractility in ECs. (A)** Wild-type mLECs were transfected with mRIP-siRNA or MYPT-siRNA or control siRNA. Seventy-two hours after transfection, mLECs were lysed and analysed by SDS-PAGE and blotting for MYPT, mRIP and β-actin proteins. **(B)** Quantification of the relative immunoreactivity of MYPT protein normalized to β-actin of three independent experiments. **(C)** Quantification of the relative immunoreactivity of mRIP protein normalized to β-actin of three independent experiments. In **(B,C)** we observed that downregulation of MYPT or mRIP affects the expression of the other protein. **(D-G)** Wild-type mLECs were transfected with MYPT-siRNA **(D,E)** or mRIP-siRNA (**F,G**). Seventy-two hours after transfection, the cells were analysed by immunoflorescence for phalloidin and pSer19-MLC and quantified intensity per cell area **(D,F)** or intensity in a selected subjuntional area **(E,G)**, n≥4 independent experiments. Error bars are SEM. *P<0,05 was considered statistically significant. Statistical analysis was performed by Mann-Whitney test.

down of MYPT led to increased actomyosin contractility. Surprisingly, no changes in the amount of F-actin and p-MLC (**Figure 4.48.D**) or in their localization were detected (**Figure 4.48.E**). Although it is not clear at the moment why we could not detect changes in p-MLC, we should consider that MYPT expression was not fully knocked-down.

MYPT1 is the regulatory domain of MLCP and its phosphorylations causes disassembling of the MLCP complex and therefore the inhibition of its phosphatase activity. By immunoprecipitating MYPT1 we aimed to show whether changes in pS445 levels could derive in MLCP delocalization from the actomyosin fibres. We immunoprecipitated MYPT in control and p110α-inactivated HEKs.

Less β-actin was immunoprecipitated in HEKs treated with p110α inhibitor compared to control, supporting that increased levels of pS445 upon p110α inactivation leads to a delocalisation of the MYPT from the actomyosin fibres and thereby impairs the proper functionality of the MLCP (**Figure 4.49**).

4.2.9.2.2 Role of mRIP downstream of p110α-PI3K signalling pathway — *Preliminary*

mRIP protein can bind RhoA, MLCP and F-actin and has been described as critical scaffold protein that localize MLCP to the actomyosin-containing filament bundles to attenuate actomyosin contractility. Furthermore, mRIP presents in its structure two PH domains, which putatively can bind to PIP_3 lipid. Phospho-proteomic screening detected that mRIP protein present a significant increase in the phosphorylation of several residues (S221/225, S364 ad S992) upon p110α inactivation (**Figure 4.46.B**). However, the functionality of these residues has not been described yet, and no antibodies against these phosphorylated residues were available limiting its study. Furthermore, the residues modified upon p110α inactivation are not localized in the binding domains that have been described to date. Taking in account that $p110\alpha^{i\Delta EC/D933A}$ ECs showed an increase in actomyosin contractility we hypothesised that the increase in the phosphorylation state of the different residues in mRIP could have an inhibitory effect, meaning that attenuate MLCP activity, either by mRIP dissociation from the actin or from the MLCP. We approached that situation by silencing mRIP in wild-type mLECs **(Figure 4.48.A,C)**. Contrary to previous data from other cells types, we didn't detect changes in phalloidin and p-MLC levels (**Figure 4.48.F**) or in their localisation (**Figure 4.48.G**) upon mRIP down-regulation. This result suggested that mRIP in ECs was not important in the regulation of MLCP activity or that the down-regulation was inefficient to detect changes similar to what happened with MYPT down-regulation. Further experiments are needed to elucidate the connexion between p110α-PI3K and mRIP and their mechanism of action.

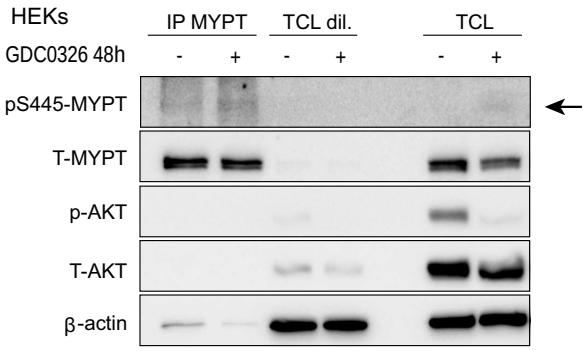

Figure 4.49: **Inactivation of p110α decreases MYPT binding to the actomyosin fibres**. Western blot analysis of MYPT immunoprecipitated from HEKs treated with DMSO (vehicle) and GDC-0326 for 48h. n=3. Ongoing experiments to include the IgG control.

5 Discussion

Class IA PI3K (PI3K) functions have been widely investigated over the last two decades. PI3K signalling is located at the crossroads of many cell surface receptors sending signals to coordinate multiple cellular functions such as cell growth, survival, motility, and metabolism. Fine-tune regulation of PI3K signalling in cells is needed to ensure the functionality of tissues and organs. However, it is still not clear how or even which PI3K isoforms are concerted into precise morphogenic events. On the other hand, PI3K activity plays central roles in several cellular processes critical for cancer progression. Hence, PI3K pathway inhibition is considered an important target for therapeutic intervention in cancer, and progress in the clinical area is being monitored by many clinical trials with PI3K inhibitors.

We were interested in investigating the role of PI3K activity in endothelial cells during the process of angiogenesis. Although ECs express all class I PI3K isoforms, only inactivation of the catalytic subunit p110α in endothelial cells (not p110β or p110δ inactivation) leads to vascular defects in the embryo (Graupera et al., 2008). This indicates that p110α activity in ECs is required in a cell-autonomous manner to ensure proper vascular development and remodelling during the embryogenesis. However, progress in the understanding of how p110α-PI3K signalling regulates the different steps of vascular morphogenesis has been hampered by embryonic lethality that both the constitutive and endothelial specific p110α mutant mice exhibit. To avoid the lethality associated to p110α inactivation our strategy was to selectively inactivate p110α in endothelial cells using a tamoxifen-inducible Pdfgb-iCreER^{T2} transgenic mouse line (Claxton et al., 2008). Taking into account that the deletion of PI3K family members leads to the disbalance of the others, complete deletion of p110α could be favouring the binding of the other p110s that normally present less affinity to the p85 regulatory subunit (Utermark et al., 2012) and/or favouring the overexpression of p85 (Bi et al., 1999), and therefore overlaying the function of p110α. For this reason, we also generated another transgenic mouse line, p110α$^{D933A/i\Delta EC}$, in which one allele was specifically deleted in ECs upon tamoxifen administration but the other allele

presented an inactivating mutation (p110α^{D933A}). Therefore, half of the p110α protein was expressed but inactive, maintaining stoichiometry (Foukas et al., 2006; Graupera et al., 2008). In this case, we should take into consideration that this mutation is present in all cells, which in the end, could also indirectly affect to the vascular development. Interestingly, although previous results in heterozygous p110α^{D933A} retinas at P5 showed defects in vascular outgrowth (Graupera et al., 2008), at P7 and P10 wild-type and heterozygous p110α^{D933A} vascular plexuses were almost indistinguishable as in adulthood (observation from Soler et al., 2015). This indicates that partial inactivation of p110α activity in all cells does not affect vascular morphogenesis and therefore, p110α$^{D933A/i\Delta EC}$ is a good model for studying the specific impact that p110α inactivation in ECs has in the sprouting angiogenic process.

My work has been focused on the study of early post-natal mouse retina, a model commonly used to study physiological angiogenesis. On the other hand, to complement the results obtained in mouse retinas we used zebrafish embryos that allow imaging of the process of angiogenesis over time. Due to the limitation of time, we approached the study using a p110α-specific inhibitor, which efficiently blocked PI3K signalling in zebrafish embryos, and morpholino oligomers. Although the reliability of morpholinos has been widely discussed over the past years, we used them as second model to validate the data obtained with the p110α-specific inhibitor. Interestingly, p110α-morphants reproduced the vascular defects observed with the inhibitor, reinforcing the importance of p110α activity in the sprouting process. The disadvantage of these approaches is target cell limitation. p110α has been shown to be expressed in zebrafish embryos (Sasore and Kennedy, 2014). Therefore, based on mouse data (Graupera and Potente, 2013) and on our results obtained upon p110α inactivation in zebrafish embryos, we speculate that p110α isoform is also important for vessel morphogenesis in zebrafish. However, it would be of interest to confirm p110α expression in vessels by *in situ* hybridization in whole-mount zebrafish embryos to discard that p110α exerts its role in the patterning of segmental vessels in a cell-nonautonomous manner (Lee et al., 2014a).

5.1 Distinct functions of p110α during vascular morphogenesis

Our study has revealed that total inactivation of p110α in endothelial cells leads to a dramatic vascular phenotype. The inactivation of p110α in ECs not only leads to pronounced morphological defects but also results in a non-functional vasculature. In this work, we provide evidence of the participation of p110α isoform on vessel formation at different stages of the angiogenic process. These functions will be discussed in depth in the following sections.

5.1.1 p110α-PI3K activity regulates EC migration

Endothelial cell migration is crucial for all aspects of vessel morphogenesis and is a mechanically integrated molecular process that involves dynamic and coordinate changes in cell adhesion, signal transduction, and cytoskeletal organization (Lamalice et al., 2007). PI3K signalling pathway is known to regulate cell motility in different cell types. Indeed, PI3K involvement in cell migration is cell-type specific and isoform-specific (Cain and Ridley, 2009). The first *in vivo* evidence of the p110α-specificity in the regulation of EC migration came from the study of heterozygous kinase-dead knock-in (KI) mice ($p110\alpha^{WT/D933A}$), in which retinal vasculature presented a delay in its outgrowth. However, it is not until now, that we have been able to assess *in vivo* the impact that total inactivation of p110α has in vascular morphogenesis in the postnatal retinas. In our study, we showed that full inactivation of p110α in ECs completely arrest endothelial migration. Differently from other vascular phenotypes where the radial expansion of the retinal vascular plexus was temporarily slowed down (Corada et al., 2013; Franco et al., 2013), the inactivation of p110α dramatically impairs EC migration reflected by the stand still of the outgrowth of the vascular plexus over time (P7,P10, P15). *In vitro* studies in which p110α isoform was inactivated using isoform-specific inhibitors (Soler et al., 2016), by siRNA (Graupera et al., 2008; Zhang et al., 2012) or genetically ($p110\alpha^{WT/D933A}$) (Graupera et al., 2008) corroborate the isoform-specific relevance of p110α in EC migration. Furthermore, we observed that both pharmacological and genetic inactivation of p110α in zebrafish embryos impair

the outgrowth of the ISVs similarly as after the inactivation of all class I PI3Ks with a pan-PI3K inhibitor (Nicoli et al., 2012). This suggests that as in mouse, p110α is the main isoform that controls vascular development through the regulation of EC migration in zebrafish embryos.

To understand the spatio-temporal regulation of the different steps of the migratory process the majority of studies have been carried out on single cell motility systems such as the amoeba Dictyostelium discoideum and leukocytes (amoeboid cell motility) (Funamoto et al., 2002; Iijima and Devreotes, 2002; Wang et al., 2002) or motile fibroblast (mesenchymal cell motility)(Sasaki et al., 2004; Haugh et al., 2000). From these data it is known that PI3K signalling pathway is important for chemotactic polarization, directional migration and the turnover of focal adhesions (Kolsch et al., 2008). PIP_2 lipid, the substrate of PI3Ks, is normally presented at high and homogeneous levels at the plasma membrane whereas basal levels of PIP_3 are very low. In response to chemotactic cues, PIP_3 presented a polarized cellular distribution at the leading edge of the migrating cell that in turn locally recruit guanine nucleotide exchange factors for the Rho-family GTPases, Rac and Cdc42 (Srinivasan et al., 2003), and activate effector kinases such as Pak, PDK1 and Akt (Primo et al., 2007; Edwards et al., 1999) which leads ultimately to actin polymerization, formation of pseudopodia and directional cell movement. The rear retracts and adhesions release in response to force and other activities. Therefore, disruption of the proper localized levels of PIP_2 and PIP_3 impair proper cell migration. However, we should take in account that *in vivo* ECs move between and among other cells (such as pericytes) and present connections with the ECM and they could be also in contact with the blood flow, making EC migration a more complex process. Endothelial cells must sense external signals and integrate and coordinate their adhesion with their surrounding in order to start and stop moving. We identified that p110α inactivation in ECs affects cytoskeleton dynamics in endothelial cells leading to an increase in actomyosin contractility in the subcortical area. Abnormal actomyosin accumulation might affect the structure and/or function of junctional complex and focal adhesion complex. This may impact not only EC migration but also other endothelial cell functions. Therefore, we believe that spatio-temporal regulation of p110α-PI3K

signalling pathway negatively controls actomyosin contractility which acts on EC junctions and focal adhesions to regulate several steps of the sprouting process as tip cell migration, sprout elongation and stabilization of new endothelial cell-cell connections. The implication of p110α-PI3K signalling pathway in endothelial cell-to-cell contacts is further discussed below. Furthermore, *in vitro* evidence about the role of PI3K signalling pathway in focal adhesion stability (di Blasio et al., 2015; Higuchi et al., 2012) prompts us to study *in vivo* its possible function on that in the future.

5.1.2 Cell rearrangements during sprout outgrowth requires p110α activity.

In concordance with Sauteur et al., sprout outgrowth is mainly driven by EC elongation and migration rather than EC number or EC proliferation. During SeA outgrowth in zebrafish embryos, ECs are connected by small junctional rings that grow while tip cell migrates to support sprout elongation. I have observed that p110α inactivation leads to a delay in the outgrowth of the SeAs. On one hand, it has already been shown that PI3K output is important in tip cells to ensure proper EC migration towards the VEGF increased gradient (Nicoli et al., 2012). On the other hand, I have also identified that in p110α-inactivated embryos, the junctional rings of angiogenic sprouts do form, but their dynamics are altered. Interestingly, p110α loss-of-function phenotype resembles the loss of VE-cadherin expression in which endothelial cells fail to elongate their inter-endothelial contacts and to induce cytoskeletal rearrangements needed to support the elongation and the formation of multicellular tubes (Gaengel et al., 2012; Sauteur et al., 2014). These observations suggest that VE-cadherin mediates, at least partially, cell elongation in a PI3K-dependent manner. In agreement with this, it has been shown that VE-cadherin can bind to p85, the so-called regulatory subunit of p110 and in turn activate PI3K signalling (Taddei et al., 2008; Graupera and Potente, 2013). In fact, VE-cadherin knock-down or blockade of VE-cadherin clustering leads to reduced Akt phosphorylation (Choi et al., 2015). However, it has been shown that PI3K signalling can promote both endothelial barrier function through the upregulation of claudin-5 upon VE-cadherin-mediated cell-cell interaction (Taddei et al., 2008) and endothelial permeability and leukocyte TEM through

the association of VE-cadherin with Pyk2, Tiam-1 and the p85 regulatory subunit upon TNF stimulation (Cain et al., 2010). This could be explained, as previously Choi et al. 2015 suggested, by the fact that PI3K signalling pathway could present different manners of activation that lead to differences in the duration and strength of the PI3K output.

According with Bentley et al., differential dynamics of VE-cadherin junctions promote endothelial cell rearrangements and EC intercalation during sprouting (Bentley et al., 2014). Our findings suggest that the spatial heterogeneity of junctional activity profiles is lost upon p110α inactivation, with an increase in VE-cadherin straight junctions, correalting with a more static behaviour of the ECs and the failure of EC rearrangements. I prompt to conclude that p110α-PI3K signalling pathway is involved in the inter-endothelial junction remodelling necessary for the extension and growing of the vasculature.

Junctional proteins and actin cytoskeleton are intimately regulating angiogenic cell-shape changes. There is increased evidence of the impact that mechanotransduction at cell-to-cell adhesions *in vivo* has in physiology in different mechanical contexts, such as at interendothelial junctions near regions of disturbed flow and during morphogenesis (Hahn and Schwartz, 2009; Schluck et al., 2013; Weber et al., 2012) making the study of the specific role that p110α-PI3K activity may exert in force transduction during vascular morphogenesis very interesting. I have observed that actin cytoskeleton organization and contractility change upon p110α inactivation in ECs. *In vitro* studies have shown that contact expansion between two cells is driven by mechanical forces, controlled by cortical tension from the actomyosin cytoskeleton and transmitted by E-cadherin (Lecuit and Yap, 2015). The maintenance of subcortical actomyosin contractility upon p110α inactivation could be avoiding the growth of the junctional ring. However, Sauteur et al. showed that only inhibition of actin polymerization rather than contractility affects the elongation of the junctional ring between stalk cells in SeAs, suggesting that this process relay more in the polymerization of actin fibres (Sauteur et al., 2014). Nevertheless, taking into account that increased actomyosin contractility generates pulling forces that promote endothelial junctional remodelling (Huveneers et al., 2012) we could not discard

that sustained actomyosin contractility in EC could affect endothelial cell-cell junctional stability, and in turn impact the extension of the interface between stalk cells that allows the outgrowth of the sprout.

5.1.3 p110α-PI3K activity contributes to cell-type specific recognition and cell-cell adhesion

Lenard et al. described that the fusion of two tip cells involve EC recognition, *de novo* polarization of EC and apical membrane invagination and fusion in zebrafish embryos. Initial contacts between filopodia are thought to be mediated through cell-type-specific cell adhesion molecules. Then upon contact of two tip cells from opposing sprouts, a spot of VE-cadherin appeared at the contact site, that is subsequently transformed into a ring as the cells expanded their contact surface (Lenard et al., 2013). We observed that inhibition of p110α in zebrafish embryos leads to the lack of stabilization of nascent contacts between two neighbouring tip cells leading to cell retraction and the appearance of disconnections in the vascular network. In the cases in which there was a contact we observed that junctional spot was not extended forming a elongated ring, similar as observed during sprout outgrowth. These results suggest that p110α is important for both favouring the stabilization of tip cell contacts and later allowing the growth of the junctional ring to form a multicellular tube. Interestingly, inactivation of p110α in the retinal vasculature led to an increase in vessel regression in the sprouting front, where we observed the increase in tip-like cells. Accordingly with the zebrafish results, p110α inactivation in mice could impair anastomosis leading to vessel regression, which in turn does not allow tip cell to terminate its fate. There is evidence that VEGF-C/VEGFR3/PI3K/FoxC2 signalling pathway regulates tip to stalk conversion by the stabilization of tip cells fusion points (Tammela et al., 2011) and therefore could explain why ECs maintain the tip cell behaviour upon p110α inactivation. We believe that this instability results from a contractility imbalance in which cellular contraction exceeds the threshold level of force, so that the adhesion becomes unstable and retracts. In accordance with p110α inactivation, specific enhance in the localization of PTEN in the membrane reproduces the defects in the stabilization of fusion contacts between two neighbouring sprouts

that result in a disconnected vasculature (stalled vessels). We also speculate that as PI3K is important in polarized migration, its inactivation could lead to the loss of polarization of migrating tip cells, which in turn could influence the localization of proteins present and necessaries in the protrusion of the tip cells to stabilize their new contacts and allow the formation of a new vascular loop. It would be of interest to perform time-lapse analysis in transgenic embryos which allow the visualization of actin, VE-cadherin and the apical membrane to better understand the impact that p110α inactivation has on this process.

5.1.4 p110α-PI3K activity may be involved in apical-basal polarity and lumen formation

The angiogenic sprouts present at least two different polarities: directional (front versus rear) and apical-basal polarity (Lizama and Zovein, 2013). Within a sprout, the tip cell acquires a directional polarity towards the chemotactic gradient, and reorient its apical-basal polarity axis. Then, when two tip cells converge, firstly they form junctions and recruit proteins that define the apical-basal polarity, followed by the apical membrane invagination and lumen formation (Lenard et al., 2013). Our data showed that p110α-PI3K is involved to some extent in these processes since its inactivation in ECs leads to the failure in the initiation of the anastomosis process and EC polarization and lumen formation is affected. In epithelial cells, PI3K and PTEN activities are required for apical-basal polarization; PIP_2 is found enriched at the apical membrane whereas PIP_3 is localized at the basolateral membrane (Gassama - Diagne et al. , 2006). Nevertheless, little is known about the contribution of the PIP_2/ PIP_3 distribution in the establishment or maintenance of the apical-basal polarity in endothelial cells. It would be very interesting to analyse the localization of these phospholipids in wild-type ECs, and then to study whether the inactivation of p110α-PI3k affects the localization of certain proteins important for the establishment of the apical-basal polarity. The Par3 complex (Par3, Par6 and atypical Protein kinase C (aPKC)) is localized at the apical membrane of the ECs but also can be part of the AMIS complex, where apical and junctional components are deposited together to start the formation of the luminal membrane. In mammalian epithelial cells,

Par3 modulates PIP_2/PIP_3 levels by directly binding to PI3K and enhance its lipid activity (Itoh et al., 2010) , and by spatially restricting the activity of PTEN (Wu et al. , 2007; Feng et al. , 2008; Itoh et al. , 2010; Krahn et al. , 2010). Furthermore, Par3 can also bind directly to both PIP_2 and PIP_3. Therefore, there is a mechanistic connection between Par3 and phosphoinositide signalling during cellular polarization (Wu et al. , 2007; Krahn et al. , 2010). However, it is not clear how phosphoinositide asymmetry arises. We have found that p110α inactivation leads to the delocalization of Par3 protein from the apical membrane suggesting that decreased in PIP_3 levels affected, at least partially, EC apical-basal polarity, what could in turn affect the proper formation of the lumen. Our study adds more evidence of the involvement of PI3K signalling in the establishment of EC apico-basal polarity and vascular lumen formation. Interestingly, a recent study has shown that lumen expansion in angiogenic sprouts depends on actomyosin contraction, making even more interesting the study of p110α-PI3K activity in this context (Gebala et al., 2016).

5.2 p110α-PI3K controls vascular morphogenesis through different effectors in ECs

p110α-PI3K inactivation in EC leads to severe vascular defects during embryonic and postnatal development. Akt is the best-characterized and principal effector of class I PI3K. Only Akt1 isoform is critical for normal angiogenesis (Yang et al., 2003; Lee et al., 2014b). However, global loss of Akt1 and postnatal endothelial deletion of Akt (both $Akt1^{iECKO}$ and $Akt1^{iECKO}/Akt2^{-/-}$) in mice only resembles some vascular defects of $p110\alpha^{i\Delta EC/D933A}$ retinal vasculature (Lee et al., 2014b). Akt inactivation does not result in any significant changes in vessel thickness or tip cell identity compared to $p110\alpha^{D933A/i\Delta EC}$ vasculature and the delay in the outgrowth of the vaculature is lower. On the other hand, the capillary area of Akt mutant retinas showed decreased vessel density and increased vessel regression similar to $p110\alpha^{D933A/i\Delta EC}$mutant suggesting that a balance and intricate regulation of PI3K-Akt signalling is required to ensure a proper remodelling and the acquisition of a normal vascular patterning (Lee et al., 2014b). These data highlight that

p110α-PI3K signalling not only exerts part of its function on ECs through Akt but also through other Akt-independent effectors during vascular morphogenesis. Interestingly, p110α-morphants displayed similar vascular defects to GDC-0326 treated embryos although p-Akt levels were not efficiently decreased, supporting the idea of Akt-indepedent functions. Arap3 is the best Akt-independent effector characterized until now in endothelial cells. Both Arap3 knock-out mouse and Arap3 point mutation knock-in mouse (which uncouples Arap3 from PIP_3), cause embryonic death in mid-gestation due to an endothelial cell-autonomous defect in sprouting angiogenesis. p110α-PI3K signals through Arap3 to control sprouting angiogenesis. Postnatal analysis of Arap3 deletion in mice retinas to understand in depth how this signalling pathway could control the different steps of the angiogenic process has not been done yet, but *in vitro* studies have shown that Arap3 can exert its function through the control of Rho and Arf family of small GTPases (Gambardella et al., 2010).

5.2.1 p110α-PI3K negatively controls actomyosin contractility independently of the Rho-A/ROCK signalling pathway.

Genetic inactivation of p110α in ECs results in an increase in actomyosin contractility specifically in the subcortical area of the EC. Although previous *in vitro* data showed that p110α-PI3K/Arap3 regulates positively RhoA-ROCK signalling (Graupera et al., 2008; Gambardella et al., 2010; Cain et al., 2010), Arap3 has been described as PI3K effector in endothelial cell acting as RhoA GAP and Arf6 GAP. Thus, we speculate that p110α-PI3K inactivation leads to a decrease in PIP_3 levels, and as a consequence, Arap3 is not translocated to the plasma membrane and cannot exert its GAP function which leads to an increase in RhoA-GTP and actomyosin contractility in the cortical area. However, our *in vitro* study in normal growing conditions showed no changes in RhoA-GTP levels between control and $p110\alpha^{D933A/i\Delta EC}$ mLECs and ROCK inhibition did not rescue $p110\alpha^{D933A/i\Delta EC}$ vascular phenotype. In contrast with previous *in vitro* data that showed that p110α-PI3K/Arap3 regulates positively or negatively RhoA-ROCK signalling (Graupera et al., 2008; Gambardella et al., 2010; Cain et al., 2010), our data indicates that PI3K-mediated actomyosin contractility independently of RhoA/ROCK signalling

pathway.

Alternatively, it would be interesting to study to which extent VEGF/p110α-PI3K/Arap3/Arf6 signalling pathway could be regulating contractility in ECs. Although the role of Arf6 in physiological angiogenesis has not been elucidated yet, studies in other systems have shown that Arf6 can regulate cortical actin organization, cell polarity and membrane traffic (Donaldson, 2003), can promote Rac1 translocation to the plasma membrane (Radhakrishna et al., 1999; Boshans et al., 2000) and may activate Rac1 through the regulation of Rac-GEFs such as Tiam1 (Burridge and Wennerberg, 2004). Thus, we cannot discard the implication of Rac1 in the p110α loss-of-function vascular phenotype. The production of PIP_3 leads to an increase in GTP-bound Rac in many cell types and several studies have shown that PI3K and Rac1 are able to interact directly with each other leading to a positive feedback loop. In ECs it is known that p110α regulates Rac1 activation through the recruitment of the Rac GEF Tiam-1 to the VE-cadherin complex (Cain et al., 2010) and that Rac-1 activation stabilize VE-cadherin adhesion and transiently counterbalance actomyosin-dependent forces reducing tension in mature AJs (Daneshjou et al., 2015). Therefore, we cannot exclude its function during sprouting angiogenesis downstream of PI3K signalling to ensure EC junctional stabilization.

We have seen that ROCK is not principally mediating the increase in the phosphorylation of MLC upon p110α inactivation. There are many kinases that have been described to phosphorylate MLC *in vitro* and *in vivo*. The fact that upon ROCK inhibition wild-type endothelial cells showed a dramatic decrease in the phosphorylation of MLC led as to think that ROCK is the main kinase responsible for MLC phosphorylation in ECs. Nonetheless, other studies have shown that MRCK also control actomyosin contractility downstream of Integrins in ECs (Yamamoto et al., 2015). In fibroblast, MLC is phosphorylated by ROCK in the centre of the cell and by MRCK at the cell periphery and their inhibition has opposite effects on the cell migration (Totsukawa et al., 2004). In this regard, subcortical contractility is maintained to certain grade upon ROCK inhibition in $p110\alpha^{i\Delta EC/D933A}$ ECs suggesting that MRCK may contribute to the subcortical increase in actomyosin contractility.

5.2.2 p110α-PI3K may regulate MLCP function

Our phosphoproteomic screening aimed to find new effectors of the p110α-PI3K signalling pathway to provide insight into the observed phenotypes in the p110α$^{i\Delta EC/D933A}$ retinal vasculature. In the present study we compared the phospho-state of proteins in control and p110α$^{i\Delta EC/D933A}$ mLECs. p110α-PI3K is not a protein kinase, so the changes in the phosphorylation state of the proteins respond to the spatial regulation of protein kinases or protein phosphatases that are captured or not to the membrane through its direct or indirect binding to PIP_3. Some known targets of Akt did not appear in the substrate list, probably because phosphorylation events are dynamic and spatially regulated. Furthermore, our phosphoscreening reflected cells under basal serum-grown conditions, whereas post-starvation stimulation with different agonist may have resulted in a larger cohort of known substrates. Interestingly, analysis on the output substrates identified several proteins related with the cytoskeleton that are significantly affected by the loss of p110α activity. To our surprise, we identified two proteins, MYPT and mRIP, intimately related with Myosin Light Chain Phosphatase (MLCP), a protein complex which reverses the phosphorylation on MLC, thus reducing actomyosin contractility. The phosphoscreening revealed that MYPT S445 phosphorylation was increased upon p110α inactivation. MYPT is the regulatory subunit of the MLCP protein complex and responsible for bringing the complex to the myosin and allowing its activity. Interestingly, Zagórska et al. showed that phosphorylation on S445, S472 and S910 of MYPT by NUAK1 promoted the interaction of MYPT with 14-3-3 proteins, thereby suppressing the phosphatase activity of MLCP (Zagorska et al., 2010). By down-regulating MYPT protein in mLECs we have not been able to observe differences in actomyosin contractility, probably due to the inefficient knock-down. However, we have detected that MYPT was less bound to the actomyosin fibres suggesting that MLCP is delocalized upon p110α inactivation. Thus, MLCP complex is not able to exert its function, and p-MLC levels are maintained. Until now, our data suggest that p110α regulates negatively actomyosin contractility through the regulation of MYPT localization, and therefore MLCP activity. Two kinases have been described to date to be able to phosphorylate MYPT on S445, NUAK1 and LATS1.

Looking for possible cross-talk interactions between these kinases and PI3K signalling pathway, I found a study showing that Akt kinase can phosphorylate NUAK1 on S600 and therefore activate its kinase activity (Suzuki, 2002). If that is the case, we should expect decreased NUAK-1 activity under p110α-PI3K inactivation, and as a consequence a decrease in the phosphorylation levels of MYPT on S445 and not the contrary, as we have observed. Therefore, to totally discern whether the increase in the phosphorylation of MYPT on S445 is or not NUAK1-dependent in p110α-inactivated ECs, we should perform in depth analysis. On the other hand, there is no clear connection between LATS and PI3K signalling pathway (Kim and Gumbiner, 2015). Furthermore, a recent study has detected that MYPT co-immunoprecipates with the p110α-p85 heterodimer (Breitkopf et al., 2016). If that come about in endothelial cells it would suggest that PI3K might regulate MYPT function in two ways: as scaffolding protein bringing MYPT to the membrane and by its lipid product PIP_3 that activates other effectors that can modify MYPT localization and function, for example, through its phosphorylation.

Another interesting target found by the phosphoproteomic analysis was mRIP protein. This protein can bind to both actin and the MLCP complex (through a direct interaction with the MYPT regulatory subunit) and it functions as a scaffolding protein (Mulder et al., 2004; Surks et al., 2003). We have observed an increase in the phospho-state of different residues of mRIP upon p110α inactivation in mLECs. However, the function of the phosphorylations in mRIP has not been described yet. *In silico* identification of protein kinases that may target these phospho-sites points to GSK3 protein as putative responsible. GSK3 is a downstream effector of PI3K signalling pathway that is phosphorylated and inactivated by Akt. Thus, p110α-PI3K inactivation should lead to an increase in GSK3 activity (decreased pGSK3) and putatively to an increase on mRIP phosphorylation. Following this hypothesis, I think that it would be interesting to perform rescue experiments using GSK3 inhibitor and to analyse its impact on the p110α loss-of-function phenotype, similar to how I have done with the ROCK inhibitor. Another report has shown that silencing of mRIP in Ao184 cells results in disassembly of the MLCP complex, increased phosphorylation

of MLC, and changes in cytoskeletal dynamics (Surks et al., 2005) what could resemble (partially) p110α$^{D933A/i\Delta EC}$ phenotype. Furthermore, treatment with ROCK inhibitor in mRIP-silenced cells does not disassemble actin fibres similar to the effect found in p110α$^{D933A/i\Delta EC}$ ECs (Surks et al., 2005). Surprisingly, down-regulation of mRIP levels in endothelial cells did not lead to changes in actomyosin contractility suggesting two possibilities: partial silencing of mRIP is not enough to resemble p110α$^{D933A/i\Delta EC}$ phenotype or mRIP presents a different regulation in endothelial cells. Interestingly, mRIP sequence has two putative PH-domains. These domains can bind phosphatidylinositol lipids within biological membranes. Through these interactions, PH domains play a role in recruiting proteins to different membranes, thus targeting them to appropriate cellular compartments or enabling them to interact with other components of the signal transduction pathways (Lemmon, 2007). We hypothesize that mRIP could bind PIP_3 (product of p110α-PI3K activity) through its PH domains and as result, bring MLCP complex to the plasma membrane. Upon p110α inactivation, PIP_3 levels will decrease and, as a consequence, mRIP would not bind to the membrane and would not bring the MLCP complex to exert its function on the actomyosin fibres of that area. The resulting effect would be the increased cortical contractility observed in my study. To probe that, first, we have to identify the specific lipid that binds to the PH domains of the mRIP protein and second, we will study the localization of mRIP control and p110α$^{D933A/i\Delta EC}$ ECs.

5.3 Cross-talk between p110α-PI3K and Notch signalling pathways

Upon p110α inactivation the strongest phenotype arose in the sprouting front of the retinal vasculature, where we observed a dramatic increase in vascular density. These vessels were thinner than those in control and heterozygous ones, and most of them were aluminazed vascular structures formed by single endothelial cells. Despite the increase in vascular structures in p110α$^{i\Delta EC/D933A}$ retinas they were not functional, resembling the effect that p110α inhibition has on tumour vessels (Soler et al., 2013, 2016). Furthermore, behind the sprouting front the

retinal vasculature grow in three-dimensions with sprouting tip cells in multiple layers showing highly dynamic formation of filopodia . At P9, this phenotype was further enhanced highlighting that although upon p110α inactivation EC migration is arrested, ECs continue in a pro-angiogenic state and create new vascular structures. In p110α$^{i\Delta EC/D933A}$ retinas staining with ESM-1 and Dll4 tip-cell markers reflected that the tip cells were extended far into the vascular plexus and not restricted to few single cells in the sprouting front. As Notch signalling limits the number of tip cell by the activation of Notch signalling on neighbouring cells via Dll4, we hypothesized that Notch signalling pathway and PI3K pathway could converge in ECs to regulate tip/stalk selection. There is experimental evidence demonstrating that the inhibition of PI3K signalling decreases Notch signalling. Several *in vitro* studies in ECs show that PI3K/AKT positively regulates Dll4/Notch signalling, and the induction of Dll4 expression and Notch signalling is abrogated by the blockade of the PI3K/Akt signalling pathway (Liu et al., 2003; Hayashi and Kume, 2008; Soler et al., 2013; Wei et al., 2013; Kerr et al., 2016). Takeshita et al. showed that VEGF stimulates presenilin proteolytic processing, γ-secretase activity, Notch1 cleavage, and Hes-1 expression, which could be blocked with the disturbance of PI3K signalling (Takeshita et al., 2007). This could explain why although inactivation of p110α leads to an increase in Dll4 ligand, Notch signalling is not activated and, therefore, there is an increase in ECs that remain as tip cells. Conversely, in our *in vivo* p110α$^{i\Delta EC/D933A}$ model Notch signalling seems to operate normally, since the expression of Dll4 and Notch target genes (Hes1 and Hey1) was similar to that in ECs from control retinas. This result contrasts previous *in vitro* data, but suggests that *in vivo* p110α-PI3K and Notch signalling pathways do not converge to regulate tip/stalk selection. Supporting our results, Serra et al. showed that neither loss nor gain of PTEN function, the phosphatase that reverts PI3K product, resulted in changes in the expression of Dll4 or Notch target genes and in the number of sprouts, further supporting that PI3K signalling is not required for tip/stalk selection (Serra et al., 2015). Normally, decreased Notch signalling correlates with an increase in EC numbers (Hellström et al., 2007), a fact that we didn't observe upon p110α inactivation. Additionally, the fact that upon p110α inactivation there were not changes in the number of sprout or filopodia in the

perimeter of the sprouting front but in the inner part support that p110α-PI3K signalling is not controlling tip/stalk selection but tip cell termination fate. On the other hand, ESM-1 is strongly expressed by endothelial tip cells during retinal angiogenesis (del Toro et al., 2010) and its expression and secretion is stimulated by VEGF and repressed by PI3K. Inactivation of PI3K with LY294002 caused a robust increase in ESM-1(Rennel et al., 2007) suggesting that increased ESM-1 staining in p110α$^{D933A/i\Delta EC}$ retinas may be due to the blocked of PI3K signalling and not as consequence of tip/stalk selection defects.

However, to further validate our data and discard a PI3K/Notch signalling crosstalk, it would be of interest to study the expression of the Notch target genes in ECs isolated directly from control and p110α$^{D933A/i\Delta EC}$ the retinas to avoid the genetic material from other cell types presented in the retina that can overlap both the specific EC gene expression profile and slight differences between conditions. On the other hand, two *in vivo* studies have shown that vascular defects associated to some extent with PI3K signalling pathway impairment in ECs were rescued by the induction of Notch signalling with the injection of Jagged1 peptide (Tammela et al., 2011; Kerr et al., 2016). Tammela et al. showed that endothelial specific deletion of VEGFR-3 leads to vascular hypervascularization which is rescued upon Jagged1 injection. VEGF-C/VEGFR-3 signals through PI3K/FoxC2 signalling pathway activating Notch signalling independently of canonical Notch ligand-receptor interactions. In addition, vascular defects associated with Akt1/Akt2 deletion in adult vessels were partially rescued upon Jagged1 injection (Kerr et al., 2016). Therefore, it would also be worth inducing Notch signalling in p110α$^{i\Delta EC/D933A}$ vasculature to detect whether there is or is not a rescue of the vascular defects and therefore, confirm that the increase in tip cell numbers in p110α loss-of-function retinas is Notch dependent or independent.

5.4 p110α inactivation in ECs decreases its proliferation

Normally excessive blood vessel branching correlates with increased endothelial proliferation (Hellström et al., 2007; Tammela et al., 2011; Serra et al., 2015). In contrast, p110α$^{D933A/i\Delta EC}$ retinal vasculature showed increased density in the

sprouting front that did not rely on an increase in EC numbers. In fact, these vessels were thinner and formed by less ECs than control ones. Although PI3K signalling has been related with proliferation in different cell types, there is no evidence of PI3K signalling pathway implication in EC proliferation. Heterozygous $p110\alpha^{WT/D933A}$ retinal vessels (Graupera et al., 2008), cultured ECs where p110α was inactivated by different strategies (Graupera et al., 2008; Soler et al., 2016) and endothelial cells in the SeAs of zebrafish embryos treated with a pan-PI3K inhibitor (Nicoli et al., 2012) showed no differences in EC proliferation. However, our study shows that complete inactivation of p110α activity in ECs dramatically impairs proliferation. Although it is difficult to discern what comes first, the fact that other studies have demonstrated that partial decrease in PI3K output firstly affects EC migration with no changes in EC proliferation (Graupera et al., 2008; Nicoli et al., 2012) and that the blockade of cell-cycle progression with the Aurora kinase inhibitor has not reproduced $p110\alpha^{i\Delta EC/D933A}$ vascular defects, suggests that the impairment of EC proliferation in $p110\alpha^{i\Delta EC/D933A}$ retinal vasculature is a consequence and not the primary cause of p110α inactivation defects in vascular morphogenesis. EC proliferation can be regulated by direct cell-cell contact and cell spreading (Nelson and Chen, 2002) and, as for migration, the dynamics of the cytoskeleton also contribute to the progression of the cell cycle.

5.5 Long-term inactivation of p110α results in EC senescence

Although no defects in survival were observed upon p110α inactivation, our data indicate that long-term inactivation of p110α in ECs derives in EC senescence, defined as an irreversible state of G1 cell cycle arrest in which cells do not respond to growth factors. Normally senescence is associated with cellular damage or stress but PI3K signalling has been described as participating not only in damage-induced senescence in adult somatic cells but also in in developmentally programmed senescence (Muñoz-Espín and Serrano, 2014). There is no evidence from the literature or from our data showing that senescence could play a role during the angiogenic process. P7 control and $p110\alpha^{i\Delta EC/D933A}$ retinas did not show SAβGAL positivity, and neither did mLECs treated for 48h with a p110α-specific inhibitor, suggesting that only sustained loss of p110α activity over time

results in EC senescence. Data from other studies showed that senescent ECs present attenuated expression and activity of eNOS (Sato et al., 1993; Matsushita et al., 2001), PI3K/Akt effector, that could be phosphorylated and activated by Akt (Dimmeler et al., 1999, 2000; Fulton et al., 1999). In contrast, other studies showed that increased PI3K/Akt signalling also induces cell senescence in endothelial cells (Miyauchi et al., 2004) and in other models (Astle et al., 2011; Chen et al., 2005b). It has become clear that either too little or too much PI3K activity can trigger senescence. *In vivo*, senescent endothelial cells have been identified specifically in the atherosclerotic regions of human coronary arteries (Wang and Bennett, 2012). However, it remains largely unknown how senescence impairs vascular functions and contributes to age-related vascular diseases over time, and the implication that endothelial p110α-PI3K activity has on it.

On the other hand, senescent cells actively secrete a plethora of factors to establish communication with the microenvironment and can trigger the establishment of senescence in neighbouring cells in a paracrine manner. Senescence in this manner modulates the ECM, enhances the transformation of predisposed cells and reinforces tumour growth (Pérez-Mancera et al., 2014). The influence that persistent anti-angiogenic therapies could have leading to EC senescence in a tumoral context has not been evaluated yet. Taking into account that long-term inactivation of p110α in ECs leads to endothelial senescence, it would be interesting to study whether anti-angiogenic therapies with p110α-specific or pan-PI3K inhibitors could lead to EC senescence in patients, and how this phenomenon would impact on tumour outgrowth and dissemination.

5.6 p110α in vessel remodelling and maturation

Although we have identified that p110α-PI3K activity is not as high in the capillary area as in the sprouting front, the decrease in vessel density in that area upon p110α inactivation indicates that p110α-PI3K regulates to some extent vessel remodelling and maturation. In this line, it has been shown that Akt, a major PI3K effector, also presents distinct function in ECs between developmental angiogenesis (Lee et al., 2014b) and mature vessels (Kerr et al., 2016). The angiopoietin/Tie (ANG/Tie) receptor system controls vascular remodelling and

vascular quiescence. Several studies have shown that PI3K signalling pathway is activated downstream of Ang-1/Tie-2 signal (Kontos et al., 1998; Jones et al., 1999; Kim et al., 2000). That results in Akt-dependent phosphorylation and nuclear exclusion of the FoxO1 transcription factor that contributes to endothelial cell survival and blood vessel stability (Daly, 2004) and phosphorylation of eNOS, which regulates vascular maturation and EC migration (Babaei et al., 2003; Chen et al., 2005a). Furthermore, p110α-PI3K signalling can not only be activated downstream of Tie2, but it is also important in the maintenance of Tie2 protein levels (Lelievre, 2005), suggesting a dual regulation of Tie2 signalling by PI3K activity. Additionally, mature vessels express high levels of miR-126, which promotes PI3K-mediated Ang-1 signalling by decreasing p85β regulatory subunit levels (Sessa et al., 2012). On the other hand, there is *in vitro* evidence showing that p110α-PI3K also can control vessels permeability during inflammation (Cain et al., 2010). Therefore, p110α-PI3K activity seems to be important not only during vascular morphogenesis but also in mature functional vessels.

5.7 Concluding remarks

The vascular system is essential for supplying all organs and tissues of the body with oxygen and nutrients, removal of waste products and also contributes to the infrastructure of the immune system. ECs respond heterogeneously to a diversity of angiogenic cues provided by other tissues and organs contributing to the proper vascular development. p110α-PI3K protein has been shown to play a key role in vascular development. Nonetheless, how p110α-PI3K controls different steps of vascular morphogenesis and its specific mechanism of action is not completely known. Therefore, I have assessed for the first time the impact that complete inactivation of p110α-PI3K activity has during the postnatal sprouting angiogenic process. Overall, p110α-PI3K activity serves as a molecular relay to orchestrate different morphogenic process such as EC migration, junctional remodelling, EC polarization and lumen formation. Furthermore, we have identified a new putative pathway in which p110α-PI3K signalling negatively controls actomyosin contractility through mRIP and/or MYPT. Therefore, these findings can serve not only to better understand normal vascular development, but also to define better

therapies against several diseases such as cancer or vascular malformation (VM) where blood vessels play a fundamental role in their progression.

6 Conclusions

1. p110α-PI3K activity is specifically enriched in the sprouting front of the retina vasculature and its inactivation leads to severe defects in vascular morphogenesis in both postnatal mouse retinas and zebrafish embryos.

2. Inactivation of p110α-PI3K in endothelial cells results in migration arrest.

3. p110α-PI3K inactivation in the retinal vasculature results in the appearance of distinct effects on vascular density between the sprouting front and capillary area suggesting that p110α signalling could regulate different steps within the angiogenic cascade.

4. Upon p110α inactivation in ECs, the most dramatic defects arise in the sprouting front where vascular density is increased but vessels are thinner and are formed by less ECs. These vessels present disorganized endothelial cell polarity which correlates with increased vessel instability and failure in lumen formation.

5. p110α-PI3K is involved in the growth of the inter-endothelial cell contacts during the outgrowth and maturation of nascent blood vessel sprouts.

6. p110α is involved in the initial steps of fusion and is necessary for proper establishment of a new connection. p110α inactivation leads to increased vascular instability and the appearance of multidirectional filopodia-like protrusions behind the sprouting front. However, this phenotype is not related with changes in Notch signalling pathway.

7. p110α-PI3K activity negatively regulates actomyosin contractility independently of Rho-ROCK signalling pathway in ECs. By performing a phosphoproteomic analysis, we have identified that p110α could regulate MLC phosphatase (MLCP) activity, and therefore, actomyosin contractility through mRIP and/or MYPT proteins. However, down-regulation of mRIP or MYPT protein expression in ECs is not enough to generate changes in p-MLC levels or localization.

8. Loss of p110α activity in ECs increases S445 phosphorylation of the MYPT leading to the uncoupling of the MLCP complex from the actin fibres, and, as a consequence, the maintenance of the p-MLC levels.

9. Inactivation of p110α also results in EC proliferation arrest. However, both (1) the fact that partial inactivation of p110α activity (heterozygous $p110\alpha^{KD}$ mouse) only results in EC migration defects, and (2) the fact that the blockage of EC proliferation *per se* (with the Aurora kinase inhibitor) does not resemble the loss of p110α activity in the retinal vasculature, suggest that EC proliferation arrest in p110α LOF retinas is not a primary defect itself, but rather a consequence of EC stretching and cytoskeleton defects.

10. Long-term inactivation of p110α in endothelial cells derives in endothelial senescence.

References

Abraham, S., Yeo, M., Montero-Balaguer, M., Paterson, H., Dejana, E., Marshall, C. J., Mavria, G., apr 2009. VE-cadherin-mediated cell-cell interaction suppresses sprouting via signaling to MLC2 phosphorylation. Current Biology 19 (8), 668–674.
URL http://dx.doi.org/10.1016/j.cub.2009.02.057

Ackah, E., Yu, J., Zoellner, S., Iwakiri, Y., Skurk, C., Shibata, R., Ouchi, N., Easton, R. M., Galasso, G., Birnbaum, M. J., Walsh, K., Sessa, W. C., Aug 2005. Akt1/protein kinase b alpha is critical for ischemic and vegf-mediated angiogenesis. J Clin Invest 115 (8), 2119–2127.
URL http://dx.doi.org/10.1172/JCI24726

Astle, M. V., Hannan, K. M., Ng, P. Y., Lee, R. S., George, A. J., Hsu, A. K., Haupt, Y., Hannan, R. D., Pearson, R. B., sep 2011. AKT induces senescence in human cells via mTORC1 and p53 in the absence of DNA damage: implications for targeting mTOR during malignancy. Oncogene 31 (15), 1949–1962.
URL https://doi.org/10.1038%2Fonc.2011.394

Augustin, H. G., Koh, G. Y., Thurston, G., Alitalo, K., mar 2009. Control of vascular morphogenesis and homeostasis through the angiopoietin-Tie system. Nature Reviews Molecular Cell Biology 10 (3), 165–177.
URL http://dx.doi.org/10.1038/nrm2639

Ausprunk, D. H., Folkman, J., jul 1977. Migration and proliferation of endothelial cells in preformed and newly formed blood vessels during tumor angiogenesis. Microvascular Research 14 (1), 53–65.
URL http://dx.doi.org/10.1016/0026-2862(77)90141-8

Babaei, S., Teichert-Kuliszewska, K., Zhang, Q., Jones, N., Dumont, D. J., Stewart, D. J., jun 2003. Angiogenic actions of Angiopoietin-1 require endothelium-derived Nitric Oxide. The American Journal of Pathology 162 (6), 1927–1936.
URL http://dx.doi.org/10.1016/S0002-9440(10)64326-X

Bazzoni, G., jul 2004. Endothelial Cell-to-Cell Junctions: Molecular organization and role in vascular homeostasis. Physiological Reviews 84 (3), 869–901.
URL http://dx.doi.org/10.1152/physrev.00035.2003

Beenken, A., Mohammadi, M., Mar 2009. The FGF family: biology, pathophysiology and therapy. Nat Rev Drug Discov 8 (3), 235–253.
URL http://dx.doi.org/10.1038/nrd2792

Benedito, R., Hellström, M., may 2013. Notch as a hub for signaling in angiogenesis. Experimental

Cell Research 319 (9), 1281–1288.
URL http://dx.doi.org/10.1016/j.yexcr.2013.01.010

Benedito, R., Roca, C., Sörensen, I., Adams, S., Gossler, A., Fruttiger, M., Adams, R. H., jun 2009. The Notch ligands Dll4 and Jagged1 have opposing effects on angiogenesis. Cell 137 (6), 1124–1135.
URL https://doi.org/10.1016%2Fj.cell.2009.03.025

Benedito, R., Rocha, S. F., Woeste, M., Zamykal, M., Radtke, F., Casanovas, O., Duarte, A., Pytowski, B., Adams, R. H., mar 2012. Notch-dependent VEGFR3 upregulation allows angiogenesis without VEGF/VEGFR2 signalling. Nature 484 (7392), 110–114.
URL https://doi.org/10.1038%2Fnature10908

Bentley, K., Franco, C. A., Philippides, A., Blanco, R., Dierkes, M., Gebala, V., Stanchi, F., Jones, M., Aspalter, I. M., Cagna, G., Weström, S., Claesson-Welsh, L., Vestweber, D., Gerhardt, H., mar 2014. The role of differential VE-cadherin dynamics in cell rearrangement during angiogenesis. Nature Cell Biology 16 (4), 309–321.
URL http://dx.doi.org/10.1038/ncb2926

Bergers, G., Song, S., Oct 2005. The role of pericytes in blood-vessel formation and maintenance. Neuro Oncol 7 (4), 452–464.
URL http://dx.doi.org/10.1215/S1152851705000232

Betsholtz, C., jan 2016. Vascular biology: Transcriptional control of endothelial energy. Nature 529 (7585), 160–161.
URL http://dx.doi.org/10.1038/nature16866

Betz, C., Lenard, A., Belting, H.-G., Affolter, M., Jul 2016. Cell behaviors and dynamics during angiogenesis. Development 143 (13), 2249–2260.
URL http://dx.doi.org/10.1242/dev.135616

Bezanilla, M., Gladfelter, A. S., Kovar, D. R., Lee, W.-L., May 2015. Cytoskeletal dynamics: a view from the membrane. J Cell Biol 209 (3), 329–337.
URL http://dx.doi.org/10.1083/jcb.201502062

Bi, L., Okabe, I., Bernard, D. J., Nussbaum, R. L., mar 2002. Early embryonic lethality in mice deficient in the p110β catalytic subunit of PI 3-kinase. Mammalian Genome 13 (3), 169–172.
URL http://dx.doi.org/10.1007/s00335-001-2123-x

Bi, L., Okabe, I., Bernard, D. J., Wynshaw-Boris, A., Nussbaum, R. L., apr 1999. Proliferative defect and embryonic lethality in mice homozygous for a deletion in the p110α subunit of phosphoinositide 3-kinase. Journal of Biological Chemistry 274 (16), 10963–10968.
URL http://dx.doi.org/10.1074/jbc.274.16.10963

Biswas, K., Yoshioka, K., Asanuma, K., Okamoto, Y., Takuwa, N., Sasaki, T., Takuwa, Y., Jan 2013. Essential role of class II phosphatidylinositol-3-kinase-C2α in sphingosine 1-phosphate receptor-1-mediated signaling and migration in endothelial cells. J Biol Chem 288 (4), 2325–2339.
URL http://dx.doi.org/10.1074/jbc.M112.409656

Blanco, R., Gerhardt, H., Oct 2012. VEGF and Notch in Tip and Stalk Cell Selection. Cold Spring Harbor Perspectives in Medicine 3 (1), a006569–a006569.
URL http://dx.doi.org/10.1101/cshperspect.a006569

Blum, Y., Belting, H.-G., Ellertsdottir, E., Herwig, L., Lüders, F., Affolter, M., apr 2008. Complex cell rearrangements during intersegmental vessel sprouting and vessel fusion in the zebrafish embryo. Developmental Biology 316 (2), 312–322.
URL http://dx.doi.org/10.1016/j.ydbio.2008.01.038

Boshans, R. L., Szanto, S., van Aelst, L., D'Souza-Schorey, C., may 2000. ADP-Ribosylation factor 6 regulates actin cytoskeleton remodeling in coordination with Rac1 and RhoA. Molecular and Cellular Biology 20 (10), 3685–3694.
URL http://dx.doi.org/10.1128/MCB.20.10.3685-3694.2000

Boudreau, N., Jones, P., May 1999. Extracellular matrix and integrin signalling: the shape of things to come. Biochem J 339 (Pt 3), 481–488.

Bouvrée, K., Larrivée, B., Lv, X., Yuan, L., DeLafarge, B., Freitas, C., Mathivet, T., Bréant, C., Tessier-Lavigne, M., Bikfalvi, A., Eichmann, A., Pardanaud, L., Jun 2008. Netrin-1 inhibits sprouting angiogenesis in developing avian embryos. Dev Biol 318 (1), 172–183.
URL http://dx.doi.org/10.1016/j.ydbio.2008.03.023

Breitkopf, S. B., Yang, X., Begley, M. J., Kulkarni, M., Chiu, Y.-H., Turke, A. B., Lauriol, J., Yuan, M., Qi, J., Engelman, J. A., Hong, P., Kontaridis, M. I., Cantley, L. C., Perrimon, N., Asara, J. M., feb 2016. A cross-species study of PI3K protein-protein interactions reveals the direct interaction of p85 and SHP2. Sci. Rep. 6, 20471.
URL http://dx.doi.org/10.1038/srep20471

Brown, J. R., Byrd, J. C., Coutre, S. E., Benson, D. M., Flinn, I. W., Wagner-Johnston, N. D., Spurgeon, S. E., Kahl, B. S., Bello, C., Webb, H. K., Johnson, D. M., Peterman, S., Li, D., Jahn, T. M., Lannutti, B. J., Ulrich, R. G., Yu, A. S., Miller, L. L., Furman, R. R., mar 2014. Idelalisib, an inhibitor of phosphatidylinositol 3-kinase p110δ, for relapsed/refractory chronic lymphocytic leukemia. Blood 123 (22), 3390–3397.
URL http://dx.doi.org/10.1182/blood-2013-11-535047

Burri, P. H., Hlushchuk, R., Djonov, V., 2004. Intussusceptive angiogenesis: Its emergence, its

characteristics, and its significance. Developmental Dynamics 231 (3), 474–488.
URL http://dx.doi.org/10.1002/dvdy.20184

Burridge, K., Wennerberg, K., jan 2004. Rho and Rac take center stage. Cell 116 (2), 167–179.
URL http://dx.doi.org/10.1016/S0092-8674(04)00003-0

Cain, R. J., Ridley, A. J., jan 2009. Phosphoinositide 3-kinases in cell migration. Biology of the Cell 101 (1), 13–29.
URL http://dx.doi.org/10.1042/BC20080079

Cain, R. J., Vanhaesebroeck, B., Ridley, A. J., mar 2010. The pi3k p110alpha isoform regulates endothelial adherens junctions via Pyk2 and Rac1. J Cell Biol 188 (6), 863–876.
URL http://dx.doi.org/10.1083/jcb.200907135

Carmeliet, P., Ferreira, V., Breier, G., Pollefeyt, S., Kieckens, L., Gertsenstein, M., Fahrig, M., Vandenhoeck, A., Harpal, K., Eberhardt, C., Declercq, C., Pawling, J., Moons, L., Collen, D., Risau, W., Nagy, A., apr 1996. Abnormal blood vessel development and lethality in embryos lacking a single VEGF allele. Nature 380 (6573), 435–439.
URL http://dx.doi.org/10.1038/380435a0

Carmeliet, P., Jain, R. K., may 2011. Molecular mechanisms and clinical applications of angiogenesis. Nature 473 (7347), 298–307.
URL http://dx.doi.org/10.1038/nature10144

Carmeliet, P., Lampugnani, M.-G., Moons, L., Breviario, F., Compernolle, V., Bono, F., Balconi, G., Spagnuolo, R., Oosthuyse, B., Dewerchin, M., Zanetti, A., Angellilo, A., Mattot, V., Nuyens, D., Lutgens, E., Clotman, F., de Ruiter, M. C., de Groot, A. G., Poelmann, R., Lupu, F., Herbert, J.-M., DésiréCollen, Dejana, E., jul 1999. Targeted deficiency or cytosolic truncation of the VE-cadherin gene in mice impairs VEGF-mediated endothelial survival and angiogenesis. Cell 98 (2), 147–157.
URL http://dx.doi.org/10.1016/S0092-8674(00)81010-7

Castel, P., Carmona, F. J., Grego-Bessa, J., Berger, M. F., Viale, A., Anderson, K. V., Bague, S., Scaltriti, M., Antonescu, C. R., Baselga, E., Baselga, J., 2016. Somatic PIK3CA mutations as a driver of sporadic venous malformations. Science Translational Medicine 8 (332), 332ra42–332ra42.
URL http://stm.sciencemag.org/content/8/332/332ra42

Castellano, E., Downward, J., Mar 2011. RAS interaction with PI3K: More than just another effector pathway. Genes Cancer 2 (3), 261–274.
URL http://dx.doi.org/10.1177/1947601911408079

Castillo, S. D., Tzouanacou, E., Zaw-Thin, M., Berenjeno, I. M., Parker, V. E., Chivite, I., Milà-Guasch, M., Pearce, W., Solomon, I., Angulo-Urarte, A., Figueiredo, A. M., Dewhurst, R. E., Knox, R. G., Clark, G. R., Scudamore, C. L., Badar, A., Kalber, T. L., Foster, J., Stuckey, D. J., David, A. L., Phillips, W. A., Lythgoe, M. F., Wilson, V., Semple, R. K., Sebire, N. J., Kinsler, V. A., Graupera, M., Vanhaesebroeck, B., 2016. Somatic activating mutations in PIK3CA cause sporadic venous malformations in mice and humans. Science Translational Medicine 8 (332), 332ra43–332ra43.
URL http://stm.sciencemag.org/content/8/332/332ra43

Chen, J., Somanath, P. R., Razorenova, O., Chen, W. S., Hay, N., Bornstein, P., Byzova, T. V., oct 2005a. Akt1 regulates pathological angiogenesis, vascular maturation and permeability in vivo. Nature Medicine 11 (11), 1188–1196.
URL http://dx.doi.org/10.1038/nm1307

Chen, Z., Trotman, L. C., Shaffer, D., Lin, H.-K., Dotan, Z. A., Niki, M., Koutcher, J. A., Scher, H. I., Ludwig, T., Gerald, W., Cordon-Cardo, C., Pandolfi, P. P., aug 2005b. Crucial role of p53-dependent cellular senescence in suppression of Pten-deficient tumorigenesis. Nature 436 (7051), 725–730.
URL https://doi.org/10.1038%2Fnature03918

Cheung, L. W. T., Walkiewicz, K. W., Besong, T. M. D., Guo, H., Hawke, D. H., Arold, S. T., Mills, G. B., Jul 2015. Regulation of the PI3K pathway through a p85α monomer-homodimer equilibrium. Elife 4, e06866.
URL http://dx.doi.org/10.7554/eLife.06866

Childs, S., Chen, J.-N., Garrity, D. M., Fishman, M. C., 2002. Patterning of angiogenesis in the zebrafish embryo. Development 129 (4), 973–982.
URL http://dev.biologists.org/content/129/4/973

Choi, H.-J., Zhang, H., Park, H., Choi, K.-S., Lee, H.-W., Agrawal, V., Kim, Y.-M., Kwon, Y.-G., may 2015. Yes-associated protein regulates endothelial cell contact-mediated expression of angiopoietin-2. Nature Communications 6, 6943.
URL https://doi.org/10.1038%2Fncomms7943

Choorapoikayil, S., Weijts, B., Kers, R., de Bruin, A., den Hertog, J., Sep 2013. Loss of Pten promotes angiogenesis and enhanced vegfaa expression in zebrafish. Dis Model Mech 6 (5), 1159–1166.
URL http://dx.doi.org/10.1242/dmm.012377

Claxton, S., Kostourou, V., Jadeja, S., Chambon, P., Hodivala-Dilke, K., Fruttiger, M., Feb 2008. Efficient, inducible Cre-recombinase activation in vascular endothelium. Genesis (New York, N.Y. : 2000) 46, 74–80.

Corada, M., Orsenigo, F., Morini, M. F., Pitulescu, M. E., Bhat, G., Nyqvist, D., Breviario, F., Conti, V., Briot, A., Iruela-Arispe, M. L., Adams, R. H., Dejana, E., oct 2013. Sox17 is indispensable for acquisition and maintenance of arterial identity. Nature Communications 4.
URL http://dx.doi.org/10.1038/ncomms3609

Coso, S., Zeng, Y., Opeskin, K., Williams, E. D., jun 2012. Vascular endothelial growth factor receptor-3 directly interacts with Phosphatidylinositol 3-Kinase to regulate lymphangiogenesis. PLoS ONE 7 (6), e39558.
URL http://dx.doi.org/10.1371/journal.pone.0039558

Costell, M., Gustafsson, E., Aszódi, A., Mörgelin, M., Bloch, W., Hunziker, E., Addicks, K., Timpl, R., Fässler, R., Nov 1999. Perlecan maintains the integrity of cartilage and some basement membranes. J Cell Biol 147 (5), 1109–1122.

Cunningham, S. A., Waxham, M. N., Arrate, P. M., Brock, T. A., sep 1995. Interaction of the Flt-1 tyrosine kinase receptor with the p85 subunit of Phosphatidylinositol 3-Kinase: MAPPING OF A NOVEL SITE INVOLVED IN BINDING. Journal of Biological Chemistry 270 (35), 20254–20257.
URL http://dx.doi.org/10.1074/jbc.270.35.20254

Daly, C., apr 2004. Angiopoietin-1 modulates endothelial cell function and gene expression via the transcription factor FKHR (FOXO1). Genes & Development 18 (9), 1060–1071.
URL http://dx.doi.org/10.1101/gad.1189704

Daneshjou, N., Sieracki, N., van Nieuw Amerongen, G. P., Conway, D. E., Schwartz, M. A., Komarova, Y. A., Malik, A. B., jan 2015. Rac1 functions as a reversible tension modulator to stabilize VE-cadherin trans-interaction. J Cell Biol 208 (1), 23–32.
URL http://dx.doi.org/10.1083/jcb.201409108

Davis, G. E., Senger, D. R., Nov 2005. Endothelial extracellular matrix: biosynthesis, remodeling, and functions during vascular morphogenesis and neovessel stabilization. Circ Res 97 (11), 1093–1107.
URL http://dx.doi.org/10.1161/01.RES.0000191547.64391.e3

Dayanir, V., mar 2001. Identification of tyrosine residues in Vascular Endothelial Growth Factor Receptor-2/FLK-1 involved in activation of Phosphatidylinositol 3-Kinase and cell proliferation. Journal of Biological Chemistry 276 (21), 17686–17692.
URL http://dx.doi.org/10.1074/jbc.M009128200

Dbouk, H. A., Vadas, O., Shymanets, A., Burke, J. E., Salamon, R. S., Khalil, B. D., Barrett, M. O., Waldo, G. L., Surve, C., Hsueh, C., Perisic, O., Harteneck, C., Shepherd, P. R., Harden, T. K., Smrcka, A. V., Taussig, R., Bresnick, A. R., Nürnberg, B., Williams, R. L., Backer, J. M., Dec 2012. G protein-coupled receptor-mediated activation of p110β by Gβγ is required for cellular

transformation and invasiveness. Sci Signal 5 (253), ra89.
URL http://dx.doi.org/10.1126/scisignal.2003264

Dejana, E., apr 2004. Endothelial cell–cell junctions: happy together. Nature Reviews Molecular Cell Biology 5 (4), 261–270.
URL http://dx.doi.org/10.1038/nrm1357

del Toro, R., Prahst, C., Mathivet, T., Siegfried, G., Kaminker, J. S., Larrivee, B., Breant, C., Duarte, A., Takakura, N., Fukamizu, A., Penninger, J., Eichmann, A., aug 2010. Identification and functional analysis of endothelial tip cell-enriched genes. Blood 116 (19), 4025–4033.
URL http://dx.doi.org/10.1182/blood-2010-02-270819

Dharaneeswaran, H., Abid, M. R., Yuan, L., Dupuis, D., Beeler, D., Spokes, K. C., Janes, L., Sciuto, T., Kang, P. M., Jaminet, S.-C. S., Dvorak, A., Grant, M. A., Regan, E. R., Aird, W. C., Jul 2014. FOXO1-mediated activation of Akt plays a critical role in vascular homeostasis. Circ Res 115 (2), 238–251.
URL http://dx.doi.org/10.1161/CIRCRESAHA.115.303227

di Blasio, L., Gagliardi, P. A., Puliafito, A., Sessa, R., Seano, G., Bussolino, F., Primo, L., jan 2015. PDK1 regulates focal adhesion disassembly by modulating endocytosis of αvβ3 integrin. Journal of Cell Science 128 (5), 863–877.
URL https://doi.org/10.1242%2Fjcs.149294

Dimmeler, S., Dernbach, E., Zeiher, A., Jul 2000. Phosphorylation of the endothelial nitric oxide synthase at ser-1177 is required for VEGF-induced endothelial cell migration. FEBS Lett 477 (3), 258–262.

Dimmeler, S., Fleming, I., Fisslthaler, B., Hermann, C., Busse, R., Zeiher, A. M., jun 1999. Activation of nitric oxide synthase in endothelial cells by Akt-dependent phosphorylation. Nature 399 (6736), 601–605.
URL https://doi.org/10.1038%2F21224

Dixelius, J., jul 2003. Ligand-induced vascular endothelial growth factor receptor-3 (VEGFR-3) heterodimerization with VEGFR-2 in primary lymphatic endothelial cells regulates tyrosine phosphorylation sites. Journal of Biological Chemistry 278 (42), 40973–40979.
URL http://dx.doi.org/10.1074/jbc.M304499200

Djonov, V., Schmid, M., Tschanz, S. A., Burri, P. H., feb 2000. Intussusceptive angiogenesis : Its role in embryonic vascular network formation. Circulation Research 86 (3), 286–292.
URL http://dx.doi.org/10.1161/01.RES.86.3.286

Domenga, V., nov 2004. Notch3 is required for arterial identity and maturation of vascular smooth muscle cells. Genes & Development 18 (22), 2730–2735.
URL http://dx.doi.org/10.1101/gad.308904

Donaldson, J. G., aug 2003. Multiple roles for Arf6: Sorting, structuring, and signaling at the plasma membrane. Journal of Biological Chemistry 278 (43), 41573–41576.
URL http://dx.doi.org/10.1074/jbc.R300026200

Dorland, Y. L., Huveneers, S., aug 2016. Cell–cell junctional mechanotransduction in endothelial remodeling. Cell. Mol. Life Sci.
URL http://dx.doi.org/10.1007/s00018-016-2325-8

Dummler, B., Hemmings, B., Apr 2007. Physiological roles of PKB/Akt isoforms in development and disease. Biochem Soc Trans 35 (Pt 2), 231–235.
URL http://dx.doi.org/10.1042/BST0350231

Dumont, D. J., oct 1998. Cardiovascular failure in mouse embryos deficient in VEGF Receptor-3. Science 282 (5390), 946–949.
URL http://dx.doi.org/10.1126/science.282.5390.946

Edwards, D. C., Sanders, L. C., Gill, G. N., Bokoch, G. M., jul 1999. Activation of LIM-kinase by Pak1 couples Rac/Cdc42 GTPase signalling to actin cytoskeletal dynamics. Nature Cell Biology 1 (5), 253–259.
URL https://doi.org/10.1038%2F12963

Ehling, M., Adams, S., Benedito, R., Adams, R. H., jun 2013. Notch controls retinal blood vessel maturation and quiescence. Development 140 (14), 3051–3061.
URL http://dx.doi.org/10.1242/dev.093351

Ellertsdóttir, E., Lenard, A., Blum, Y., Krudewig, A., Herwig, L., Affolter, M., Belting, H.-G., 2010. Vascular morphogenesis in the zebrafish embryo. Developmental Biology 341 (1), 56 – 65, special Section: Morphogenesis.
URL http://www.sciencedirect.com/science/article/pii/S0012160609013116

Ferrara, N., Carver-Moore, K., Chen, H., Dowd, M., Lu, L., O'Shea, K. S., Powell-Braxton, L., Hillan, K. J., Moore, M. W., apr 1996. Heterozygous embryonic lethality induced by targeted inactivation of the VEGF gene. Nature 380 (6573), 439–442.
URL http://dx.doi.org/10.1038/380439a0

Fish, J. E., Santoro, M. M., Morton, S. U., Yu, S., Yeh, R.-F., Wythe, J. D., Ivey, K. N., Bruneau, B. G., Stainier, D. Y., Srivastava, D., aug 2008. miR-126 regulates angiogenic signaling and vascular integrity. Developmental Cell 15 (2), 272–284.
URL http://dx.doi.org/10.1016/j.devcel.2008.07.008

Fong, G.-H., Rossant, J., Gertsenstein, M., Breitman, M. L., jul 1995. Role of the Flt-1 receptor tyrosine kinase in regulating the assembly of vascular endothelium. Nature 376 (6535), 66–70.
URL http://dx.doi.org/10.1038/376066a0

Foukas, L. C., Claret, M., Pearce, W., Okkenhaug, K., Meek, S., Peskett, E., Sancho, S., Smith, A. J. H., Withers, D. J., Vanhaesebroeck, B., apr 2006. Critical role for the p110alpha phosphoinositide-3-OH kinase in growth and metabolic regulation. Nature 441 (7091), 366–370.
URL http://dx.doi.org/10.1038/nature04694

Franco, C. A., Blanc, J., Parlakian, A., Blanco, R., Aspalter, I. M., Kazakova, N., Diguet, N., Mylonas, E., Gao-Li, J., Vaahtokari, A., Penard-Lacronique, V., Fruttiger, M., Rosewell, I., Mericskay, M., Gerhardt, H., Li, Z., may 2013. SRF selectively controls tip cell invasive behavior in angiogenesis. Development 140 (11), 2321–2333.
URL http://dx.doi.org/10.1242/dev.091074

Franco, C. A., Jones, M. L., Bernabeu, M. O., Geudens, I., Mathivet, T., Rosa, A., Lopes, F. M., Lima, A. P., Ragab, A., Collins, R. T., Phng, L.-K., Coveney, P. V., Gerhardt, H., May 2015a. Correction: Dynamic endothelial cell rearrangements drive developmental vessel regression. PLoS Biol 13 (5), e1002163.
URL http://dx.doi.org/10.1371/journal.pbio.1002163

Franco, C. A., Jones, M. L., Bernabeu, M. O., Geudens, I., Mathivet, T., Rosa, A., Lopes, F. M., Lima, A. P., Ragab, A., Collins, R. T., Phng, L.-K., Coveney, P. V., Gerhardt, H., Apr 2015b. Dynamic endothelial cell rearrangements drive developmental vessel regression. PLoS Biol 13 (4), e1002125.
URL http://dx.doi.org/10.1371/journal.pbio.1002125

Fritsch, R., de Krijger, I., Fritsch, K., George, R., Reason, B., Kumar, M. S., Diefenbacher, M., Stamp, G., Downward, J., may 2013. RAS and RHO families of GTPases directly regulate distinct Phosphoinositide 3-Kinase isoforms. Cell 153 (5), 1050–1063.
URL http://dx.doi.org/10.1016/j.cell.2013.04.031

Fruman, D., Mauvais-Jarvis, F., Pollard, D., Yballe, C., Brazil, D., Bronson, R., Kahn, C., Cantley, L., Nov 2000. Hypoglycaemia, liver necrosis and perinatal death in mice lacking all isoforms of phosphoinositide 3-kinase p85 alpha. Nat Genet 26 (3), 379–382.
URL http://dx.doi.org/10.1038/81715

Fujita, M., Cha, Y. R., Pham, V. N., Sakurai, A., Roman, B. L., Gutkind, J. S., Weinstein, B. M., mar 2011. Assembly and patterning of the vascular network of the vertebrate hindbrain. Development 138 (9), 1705–1715.
URL http://dx.doi.org/10.1242/dev.058776

Fulton, D., Gratton, J.-P., McCabe, T. J., Fontana, J., Fujio, Y., Walsh, K., Franke, T. F., Papapetropoulos, A., Sessa, W. C., jun 1999. Regulation of endothelium-derived nitric oxide production by the protein kinase Akt. Nature 399 (6736), 597–601.
URL https://doi.org/10.1038%2F21218

Funamoto, S., Meili, R., Lee, S., Parry, L., Firtel, R. A., may 2002. Spatial and temporal regulation of 3-phosphoinositides by PI 3-Kinase and PTEN mediates chemotaxis. Cell 109 (5), 611–623. URL https://doi.org/10.1016%2Fs0092-8674%2802%2900755-9

Gaengel, K., Genova, G., Armulik, A., Betsholtz, C., May 2009. Endothelial-mural cell signaling in vascular development and angiogenesis. Arterioscler Thromb Vasc Biol 29 (5), 630–638. URL http://dx.doi.org/10.1161/ATVBAHA.107.161521

Gaengel, K., Niaudet, C., Hagikura, K., Laviña, B., Muhl, L., Hofmann, J. J., Ebarasi, L., Nyström, S., Rymo, S., Chen, L. L., Pang, M.-F., Jin, Y., Raschperger, E., Roswall, P., Schulte, D., Benedito, R., Larsson, J., Hellström, M., Fuxe, J., Uhlén, P., Adams, R., Jakobsson, L., Majumdar, A., Vestweber, D., Uv, A., Betsholtz, C., sep 2012. The Sphingosine-1-Phosphate Receptor S1PR1 restricts sprouting angiogenesis by regulating the interplay between VE-cadherin and VEGFR2. Developmental Cell 23 (3), 587–599. URL https://doi.org/10.1016%2Fj.devcel.2012.08.005

Galvagni, F., Pennacchini, S., Salameh, A., Rocchigiani, M., Neri, F., Orlandini, M., Petraglia, F., Gotta, S., Sardone, G. L., Matteucci, G., Terstappen, G. C., Oliviero, S., apr 2010. Endothelial cell adhesion to the extracellular matrix induces c-src-dependent VEGFR-3 phosphorylation without the activation of the receptor intrinsic kinase activity. Circulation Research 106 (12), 1839–1848. URL http://dx.doi.org/10.1161/CIRCRESAHA.109.206326

Gambardella, L., Hemberger, M., Hughes, B., Zudaire, E., Andrews, S., Vermeren, S., Oct 2010. PI3K signaling through the dual GTPase-activating protein ARAP3 is essential for developmental angiogenesis. Sci Signal 3 (145), ra76. URL http://dx.doi.org/10.1126/scisignal.2001026

García, Z., Silio, V., Marqués, M., Cortés, I., Kumar, A., Hernandez, C., Checa, A. I., Serrano, A., Carrera, A. C., Oct 2006. A PI3K activity-independent function of p85 regulatory subunit in control of mammalian cytokinesis. EMBO J 25 (20), 4740–4751. URL http://dx.doi.org/10.1038/sj.emboj.7601324

Gariano, R. F., Gardner, T. W., Dec 2005. Retinal angiogenesis in development and disease. Nature 438 (7070), 960–966. URL http://dx.doi.org/10.1038/nature04482

Gebala, V., Collins, R., Geudens, I., Phng, L.-K., Gerhardt, H., feb 2016. Blood flow drives lumen formation by inverse membrane blebbing during angiogenesis in vivo. Nature Cell Biology 18 (4), 443–450. URL http://dx.doi.org/10.1038/ncb3320

Geering, B., Cutillas, P. R., Nock, G., Gharbi, S. I., Vanhaesebroeck, B., May 2007. Class IA phosphoinositide 3-kinases are obligate p85-p110 heterodimers. Proc Natl Acad Sci U S A 104 (19), 7809–7814.
URL http://dx.doi.org/10.1073/pnas.0700373104

Gerhardt, H., Golding, M., Fruttiger, M., Ruhrberg, C., Lundkvist, A., Abramsson, A., Jeltsch, M., Mitchell, C., Alitalo, K., Shima, D., Betsholtz, C., jun 2003. VEGF guides angiogenic sprouting utilizing endothelial tip cell filopodia. J Cell Biol 161 (6), 1163–1177.
URL http://dx.doi.org/10.1083/jcb.200302047

Giannotta, M., Trani, M., Dejana, E., sep 2013. VE-cadherin and endothelial adherens junctions: Active guardians of vascular integrity. Developmental Cell 26 (5), 441–454.
URL http://dx.doi.org/10.1016/j.devcel.2013.08.020

Glaser, B., Kalebic, T., Garbisa, S., Connor, T. B., Liotta, L. A., may 2008. Degradation of basement membrane components by vascular endothelial cells: Role in neovascularization. In: Ciba/Development. Wiley-Blackwell, pp. 150–162.
URL http://dx.doi.org/10.1002/9780470720813.ch10

González-García, A., Carrera, A. C., 2012. p85β increases phosphoinositide 3-kinase activity and accelerates tumor progression. Cell Cycle 11 (19), 3523–3524, pMID: 22935711.
URL http://dx.doi.org/10.4161/cc.21961

Gore, A. V., Monzo, K., Cha, Y. R., Pan, W., Weinstein, B. M., May 2012. Vascular development in the zebrafish. Cold Spring Harb Perspect Med 2 (5), a006684.
URL http://dx.doi.org/10.1101/cshperspect.a006684

Gory-Faure, S., Prandini, M., Pointu, H., Roullot, V., Pignot-Paintrand, I., Vernet, M., Huber, P., 1999. Role of vascular endothelial-cadherin in vascular morphogenesis. Development 126 (10), 2093–2102.
URL http://dev.biologists.org/content/126/10/2093

Grassie, M. E., Moffat, L. D., Walsh, M. P., MacDonald, J. A., Jun 2011. The myosin phosphatase targeting protein (MYPT) family: a regulated mechanism for achieving substrate specificity of the catalytic subunit of protein phosphatase type 1. Arch Biochem Biophys 510 (2), 147–159.
URL http://dx.doi.org/10.1016/j.abb.2011.01.018

Graupera, M., Guillermet-Guibert, J., Foukas, L. C., Phng, L.-K., Cain, R. J., Salpekar, A., Pearce, W., Meek, S., Millan, J., Cutillas, P. R., Smith, A. J. H., Ridley, A. J., Ruhrberg, C., Gerhardt, H., Vanhaesebroeck, B., apr 2008. Angiogenesis selectively requires the p110α isoform of PI3K to control endothelial cell migration. Nature 453 (7195), 662–666.
URL http://dx.doi.org/10.1038/nature06892

Graupera, M., Potente, M., may 2013. Regulation of angiogenesis by PI3K signaling networks. Experimental Cell Research 319 (9), 1348–1355.
URL http://dx.doi.org/10.1016/j.yexcr.2013.02.021

Gu, C., Yoshida, Y., Livet, J., Reimert, D. V., Mann, F., Merte, J., Henderson, C. E., Jessell, T. M., Kolodkin, A. L., Ginty, D. D., Jan 2005. Semaphorin 3E and plexin-D1 control vascular pattern independently of neuropilins. Science 307 (5707), 265–268.
URL http://dx.doi.org/10.1126/science.1105416

Gupta, S., Ramjaun, A. R., Haiko, P., Wang, Y., Warne, P. H., Nicke, B., Nye, E., Stamp, G., Alitalo, K., Downward, J., jun 2007. Binding of Ras to phosphoinositide 3-Kinase p110α is required for Ras- driven tumorigenesis in mice. Cell 129 (5), 957–968.
URL http://dx.doi.org/10.1016/j.cell.2007.03.051

Haiko, P., Makinen, T., Keskitalo, S., Taipale, J., Karkkainen, M. J., Baldwin, M. E., Stacker, S. A., Achen, M. G., Alitalo, K., jun 2008. Deletion of vascular endothelial growth factor c (VEGF-c) and VEGF-d is not equivalent to VEGF receptor 3 deletion in mouse embryos. Molecular and Cellular Biology 28 (15), 4843–4850.
URL http://dx.doi.org/10.1128/MCB.02214-07

Hamada, K., Sasaki, T., Koni, P. A., Natsui, M., Kishimoto, H., Sasaki, J., Yajima, N., Horie, Y., Hasegawa, G., Naito, M., Miyazaki, J.-I., Suda, T., Itoh, H., Nakao, K., Mak, T. W., Nakano, T., Suzuki, A., Sep 2005. The PTEN/PI3K pathway governs normal vascular development and tumor angiogenesis. Genes Dev 19 (17), 2054–2065.
URL http://dx.doi.org/10.1101/gad.1308805

Hanada, M., Feng, J., Hemmings, B. A., Mar 2004. Structure, regulation and function of PKB/AKT–a major therapeutic target. Biochim Biophys Acta 1697 (1-2), 3–16.
URL http://dx.doi.org/10.1016/j.bbapap.2003.11.009

Hare, L. M., Schwarz, Q., Wiszniak, S., Gurung, R., Montgomery, K. G., Mitchell, C. A., Phillips, W. A., Aug 2015. Heterozygous expression of the oncogenic Pik3ca(H1047R) mutation during murine development results in fatal embryonic and extraembryonic defects. Dev Biol 404 (1), 14–26.
URL http://dx.doi.org/10.1016/j.ydbio.2015.04.022

Harrington, L. S., Sainson, R. C. A., Williams, C. K., Taylor, J. M., Shi, W., Li, J.-L., Harris, A. L., Mar 2008. Regulation of multiple angiogenic pathways by Dll4 and Notch in human umbilical vein endothelial cells. Microvasc Res 75 (2), 144–154.
URL http://dx.doi.org/10.1016/j.mvr.2007.06.006

Haugh, J. M., Codazzi, F., Teruel, M., Meyer, T., dec 2000. Spatial sensing in fibroblasts mediated

by 3' phosphoinositides. The Journal of Cell Biology 151 (6), 1269–1280.
URL https://doi.org/10.1083%2Fjcb.151.6.1269

Hayashi, H., Kume, T., Jun 2008. Foxc transcription factors directly regulate Dll4 and Hey2 expression by interacting with the VEGF-Notch signaling pathways in endothelial cells. PLoS One 3 (6), e2401.
URL http://dx.doi.org/10.1371/journal.pone.0002401

Helker, C. S. M., Schuermann, A., Karpanen, T., Zeuschner, D., Belting, H.-G., Affolter, M., Schulte-Merker, S., Herzog, W., may 2013. The zebrafish common cardinal veins develop by a novel mechanism: lumen ensheathment. Development 140 (13), 2776–2786.
URL http://dx.doi.org/10.1242/dev.091876

Hellström, M., Phng, L.-K., Hofmann, J. J., Wallgard, E., Coultas, L., Lindblom, P., Alva, J., Nilsson, A.-K., Karlsson, L., Gaiano, N., Yoon, K., Rossant, J., Iruela-Arispe, M. L., Kalén, M., Gerhardt, H., Betsholtz, C., Feb 2007. Dll4 signalling through notch1 regulates formation of tip cells during angiogenesis. Nature 445 (7129), 776–780.
URL http://dx.doi.org/10.1038/nature05571

Hemmings, B. A., Restuccia, D. F., sep 2012. PI3K-PKB/Akt pathway. Cold Spring Harbor Perspectives in Biology 4 (9), a011189–a011189.
URL http://dx.doi.org/10.1101/cshperspect.a011189

Herbert, S. P., Huisken, J., Kim, T. N., Feldman, M. E., Houseman, B. T., Wang, R. A., Shokat, K. M., Stainier, D. Y. R., oct 2009. Arterial-venous segregation by selective cell sprouting: An alternative mode of blood vessel formation. Science 326 (5950), 294–298.
URL http://dx.doi.org/10.1126/science.1178577

Herbert, S. P., Stainier, D. Y. R., aug 2011. Molecular control of endothelial cell behaviour during blood vessel morphogenesis. Nature Reviews Molecular Cell Biology 12 (9), 551–564.
URL http://dx.doi.org/10.1038/nrm3176

Higuchi, M., Kihara, R., Okazaki, T., Aoki, I., Suetsugu, S., Gotoh, Y., dec 2012. Akt1 promotes focal adhesion disassembly and cell motility through phosphorylation of FAK in growth factor-stimulated cells. Journal of Cell Science 126 (3), 745–755.
URL https://doi.org/10.1242%2Fjcs.112722

Hlushchuk, R., Ehrbar, M., Reichmuth, P., Heinimann, N., Styp-Rekowska, B., Escher, R., Baum, O., Lienemann, P., Makanya, A., Keshet, E., Djonov, V., sep 2011. Decrease in VEGF expression induces intussusceptive vascular pruning. Arteriosclerosis, Thrombosis, and Vascular Biology 31 (12), 2836–2844.
URL http://dx.doi.org/10.1161/ATVBAHA.111.231811

Hlushchuk, R., Riesterer, O., Baum, O., Wood, J., Gruber, G., Pruschy, M., Djonov, V., oct 2008. Tumor recovery by angiogenic switch from sprouting to intussusceptive angiogenesis after treatment with PTK787/ZK222584 or ionizing radiation. The American Journal of Pathology 173 (4), 1173–1185.
URL http://dx.doi.org/10.2353/ajpath.2008.071131

Hogan, B. M., Herpers, R., Witte, M., Heloterä, H., Alitalo, K., Duckers, H. J., Schulte-Merker, S., Dec 2009. Vegfc/Flt4 signalling is suppressed by Dll4 in developing zebrafish intersegmental arteries. Development 136 (23), 4001–4009.
URL http://dx.doi.org/10.1242/dev.039990

Hopkins, B. D., Hodakoski, C., Barrows, D., Mense, S. M., Parsons, R. E., Apr 2014. PTEN function: the long and the short of it. Trends Biochem Sci 39 (4), 183–190.
URL http://dx.doi.org/10.1016/j.tibs.2014.02.006

Hudry-Clergeon, H., apr 2005. Platelet-activating factor increases VE-cadherin tyrosine phosphorylation in mouse endothelial cells and its association with the PtdIns3'-kinase. The FASEB Journal 19 (6), 512–520.
URL http://dx.doi.org/10.1096/fj.04-2202com

Huveneers, S., de Rooij, J., jan 2013. Mechanosensitive systems at the cadherin-F-actin interface. Journal of Cell Science 126 (2), 403–413.
URL http://dx.doi.org/10.1242/jcs.109447

Huveneers, S., Oldenburg, J., Spanjaard, E., van der Krogt, G., Grigoriev, I., Akhmanova, A., Rehmann, H., de Rooij, J., Mar 2012. Vinculin associates with endothelial VE-cadherin junctions to control force-dependent remodeling. J Cell Biol 196 (5), 641–652.
URL http://dx.doi.org/10.1083/jcb.201108120

Iijima, M., Devreotes, P., may 2002. Tumor suppressor PTEN mediates sensing of chemoattractant gradients. Cell 109 (5), 599–610.
URL https://doi.org/10.1016%2Fs0092-8674%2802%2900745-6

Inoki, K., Li, Y., Zhu, T., Wu, J., Guan, K.-L., Sep 2002. TSC2 is phosphorylated and inhibited by Akt and suppresses mTOR signalling. Nat Cell Biol 4 (9), 648–657.
URL http://dx.doi.org/10.1038/ncb839

Inukai, K., Funaki, M., Anai, M., Ogihara, T., Katagiri, H., Fukushima, Y., Sakoda, H., Onishi, Y., Ono, H., Fujishiro, M., Abe, M., Oka, Y., Kikuchi, M., Asano, T., Feb 2001. Five isoforms of the phosphatidylinositol 3-kinase regulatory subunit exhibit different associations with receptor tyrosine kinases and their tyrosine phosphorylations. FEBS Lett 490 (1-2), 32–38.

Iso, T., Kedes, L., Hamamori, Y., jan 2003. HES and HERP families: Multiple effectors of the notch signaling pathway. Journal of Cellular Physiology 194 (3), 237–255.
URL https://doi.org/10.1002%2Fjcp.10208

Isogai, S., Horiguchi, M., Weinstein, B., Feb 2001. The vascular anatomy of the developing zebrafish: an atlas of embryonic and early larval development. Dev Biol 230 (2), 278–301.
URL http://dx.doi.org/10.1006/dbio.2000.9995

Isogai, S., Lawson, N. D., Torrealday, S., Horiguchi, M., Weinstein, B. M., Nov 2003. Angiogenic network formation in the developing vertebrate trunk. Development 130 (21), 5281–5290.
URL http://dx.doi.org/10.1242/dev.00733

Jakobsson, L., Franco, C. A., Bentley, K., Collins, R. T., Ponsioen, B., Aspalter, I. M., Rosewell, I., Busse, M., Thurston, G., Medvinsky, A., Schulte-Merker, S., Gerhardt, H., sep 2010. Endothelial cells dynamically compete for the tip cell position during angiogenic sprouting. Nature Cell Biology 12 (10), 943–953.
URL http://dx.doi.org/10.1038/ncb2103

Jean, S., Kiger, A. A., Mar 2014. Classes of phosphoinositide 3-kinases at a glance. J Cell Sci 127 (Pt 5), 923–928.
URL http://dx.doi.org/10.1242/jcs.093773

Jin, S.-W., dec 2005. Cellular and molecular analyses of vascular tube and lumen formation in zebrafish. Development 132 (23), 5199–5209.
URL http://dx.doi.org/10.1242/dev.02087

Jones, C. A., London, N. R., Chen, H., Park, K. W., Sauvaget, D., Stockton, R. A., Wythe, J. D., Suh, W., Larrieu-Lahargue, F., Mukouyama, Y.-S., Lindblom, P., Seth, P., Frias, A., Nishiya, N., Ginsberg, M. H., Gerhardt, H., Zhang, K., Li, D. Y., Apr 2008. Robo4 stabilizes the vascular network by inhibiting pathologic angiogenesis and endothelial hyperpermeability. Nat Med 14 (4), 448–453.
URL http://dx.doi.org/10.1038/nm1742

Jones, N., Master, Z., Jones, J., Bouchard, D., Gunji, Y., Sasaki, H., Daly, R., Alitalo, K., Dumont, D., Oct 1999. Identification of Tek/Tie2 binding partners. binding to a multifunctional docking site mediates cell survival and migration. J Biol Chem 274 (43), 30896–30905.

Kalluri, R., Jun 2003. Basement membranes: structure, assembly and role in tumour angiogenesis. Nat Rev Cancer 3 (6), 422–433.
URL http://dx.doi.org/10.1038/nrc1094

Kartopawiro, J., Bower, N. I., Karnezis, T., Kazenwadel, J., Betterman, K. L., Lesieur, E., Koltowska, K., Astin, J., Crosier, P., Vermeren, S., Achen, M. G., Stacker, S. A., Smith, K. A.,

Harvey, N. L., François, M., Hogan, B. M., Mar 2014. Arap3 is dysregulated in a mouse model of hypotrichosis-lymphedema-telangiectasia and regulates lymphatic vascular development. Hum Mol Genet 23 (5), 1286–1297.
URL http://dx.doi.org/10.1093/hmg/ddt518

Kearney, J. B., feb 2004. The VEGF receptor flt-1 (VEGFR-1) is a positive modulator of vascular sprout formation and branching morphogenesis. Blood 103 (12), 4527–4535.
URL http://dx.doi.org/10.1182/blood-2003-07-2315

Kerr, B. A., West, X. Z., Kim, Y.-W., Zhao, Y., Tischenko, M., Cull, R. M., Phares, T. W., Peng, X.-D., Bernier-Latmani, J., Petrova, T. V., Adams, R. H., Hay, N., Prasad, S. V. N., Byzova, T. V., mar 2016. Stability and function of adult vasculature is sustained by Akt/Jagged1 signalling axis in endothelium. Nature Communications 7, 10960.
URL http://dx.doi.org/10.1038/ncomms10960

Kim, I., Kim, H., So, J., Kim, J., Kwak, H., Koh, G., 2000. Angiopoietin-1 regulates endothelial cell survival through the phosphatidylinositol 3'-kinase/Akt signal transduction pathway. Circ Res 86 (1), 24–29.

Kim, N.-G., Gumbiner, B. M., jul 2015. Adhesion to fibronectin regulates Hippo signaling via the FAK/Src/PI3K pathway. The Journal of Cell Biology 210 (3), 503–515.
URL https://doi.org/10.1083%2Fjcb.201501025

Kochhan, E., Lenard, A., Ellertsdottir, E., Herwig, L., Affolter, M., Belting, H.-G., Siekmann, A. F., 2013. Blood flow changes coincide with cellular rearrangements during blood vessel pruning in zebrafish embryos. PloS one 8, e75060.

Koga, Y., Ikebe, M., nov 2004. p116 rip decreases myosin II phosphorylation by activating myosin light chain phosphatase and by inactivating RhoA. Journal of Biological Chemistry 280 (6), 4983–4991.
URL http://dx.doi.org/10.1074/jbc.M410909200

Kolsch, V., Charest, P. G., Firtel, R. A., feb 2008. The regulation of cell motility and chemotaxis by phospholipid signaling. Journal of Cell Science 121 (5), 551–559.
URL https://doi.org/10.1242%2Fjcs.023333

Kontos, C., Stauffer, T., Yang, W., York, J., Huang, L., Blanar, M., Meyer, T., Peters, K., Jul 1998. Tyrosine 1101 of Tie2 is the major site of association of p85 and is required for activation of phosphatidylinositol 3-kinase and Akt. Mol Cell Biol 18 (7), 4131–4140.

Kopan, R., Ilagan, M. X. G., apr 2009. The canonical Notch signaling pathway: Unfolding the activation mechanism. Cell 137 (2), 216–233.
URL http://dx.doi.org/10.1016/j.cell.2009.03.045

Korn, C., Augustin, H. G., Jul 2015. Mechanisms of vessel pruning and regression. Dev Cell 34 (1), 5–17.
URL http://dx.doi.org/10.1016/j.devcel.2015.06.004

Krueger, J., Liu, D., Scholz, K., Zimmer, A., Shi, Y., Klein, C., Siekmann, A., Schulte-Merker, S., Cudmore, M., Ahmed, A., le Noble, F., apr 2011. Flt1 acts as a negative regulator of tip cell formation and branching morphogenesis in the zebrafish embryo. Development 138 (10), 2111–2120.
URL http://dx.doi.org/10.1242/dev.063933

Krugmann, S., Anderson, K., Ridley, S., Risso, N., McGregor, A., Coadwell, J., Davidson, K., Eguinoa, A., Ellson, C., Lipp, P., Manifava, M., Ktistakis, N., Painter, G., Thuring, J., Cooper, M., Lim, Z.-Y., Holmes, A., Dove, S., Michell, R., Grewal, A., Nazarian, A., Erdjument-Bromage, H., Tempst, P., Stephens, L., Hawkins, P., Jan 2002. Identification of ARAP3, a novel PI3K effector regulating both Arf and Rho GTPases, by selective capture on phosphoinositide affinity matrices. Mol Cell 9 (1), 95–108.

Krugmann, S., Williams, R., Stephens, L., Hawkins, P. T., Aug 2004. ARAP3 is a PI3K- and rap-regulated GAP for RhoA. Curr Biol 14 (15), 1380–1384.
URL http://dx.doi.org/10.1016/j.cub.2004.07.058

Kurek, K. C., Luks, V. L., Ayturk, U. M., Alomari, A. I., Fishman, S. J., Spencer, S. A., Mulliken, J. B., Bowen, M. E., Yamamoto, G. L., Kozakewich, H. P. W., Warman, M. L., Jun 2012. Somatic mosaic activating mutations in PIK3CA cause CLOVES syndrome. Am J Hum Genet 90 (6), 1108–1115.
URL http://dx.doi.org/10.1016/j.ajhg.2012.05.006

Lamalice, L., Le Boeuf, F., Huot, J., Mar 2007. Endothelial cell migration during angiogenesis. Circ Res 100 (6), 782–794.
URL http://dx.doi.org/10.1161/01.RES.0000259593.07661.1e

Lawson, N. D., Scheer, N., Pham, V. N., Kim, C.-H., Chitnis, A. B., Campos-Ortega, J. A., Weinstein, B. M., 2001. Notch signaling is required for arterial-venous differentiation during embryonic vascular development. Development 128 (19), 3675–3683.
URL http://dev.biologists.org/content/128/19/3675

Lawson, N. D., Weinstein, B. M., aug 2002. In vivo imaging of embryonic vascular development using transgenic zebrafish. Developmental Biology 248 (2), 307–318.
URL http://dx.doi.org/10.1006/dbio.2002.0711

Lecuit, T., Yap, A. S., apr 2015. E-cadherin junctions as active mechanical integrators in tissue dynamics. Nature Cell Biology 17 (5), 533–539.
URL https://doi.org/10.1038%2Fncb3136

Lee, H.-C., Lin, Y.-Z., Lai, Y.-T., Huang, W.-J., Hu, J.-R., Tsai, J.-N., Tsai, H.-J., aug 2014a. Glycogen synthase kinase 3 beta in somites plays a role during the angiogenesis of zebrafish embryos. FEBS Journal 281 (19), 4367–4383.
URL http://dx.doi.org/10.1111/febs.12942

Lee, M. Y., Luciano, A. K., Ackah, E., Rodriguez-Vita, J., Bancroft, T. A., Eichmann, A., Simons, M., Kyriakides, T. R., Morales-Ruiz, M., Sessa, W. C., Sep 2014b. Endothelial Akt1 mediates angiogenesis by phosphorylating multiple angiogenic substrates. Proc Natl Acad Sci U S A 111 (35), 12865–12870.
URL http://dx.doi.org/10.1073/pnas.1408472111

Lelievre, E., may 2005. Deficiency in the p110alpha subunit of PI3K results in diminished Tie2 expression and Tie2-/- like vascular defects in mice. Blood 105 (10), 3935–3938.
URL http://dx.doi.org/10.1182/blood-2004-10-3955

Lemmon, M. A., dec 2007. Pleckstrin homology (PH) domains and phosphoinositides. Biochemical Society Symposium 74 (1), 81.
URL https://doi.org/10.1042%2Fbss0740081

Lenard, A., Daetwyler, S., Betz, C., Ellertsdottir, E., Belting, H.-G., Huisken, J., Affolter, M., Apr 2015. Endothelial cell self-fusion during vascular pruning. PLoS Biol 13 (4), e1002126.
URL http://dx.doi.org/10.1371/journal.pbio.1002126

Lenard, A., Ellertsdottir, E., Herwig, L., Krudewig, A., Sauteur, L., Belting, H.-G., Affolter, M., jun 2013. In vivo analysis reveals a highly stereotypic morphogenetic pathway of vascular anastomosis. Developmental Cell 25 (5), 492–506.
URL http://dx.doi.org/10.1016/j.devcel.2013.05.010

Leslie, J. D., Ariza-McNaughton, L., Bermange, A. L., McAdow, R., Johnson, S. L., Lewis, J., Mar 2007. Endothelial signalling by the Notch ligand Delta-like 4 restricts angiogenesis. Development 134 (5), 839–844.
URL http://dx.doi.org/10.1242/dev.003244

Limaye, N., Kangas, J., Mendola, A., Godfraind, C., Schlögel, M. J., Helaers, R., Eklund, L., Boon, L. M., Vikkula, M., dec 2015. Somatic Activating PIK3CA Mutations Cause Venous Malformation. The American Journal of Human Genetics 97 (6), 914–921.
URL http://dx.doi.org/10.1016/j.ajhg.2015.11.011

Limbourg, A., Ploom, M., Elligsen, D., Sorensen, I., Ziegelhoeffer, T., Gossler, A., Drexler, H., Limbourg, F. P., feb 2007. Notch Ligand Delta-Like 1 Is Essential for Postnatal Arteriogenesis. Circulation Research 100 (3), 363–371.
URL http://dx.doi.org/10.1161/01.RES.0000258174.77370.2c

Lindsay, Y., McCoull, D., Davidson, L., Leslie, N. R., Fairservice, A., Gray, A., Lucocq, J., Downes, C. P., Dec 2006. Localization of agonist-sensitive PtdIns(3,4,5)P3 reveals a nuclear pool that is insensitive to PTEN expression. J Cell Sci 119 (Pt 24), 5160–5168.
URL http://dx.doi.org/10.1242/jcs.000133

Liu, Z.-J., Shirakawa, T., Li, Y., Soma, A., Oka, M., Dotto, G. P., Fairman, R. M., Velazquez, O. C., Herlyn, M., Jan 2003. Regulation of Notch1 and Dll4 by vascular endothelial growth factor in arterial endothelial cells: implications for modulating arteriogenesis and angiogenesis. Mol Cell Biol 23 (1), 14–25.

Lizama, C. O., Zovein, A. C., may 2013. Polarizing pathways: Balancing endothelial polarity, permeability, and lumen formation. Experimental Cell Research 319 (9), 1247–1254.
URL https://doi.org/10.1016%2Fj.yexcr.2013.03.028

Lobov, I. B., Renard, R. A., Papadopoulos, N., Gale, N. W., Thurston, G., Yancopoulos, G. D., Wiegand, S. J., feb 2007. Delta-like ligand 4 (Dll4) is induced by VEGF as a negative regulator of angiogenic sprouting. Proceedings of the National Academy of Sciences 104 (9), 3219–3224.
URL http://dx.doi.org/10.1073/pnas.0611206104

Lu, X., Le Noble, F., Yuan, L., Jiang, Q., De Lafarge, B., Sugiyama, D., Bréant, C., Claes, F., De Smet, F., Thomas, J.-L., Autiero, M., Carmeliet, P., Tessier-Lavigne, M., Eichmann, A., Nov 2004. The netrin receptor UNC5B mediates guidance events controlling morphogenesis of the vascular system. Nature 432 (7014), 179–186.
URL http://dx.doi.org/10.1038/nature03080

Lubarsky, B., Krasnow, M. A., jan 2003. Tube morphogenesis. Cell 112 (1), 19–28.
URL http://dx.doi.org/10.1016/S0092-8674(02)01283-7

Luks, V. L., Kamitaki, N., Vivero, M. P., Uller, W., Rab, R., BovÃ©e, J. V. M. G., Rialon, K. L., Guevara, C. J., Alomari, A. I., Greene, A. K., Fishman, S. J., Kozakewich, H. P. W., Maclellan, R. A., Mulliken, J. B., Rahbar, R., Spencer, S. A., Trenor, 3rd, C. C., Upton, J., Zurakowski, D., Perkins, J. A., Kirsh, A., Bennett, J. T., Dobyns, W. B., Kurek, K. C., Warman, M. L., McCarroll, S. A., Murillo, R., Apr 2015. Lymphatic and other vascular malformative/overgrowth disorders are caused by somatic mutations in PIK3CA. J Pediatr 166 (4), 1048–54.e1–5.
URL http://dx.doi.org/10.1016/j.jpeds.2014.12.069

Luo, J., Cantley, L. C., Oct 2005. The negative regulation of phosphoinositide 3-kinase signaling by p85 and it's implication in cancer. Cell Cycle 4 (10), 1309–1312.
URL http://dx.doi.org/10.4161/cc.4.10.2062

Makanya, A. N., Hlushchuk, R., Djonov, V. G., feb 2009. Intussusceptive angiogenesis and its role in vascular morphogenesis, patterning, and remodeling. Angiogenesis 12 (2), 113–123.
URL http://dx.doi.org/10.1007/s10456-009-9129-5

Makinen, T., sep 2001. Isolated lymphatic endothelial cells transduce growth, survival and migratory signals via the VEGF-C/D receptor VEGFR-3. The EMBO Journal 20 (17), 4762–4773.
URL http://dx.doi.org/10.1093/emboj/20.17.4762

Manning, B. D., Cantley, L. C., Jun 2007. AKT/PKB signaling: navigating downstream. Cell 129 (7), 1261–1274.
URL http://dx.doi.org/10.1016/j.cell.2007.06.009

Manning, G., Plowman, G. D., Hunter, T., Sudarsanam, S., Oct 2002. Evolution of protein kinase signaling from yeast to man. Trends Biochem Sci 27 (10), 514–520.

Margaris, K. N., Black, R. A., jan 2012. Modelling the lymphatic system: challenges and opportunities. Journal of The Royal Society Interface 9 (69), 601–612.
URL http://dx.doi.org/10.1098/rsif.2011.0751

Massacesi, C., Tomaso, E. D., Urban, P., Germa, C., Quadt, C., Trandafir, L., Aimone, P., Fretault, N., Dharan, B., Tavorath, R., Hirawat, S., jan 2016. PI3K inhibitors as new cancer therapeutics: implications for clinical trial design. OTT, 203.
URL http://dx.doi.org/10.2147/OTT.S89967

Matsushita, H., Chang, E., Glassford, A. J., Cooke, J. P., Chiu, C.-P., Tsao, P. S., sep 2001. eNOS activity is reduced in senescent human endothelial cells: Preservation by hTERT immortalization. Circulation Research 89 (9), 793–798.
URL http://dx.doi.org/10.1161/hh2101.098443

Mauvais-Jarvis, F., Ueki, K., Fruman, D. A., Hirshman, M. F., Sakamoto, K., Goodyear, L. J., Iannacone, M., Accili, D., Cantley, L. C., Kahn, C. R., Jan 2002. Reduced expression of the murine p85alpha subunit of phosphoinositide 3-kinase improves insulin signaling and ameliorates diabetes. J Clin Invest 109 (1), 141–149.
URL http://dx.doi.org/10.1172/JCI13305

Mellor, P., Furber, L. A., Nyarko, J. N. K., Anderson, D. H., Jan 2012. Multiple roles for the p85α isoform in the regulation and function of PI3K signalling and receptor trafficking. Biochem J 441 (1), 23–37.
URL http://dx.doi.org/10.1042/BJ20111164

Milde, F., Lauw, S., Koumoutsakos, P., Iruela-Arispe, M. L., Dec 2013. The mouse retina in 3D: quantification of vascular growth and remodeling. Integr Biol (Camb) 5 (12), 1426–1438.
URL http://dx.doi.org/10.1039/c3ib40085a

Millan, J., Cain, R. J., Reglero-Real, N., Bigarella, C., Marcos-Ramiro, B., Fernandez-Martin, L., Correas, I., Ridley, A. J., 2010. Adherens junctions connect stress fibers between adjacent

endothelial cells. BMC Biology 8 (1), 11.
URL http://dx.doi.org/10.1186/1741-7007-8-11

Miyauchi, H., Minamino, T., Tateno, K., Kunieda, T., Toko, H., Komuro, I., jan 2004. Akt negatively regulates the in vitro lifespan of human endothelial cells via a p53/p21-dependent pathway. The EMBO Journal 23 (1), 212–220.
URL https://doi.org/10.1038%2Fsj.emboj.7600045

Montero-Balaguer, M., Swirsding, K., Orsenigo, F., Cotelli, F., Mione, M., Dejana, E., jun 2009. Stable vascular connections and remodeling require full expression of VE-cadherin in zebrafish embryos. PLoS ONE 4 (6), e5772.
URL http://dx.doi.org/10.1371/journal.pone.0005772

Mulder, J., Ariaens, A., van den Boomen, D., Moolenaar, W. H., Dec 2004. p116Rip targets myosin phosphatase to the actin cytoskeleton and is essential for RhoA/ROCK-regulated neuritogenesis. Mol Biol Cell 15 (12), 5516–5527.
URL http://dx.doi.org/10.1091/mbc.E04-04-0275

Mulder, J., Poland, M., Gebbink, M. F. B. G., Calafat, J., Moolenaar, W. H., Kranenburg, O., Jul 2003. p116Rip is a novel filamentous actin-binding protein. J Biol Chem 278 (29), 27216–27223.
URL http://dx.doi.org/10.1074/jbc.M302399200

Muñoz-Espín, D., Serrano, M., Jul 2014. Cellular senescence: from physiology to pathology. Nat Rev Mol Cell Biol 15 (7), 482–496.
URL http://dx.doi.org/10.1038/nrm3823

Nelson, C. M., Chen, C. S., feb 2002. Cell-cell signaling by direct contact increases cell proliferation via a PI3K-dependent signal. FEBS Letters 514 (2-3), 238–242.
URL http://dx.doi.org/10.1016/S0014-5793(02)02370-0

Nguyen, H.-N., Yang, J.-M., Miyamoto, T., Itoh, K., Rho, E., Zhang, Q., Inoue, T., Devreotes, P. N., Sesaki, H., Iijima, M., Jul 2015. Opening the conformation is a master switch for the dual localization and phosphatase activity of PTEN. Sci Rep 5, 12600.
URL http://dx.doi.org/10.1038/srep12600

Nicoli, S., Knyphausen, C.-P., Zhu, L. J., Lakshmanan, A., Lawson, N. D., feb 2012. miR-221 is required for endothelial tip cell behaviors during vascular development. Developmental Cell 22 (2), 418–429.
URL http://dx.doi.org/10.1016/j.devcel.2012.01.008

Nilsson, I., Bahram, F., Li, X., Gualandi, L., Koch, S., Jarvius, M., Söderberg, O., Anisimov, A., Kholová, I., Pytowski, B., Baldwin, M., Ylä-Herttuala, S., Alitalo, K., Kreuger, J., Claesson-Welsh, L., mar 2010. VEGF receptor 2/-3 heterodimers detected in situ by proximity ligation on

angiogenic sprouts. The EMBO Journal 29 (8), 1377–1388.
URL http://dx.doi.org/10.1038/emboj.2010.30

Oellerich, M. F., Potente, M., apr 2012. FOXOs and Sirtuins in Vascular Growth, Maintenance, and Aging. Circulation Research 110 (9), 1238–1251.
URL http://dx.doi.org/10.1161/CIRCRESAHA.111.246488

Oikawa, T., Shimamura, M., Dec 1996. Potent inhibition of angiogenesis by wortmannin, a fungal metabolite. Eur J Pharmacol 318 (1), 93–96.

Okkenhaug, K., Graupera, M., Vanhaesebroeck, B., 2016. Targeting PI3K in Cancer: Impact on Tumor Cells, Their Protective Stroma, Angiogenesis, and Immunotherapy. Cancer Discovery 6 (10), 1090–1105.
URL http://cancerdiscovery.aacrjournals.org/content/6/10/1090

Papapetropoulos, A., mar 2000. Angiopoietin-1 Inhibits Endothelial Cell Apoptosis via the Akt/Survivin Pathway. Journal of Biological Chemistry 275 (13), 9102–9105.
URL http://dx.doi.org/10.1074/jbc.275.13.9102

Perryn, E. D., Czirók, A., Little, C. D., jan 2008. Vascular sprout formation entails tissue deformations and VE-cadherin-dependent cell-autonomous motility. Developmental Biology 313 (2), 545–555.
URL http://dx.doi.org/10.1016/j.ydbio.2007.10.036

Phng, L.-K., Potente, M., Leslie, J. D., Babbage, J., Nyqvist, D., Lobov, I., Ondr, J. K., Rao, S., Lang, R. A., Thurston, G., Gerhardt, H., jan 2009. Nrarp coordinates endothelial Notch and Wntsignaling to control vessel density in angiogenesis. Developmental Cell 16 (1), 70–82.
URL http://dx.doi.org/10.1016/j.devcel.2008.12.009

Pitulescu, M. E., Schmidt, I., Benedito, R., Adams, R. H., Sep 2010. Inducible gene targeting in the neonatal vasculature and analysis of retinal angiogenesis in mice. Nat Protoc 5 (9), 1518–1534.
URL http://dx.doi.org/10.1038/nprot.2010.113

Poschl, E., Schlotzer-Schrehardt, U., Brachvogel, B., Saito, K., Ninomiya, Y., Mayer, U., Apr 2004. Collagen IV is essential for basement membrane stability but dispensable for initiation of its assembly during early development. Development 131 (7), 1619–1628.
URL http://dx.doi.org/10.1242/dev.01037

Potente, M., Gerhardt, H., Carmeliet, P., Sep 2011. Basic and therapeutic aspects of angiogenesis. Cell 146 (6), 873–887.
URL http://dx.doi.org/10.1016/j.cell.2011.08.039

Potente, M., Urbich, C., Sasaki, K.-i., Hofmann, W. K., Heeschen, C., Aicher, A., Kollipara, R., DePinho, R. A., Zeiher, A. M., Dimmeler, S., Sep 2005. Involvement of Foxo transcription factors in angiogenesis and postnatal neovascularization. J Clin Invest 115 (9), 2382–2392.
URL http://dx.doi.org/10.1172/JCI23126

Prasain, N., Stevens, T., Jan 2009. The actin cytoskeleton in endothelial cell phenotypes. Microvasc Res 77 (1), 53–63.
URL http://dx.doi.org/10.1016/j.mvr.2008.09.012

Pérez-Mancera, P. A., Young, A. R. J., Narita, M., Aug 2014. Inside and out: the activities of senescence in cancer. Nat Rev Cancer 14 (8), 547–558.
URL http://dx.doi.org/10.1038/nrc3773

Primo, L., di Blasio, L., Roca, C., Droetto, S., Piva, R., Schaffhausen, B., Bussolino, F., mar 2007. Essential role of PDK1 in regulating endothelial cell migration. The Journal of Cell Biology 176 (7), 1035–1047.
URL https://doi.org/10.1083%2Fjcb.200607053

Quillien, A., Moore, J. C., Shin, M., Siekmann, A. F., Smith, T., Pan, L., Moens, C. B., Parsons, M. J., Lawson, N. D., mar 2014. Distinct Notch signaling outputs pattern the developing arterial system. Development 141 (7), 1544–1552.
URL http://dx.doi.org/10.1242/dev.099986

Radhakrishna, H., Al-Awar, O., Khachikian, Z., Donaldson, J., 1999. ARF6 requirement for Rac ruffling suggests a role for membrane trafficking in cortical actin rearrangements. Journal of Cell Science 112 (6), 855–866.
URL http://jcs.biologists.org/content/112/6/855

Rennel, E., Mellberg, S., Dimberg, A., Petersson, L., Botling, J., Ameur, A., Westholm, J. O., Komorowski, J., Lassalle, P., Cross, M. J., Gerwins, P., Apr 2007. Endocan is a VEGF-A and PI3K regulated gene with increased expression in human renal cancer. Exp Cell Res 313 (7), 1285–1294.
URL http://dx.doi.org/10.1016/j.yexcr.2007.01.021

Rensen, S. S. M., Doevendans, P. A. F. M., van Eys, G. J. J. M., 2007. Regulation and characteristics of vascular smooth muscle cell phenotypic diversity. Neth Heart J 15 (3), 100–108.

Ricard, N., Simons, M., May 2015. When it is better to regress: dynamics of vascular pruning. PLoS Biol 13 (5), e1002148.
URL http://dx.doi.org/10.1371/journal.pbio.1002148

Risau, W., apr 1997. Mechanisms of angiogenesis. Nature 386 (6626), 671–674.
URL http://dx.doi.org/10.1038/386671a0

Risau, W., Flamme, I., nov 1995. Vasculogenesis. Annual Review of Cell and Developmental Biology 11 (1), 73–91.
URL http://dx.doi.org/10.1146/annurev.cb.11.110195.000445

Roca, C., Adams, R. H., Oct 2007. Regulation of vascular morphogenesis by Notch signaling. Genes Dev 21 (20), 2511–2524.
URL http://dx.doi.org/10.1101/gad.1589207

Roy, A., Skibo, J., Kalume, F., Ni, J., Rankin, S., Lu, Y., Dobyns, W. B., Mills, G. B., Zhao, J. J., Baker, S. J., Millen, K. J., dec 2015. Mouse models of human PIK3CA-related brain overgrowth have acutely treatable epilepsy. eLife 4, e12703.
URL https://dx.doi.org/10.7554/eLife.12703

Ruan, G.-X., Kazlauskas, A., feb 2012. Axl is essential for VEGF-A-dependent activation of PI3K/Akt. The EMBO Journal 31 (7), 1692–1703.
URL http://dx.doi.org/10.1038/emboj.2012.21

Sarbassov, D., Guertin, D. A., Ali, S. M., Sabatini, D. M., Feb 2005. Phosphorylation and regulation of Akt/PKB by the rictor-mTOR complex. Science 307 (5712), 1098–1101.
URL http://dx.doi.org/10.1126/science.1106148

Sasaki, A. T., Chun, C., Takeda, K., Firtel, R. A., nov 2004. Localized Ras signaling at the leading edge regulates PI3K, cell polarity, and directional cell movement. The Journal of Cell Biology 167 (3), 505–518.
URL https://doi.org/10.1083%2Fjcb.200406177

Sasore, T., Kennedy, B., aug 2014. Deciphering combinations of PI3K/AKT/mTOR pathway drugs augmenting anti-angiogenic efficacy in vivo. PLoS ONE 9 (8), e105280.
URL http://dx.doi.org/10.1371/journal.pone.0105280

Sato, I., Morita, I., Kaji, K., Ikeda, M., Nagao, M., Murota, S., sep 1993. Reduction of nitric oxide producing activity associated with in vitro aging in cultured human umbilical vein endothelial cell. Biochemical and Biophysical Research Communications 195 (2), 1070–1076.
URL http://dx.doi.org/10.1006/bbrc.1993.2153

Sauteur, L., Krudewig, A., Herwig, L., Ehrenfeuchter, N., Lenard, A., Affolter, M., Belting, H.-G., oct 2014. Cdh5/VE-cadherin promotes endothelial cell interface elongation via cortical actin polymerization during angiogenic sprouting. Cell Reports 9 (2), 504–513.
URL http://dx.doi.org/10.1016/j.celrep.2014.09.024

Senger, D. R., Davis, G. E., Aug 2011. Angiogenesis. Cold Spring Harb Perspect Biol 3 (8), a005090.
URL http://dx.doi.org/10.1101/cshperspect.a005090

Serra, H., Chivite, I., Angulo-Urarte, A., Soler, A., Sutherland, J. D., Arruabarrena-Aristorena, A., Ragab, A., Lim, R., Malumbres, M., Fruttiger, M., Potente, M., Serrano, M., Fabra, A., Viñals, F., Casanovas, O., Pandolfi, P. P., Bigas, A., Carracedo, A., Gerhardt, H., Graupera, M., jul 2015. PTEN mediates Notch-dependent stalk cell arrest in angiogenesis. Nature Communications 6, 7935.
URL http://dx.doi.org/10.1038/ncomms8935

Sessa, R., Seano, G., di Blasio, L., Gagliardi, P. A., Isella, C., Medico, E., Cotelli, F., Bussolino, F., Primo, L., oct 2012. The miR-126 regulates angiopoietin-1-signaling and vessel maturation by targeting p85beta. Biochimica et Biophysica Acta (BBA) - Molecular Cell Research 1823 (10), 1925–1935.
URL https://doi.org/10.1016%2Fj.bbamcr.2012.07.011

Shalaby, F., Rossant, J., Yamaguchi, T. P., Gertsenstein, M., Wu, X.-F., Breitman, M. L., Schuh, A. C., jul 1995. Failure of blood-island formation and vasculogenesis in Flk-1-deficient mice. Nature 376 (6535), 62–66.
URL http://dx.doi.org/10.1038/376062a0

Siekmann, A. F., Affolter, M., Belting, H.-G., may 2013. The tip cell concept 10 years after: New players tune in for a common theme. Experimental Cell Research 319 (9), 1255–1263.
URL http://dx.doi.org/10.1016/j.yexcr.2013.01.019

Siekmann, A. F., Lawson, N. D., jan 2007. Notch signalling limits angiogenic cell behaviour in developing zebrafish arteries. Nature 445 (7129), 781–784.
URL http://dx.doi.org/10.1038/nature05577

Simons, M., Gordon, E., Claesson-Welsh, L., jul 2016. Mechanisms and regulation of endothelial VEGF receptor signalling. Nature Reviews Molecular Cell Biology 17 (10), 611–625.
URL http://dx.doi.org/10.1038/nrm.2016.87

Soler, A., Angulo-Urarte, A., Graupera, M., feb 2015. PI3K at the crossroads of tumor angiogenesis signaling pathways. Molecular & Cellular Oncology 2 (2), e975624.
URL http://dx.doi.org/10.4161/23723556.2014.975624

Soler, A., Figueiredo, A. M., Castel, P., Martin, L., Monelli, E., Angulo-Urarte, A., Mila-Guasch, M., Viñals, F., Baselga, J., Casanovas, O., Graupera, M., May 2016. Therapeutic benefit of selective inhibition of p110α PI3-kinase in pancreatic neuroendocrine tumors. Clin Cancer Res.
URL http://dx.doi.org/10.1158/1078-0432.CCR-15-3051

Soler, A., Serra, H., Pearce, W., Angulo, A., Guillermet-Guibert, J., Friedman, L. S., Viñals, F., Gerhardt, H., Casanovas, O., Graupera, M., Vanhaesebroeck, B., Sep 2013. Inhibition of the p110α isoform of PI 3-kinase stimulates nonfunctional tumor angiogenesis. J Exp Med 210 (10),

1937–1945.
URL http://dx.doi.org/10.1084/jem.20121571

Soriano, P., Jan 1999. Generalized lacZ expression with the ROSA26 Cre reporter strain. Nat Genet 21 (1), 70–71.
URL http://dx.doi.org/10.1038/5007

Srinivasan, S., Wang, F., Glavas, S., Ott, A., Hofmann, F., Aktories, K., Kalman, D., Bourne, H. R., jan 2003. Rac and cdc42 play distinct roles in regulating PI(3,4,5)p3and polarity during neutrophil chemotaxis. The Journal of Cell Biology 160 (3), 375–385.
URL https://doi.org/10.1083%2Fjcb.200208179

Strasser, G. A., Kaminker, J. S., Tessier-Lavigne, M., feb 2010. Microarray analysis of retinal endothelial tip cells identifies CXCR4 as a mediator of tip cell morphology and branching. Blood 115 (24), 5102–5110.
URL http://dx.doi.org/10.1182/blood-2009-07-230284

Stratman, A. N., Malotte, K. M., Mahan, R. D., Davis, M. J., Davis, G. E., Dec 2009. Pericyte recruitment during vasculogenic tube assembly stimulates endothelial basement membrane matrix formation. Blood 114 (24), 5091–5101.
URL http://dx.doi.org/10.1182/blood-2009-05-222364

Strilic, B., Kucera, T., Eglinger, J., Hughes, M. R., McNagny, K. M., Tsukita, S., Dejana, E., Ferrara, N., Lammert, E., oct 2009. The molecular basis of vascular lumen formation in the developing mouse aorta. Developmental Cell 17 (4), 505–515.
URL http://dx.doi.org/10.1016/j.devcel.2009.08.011

Stumpf, M., den Hertog, J., 2016. Differential requirement for pten lipid and protein phosphatase activity during zebrafish embryonic development. PLoS One 11 (2), e0148508.
URL http://dx.doi.org/10.1371/journal.pone.0148508

Suchting, S., Freitas, C., le Noble, F., Benedito, R., Bríant, C., Duarte, A., Eichmann, A., Feb 2007. The Notch ligand Delta-like 4 negatively regulates endothelial tip cell formation and vessel branching. Proc Natl Acad Sci U S A 104 (9), 3225–3230.
URL http://dx.doi.org/10.1073/pnas.0611177104

Surks, H. K., Richards, C. T., Mendelsohn, M. E., Dec 2003. Myosin phosphatase-Rho interacting protein. A new member of the myosin phosphatase complex that directly binds RhoA. J Biol Chem 278 (51), 51484–51493.
URL http://dx.doi.org/10.1074/jbc.M305622200

Surks, H. K., Riddick, N., i. Ohtani, K., oct 2005. M-RIP targets myosin phosphatase to stress fibers to regulate myosin light chain phosphorylation in vascular smooth muscle cells. Journal

of Biological Chemistry 280 (52), 42543–42551.
URL http://dx.doi.org/10.1074/jbc.M506863200

Suzuki, A., oct 2002. Identification of a novel protein kinase mediating Akt survival signaling to the ATM protein. Journal of Biological Chemistry 278 (1), 48–53.
URL https://doi.org/10.1074%2Fjbc.m206025200

Swartz, M., aug 2001. The physiology of the lymphatic system. Advanced Drug Delivery Reviews 50 (1-2), 3–20.
URL http://dx.doi.org/10.1016/S0169-409X(01)00150-8

Taddei, A., Giampietro, C., Conti, A., Orsenigo, F., Breviario, F., Pirazzoli, V., Potente, M., Daly, C., Dimmeler, S., Dejana, E., jul 2008. Endothelial adherens junctions control tight junctions by VE-cadherin-mediated upregulation of claudin-5. Nature Cell Biology 10 (8), 923–934.
URL http://dx.doi.org/10.1038/ncb1752

Takeshita, K., Satoh, M., Ii, M., Silver, M., Limbourg, F. P., Mukai, Y., Rikitake, Y., Radtke, F., Gridley, T., Losordo, D. W., Liao, J. K., Jan 2007. Critical role of endothelial Notch1 signaling in postnatal angiogenesis. Circ Res 100 (1), 70–78.
URL http://dx.doi.org/10.1161/01.RES.0000254788.47304.6e

Tamagnone, L., Comoglio, P., Sep 2000. Signalling by semaphorin receptors: cell guidance and beyond. Trends Cell Biol 10 (9), 377–383.

Tammela, T., Zarkada, G., Nurmi, H., Jakobsson, L., Heinolainen, K., Tvorogov, D., Zheng, W., Franco, C. A., Murtomäki, A., Aranda, E., Miura, N., Ylä-Herttuala, S., Fruttiger, M., Mäkinen, T., Eichmann, A., Pollard, J. W., Gerhardt, H., Alitalo, K., sep 2011. VEGFR-3 controls tip to stalk conversion at vessel fusion sites by reinforcing Notch signalling. Nature Cell Biology 13 (10), 1202–1213.
URL http://dx.doi.org/10.1038/ncb2331

Tammela, T., Zarkada, G., Wallgard, E., Murtomäki, A., Suchting, S., Wirzenius, M., Waltari, M., Hellström, M., Schomber, T., Peltonen, R., Freitas, C., Duarte, A., Isoniemi, H., Laakkonen, P., Christofori, G., Ylä-Herttuala, S., Shibuya, M., Pytowski, B., Eichmann, A., Betsholtz, C., Alitalo, K., jun 2008. Blocking VEGFR-3 suppresses angiogenic sprouting and vascular network formation. Nature 454 (7204), 656–660.
URL http://dx.doi.org/10.1038/nature07083

Thorpe, L. M., Yuzugullu, H., Zhao, J. J., dec 2014. PI3K in cancer: divergent roles of isoforms, modes of activation and therapeutic targeting. Nature Reviews Cancer 15 (1), 7–24.
URL http://dx.doi.org/10.1038/nrc3860

Thyboll, J., Kortesmaa, J., Cao, R., Soininen, R., Wang, L., Iivanainen, A., Sorokin, L., Risling, M., Cao, Y., Tryggvason, K., Feb 2002. Deletion of the laminin alpha4 chain leads to impaired microvessel maturation. Mol Cell Biol 22 (4), 1194–1202.

Torres-Vazquez, J., Gitler, A. D., Fraser, S. D., Berk, J. D., Van N Pham, Fishman, M. C., Childs, S., Epstein, J. A., Weinstein, B. M., Jul 2004. Semaphorin-plexin signaling guides patterning of the developing vasculature. Dev Cell 7 (1), 117–123.
URL http://dx.doi.org/10.1016/j.devcel.2004.06.008

Totsukawa, G., Wu, Y., Sasaki, Y., Hartshorne, D. J., Yamakita, Y., Yamashiro, S., Matsumura, F., feb 2004. Distinct roles of MLCK and ROCK in the regulation of membrane protrusions and focal adhesion dynamics during cell migration of fibroblasts. J Cell Biol 164 (3), 427–439.
URL http://dx.doi.org/10.1083/jcb.200306172

Totsukawa, G., Yamakita, Y., Yamashiro, S., Hartshorne, D., Sasaki, Y., Matsumura, F., Aug 2000. Distinct roles of ROCK (Rho-kinase) and MLCK in spatial regulation of MLC phosphorylation for assembly of stress fibers and focal adhesions in 3T3 fibroblasts. J Cell Biol 150 (4), 797–806.

Ueki, K., Fruman, D. A., Brachmann, S. M., Tseng, Y.-H., Cantley, L. C., Kahn, C. R., Feb 2002. Molecular balance between the regulatory and catalytic subunits of phosphoinositide 3-kinase regulates cell signaling and survival. Mol Cell Biol 22 (3), 965–977.

Utermark, T., Rao, T., Cheng, H., Wang, Q., Lee, S. H., Wang, Z. C., Iglehart, J. D., Roberts, T. M., Muller, W. J., Zhao, J. J., Jul 2012. The p110alpha and p110beta isoforms of PI3K play divergent roles in mammary gland development and tumorigenesis. Genes Dev 26 (14), 1573–1586.
URL http://dx.doi.org/10.1101/gad.191973.112

Vallenius, T., Vaahtomeri, K., Kovac, B., Osiceanu, A.-M., Viljanen, M., Mäkelä, T. P., Feb 2011. An association between NUAK2 and MRIP reveals a novel mechanism for regulation of actin stress fibers. J Cell Sci 124 (Pt 3), 384–393.
URL http://dx.doi.org/10.1242/jcs.072660

van Geemen, D., Smeets, M. W. J., van Stalborch, A.-M. D., Woerdeman, L. A. E., Daemen, M. J. A. P., Hordijk, P. L., Huveneers, S., jul 2014. F-actin-anchored focal adhesions distinguish endothelial phenotypes of human arteries and veins. Arteriosclerosis, Thrombosis, and Vascular Biology 34 (9), 2059–2067.
URL http://dx.doi.org/10.1161/ATVBAHA.114.304180

Vanhaesebroeck, B., Guillermet-Guibert, J., Graupera, M., Bilanges, B., May 2010. The emerging mechanisms of isoform-specific PI3K signalling. Nat Rev Mol Cell Biol 11 (5), 329–341.
URL http://dx.doi.org/10.1038/nrm2882

Vicente-Manzanares, M., Ma, X., Adelstein, R. S., Horwitz, A. R., Nov 2009. Non-muscle myosin ii takes centre stage in cell adhesion and migration. Nat Rev Mol Cell Biol 10 (11), 778–790.
URL http://dx.doi.org/10.1038/nrm2786

Wallez, Y., Huber, P., Mar 2008. Endothelial adherens and tight junctions in vascular homeostasis, inflammation and angiogenesis. Biochim Biophys Acta 1778 (3), 794–809.
URL http://dx.doi.org/10.1016/j.bbamem.2007.09.003

Wang, F., Herzmark, P., Weiner, O. D., Srinivasan, S., Servant, G., Bourne, H. R., jun 2002. Lipid products of PI(3)Ks maintain persistent cell polarity and directed motility in neutrophils. Nature Cell Biology 4 (7), 513–518.
URL https://doi.org/10.1038%2Fncb810

Wang, J. C., Bennett, M., jul 2012. Aging and atherosclerosis: Mechanisms, functional consequences, and potential therapeutics for cellular senescence. Circulation Research 111 (2), 245–259.
URL http://dx.doi.org/10.1161/CIRCRESAHA.111.261388

Wang, R., Brattain, M. G., Oct 2006. AKT can be activated in the nucleus. Cell Signal 18 (10), 1722–1731.
URL http://dx.doi.org/10.1016/j.cellsig.2006.01.020

Wang, Y., Kaiser, M. S., Larson, J. D., Nasevicius, A., Clark, K. J., Wadman, S. A., Roberg-Perez, S. E., Ekker, S. C., Hackett, P. B., McGrail, M., Essner, J. J., aug 2010. Moesin1 and Ve-cadherin are required in endothelial cells during in vivo tubulogenesis. Development 137 (18), 3119–3128.
URL http://dx.doi.org/10.1242/dev.048785

Warren, C. M., Iruela-Arispe, M. L., May 2010. Signaling circuitry in vascular morphogenesis. Curr Opin Hematol 17 (3), 213–218.
URL http://dx.doi.org/10.1097/MOH.0b013e32833865d1

Wei, Y., Gong, J., Thimmulappa, R. K., Kosmider, B., Biswal, S., Duh, E. J., Oct 2013. Nrf2 acts cell-autonomously in endothelium to regulate tip cell formation and vascular branching. Proc Natl Acad Sci U S A 110 (41), E3910–E3918.
URL http://dx.doi.org/10.1073/pnas.1309276110

Weinstein, B., Stemple, D., Driever, W., Fishman, M., Nov 1995. Gridlock, a localized heritable vascular patterning defect in the zebrafish. Nat Med 1 (11), 1143–1147.

Westerfield, M., 2007. THE ZEBRAFISH BOOK, 5th Edition; A guide for the laboratory use of zebrafish (Danio rerio). Eugene, University of Oregon Press.

Wilhelm, K., Happel, K., Eelen, G., Schoors, S., Oellerich, M. F., Lim, R., Zimmermann, B., Aspalter, I. M., Franco, C. A., Boettger, T., Braun, T., Fruttiger, M., Rajewsky, K., Keller, C., Brüning, J. C., Gerhardt, H., Carmeliet, P., Potente, M., Jan 2016. FOXO1 couples metabolic activity and growth state in the vascular endothelium. Nature 529 (7585), 216–220.
URL http://dx.doi.org/10.1038/nature16498

Wilkes, E. H., Terfve, C., Gribben, J. G., Saez-Rodriguez, J., Cutillas, P. R., jun 2015. Empirical inference of circuitry and plasticity in a kinase signaling network. Proceedings of the National Academy of Sciences 112 (25), 7719–7724.
URL https://doi.org/10.1073%2Fpnas.1423344112

Xia, X., Serrero, G., aug 1999. Multiple forms of p55PIK, a regulatory subunit of phosphoinositide 3-kinase, are generated by alternative initiation of translation. Biochem. J. 341 (3), 831–837.
URL http://dx.doi.org/10.1042/bj3410831

Xu, K., Cleaver, O., dec 2011. Tubulogenesis during blood vessel formation. Seminars in Cell & Developmental Biology 22 (9), 993–1004.
URL http://dx.doi.org/10.1016/j.semcdb.2011.05.001

Xue, G., Hemmings, B. A., Mar 2013. PKB/Akt-dependent regulation of cell motility. J Natl Cancer Inst 105 (6), 393–404.
URL http://dx.doi.org/10.1093/jnci/djs648

Yamamoto, H., Ehling, M., Kato, K., Kanai, K., van Lessen, M., Frye, M., Zeuschner, D., Nakayama, M., Vestweber, D., Adams, R. H., mar 2015. Integrin β1 controls VE-cadherin localization and blood vessel stability. Nature Communications 6, 6429.
URL http://dx.doi.org/10.1038/ncomms7429

Yang, S., Kim, H.-M., apr 2012. The RhoA-ROCK-PTEN pathway as a molecular switch for anchorage dependent cell behavior. Biomaterials 33 (10), 2902–2915.
URL http://dx.doi.org/10.1016/j.biomaterials.2011.12.051

Yang, Z.-Z., Tschopp, O., Hemmings-Mieszczak, M., Feng, J., Brodbeck, D., Perentes, E., Hemmings, B. A., Aug 2003. Protein kinase B alpha/Akt1 regulates placental development and fetal growth. J Biol Chem 278 (34), 32124–32131.
URL http://dx.doi.org/10.1074/jbc.M302847200

Yoshioka, K., Yoshida, K., Cui, H., Wakayama, T., Takuwa, N., Okamoto, Y., Du, W., Qi, X., Asanuma, K., Sugihara, K., Aki, S., Miyazawa, H., Biswas, K., Nagakura, C., Ueno, M., Iseki, S., Schwartz, R. J., Okamoto, H., Sasaki, T., Matsui, O., Asano, M., Adams, R. H., Takakura, N., Takuwa, Y., Oct 2012. Endothelial PI3K-C2alpha, a class II PI3K, has an essential role in angiogenesis and vascular barrier function. Nat Med 18 (10), 1560–1569.
URL http://dx.doi.org/10.1038/nm.2928

Yu, J. A., Castranova, D., Pham, V. N., Weinstein, B. M., aug 2015. Single-cell analysis of endothelial morphogenesis in vivo. Development 142 (17), 2951–2961.
URL http://dx.doi.org/10.1242/dev.123174

Yuan, T. L., Choi, H. S., Matsui, A., Benes, C., Lifshits, E., Luo, J., Frangioni, J. V., Cantley, L. C., jul 2008. Class 1A PI3K regulates vessel integrity during development and tumorigenesis. Proceedings of the National Academy of Sciences 105 (28), 9739–9744.
URL http://dx.doi.org/10.1073/pnas.0804123105

Zagorska, A., Deak, M., Campbell, D. G., Banerjee, S., Hirano, M., Aizawa, S., Prescott, A. R., Alessi, D. R., mar 2010. New roles for the LKB1-NUAK pathway in controlling myosin phosphatase complexes and cell adhesion. Science Signaling 3 (115), ra25–ra25.
URL http://dx.doi.org/10.1126/scisignal.2000616

Zhang, L., Zhou, F., Han, W., Shen, B., Luo, J., Shibuya, M., He, Y., aug 2010. VEGFR-3 ligand-binding and kinase activity are required for lymphangiogenesis but not for angiogenesis. Cell Research 20 (12), 1319–1331.
URL http://dx.doi.org/10.1038/cr.2010.116

Zhang, L.-J., Tao, B.-B., Wang, M.-J., Jin, H.-M., Zhu, Y.-C., 2012. PI3K p110alpha isoform-dependent Rho GTPase Rac1 activation mediates H2S-promoted endothelial cell migration via actin cytoskeleton reorganization. PLoS One 7 (9), e44590.
URL http://dx.doi.org/10.1371/journal.pone.0044590

Zhou, G.-L., Tucker, D. F., Bae, S. S., Bhatheja, K., Birnbaum, M. J., Field, J., Nov 2006. Opposing roles for Akt1 and Akt2 in Rac/Pak signaling and cell migration. J Biol Chem 281 (47), 36443–36453.
URL http://dx.doi.org/10.1074/jbc.M600788200

Zygmunt, T., Trzaska, S., Edelstein, L., Walls, J., Rajamani, S., Gale, N., Daroles, L., Ramírez, C., Ulrich, F., Torres-Vázquez, J., 2012. 'In parallel' interconnectivity of the dorsal longitudinal anastomotic vessels requires both VEGF signaling and circulatory flow. J Cell Sci 125 (Pt 21), 5159–5167.
URL http://dx.doi.org/10.1242/jcs.108555

Appendix

A first author manuscript based on my thesis work is under preparation to be submitted to an international journal relevant to the field. In addition, during this period I have participated in several enriching collaborations that have given rise to the following publications:

- Soler, A., Serra, H., Pearce, W., **Angulo, A.**, Guillermet-Guibert, J., Friedman, L. S., Viñals, F., Gerhardt, H., Casanovas, O., Graupera, M., Vanhaesebroeck, B., (2013) *Inhibition of the p110α isoform of PI 3-kinase stimulates nonfunctional tumor angiogenesis*. J Exp Med 210 (10), 1937–1945.

  URL http://dx.doi.org/10.1084/jem.20121571

- Soler, A.*, **Angulo-Urarte, A**.*, Graupera, M., (2015) *PI3K at the crossroads of tumor angiogenesis signaling pathways.* Review. Molecular & Cellular Oncology 2 (2), e975624.

  URL http://dx.doi.org/10.4161/23723556.2014.975624

- Serra, H., Chivite, I., **Angulo-Urarte, A.**, Soler, A., Sutherland, J. D., Arruabarrena-Aristorena, A., Ragab, A., Lim, R., Malumbres, M., Fruttiger, M., Potente, M., Serrano, M., Fabra, A., Viñals, F., Casanovas, O., Pandolfi, P. P., Bigas, A., Carracedo, A., Gerhardt, H., Graupera, M., (2015) *PTEN mediates Notch-dependent stalk cell arrest in angiogenesis.* Nature Communications 6, 7935.

  URL http://dx.doi.org/10.1038/ncomms8935

- Calderone, V., Gallego, J., Fernandez-Miranda, G., Garcia-Pras, E., Maillo, C., Berzigotti, A., Mejias, M., Bava, F.-A., **Angulo-Urarte, A.**, Graupera, M., Navarro, P., Bosch, J., Fernandez, M., Mendez, R., (2016) *Sequential functions of CPEB1 and CPEB4 regulate pathologic expression of vascular endothelial growth factor and angiogenesis in chronic liver disease.* Gastroenterology 150 (4), 982–997.e30.

  URL https://doi.org/10.1053%2Fj.gastro.2015.11.038

- Castillo, S. D., Tzouanacou, E., Zaw-Thin, M., Berenjeno, I. M., Parker, V. E., Chivite, I., Milà-Guasch, M., Pearce, W., Solomon, I., **Angulo- Urarte, A**., Figueiredo, A. M., Dewhurst, R. E., Knox, R. G., Clark, G. R., Scudamore, C. L., Badar, A., Kalber, T. L., Foster, J., Stuckey, D. J., David, A. L., Phillips,

W. A., Lythgoe, M. F., Wilson, V., Semple, R. K., Sebire, N. J., Kinsler, V. A., Graupera, M., Vanhaesebroeck, B., (2016) *Somatic activating mutations in PIK3CA cause sporadic venous malformations in mice and humans.* Science Translational Medicine 8 (332), 332ra43–332ra43.

URL http://stm.sciencemag.org/content/8/332/332ra43

- Soler, A., Figueiredo, A. M., Castel, P., Martin, L., Monelli, E., **Angulo- Urarte, A.**, Mila-Guasch, M., Viñals, F., Baselga, J., Casanovas, O., Graupera, M., (2016) *Therapeutic benefit of selective inhibition of p110α PI3-kinase in pancreatic neuroendocrine tumors.* Clin Cancer Res.

  URL http://dx.doi.org/10.1158/1078-0432.CCR-15-3051

- Ola, R., Dubrac, A., Han, J., Zhang, F., Fang, J. S., Larrivée, B., Lee, M., **Urarte, A. A.**, Kraehling, J. R., Genet, G., Hirschi, K. K., Sessa, W. C., Canals, F. V., Graupera, M., Yan, M., Young, L. H., Oh, P. S., Eichmann, A., (2016) *PI3-kinase inhibition improves vascular malformations in mouse models of hereditary haemorrhagic telangiectasia.* Nature Communications 7, 13650.

  URL https://doi.org/10.1038%2Fncomms13650